

Investigation of Ethylene Tetramerization Catalysis from Structurally-  
Defined Organochromium Compounds

Thesis by  
Nathanael Allen Hirscher

In Partial Fulfillment of the Requirements  
for the Degree of Doctor of Philosophy

CALIFORNIA INSTITUTE OF TECHNOLOGY  
Division of Chemistry and Chemical Engineering  
Pasadena, California

2020

(Defended on July 18<sup>th</sup>, 2019)

©2020

Nathanael Allen Hirscher  
ORCID: 0000-0002-6847-0012

## Acknowledgements

As I complete my Ph.D., I need to take the time to acknowledge the many, many people who have contributed to me accomplishing this work. I certainly cannot include every name, but am thankful for the associates, coworkers, collaborators, friends, and mentors I have encountered over the years of my academic life so far.

Everything started with my parents, Randy and Julie. They homeschooled me for thirteen years, and contributed primarily to my intellectual and personal development through steadfast love and wisdom. I thank my siblings, Alisa, Jonathan, Joshua, and Elizabeth for their love and support as well. My father instilled in me a sense of the importance of hard work. He also frequently gave the advice to “get all the information” before making a decision. I recall those words often. I definitely inherited any patience I have from my mother. This is one of the most important qualities for a scientist, and I would not be here without it. My wife, Emily, has been a wonderful partner, supportive in every way throughout my Ph.D.

I need to acknowledge some of the educators I have benefited from. My high-school chemistry teacher, Sandy Kelly, sparked my initial interest in the subject. I thank Professor Dean Harman at the University of Virginia for demonstrating his passion for teaching and research. He also facilitated my involvement in the undergraduate research program at the University of Virginia (UVA).

As an undergraduate, I had the benefit of working in the lab of Professor Brent Gunnoe at UVA. I thank him for his commitment to my development as a scientist. I acknowledge Jeremy Andreatta for teaching me the basic elements of being a research scientist, and training me in the fundamentals of inorganic synthesis. I also specifically thank Tristan, Laurel, and Ted for the time invested in mentoring me during that time. Many others in the

lab were very welcoming and inspiring colleagues: thank you to Joanna, Brad, Samantha, Evan, Jiajun, Steve, Mark, George, Matt, Ben, and Mike.

I thank Professor Oleg Ozerov for welcoming me to his lab at Texas A&M University when I was an undergraduate. I decided to pursue a Ph.D. in chemistry at the conclusion of that three month appointment. Despite our short time together, his role in my intellectual formation has been incredible. Further, I thank Chun-I Lee, who guided my research progress at Texas A&M. The rest of the group was wonderful to me: thanks to Jess, Chris, Loren, Chandra, Wei-Chun, Morgan, Sam, Jill, and Chelsea.

Caltech has been a whirlwind. Despite the long hours and days, altogether it seems like no time has passed at all. I thank Professor Theo Agapie for his steady mentorship over these years. His outlook, methods, and mannerisms have left an indelible mark on my scientific psyche. This is how it should be, and I can say I am honored to have passed through the Caltech chemistry program under his tutelage. It is worth remarking that my thesis topic is closely related to Theo's own, from the previous decade. I never felt like Theo had special expectations because of this, and I thank him for giving me a high degree of autonomy in the pursuit of my project goals.

Other faculty at Caltech have been influential in my scientific development. I thank Professor Jonas Peters for his advice and guidance. Professors Brian Stoltz and Bob Grubbs have both provided great career advice to me. I also thank Professor John Bercaw for his mentorship. I have had the honor to work directly with John in the lab, and my thesis is indebted to the research done in his group over the years. Professor Harry Gray has been an inspiration. I thank other scholars at Caltech who I've learned from, especially Mike Takase, and Professors Sarah Reisman and Greg Fu, for teaching me fundamentals necessary to my training. I acknowledge Larry Henling for his unending patience in wrangling the crystal

queue and teaching me how to operate the diffractometer. Paul Oyala has been a great collaborator on the EPR studies. Jay Labinger was very helpful in discussing mechanism ideas.

I had the opportunity to interface with several Dow scientists via web conference and in-person meetings. Dr. Sean Ewart was the head of that Dow team, and was always wonderful to work with. He was also very hospitable during my visit to the Dow site in Lake Jackson, TX. I thank Jerzy, Mari, David L., David K., and Alejo for their experimental contributions and feedback on my project. I wish them all the best regarding the development of ethylene tetramerization!

I thank all my coworkers at Caltech for their friendship and guidance. Josh Buss, Aimee Bryan, Jessica Sampson, Marcus Low, and HB Lee all showed me how to make the science happen in the lab. Without their words of wisdom, I am certain that my chemistry would never have taken off. I thank Davide, Guy, Sandy, Kyle, and Justin for tolerating me in the early days. Thanks to Chris Reed for being a great sounding board throughout the years; good luck at Urbana-Champaign! I appreciate Danny Perez for his contributions on this project. I have learned so much from all the postdocs and visiting scholars in the group: Graham, Shin, Zhiji, Siti, Masa, Naoki, Naofumi, Miku, Hitoshi, Yohei, David, Till, and Davit. I thank the current group for taking the reins in the lab: Arnaud, Gwen, Manar, Ryan, Charlie, Anna, Angela, Meaghan, Sam, Gavin, and Linh. You are all a pleasure to work with. Others in the inorganic division at Caltech have been great friends and colleagues: Dinesh, Alonso, Nina, Meaghan, Matt, Javier, and Dirk. Best wishes for your careers at Caltech and beyond.

## Abstract

Chapter 1 is a general introduction to the topic of ethylene tetramerization catalysis.

Chapter 2 presents the synthesis and catalytic utility of chromium multi-aryl complexes that were the first examples of ethylene tetramerization catalysts that could be produced without excess alkyl aluminum reagents.

Chapter 3 describes the mechanistic analysis of the ethylene tetramerization reaction using isotopically labelled ethylene. Co-production of 1-hexene along with 1-octene was determined to be intrinsic to the reaction mechanism. This is due to the intermediacy of a chromacyclic species that can either eliminate 1-hexene or insert a fourth ethylene.

Chapter 4 presents the synthesis of additional Cr tris(aryl) complexes, which are coordinatively saturated, and were used to generate a crystallographically-characterized Cr(III) cationic species. This was the first reported single-component precatalyst for ethylene tetramerization.

Chapter 5 describes the isotopic labelling of a well-defined ethylene tetramerization precatalyst with a deuteriomethyl group. This label was tracked following protonation of the neutral Cr complex via pulse EPR. Successful detection of deuterium on Cr-alkyl ligands led to *in situ* analysis of the catalytic mixture. A low-spin species derived from deuterated ethylene was observed.

Appendix 1 describes the synthesis of various Cr aryl amine complexes. Appendix 2 provides the results of additional catalytic experiments for ethylene tetramerization, including those with a more soluble precatalyst, and those at higher ethylene pressure. Appendix 3 details the synthesis of a molecular Re catalyst for CO<sub>2</sub> electroreduction which was used to modify electrodes. Appendix 4 lists various X-ray crystal structures that were obtained, but not related elsewhere in the thesis.

## Published Content and Contributions

Several published articles were adapted or reproduced as a part of this thesis. Permissions are indicated on the title page of the corresponding chapter. Contributions of the co-authors are indicated below.

### Chapter 2.

Nathanael A. Hirscher and Theodor Agapie. (2017). “Stoichiometrically Activated Catalysts for Ethylene Tetramerization using Diphosphinoamine-Ligated Cr Tris(hydrocarbyl) Complexes”. In: *Organometallics*, 36 (21), pp 4107-4110. doi: 10.1021/acs.organomet.7b00706.  
N.A.H. performed experiments and wrote the manuscript.

### Chapter 3.

Nathanael A. Hirscher, Jay A. Labinger, and Theodor Agapie. (2019). “Isotopic labelling in ethylene oligomerization: addressing the issue of 1-octene vs. 1-hexene selectivity”. In: *Dalton Transactions*, 48, pp 40-44. doi: 10.1039/C8DT04509G.  
N.A.H. performed experiments and wrote the manuscript.  
J.A.L. contributed to experiment design and data interpretation.

### Chapter 4.

Nathanael A. Hirscher, Danny Perez Sierra, and Theodor Agapie. (2019). “Robust Chromium Precursors for Catalysis: Isolation and Structure of a Single-Component Ethylene Tetramerization Precatalyst”. In: *Journal of the American Chemical Society*, 141 (14), pp 6022-6029. doi: 10.1021/jacs.9b01387.  
N.A.H. performed experiments and wrote the manuscript.  
D.P.S. performed synthesis experiments.

### Chapter 5.

Nathanael A. Hirscher, Charles H. Arnett, Paul H. Oyala, and Theodor Agapie. (2020). “Characterization of Cr-Hydrocarbyl Species via Pulse EPR in the Study of Ethylene Tetramerization Catalysis”. In: *Organometallics* **Article ASAP**. doi: 10.1021/acs.organomet.0c00521  
N.A.H. performed synthesis experiments, prepared EPR samples and wrote the chapter.  
C.H.A. performed DFT calculations.  
P. H.O. performed EPR spectroscopy, simulated EPR spectra, and contributed writing.

## Table of Contents

<b>Acknowledgements</b>	<b>iii</b>
<b>Abstract</b>	<b>vi</b>
<b>Published Content and Contributions</b>	<b>vii</b>
<b>Table of Contents</b>	<b>viii</b>
<b>Chapter 1</b>	<b>1</b>
General Introduction	
<b>Chapter 2</b>	<b>8</b>
Stoichiometrically-Activated Catalysts for Ethylene Tetramerization using Diphosphinoamine-Ligated Cr Tris(hydrocarbyl) Complexes	
Abstract	<b>9</b>
Introduction	<b>10</b>
Results and Discussion	<b>11</b>
Conclusion	<b>41</b>
Experimental Section	<b>42</b>
References	<b>60</b>
<b>Chapter 3</b>	<b>65</b>
Isotopic Labelling in Ethylene Oligomerization: Addressing the Issue of 1-Octene vs. 1-Hexene Selectivity	

Abstract	66
Introduction	67
Results and Discussion	69
Conclusion	77
Experimental Section	77
References	90
<b>Chapter 4</b>	<b>93</b>
Robust Chromium Precursors for Catalysis: Isolation and Structure of a Single-Component Ethylene Tetramerization Precatalyst	
Abstract	94
Introduction	95
Results and Discussion	98
Conclusion	106
Experimental Section	107
References	122
<b>Chapter 5</b>	<b>127</b>
Structural Determination of Cr-Hydrocarbyl Species via Pulse EPR in the Study of Ethylene Tetramerization Catalysis	
Abstract	128
Introduction	129
Results and Discussion	130
Conclusion	142

Experimental Section	143
References	162
<b>Appendix 1</b>	<b>165</b>
Chromium Complexes of Bidentate Aryl Amines and Tridentate Aryl Diamines	
Abstract	166
Introduction	167
Results and Discussion	169
Conclusion	179
Experimental Section	180
References	187
<b>Appendix 2</b>	<b>188</b>
Soluble Cr Species for Ethylene Tetramerization in Methylcyclohexane, and High-Pressure Catalytic Trials of a Single-Component Precatalyst	
Abstract	189
Introduction	190
Results and Discussion	190
Conclusion	197
Experimental Section	198
References	201

<b>Appendix 3</b>	<b>202</b>
Deposition of a Bipyridine Re Carbonyl Complex onto Electrodes for CO <sub>2</sub> Reduction	
Abstract	<b>203</b>
Introduction	<b>204</b>
Results and Discussion	<b>204</b>
Conclusion	<b>206</b>
Experimental Section	<b>207</b>
References	<b>213</b>
<b>Appendix 4</b>	<b>215</b>
Miscellaneous X-Ray Crystal Structures	
<b>About the Author</b>	<b>226</b>

## Chapter 1

General Introduction

The discovery, development, and optimization of catalytic processes is a major goal of chemical research and its broader applications. Transition metals are particularly suited for catalysis due to their diverse coordination environments and reactivity.<sup>1</sup> To develop known catalysts by improving their selectivity, rates, and longevity, fundamental study of the properties of the transition metal species is necessary.<sup>2</sup> Mechanistic, spectroscopic, and synthetic methodologies must be employed to probe the features of transition metal complexes in order to make these improvements.

Of particular interest are first-row transition metals due to their low cost compared to second- and third-row congeners.<sup>3</sup> A defining characteristic of complexes of first-row metals is their propensity to contain unpaired electrons (paramagnetism).<sup>4</sup> This is due either to the stability of metal oxidation states with odd-numbers of electrons, or stabilized high-spin states (for even-numbered electron counts) due to small d-orbital splitting. Ultimately, consideration of paramagnetism is required to understand certain reaction mechanisms of first-row metals for the purposes of improving catalysis.<sup>5</sup>

Due to the paramagnetism of first-row metals, they are often not suitable for characterization by the ubiquitous nuclear magnetic resonance (NMR) spectroscopy.<sup>6</sup> This has hindered the understanding of the speciation of transition metals relevant to catalysis, except where electron paramagnetic resonance (EPR) spectroscopy can be employed. Chromium complexes tend to be particularly challenging to characterize by spectroscopic methods. Although Cr(III) is a common oxidation state, the high spin multiplicity ( $S = 3/2$ ) leads to broad EPR spectra for which hyperfine parameters cannot be extracted.<sup>7</sup> Another common oxidation state, Cr(II), is often  $S = 2$ , and its transitions are formally forbidden by conventional EPR (perpendicular mode).<sup>8</sup>

The work herein addresses the broader scientific interest in the characterization of paramagnetic Cr species in the context of an industrially-relevant catalytic process: ethylene tetramerization. Chromium has been targeted for selective ethylene tetramerization since 2004.<sup>9</sup> Catalysts typically are formed by ill-defined processes using alkyl aluminum reagents, and starting from Cr(III) precatalysts. Although analogies can be derived from reactions of group IV metals,<sup>10</sup> the aforementioned spectroscopic challenges for Cr have hindered the systematic study of ethylene tetramerization.

An important point regarding ethylene tetramerization catalysis is that it uses aminodiphosphine (PNP) ligands that bind in a bidentate fashion, yet with an acute bite angle ( $< 70^\circ$ ) due to the four-membered ring.<sup>11</sup> This leads to weak binding, and complicates the synthesis of PNP-Cr species, since PNP will dissociate from Cr(III) in favor of ligands such as tetrahydrofuran (THF). Furthermore, PNP has been observed in several cases to undergo isomerization to PPN structures.<sup>12</sup> This has even led to P-P bond cleavage in the presence of alkyl-aluminum reagents.<sup>13</sup> Finally, aminodiphosphines also can support metal-metal bonded motifs.<sup>14</sup> Although the work described here has not directly evaluated these complexities in the context of the Cr catalysis, they are worth keeping in mind.

Pursuant to our aim of understanding and improving the Cr-based ethylene tetramerization catalyst, we sought well-defined PNP-Cr precatalysts so that large excesses of alkyl aluminum reagents are not required. This was important not only due to the practical aspects of safety and cost, but also for fundamental understanding. The activator *du jour* is modified methylaluminoxane (MMAO), one commercially-available formulation (MMAO-3A) is known to be a partially hydrolyzed mixture of trimethylaluminum and triisobutylaluminum (in a 2:1 ratio).<sup>15</sup> Drawing from knowledge of group IV chemistry, MMAO-3A likely serves to generate an alkylated and cationic Cr species *in situ*.<sup>16</sup> The

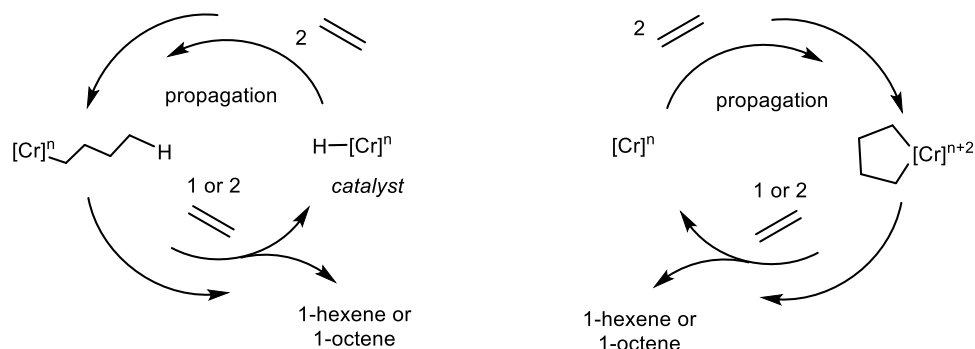
composition, structure, and stability of methylaluminoxanes is the subject of research in its own right.<sup>17</sup> Therefore, to eliminate the uncertainty in the composition of our catalysts due to the use of MMAO, we designed “pre-alkylated” Cr complexes that could be activated by protonation (Chapter 2).

The Cr ethylene tetramerization catalyst had been demonstrated by Sasol researchers to proceed through a metallacyclic chain-growth mechanism (Scheme 1, right).<sup>18</sup> This is similar to Cr (and other metal-based) ethylene trimerization catalysts.<sup>19</sup> The metallacyclic mechanism provides a means of selecting for certain chain lengths on the basis of strain in the metallacycle, in contrast to a linear chain growth mechanism (Scheme 1, left). We have revisited this mechanistic study, in order to rationalize an isotope effect on the selectivity between 1-octene and 1-hexene, the major co-product (Chapter 3). This analysis confirmed that both products are formed by the *same* catalyst species, and hydride transfer v. ethylene insertion governs the selectivity between the two products.

Following the successful stoichiometric activation of PNP-Cr tris(hydrocarbyl) precatalysts, an expanded series of homoleptic Cr tris(aryl) precursors was synthesized (Chapter 4). A study of analogs distinguished by the chelate ring size was performed, demonstrating differences in stability and structure. These precursors enabled the synthesis of a cationic, PNP Cr(III) diaryl species, which was crystallographically characterized, and demonstrated to be a single-component ethylene tetramerization precatalyst.

The original Cr tris(hydrocarbyl) precursors included a Cr-methyl example, which was well-suited for isotopic labelling to the Cr-CD<sub>3</sub> analog (Chapter 5). This provided a handle for pulse EPR techniques, which were employed for the characterization of reactive Cr intermediates. As well, EPR analysis of catalysis was possible using C<sub>2</sub>D<sub>4</sub> gas. An off-path intermediate was observed, with spectral features consistent with a Cr-alkene species.

**Scheme 1.** Linear chain growth process (left) vs. metallacyclic chain growth process (right).



In summary, the synthesis of new, paramagnetic Cr complexes allowed for ethylene tetramerization catalysis from well-defined (crystallographically-characterized) organochromium starting materials. This strategy was extended to the discovery of a single-component catalyst. Therefore, the elimination of the need for alkyl aluminum activators (and activators of any kind) was achieved. Analysis of an isotopically-labelled ethylene gas mixture showed that 1-hexene cannot be produced independently of 1-octene using this catalyst. Isotopic labelling of an organochromium precatalyst provided a spectroscopic handle for pulse EPR, which enabled *in situ* characterization of a species derived from the catalytic mixture. These studies highlight the importance of synthesizing the necessary organometallic complexes to study complicated catalytic processes.

## References.

- (1) (a) Nicolaou, K. C.; Bulger, P. G.; Sarlah, D. *Angewandte Chemie International Edition* **2005**, *44*, 4442. (b) Magano, J.; Dunetz, J. R. *Chemical Reviews* **2011**, *111*, 2177. (c) Gattrell, M.; Gupta, N.; Co, A. *Journal of Electroanalytical Chemistry* **2006**, *594*, 1. (d) Baier, M. C.; Zuideveld, M. A.; Mecking, S. *Angewandte Chemie International Edition* **2014**, *53*, 9722.

- (2) Crabtree, R. H. *Chemical Reviews* **2015**, *115*, 127.
- (3) Chirik, P.; Morris, R. *Accounts of Chemical Research* **2015**, *48*, 2495.
- (4) Poli, R. *Chemical Reviews* **1996**, *96*, 2135.
- (5) Holland, P. L. *Accounts of Chemical Research* **2015**, *48*, 1696.
- (6) (a) Fernández, P.; Pritzkow, H.; Carbó, J. J.; Hofmann, P.; Enders, M. *Organometallics* **2007**, *26*, 4402. (b) Krzystek, J.; Kohl, G.; Hansen, H.-B.; Enders, M.; Telser, J. *Organometallics* **2019**.
- (7) Pedersen, E.; Toftlund, H. *Inorganic Chemistry* **1974**, *13*, 1603.
- (8) (a) Alonso, P. J.; Forniés, J.; García-Monforte, M. A.; Martín, A.; Menjón, B.; Rillo, C. *Chemistry – A European Journal* **2002**, *8*, 4056. (b) Bucinsky, L.; Breza, M.; Malček, M.; Powers, D. C.; Hwang, S. J.; Krzystek, J.; Nocera, D. G.; Telser, J. *Inorganic Chemistry* **2019**, *58*, 4907. (c) Telser, J.; Pardi, L. A.; Krzystek, J.; Brunel, L.-C. *Inorganic Chemistry* **1998**, *37*, 5769.
- (9) Bollmann, A.; Blann, K.; Dixon, J. T.; Hess, F. M.; Killian, E.; Maumela, H.; McGuinness, D. S.; Morgan, D. H.; Neveling, A.; Otto, S.; Overett, M.; Slawin, A. M. Z.; Wasserscheid, P.; Kuhlmann, S. *Journal of the American Chemical Society* **2004**, *126*, 14712.
- (10) Bochmann, M. *Organometallics* **2010**, *29*, 4711.
- (11) Fliedel, C.; Ghisolfi, A.; Braunstein, P. *Chemical Reviews* **2016**, *116*, 9237.
- (12) Haddow, M. F.; Jaltai, J.; Hanton, M.; Pringle, P. G.; Rush, L. E.; Sparkes, H. A.; Woodall, C. H. *Dalton Transactions* **2016**, *45*, 2294.
- (13) Lifschitz, A. M.; Hirscher, N. A.; Lee, H. B.; Buss, J. A.; Agapie, T. *Organometallics* **2017**, *36*, 1640.
- (14) (a) Ahuja, R.; Nethaji, M.; Samuelson, A. G. *Inorganica Chimica Acta* **2011**, *372*, 220. (b) Balakrishna, M. S.; Reddy, V. S.; Krishnamurthy, S. S.; Nixon, J. F.; Laurent, J. C. T. R. B.

S. *Coordination Chemistry Reviews* **1994**, *129*, 1. (c) Pal, S.; Kathewad, N.; Pant, R.; Khan, S. *Inorganic Chemistry* **2015**, *54*, 10172.

(15) Zijlstra, H. S.; Harder, S. *European Journal of Inorganic Chemistry* **2015**, *2015*, 19.

(16) Chen, E. Y.-X.; Marks, T. J. *Chemical Reviews* **2000**, *100*, 1391.

(17) (a) Zijlstra, H. S.; Linnolahti, M.; Collins, S.; McIndoe, J. S. *Organometallics* **2017**, *36*, 1803. (b) Trefz, T. K.; Henderson, M. A.; Wang, M. Y.; Collins, S.; McIndoe, J. S. *Organometallics* **2013**, *32*, 3149.

(18) Overett, M. J.; Blann, K.; Bollmann, A.; Dixon, J. T.; Haasbroek, D.; Killian, E.; Maumela, H.; McGuinness, D. S.; Morgan, D. H. *Journal of the American Chemical Society* **2005**, *127*, 10723.

(19) Agapie, T.; Labinger, J. A.; Bercaw, J. E. *Journal of the American Chemical Society* **2007**, *129*, 14281.

## Chapter 2

Stoichiometrically-Activated Catalysts for Ethylene Tetramerization using  
Diphosphinoamine-Ligated Cr Tris(hydrocarbyl) Complexes

Adapted with permission from:

*Organometallics*, **2017**, 36 (21), pp 4107-4110

Copyright 2017 American Chemical Society

**Abstract**

A new, stoichiometric, activation mode is presented for Cr-PNP (PNP = diphosphinoamine) complexes for ethylene tetramerization catalysis. To access suitable precatalysts, two robust Cr(III) multiaryl compounds were synthesized as THF adducts. These complexes are supported by a facially coordinated bis(aryl) ligand with an additional ether donor. From these precursors, Cr-PNP trishydrocarbyl complexes were synthesized. Using a single equivalent of Brønsted acid as activator, an active species for the catalytic tetramerization of ethylene was produced, without the need for excess alkyl aluminum reagents.

## Introduction

Linear  $\alpha$ -olefins (LAOs) are co-monomers in the production of linear low density polyethylene (LLDPE), and traditionally have been produced via non-selective ethylene oligomerization.<sup>1</sup> Due to the high demand for pure fractions of specific LAOs (typically 1-hexene or 1-octene), selective ethylene oligomerization catalysts have been targeted for use on an industrial scale.<sup>2</sup> For 1-octene synthesis, the best catalyst with respect to activity and selectivity is Cr-PNP (PNP = diphosphinoamine, Scheme 1).<sup>3</sup> Despite many studies investigating the role of the PNP ligand and the activator, this system still suffers from generation of significant amounts of polymer or undesired oligomers.<sup>3a,4</sup> Additionally, ill-defined activators such as modified methylaluminoxane (MMAO) are required in hundreds-fold excess relative to the Cr precatalyst. Rational improvement of catalysis has been hindered by a lack of mechanistic understanding related to the oxidation state, coordination environment, and Cr nuclearity of the active species.<sup>5</sup> Using a single well-defined activator in stoichiometric amounts is important for addressing mechanistic questions as well as for industrial applications.<sup>6</sup>

Toward developing catalysts for olefin upgrading, a variety of organochromium complexes have been studied recently.<sup>7</sup> Several Cr compounds require no exogenous activators for ethylene trimerization or non-selective oligomerization.<sup>7a,8</sup> Ethylene trimerization catalysts have also been generated from Cr-triphenyl and Cr-diaryl-halide complexes via stoichiometric treatment with acid or abstraction of halide.<sup>7j-1</sup> Herein, we describe the synthesis of a Cr-PNP precursor suitable for stoichiometric activation and demonstrate, for the first time, the generation of ethylene tetramerization catalysts upon protonation. Remarkably, these catalysts perform comparably to the MMAO system using  $\text{CrCl}_3$  precursors.

Chromium compounds featuring three alkyl or aryl ligands are typically thermally unstable,<sup>7g,i,9</sup> although some Cr-aryls are stabilized using chelating interactions.<sup>10</sup> Recently, a Cr compound featuring chelating alkyl ligands was used to generate an active tetramerization catalyst using excess aluminum activators, albeit with significantly lower activity than the chlorinated Cr precatalyst.<sup>11</sup> Separately, the protonolysis of a Cr-triaryl complex was reported, but no oligomerization activity was observed.<sup>7c</sup>

## Results and Discussion

**Synthesis of Cr(III) Tris(hydrocarbyl) Complexes Using a Tridentate Bis(aryl)ether Ligand.** Initial attempts to use  $\text{CrPh}_3(\text{THF})_3$  as precursor were not promising due to its instability;<sup>9b</sup> the generation of a five-coordinate species likely contributed to decomposition. To access a robust Cr-PNP complex, we used a chelating, tridentate bis(aryl)ether ligand. Treatment of  $\text{CrCl}_2(\text{p-tolyl})(\text{THF})_3$  or  $\text{CrCl}_2\text{Me}(\text{THF})_3$  precursors with a bis(aryl)ether organomagnesium reagent results in isolation of **1** or **2**, respectively, as red crystalline solids (see Scheme 2, and Figures 1 and 2). Single crystal X-ray diffraction (XRD) studies of **1** and **2** reveal similar geometries about Cr (see Table 1 for bond metrics). The three hydrocarbyl ligands bind to Cr facially, as in  $\text{CrPh}_3(\text{THF})_3$ .<sup>9a,9c</sup> Consequently, the bis(aryl)ether ligand also binds facially; the coordination sphere is completed by two THF ligands.

To employ compounds **1** and **2** as practical precursors for organometallic catalysis, stability is important. Complex **1** was compared to  $\text{CrPh}_3(\text{THF})_3$ .  $\text{CrPh}_3(\text{THF})_3$  completely decomposes within seconds upon dissolution in toluene or  $\text{Et}_2\text{O}$ , with formation of biphenyl as tracked by gas chromatography/mass spectrometry (GC/MS). In the presence of 100



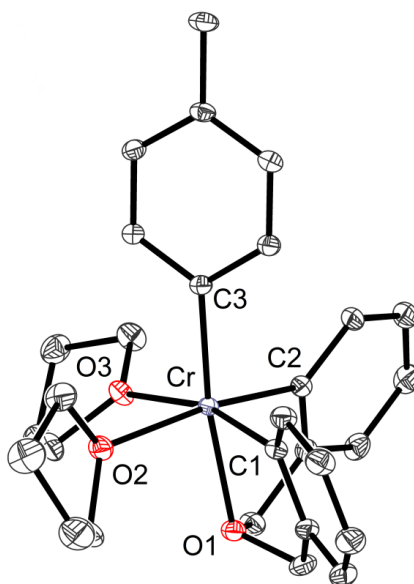


**Figure 1.** Molecular structure of **1** with thermal ellipsoids at the 50% probability level. Selected bond distances/angle shown in table 1. H atoms have been omitted for clarity. There are two molecules in the asymmetric unit, with C1 corresponding to C30, C2 to C31, and C3 to C32. For oxygen, O1 corresponds to O4, O2 to O5, and O3 to O6.

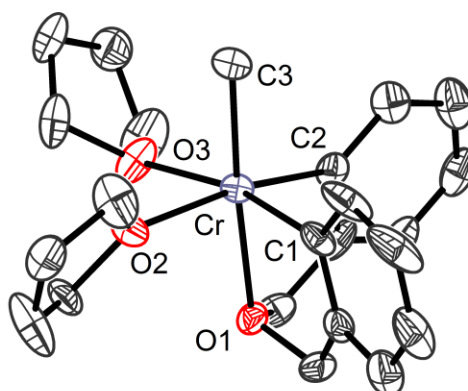


**Figure 2.** Molecular structure of **2** with thermal ellipsoids at the 50% probability level. Selected bond distances/angle shown in table 1. H atoms have been omitted for clarity. There are three molecules in the asymmetric unit, with C1 corresponding to C24 & C47, C2 to C25 & C48, and C3 to C26 & C49. For oxygen, O1 corresponds to O4 & O7, O2 to O5 & O8, and O3 to O6 & O9.

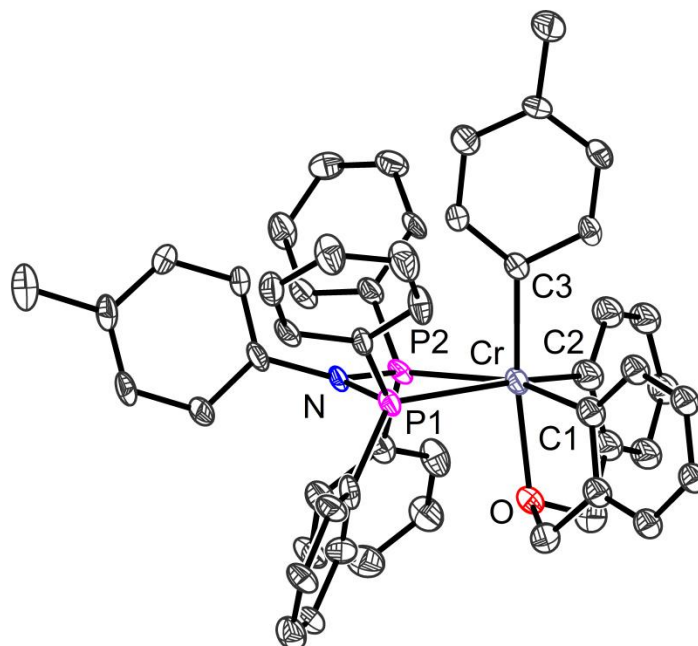


**Figure 3.** Molecular structure of **3** with thermal ellipsoids at the 50% probability level. H atoms and pentane solvent molecule have been omitted for clarity. Selected bond distances/angle shown in table 2.

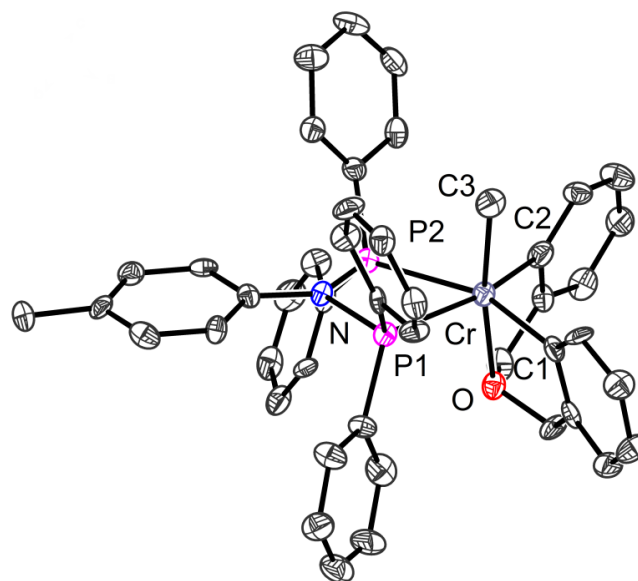


**Figure 4.** Molecular structure of **4** with thermal ellipsoids at the 50% probability level. Selected bond distances/angle shown in table 2. H atoms and toluene solvent molecules have been omitted for clarity. There are two molecules in the asymmetric unit, with C1 corresponding to C47, C2 to C48, and C3 to C49. For phosphorus, P1 corresponds to P3, and P2 to P4.

**Table 1.** Selected bond angles and distances for complexes **1** and **2**.

Bond Distance (Å) Averages <sup>a</sup>	Complex	
	1	2
Cr-C1	2.0664(11)	2.056(5)
Cr-C2	2.0637(11)	2.056(5)
Cr1-C3	2.0557(10)	2.069(5)
Cr1-O1	2.1522(8)	2.181(4)
Cr1-O2	2.1673(8)	2.158(3)
Cr1-O3	2.1794(8)	2.162(3)
<b>Bond Angles (°) Averages<sup>a</sup></b>		
C1-Cr1-C2	100.06(4)	93.9(3)

<sup>a</sup> Average metrics calculated for two (compound **1**) or three (compound **2**) molecules present in the asymmetric unit.

**Table 2.** Selected bond angles and distances for complexes **3** and **4**.

Bond Distance (Å) Averages <sup>a</sup>	Complex	
	3	4
Cr1-C1	2.087(9)	2.032(12)
Cr1-C2	2.060(9)	2.062(12)
Cr1-C3	2.069(8)	2.080(13)
Cr1-P1	2.591(2)	2.493(4)
Cr1-P2	2.538(3)	2.500(3)
Cr1-O1	2.154(6)	2.171(8)
<b>Bond Angles (°) Averages<sup>a</sup></b>		
C1-Cr1-C2	102.5(4)	105.9(5)
P1-Cr1-P2	65.22(8)	65.48(11)

<sup>a</sup> Average metrics calculated for two (compound **4**) molecules present in the asymmetric unit.

equiv. THF,  $\text{CrPh}_3(\text{THF})_3$  completely decomposes within 3 hours in toluene ( $[\text{Cr}] \approx 4 \text{ mM}$ ). Complex **1** decomposes in solution, producing 0.2 equiv. 4,4'-dimethylbiphenyl within 1 h in toluene or 5 h in  $\text{Et}_2\text{O}$  ( $[\text{Cr}] = 4 \text{ mM}$ ). No other aryl-aryl bond formation product is observed, suggesting that the reductive elimination is an intermolecular process. The partial decomposition observed over these longer periods indicate higher stability for **1** relative to  $\text{CrPh}_3(\text{THF})_3$ . In the presence of THF (100 equiv.), no decomposition of **1** was observed in toluene after 2 days. The significant stability of **1** compared to  $\text{CrPh}_3(\text{THF})_3$  is attributed to the chelating bis(aryl)ether ligand. Increased stability has been reported for bidentate aryl ligands, albeit with amine donors.<sup>10b-d</sup>

As designed, **1** or **2** display two THF ligands prone to substitution for bidentate PNP. Indeed, treatment of **1** or **2** with (*p*-tol)N( $\text{PPh}_2$ )<sub>2</sub> (<sup>tol</sup>PNP) yields **3** (47% yield) and **4** (49% yield), respectively (Scheme 2). Metallation of <sup>i</sup>PrN( $\text{PPh}_2$ )<sub>2</sub> (<sup>iPr</sup>PNP) under similar conditions has not provided the analogous complexes in practical amounts. XRD analysis (Figure 3 and 4) shows that the three hydrocarbyl ligands remain in a facial arrangement with the phosphorus atoms of <sup>tol</sup>PNP binding trans to the chelating aryl donors, in the sites previously occupied by THF ligands in **1** and **2**. Compounds **3** and **4** represent the first structurally characterized Cr(III) tris(hydrocarbyl) complexes that display an ancillary ligand established to support selective ethylene tetramerization catalysis. Notably, compounds **3** and **4** are reminiscent of multiaryl Cr-PNP precatalysts for ethylene trimerization.<sup>7j-l</sup> In those compounds, the ether moiety is linked to the PNP ligand ( $\text{PNP}^{\text{OMe}^+}$ ), limiting catalytic selectivity to trimerization. In compounds **1-4**, the stabilizing ether donor is not a part of the ancillary PNP ligand, ultimately allowing for ethylene tetramerization activity.

### **Ethylene Oligomerization Catalysis Using Cr(III) Tris(hydrocarbyl) Complexes.**

With complexes **1-4** in hand, catalytic trials were performed upon stoichiometric activation

with a Brønsted acid,  $[\text{H}(\text{Et}_2\text{O})_2][\text{BAR}'_4]$  ( $\text{Ar}' = 3,5\text{-(CF}_3)_2\text{-C}_6\text{H}_3$ ). Precursors **1** or **2** were mixed with PNP ligands to generate the Cr-PNP species in situ, while **3** and **4** were used directly. Upon addition of ethylene (100 psi) to the activated Cr species, mixtures of 1-hexene and 1-octene were produced (Table 3). Pre-ligated complexes **3** and **4** give substantially higher activity than **1** and **2** (entries 3-6, Table 3). This may be due to partial decomposition of precursors **1** and **2** or their protonation products before substitution of  $^{\text{tol}}$ PNP for THF ligands. Additionally, the presence of two THF equivalents could inhibit catalysis (*vide infra*). Catalytic activities as high as 3700 g/g Cr ( $\approx 6900$  equiv.  $\text{C}_2\text{H}_4$  consumed) were obtained using **4**, with selectivity for 1-octene as high as 44 wt%. Very small amounts of polymer were produced in the experiments using stoichiometric activation (entries 1-6, Table 3). In the trials showing higher activity, oligomers resulting from co-trimerization/-tetramerization of ethylene and 1-hexene or 1-octene ( $\text{C}_{10}\text{-C}_{14}$  branched  $\alpha$ -olefins) were produced in larger amounts.<sup>4i</sup> Most notably, the catalytic performance using **3** or **4** and 1 equiv.  $[\text{H}(\text{Et}_2\text{O})_2][\text{BAR}'_4]$  is very close to that obtained using 300 equiv. MMAO to activate a mixture of  $\text{CrCl}_3(\text{THF})_3$  and  $^{\text{tol}}$ PNP or  $^{\text{iPr}}$ PNP (Table 3, entries 5-6, 12-13). These results demonstrate for the first time that large excesses of Al activators are not required for 1-octene generation. Additionally, very low (or undetectable) levels of polymer are generated under these conditions. Both of these features are important for potential large scale practical applications.

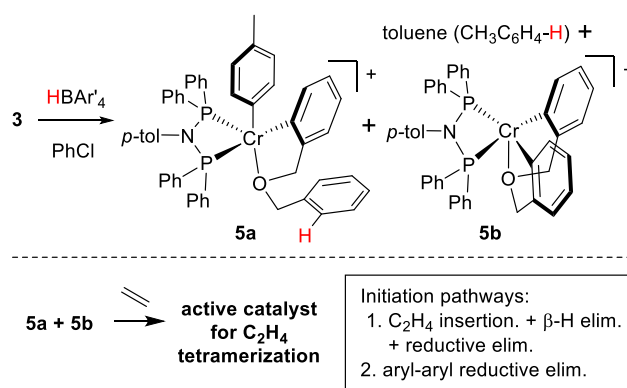
When the catalysts are prepared from **1** or **2** and PNP in situ, two equivalents of THF are present in the mixture, in contrast to activation of **3** or **4**. Catalytic trials were performed in the presence of a small amount of MMAO (5 equiv.) toward binding any THF ligands that may compete with ethylene coordination to Cr. Significantly improved oligomerization

**Table 3.** Results of catalysis using stoichiometric activation (entries 1-6), with 5 equiv. MMAO (entries 7-11), compared to activation of CrCl<sub>3</sub> precatalysts using excess MMAO (entries 12-13).

Entry	Cr. Source/ PNP	n HBAR <sup>F</sup> <sub>4</sub> / n MMAO	g/g Cr	PE <sup>a</sup>	C <sub>6</sub> <sup>a</sup>	1-C <sub>8</sub> <sup>a</sup>	C <sub>10</sub> -C <sub>14</sub> <sup>a</sup>	% 1-C <sub>6</sub> in C <sub>6</sub> <sup>a</sup>	1-octene: 1-hexene <sup>b</sup>
1	1 / <i>i</i> PtPNP	1 / 0	1600	<1%	75%	22%	3%	97%	0.23
2	2 / <i>i</i> PtPNP	1 / 0	500	0%	77%	21%	2%	97%	0.22
3	1 / <i>tol</i> PNP	1 / 0	980	0%	62%	36%	2%	87%	0.51
4	2 / <i>tol</i> PNP	1 / 0	260	0%	66%	34%	<1%	88%	0.44
5	3 / --	1 / 0	3300	<1%	46%	43%	11%	75%	0.93
6	4 / --	1 / 0	3700	<1%	43%	44%	13%	75%	1.0
7	1 / <i>i</i> PtPNP	1 / 5	4200	<1%	47%	37%	16%	92%	0.64
8	1 / <i>tol</i> PNP	1 / 5	1500	1%	46%	48%	5%	77%	1.0
9	2 / <i>tol</i> PNP	1 / 5	1900	0%	52%	43%	5%	81%	0.75
10	3 / --	1 / 5	3900	2%	42%	40%	16%	78%	0.92
11	4 / --	1 / 5	4500	1%	48%	36%	15%	81%	0.70
12	CrCl <sub>3</sub> (THF) <sub>3</sub> / <i>i</i> PtPNP	0 / 300	5200	<1%	43%	41%	16%	89%	0.80
13	CrCl <sub>3</sub> (THF) <sub>3</sub> / <i>tol</i> PNP	0 / 300	3100	<1%	40%	50%	10%	73%	1.3

Conditions: [Cr] = 1 mM, Solvent: 7.5 mL PhCl. Pressure: 100 psig C<sub>2</sub>H<sub>4</sub>. Temperature: 25°C. Reaction time: 45 min. <sup>a</sup> wt% (total) <sup>b</sup> molar ratio

**Scheme 3.** Stoichiometric activation of **3** via protonation.



activity was observed in all cases when precatalysts **1** and **2** were used (entries 1, 3-4, 7-9, Table 3). The 1-octene:1-hexene ratio increased by a factor of 2, on average, upon MMAO addition in these experiments. It is proposed that Al species in MMAO abstract THF ligands, generating a more sterically open and electronically deficient Cr center and causing an increase in activity and 1-octene selectivity. However, the possibility that the MMAO alkylates the Cr center or otherwise changes the mechanism of activation following protonation cannot be excluded. In agreement with the above proposal, addition of MMAO (5 equiv.) following protonation of **3** or **4**, which lack THF, results in smaller effects on oligomerization activity and selectivity (entries 5-6, 10-11, Table 3).

**Analysis of Aryl Residues by  $^1\text{H}$  NMR and GC/MS.** Analysis of organic byproducts of Cr-aryl precatalysts has been used to infer possible activation mechanisms.<sup>7c,7i,7l</sup> Upon protonation of **3**, 0.3 equiv. of toluene were observed by  $^1\text{H}$  NMR ( $\text{C}_6\text{D}_5\text{Cl}$ ), suggesting a ratio of 2:1 for putative cationic species **5a** and **5b** (Scheme 3). Quenching with excess  $\text{CD}_3\text{OD}$  shows dibenzylether- $\text{d}_2$  via GC/MS, indicating that the hydrocarbyl ligands remain bound to Cr. GC/MS analysis also shows the gradual formation of p-tolyl-substituted dibenzylether over 1 hour at RT, consistent with reductive elimination from **5a** to generate a Cr(I) species. The catalytic activity was found to decrease upon storing the activated mixture at room temperature in the absence of ethylene, indicating that the resulting Cr(I) species is prone to decomposition in the absence of monomer. Under normal activation conditions, the same aryl-aryl reductive elimination is also observed following catalysis (see Figure 5). Additionally, species consistent with one, two and three ethylene insertions, followed by  $\beta$ -H elimination and C-H reductive elimination are observed; their potential relevance to catalyst initiation is discussed in the next section. These products are similar to the ones observed for the stoichiometric activation of well-defined Cr-PNP<sup>(OMe)<sub>4</sub></sup> precatalysts for ethylene

trimerization.<sup>7i,7l</sup> In contrast, aryl-aryl reductive elimination was not observed in that case. This difference in initiation could be a consequence of the lower denticity of the PNP ligands selective for ethylene tetramerization.<sup>12</sup> Species corresponding to ethylene insertion followed by reductive elimination with C-C bond formation are not observed.

Notably, following catalysis using complexes **1-4**, a major set of organic species is apparent by GC/MS (**C** and **D** in Figure 5). Because of their relative prominence, it was surmised that they could have significance to the reactivity of the activated Cr species with ethylene. The presence of  $m/z = 91, 106$  mass fragments strongly suggests **C** and **D** are derived from the bis(aryl)ether. The mass analysis further suggests these are derived from insertion of *three* ethylene units into the Cr-aryl bond ( $m/z = 172, 181, 189$ ). Furthermore, a separate pair of organic residues corresponding to *four* ethylenes was observed in relative concentrations that were correlated to the 1-octene:1-hexene ratio (not shown in Figure 5). Therefore, **C** and **D** are derived from the Cr precatalyst and ethylene, and the formation of **C** and **D** is correlated to the activity and selectivity of the Cr catalyst.

Two obvious potential explanations for the formation of these species were considered. Firstly, insertion of 1-hexene (product) into an intact Cr-aryl bond would lead to one of 5 possible hexenyl-bis(aryl)ether isomers (depending on the regioselectivity of the insertion and subsequent  $\beta$ -hydride elimination). However, in a separate experiment, 1-hexene (100 equiv.) was added to an activated mixture of **1** and the reaction mixture was quenched. The GC/MS analysis showed two new species (**E** and **F**) that were confirmed to be distinct from **C** and **D** (Figure 6). Therefore, **C** and **D** are not derived from 1-hexene re-insertion into a Cr-aryl bond.

The second explanation for **C** and **D** is three consecutive insertions of ethylene into a

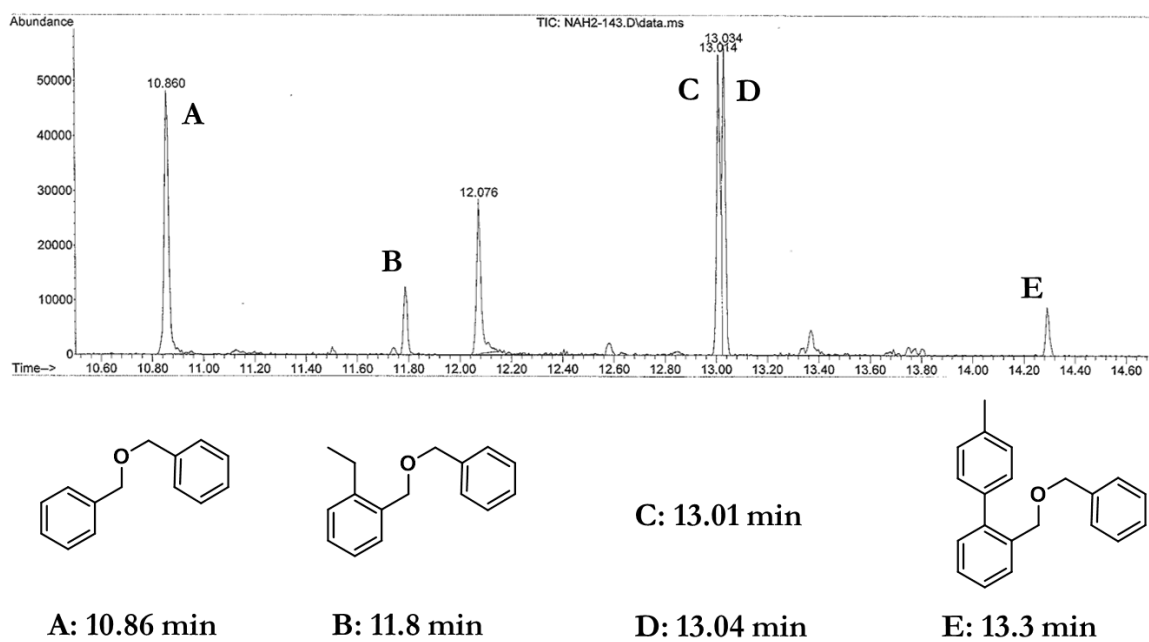


**Figure 5.** Representative GC/MS trace (retention time: 10.5 to 14.7 min) following quenching of catalytic process, and filtration of the solution.

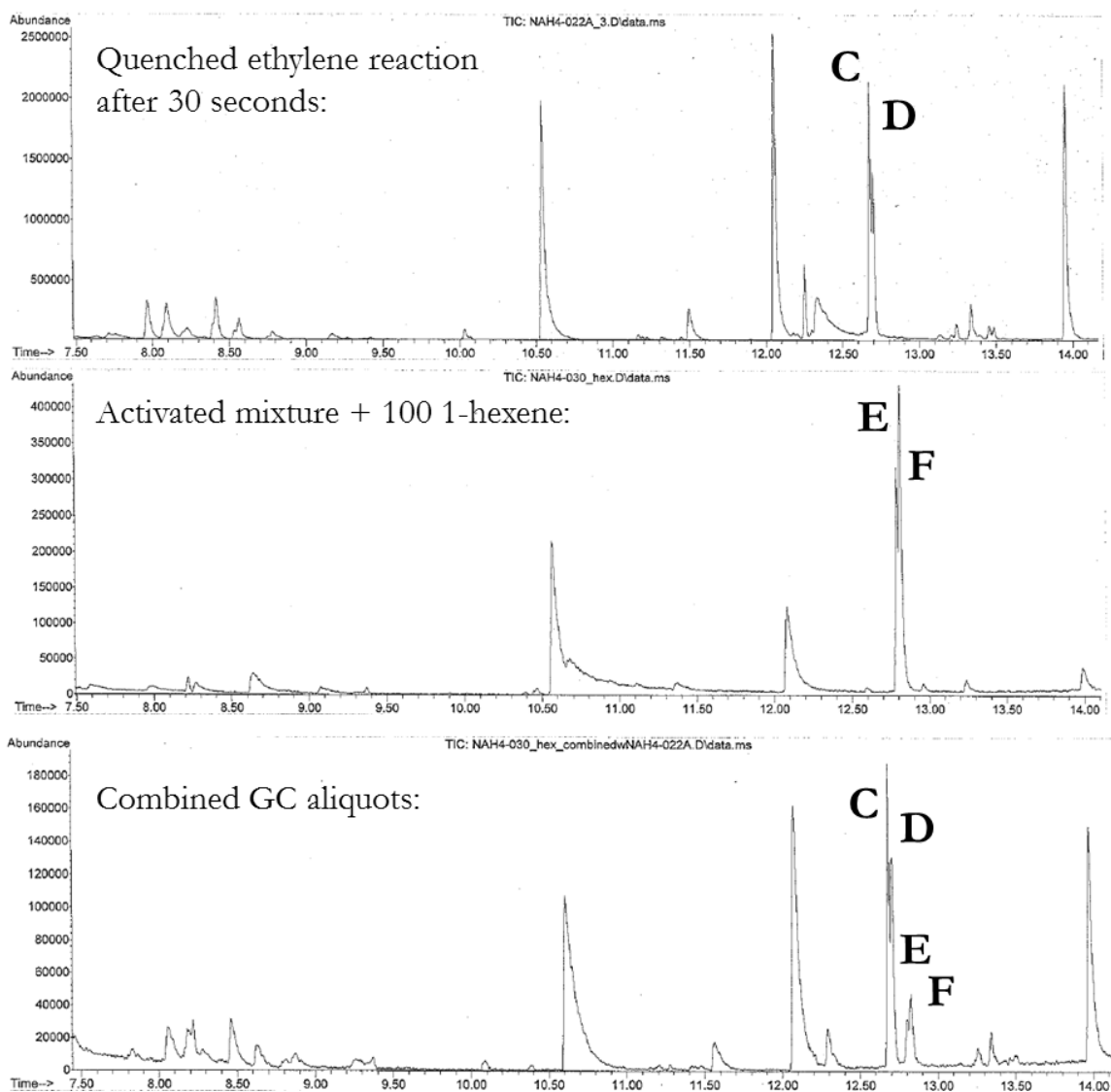
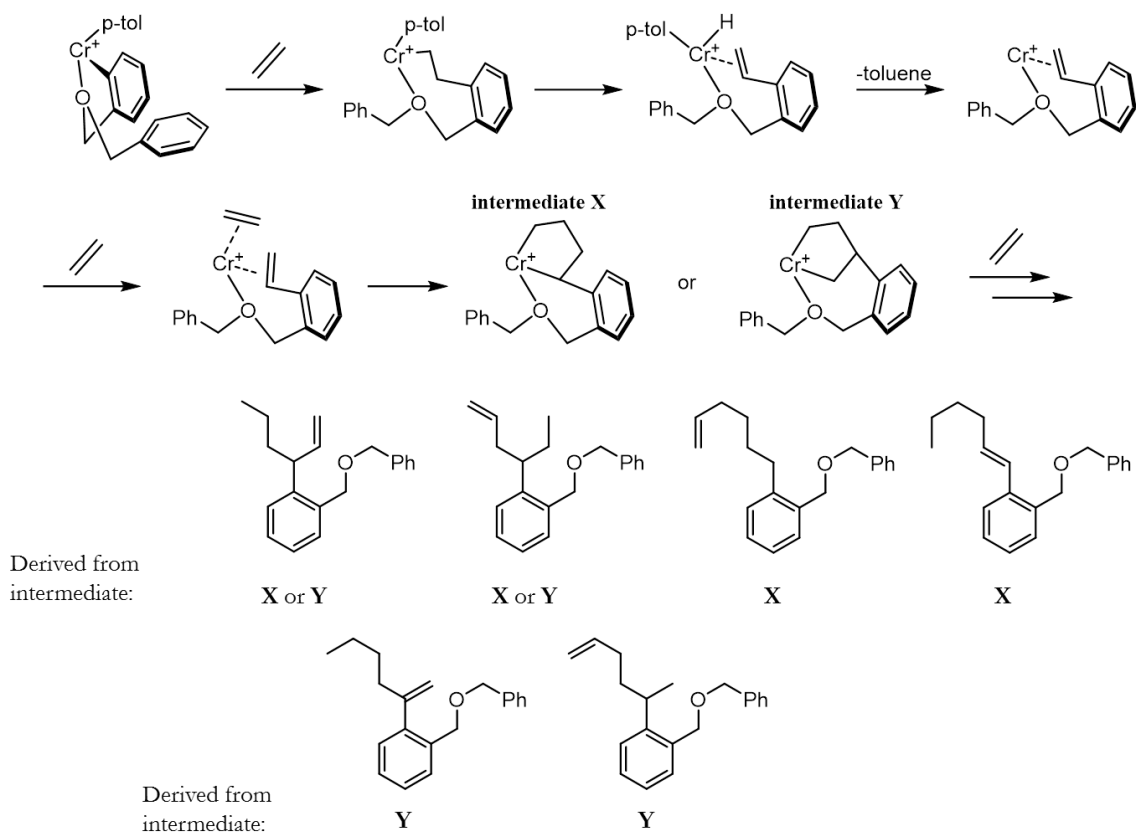


**Figure 6.** Comparison between GC/MS traces following ethylene oligomerization catalysis leading to species C and D (top), and 1-hexene addition (in the absence of ethylene) leading to E and F (middle). Both GC samples were mixed together and co-eluted to confirm the resolution of C, D, E, and F as distinct species (bottom).

**Scheme 4.** Proposed catalyst initiation pathway, leading to a Cr(I) cationic active species bound to vinyl-bis(aryl)ether. Consumption of the vinyl-bis(aryl)ether by oxidative coupling with ethylene could eventually lead to one of six different hexenyl-bis(aryl)ether isomers.



Cr-aryl bond. Or, formation of a chromacycloheptane on a species with an intact Cr-aryl bond could lead to **C** and **D** following reductive elimination. This linear hexenyl isomer was prepared independently by Pd-catalyzed cross-coupling of  $\text{BrZn}(\text{CH}_2)_4\text{CH}=\text{CH}_2$  and 1-((benzyloxy)methyl)-2-bromobenzene under Negishi conditions. Analysis of the crude reaction mixture by GC/MS showed that the linear hexenyl-bis(aryl)ether had a distinct retention time (13.2 min), ruling out this particular isomer as the identity of **C** and **D**.

From the above experiments, it was inferred that **C** and **D** are *branched* hexenyl-bis(aryl)ether isomers based on the similar retention times and mass spectral patterns as **E** and **F**. A remaining mechanistic possibility is that a vinyl-bis(aryl)ether residue undergoes oxidative coupling with ethylene, followed by a subsequent ethylene insertion (Scheme 4). This would correspond to the first turnover of the Cr catalyst, where vinyl-bis(aryl)ether is an available olefin substrate. Depending on the regioselectivity of these couplings and insertions, up to six different isomers are possible (see Scheme 4). Due to the possibilities, positive identification of the exact structure by independent synthesis was not pursued further. However, the implication of this proposal is that the catalytically active species has a vinyl-bis(aryl)ether bound to Cr following initiation. This strongly suggests that the active species is Cr(I) derived from the initiation pathway shown in Scheme 4. Of course, the same hypothesis was based on earlier reports where vinylarenes were prominent organic residues. In contrast to those examples (from Cr-phenyl or Cr-biphenyldiyl intermediates) the Cr aryl species here have a coordinating ether built into the aryl ligand, which probably prevents the dissociation of the resulting Cr-vinyl species. Therefore, the vinyl-bis(aryl)ether could preferentially undergo oxidative coupling rather than displacement by ethylene.

**Complexes That Highlight a Diversity of Bis(aryl)ether Binding Modes.** Key to the isolation and clean reactivity of complexes **1-4** is the complete removal of chloride

ligands from  $\text{CrCl}_3(\text{THF})_3$  and subsequent reactive intermediates. Furthermore, **1** and **2** are not indefinitely stable in non-THF solvents, presumably decomposition occurs following the loss of THF, in analogy to  $\text{CrPh}_3(\text{THF})_3$ . Crystals of  $\text{CrCl}((o\text{-C}_6\text{H}_4\text{CH}_2)_2\text{O})(\text{THF})_2$  (**6**·**THF**) could be obtained, as well as the related dimer (based on loss of THF):  $[\text{CrCl}((o\text{-C}_6\text{H}_4\text{CH}_2)_2\text{O})(\text{THF})]_2$  (**[6]**<sub>2</sub>) which happened to co-crystallize with the monomer. Ultimately, based on the similar solubility of these complexes, they were not isolated independently.

Crystals of a decomposition product derived from the synthesis of **1** were obtained. This revealed a dimeric Cr(II)-Cr(II) structure (**7**) where the bis(aryl)ether ligands bridge the Cr centers. This structure is a coordination polymer since the ethereal ligand is the ditopic 1,4-dioxane (used in the synthesis to precipitate Mg-halide salts). Decomposition of Cr(III) hydrocarbyl species to Cr(II) dinuclear species is well-precedented.<sup>13</sup> It is proposed that a similar species is the product of decomposition of clean **1** or **2** (where the ethereal ligand is THF rather than 1,4-dioxane), although this has not been definitively established by spectroscopic or crystallographic evidence.

Concerns about the stability of **1** and **2** due to this possible decomposition mode led to the exploration of more strongly-binding neutral donors. In particular, the dimethoxyethane (**8**) and bis(pyridine) (**9**) analogs were isolated and structures determined by X-ray diffraction. The bis(pyridine) complex (**9**) was surprisingly found to exhibit the bis(aryl)ether ligand in a tridentate, yet meridional coordination geometry. This was our first observation of such behavior, yet substitution of the THF ligands on **1** for  $\text{Ph}_2\text{PMe}$  also allowed for the crystallographic characterization of another six-coordinate Cr(III) species with the meridional bis(aryl)ether:  $\text{Cr}((o\text{-C}_6\text{H}_4\text{CH}_2)_2\text{O})(p\text{-tol})(\text{Ph}_2\text{PMe})_2$  (**10**). These structures can be

**Scheme 5.** Attempted synthesis of mono-chloride bis(aryl)ether leads to mixture of monomeric and dimeric forms (isolated as individual crystals or cocrystals).

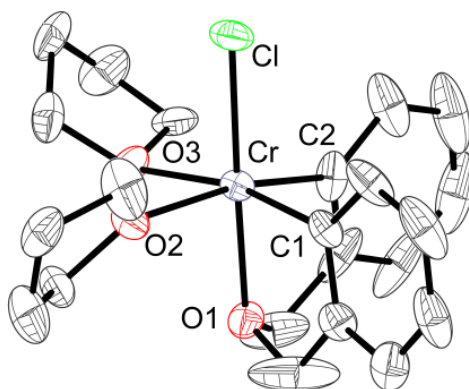
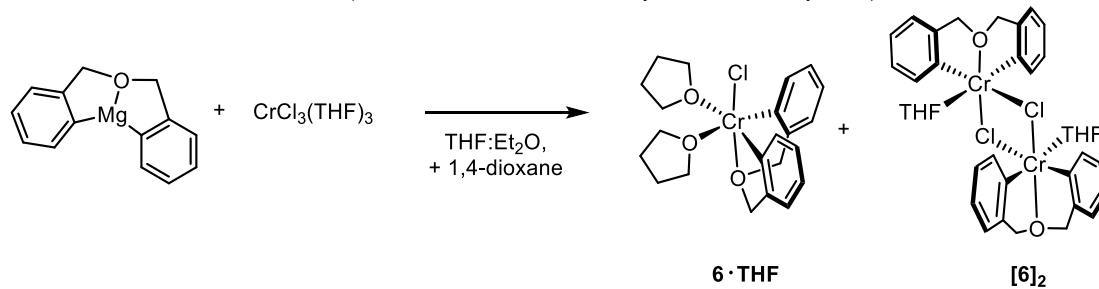


**Figure 7.** Structure of monomeric,  $\text{CrCl}((o\text{-C}_6\text{H}_4\text{CH}_2)_2\text{O})(\text{THF})_2$  ( $6 \cdot \text{THF}$ ) determined via single-crystal XRD. H-atoms are not shown (for clarity). Thermal ellipsoids are displayed at the 50% probability level.

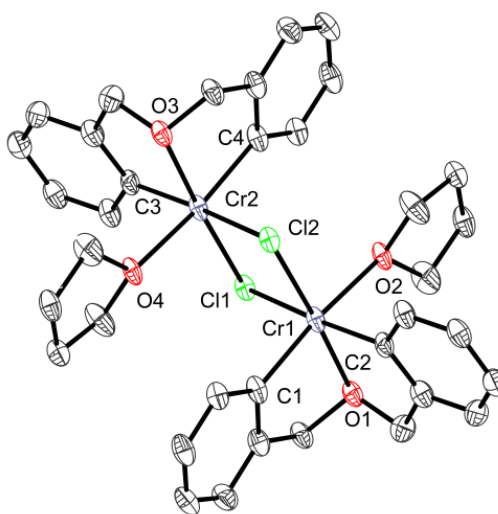


**Figure 8.** Structure of dimeric,  $[\text{CrCl}((o\text{-C}_6\text{H}_4\text{CH}_2)_2\text{O})(\text{THF})]_2$  ( $[6]_2$ ), determined via single-crystal XRD. Also present in the asymmetric unit is an equivalent of  $6 \cdot \text{THF}$  and a disordered molecule of THF. H-atoms are not shown (for clarity). Thermal ellipsoids are displayed at the 50% probability level.

**Scheme 6.** Top: side-product from synthesis of **1** is revealed to be Cr-Cr dinuclear species that exists as a coordination polymer due to 1,4-dioxane. Bottom: proposed bimolecular decomposition of **1** in the absence of THF, to generate similar complex as **7**.

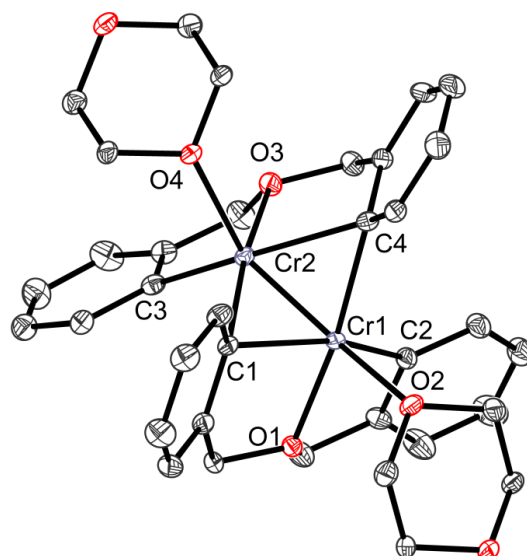
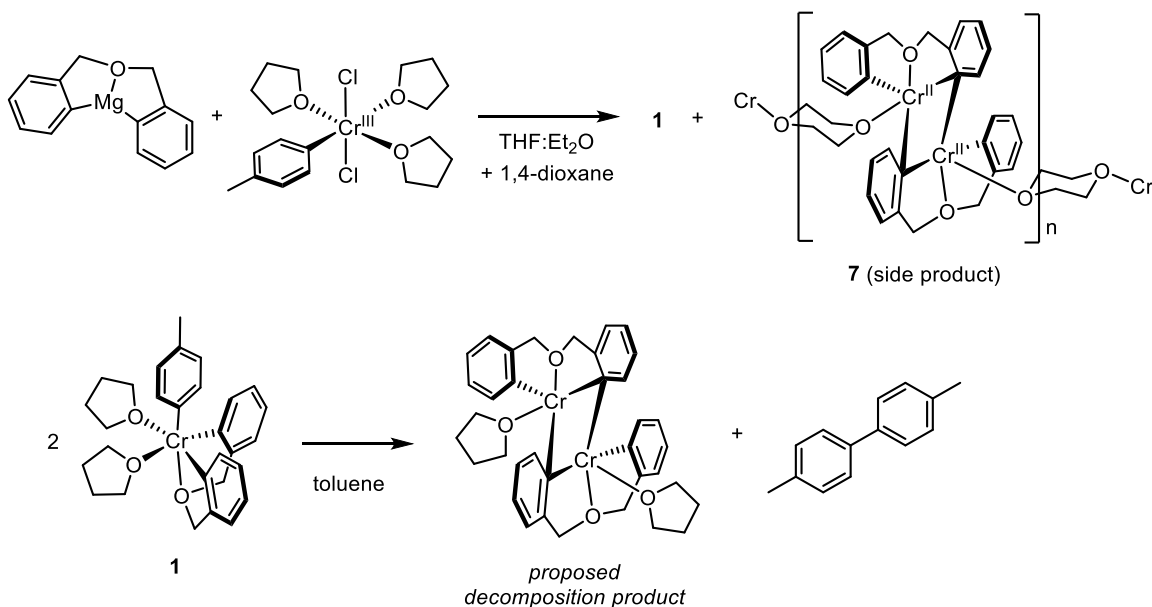


**Figure 9.** Structure of the dinuclear unit  $\text{Cr}((o\text{-C}_6\text{H}_4\text{CH}_2)_2\text{O})(1,4\text{-dioxane})$  (**7**). The asymmetric unit only includes one 1,4-dioxane ligand, but the Cr coordination spheres are shown completed, and H-atoms are not shown for clarity. Thermal ellipsoids are displayed at the 50% probability level.

**Scheme 7.** Reactions of **1** with strongly donating ligands leads to substitution of THF for either dimethoxyethane (**8**), pyridine (**9**), or  $\text{Ph}_2\text{PMe}$  (**10**).

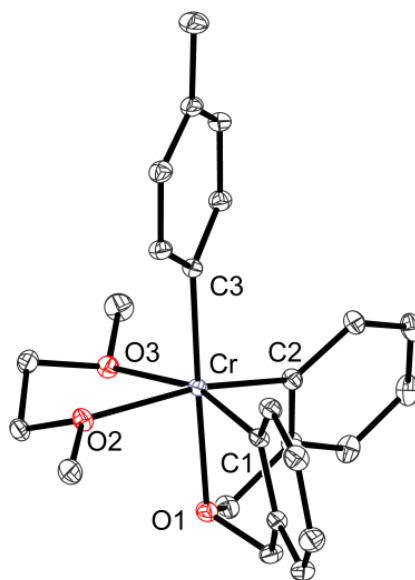
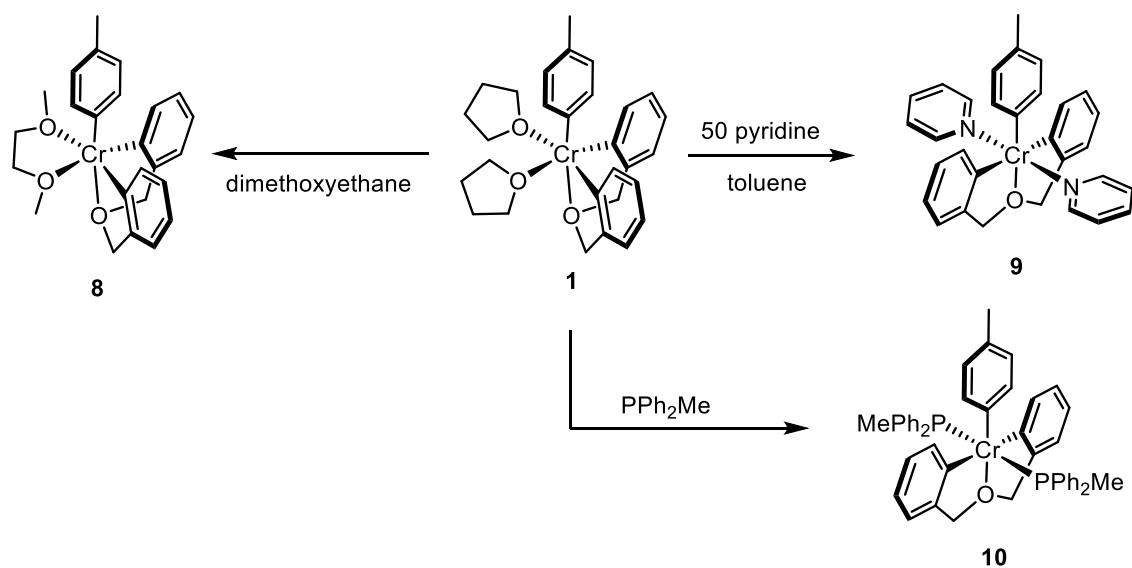


**Figure 10.** Structure of  $\text{Cr}((o\text{-C}_6\text{H}_4\text{CH}_2)_2\text{O})(p\text{-tol})(\text{dimethoxyethane})$  (**8**), determined via single-crystal XRD. H-atoms are not shown for clarity and thermal ellipsoids are displayed at the 50% probability level.

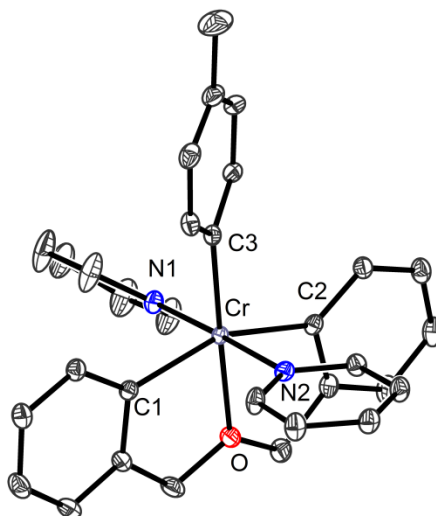


**Figure 11.** Structure of  $\text{Cr}((o\text{-C}_6\text{H}_4\text{CH}_2)_2\text{O})(p\text{-tol})(\text{pyridine})_2$  (**9**), determined via single-crystal XRD. H-atoms and toluene solvent molecule are not shown for clarity and thermal ellipsoids are displayed at the 50% probability level.

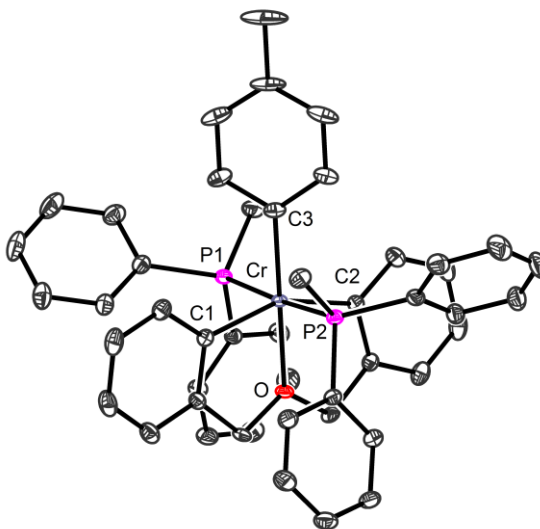


**Figure 12.** Structure of  $\text{Cr}((o\text{-C}_6\text{H}_4\text{CH}_2)_2\text{O})(p\text{-tol})(\text{Ph}_2\text{PMe})_2$  (**10**), determined via single-crystal XRD. H-atoms and toluene solvent molecule are not shown for clarity and thermal ellipsoids are displayed at the 50% probability level.

rationalized due to the relative trans-influence of Ph<sub>2</sub>PMe and pyridine compared to THF. This suggests that the meridional coordination geometry of the bis(aryl)ether is actually less-strained than the facial geometry. Steric reasons probably contribute to the trans-disposition of the phosphine ligands in **10**, but the pyridine ligands of **9** should not be sterically prevented from binding in a cis-fashion.

Analysis of the decomposition of toluene solutions of **1** showed 4,4-dimethylbiphenyl (*vide supra*) over time and cw X-band EPR spectroscopy showed the appearance of an axial signal at  $g \approx 2$ , or 3400 Gauss (Figure 13). Since Cr(II)-Cr(II) dimers (or intermediate Cr(III)-Cr(III)) dimers would have integer spin, it is difficult to assign this signal to such species without more detailed knowledge of the electronic structure. The possibility of a low-spin ( $S = 1/2$ ) Cr(III) intermediate has been considered, but such spin state is unlikely given the ligands present on Cr.<sup>14</sup> There are many examples of five-coordinate quartet spin Cr(III) species.<sup>7h,15</sup> The axial  $g \approx 2$  signal was reproduced by abstraction of pyridine from **9** using B(C<sub>6</sub>F<sub>5</sub>)<sub>3</sub> (Figure 14). Without adding B(C<sub>6</sub>F<sub>5</sub>)<sub>3</sub>, this signal is not seen in the toluene solution of **9**. Ultimately, the  $g \approx 2$  signal was correlated to ligand dissociation from Cr(III) and possible dimer formation, yet not conclusively to any structure, so it has been simply regarded as evidence of Cr(III) decomposition.

**Synthesis of a Symmetrical Cr(III) Tris(aryl) Precatalyst.** Elucidation of the reactivity of the Cr activated species mentioned above was complicated by the fact that protonation of complexes **1-4** was nonselective. That is, two possible cationic species resulted since either the tolyl (or methyl) or bis(aryl)ether ligand could be protonated. Nonetheless, such reactions were characterized in detail by EPR spectroscopy (see Chapter 5). To achieve a more tractable activation process, a completely symmetric chelating tris(aryl) ligand was envisioned. Two desired species are shown in Figure 15. In analogy to the

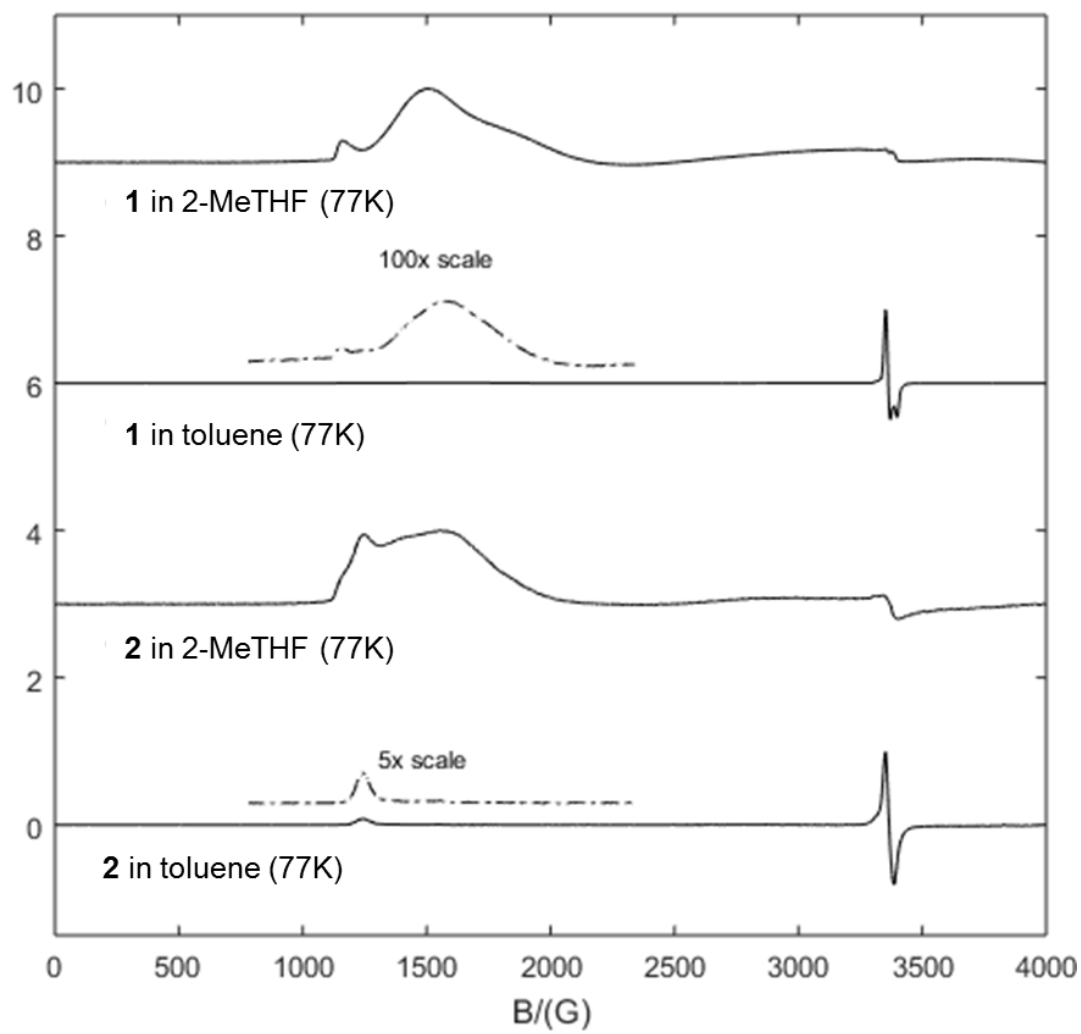


**Figure 13.** Comparison of EPR spectra of **1** and **2** in 2-MeTHF vs. toluene, where a signal at  $g \approx 2$  (or  $B \approx 3400$  Gauss) shows up in the non-coordinating solvent.

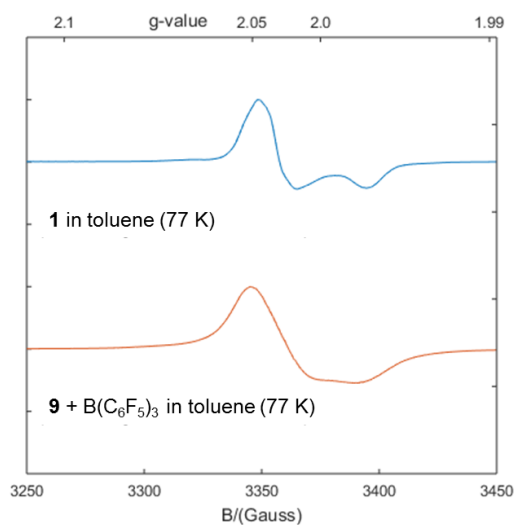


**Figure 14.** Comparison of  $g \approx 2$  region of **1** in toluene with the reaction mixture of **9** +  $B(C_6F_5)_3$ , where a similar signal appears, presumably due to abstraction of pyridine from **9**.

syntheses of **3** and **4**, THF-bound precursors were targeted as intermediates.

In the case of the trisaryl(amine) version, several reactions of the corresponding Grignard reagent were attempted with  $CrCl_3(THF)_3$ . The reactions were not tractable; the only isolated crystals whose structure was determined were those of a Cr(IV) trigonal bipyramidal complex presumably derived from disproportionation of Cr(III) intermediates.<sup>7b,16</sup> The presence of an outer sphere cation ( $Li^+$ ) cannot be excluded due to the poor data quality; in that case, the oxidation state assignment of **11** would be Cr(III). It is possible that the strong trans influence of the aryl ligands disfavors the six-coordinate geometry expected of the Cr(III) precursor. The aryl ligands cannot be co-facial like they are in complexes **1** and **3**. However, we have observed two cases where aryl ligands coordinate to Cr in a trans-fashion (**9** and **10**). The more likely explanation for the suspected instability of the desired six-coordinate Cr product is that the preferred pyramidal (or tetrahedral)

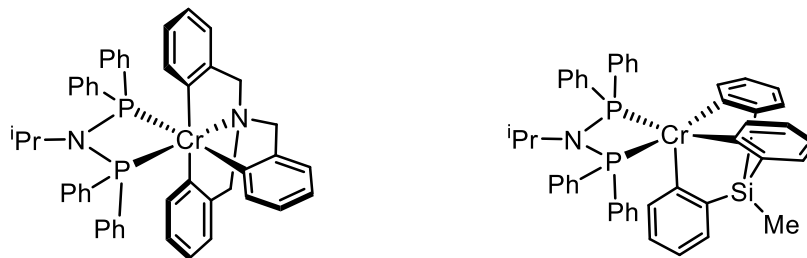


**Figure 15.** Targeted symmetrical PNP-Cr(III) tris(aryl) species, utilizing amine- or silane-based tethers.

**Scheme 8.** A Cr(IV) species (**11**) was isolated from the attempted synthesis of a Cr(III) bis-THF complex.

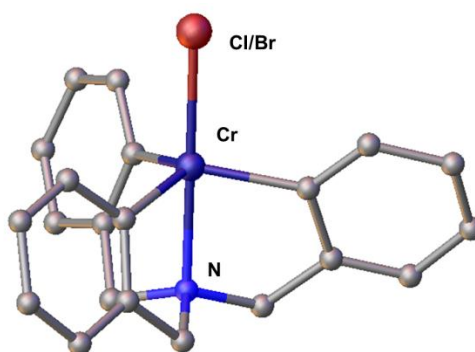
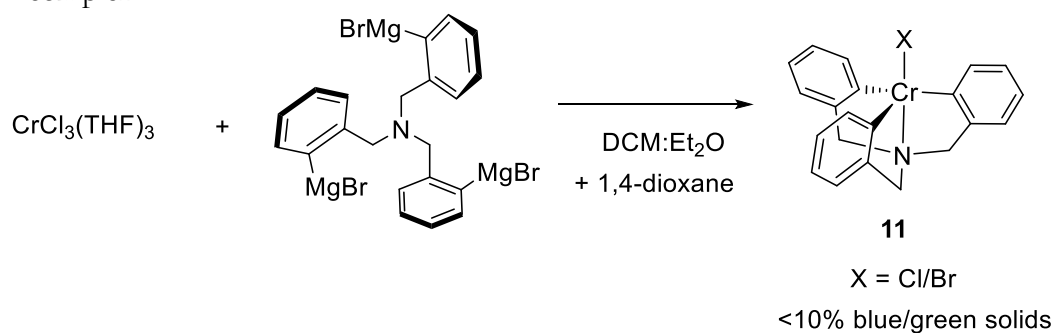


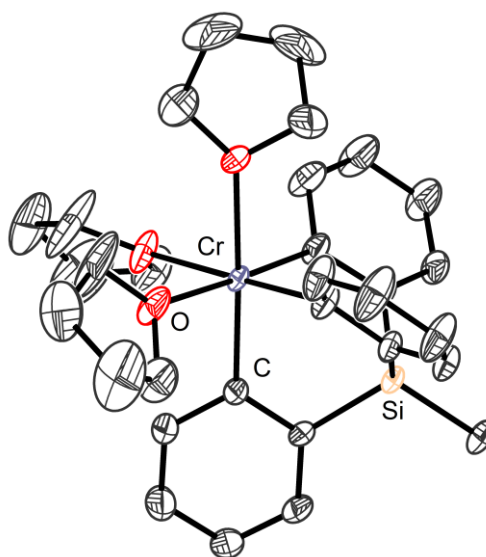
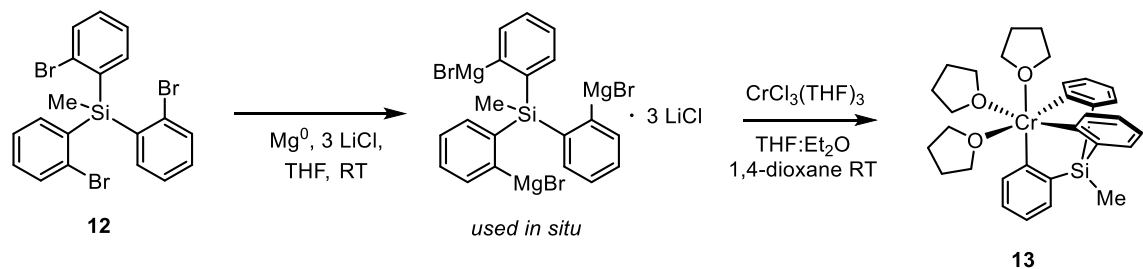
**Figure 16.** Solid-state structure of **11** determined from single-crystal XRD. The crystals did not yield a high-quality data set, so thermal ellipsoids are not represented. H-atoms are omitted for clarity. The halogen (orange) atom is modeled as a mixture of Cl/Br.

geometry about the amine nitrogen is not possible.

The second targeted complex incorporated a symmetric tris(aryl) ligand based on a silyl-backbone. This design was attractive since no neutral donor atoms are involved, the tris(aryl) motif would be stabilized by the triptycene-like chelating geometry. To our knowledge, there are no triptycene derivatives with transition metals at the vertices. We successfully employed the synthetic strategy shown in Scheme 9 to form the appropriate tris-Grignard reagent in situ, followed by reaction with  $\text{CrCl}_3(\text{THF})_3$  to form  $\text{Cr}((o\text{-C}_6\text{H}_4)_3\text{SiMe})(\text{THF})_3$  (**13**). Several challenges in this route were apparent. Firstly, the synthesis of the tribromide **12** was low-yielding due the use of thermally-sensitive *ortho*-bromophenyllithium and the relatively sterically encumbered silyl chloride intermediates. Secondly, the activation of **12** to form the tris-Grignard could not be achieved without LiCl additive, as has been noted for other aryl bromides.<sup>17</sup> Unfortunately, the remaining LiCl is difficult to remove completely from the mixtures containing **13**. This has been exemplified by examples of LiCl cocrystallizing with an analogous complex to **13** (shown in Appendix 4, Figure 7). Small amounts of LiCl-free **13** that were obtained could be used for reactions with <sup>i</sup>PrPNP, from which green crystals of the desired product, **14**, could be grown. This is a rare example of a structurally-characterized Cr tris(hydrocarbyl) species with the bidentate PNP-ligand bound. A comparison of bond metrics between **14**, **3** and **4**, as well as **15**, the <sup>i</sup>PrPNP analog of **3** (bulk isolation of **15** was not achieved) is discussed in the next section.

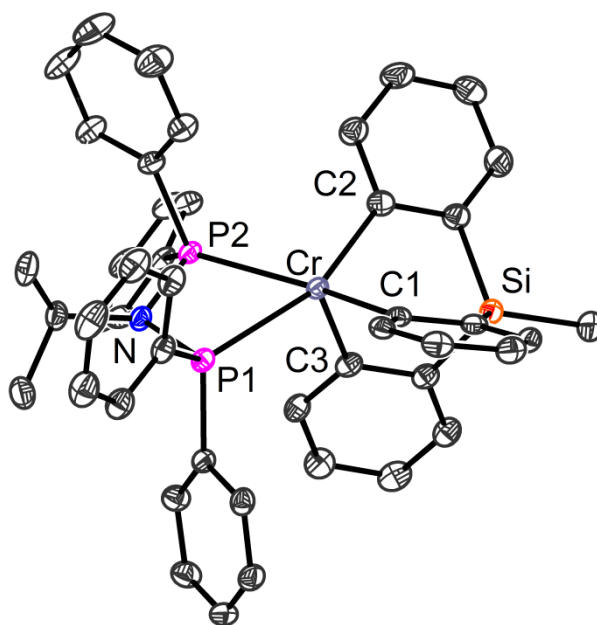
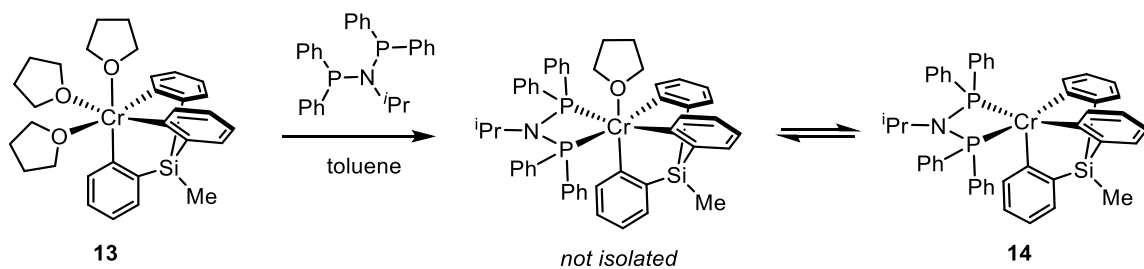
Ultimately, the following issues with the synthesis of **14** precluded isolation in significant amounts. It is suspected that traces of THF lead to a six-coordinate coproduct (brown in color). Also, **14** seemed to be light-sensitive and/or thermally sensitive since aryl-aryl

**Scheme 9.** Synthetic scheme for complex **13**, by reaction of tris-Grignard derived from tribromide **12**, with  $\text{CrCl}_3(\text{THF})_3$ .



**Figure 17.** Structure of  $\text{Cr}((o\text{-C}_6\text{H}_4)_3\text{SiMe})(\text{THF})_3$  (**13**), determined via single-crystal XRD. The asymmetric unit lies on a 3-fold axis of symmetry that contains the Cr-Si vector. H-atoms omitted for clarity and thermal ellipsoids are displayed at the 50% probability level.

**Scheme 10.** Reaction of **13** with  $i^{\text{Pr}}$ PNP leads to five-coordinate **14**, which is suspected to be formed along with six-coordinate THF-bound species.

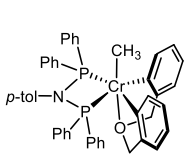
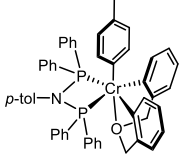
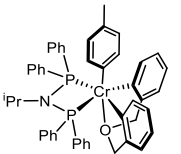
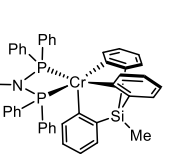
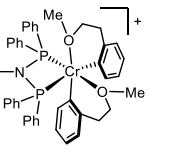


**Figure 18.** Structure of  $(i^{\text{Pr}}\text{PNP})\text{Cr}((o\text{-C}_6\text{H}_4)_3\text{SiMe})$  (**14**), determined via single-crystal XRD. H-atoms and toluene solvent omitted for clarity and thermal ellipsoids are displayed at the 50% probability level.

reductive elimination would occur in solution over time; the organic residue with  $m/z = 272$  was resolved by GC/MS. These issues precluded a focus of study on **13** and **14**, but **13** was tested for ethylene oligomerization activity using  $^{iPr}$ PNP as the ligand and  $HBAr'_4$  as the activator, in conditions analogous to those for complexes **1-4** (Table 3). The productivity was 500 g/g Cr, and 1-octene selectivity was 15% (1-hexene selectivity was 74%). This was close to the selectivity values for precursors **1** and **2** given in Table 3, where THF equivalents are suspected to affect the selectivity (*vide supra*). Analysis of the aryl residues by GC/MS following catalysis showed vinyl- ( $m/z = 300$ ) and butenyl- ( $m/z = 328$ ) triarylsilanes as the major byproducts. This is consistent with the ethylene insertion initiation pathway discussed above; notably, this scenario does not involve built-in ethereal oxygen donors that would prohibit substitution of the alkene derived from the triarylsilane by ethylene. Therefore, no branched hexenyl product is seen from this precatalyst. The C-C coupled reductive elimination product ( $m/z = 272$ ) was seen in minor amounts. Therefore, Cr(I) could also form by a reductive elimination process.

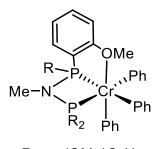
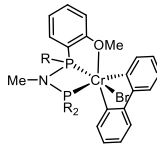
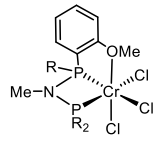
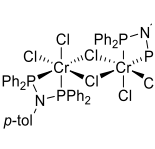
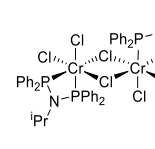
**Structural Comparison of PNP-Cr Multiaryl Complexes.** Structurally-characterized Cr-hydrocarbyl species ligated by PNP ligands are quite rare, so a close analysis of their bond metrics is undertaken here. Of particular interest is complex **15**, which is analogous to compound **3**, with  $^{iPr}$ PNP bound instead of  $^{tol}$ PNP. It was not isolated in bulk amounts, likely due to the propensity of  $^{iPr}$ PNP to dissociate. However, the XRD data provides a direct comparison of the two PNP ligand types (Table 4). The average Cr-P bond distance for the neutral,  $^{iPr}$ PNP complexes is 2.6074 Å (from complexes **14** and **15**). The corresponding average value for  $^{tol}$ PNP (from complexes **3** and **4**) is 2.5305 Å, a difference of 0.077 Å. This suggests, on average, tighter binding of  $^{tol}$ PNP than  $^{iPr}$ PNP, in agreement with the anecdotal experimental evidence. It is interesting that the average Cr-P distance in

Table 4.

					
Bond Lengths (Å)	<b>4<sup>a</sup></b>	<b>3</b>	<b>15</b>	<b>14</b>	from chap. 4
Cr-P1:	2.493(4)	2.591(2)	2.6437(9)	2.6354(7)	2.5088(4)
Cr-P2:	2.500(3)	2.538(3)	2.6027(9)	2.5476(6)	2.7501(5)
Cr-O1:	2.171(8)	2.154(6)	2.176(2)	--	2.181(1)
Cr-O2:	--	--	--	--	2.108(1)
Cr-C1:	2.032(12)	2.087(9)	2.050(3)	2.068(2)	2.056(2)
Cr-C2:	2.062(12)	2.060(9)	2.087(3)	2.082(2)	2.072(2)
Cr-C3:	2.080(13)	2.069(8)	2.062(3)	2.041(1)	--
Bond Angles (°)					
P1-Cr-P2	65.48(11)	65.22(8)	62.82(3)	63.84(2)	62.62(1)
C1-Cr-C2	105.9(5)	102.5(4)	90.3(1)	94.07(9)	98.65(6)
C1-Cr-C3	96.1(5)	97.0(3)	96.4(1)	95.34(8)	--
C2-Cr-C3	96.2(5)	95.6(3)	97.9(1)	93.89(9)	--

<sup>a</sup>Metrics derived by averaging values from both molecules in asymmetric unit.

Table 5.

Bond Lengths (Å)					
	from <sup>a,b</sup> ref. 7k	from <sup>b</sup> ref. 7k	from <sup>b</sup> ref. 7k	from <sup>b</sup> ref. 4k	from <sup>a,b</sup> ref. 4k
Cr-P1:	2.638(1)	2.6608(8)	2.3855(7)	2.4947(4)	2.5052(5)
Cr-P2:	2.497(1)	2.4261(8)	2.5098(7)	2.4074(4)	2.4410(5)
Cr-O1:	2.286(3)	—	2.156(2)	—	—
Cr-O2:	—	—	—	—	—
Cr-C1:	2.097(4) <sup>c</sup>	2.058(3)	—	—	—
Cr-C2:	2.078(4) <sup>c</sup>	2.035(3)	—	—	—
Cr-C3:	2.051(4) <sup>c</sup>	—	—	—	—
Bond Angles (°)					
P1-Cr-P2	64.02(4)	64.89(2)	66.56(2)	66.62(1)	66.47(2)
C1-Cr-C2	98.67(2)	81.95(1)	—	—	—
C1-Cr-C3	96.99(1)	—	—	—	—
C2-Cr-C3	93.46(1)	—	—	—	—

<sup>a</sup>Metrics derived by averaging values from both molecules in asymmetric unit. <sup>b</sup>Atoms are renumbered from published versions. <sup>c</sup>C1 is *trans* to P2, C2 is *trans* to P1, and C3 is *trans* to O.

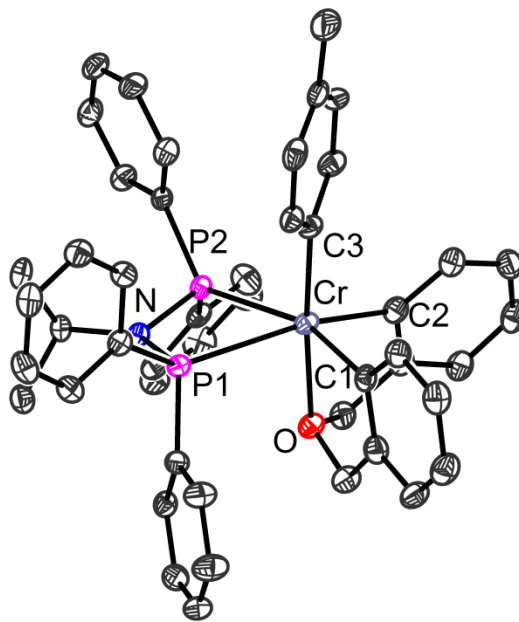


**Figure 19.** Molecular structure of  $(iPrPNP)Cr((o-C_6H_4CH_2)_2O)(p-tol)$  (**15**) with thermal ellipsoids at the 50% probability level. H-atoms and toluene solvent are omitted for clarity.

the cationic species (discussed in Chapter 4) is 2.6295 Å, which is slightly longer than in neutral **15**. However, the steric environments are not identical, so the influence of the Cr charge (cationic vs. neutral) on the Cr-P distance is not clear. The P-Cr-P bond angles are less than 66° in all cases, highlighting the poor overlap of the diphosphines with the Cr d-orbitals. These metrics are similar to those in the Cr complexes of the tridentate PNP ligands (with an additional ether-donor) from Bercaw et. al., as well as CrCl<sub>3</sub> examples (Table 5).

## Conclusion

In summary, the first example of Cr catalysis for ethylene tetramerization upon stoichiometric activation was demonstrated. Access to appropriate Cr-tris(hydrocarbyl) precursors is instrumental for activation via protonation. The use of chelating bis(aryl)ether ligands affords organometallic Cr precursors that are suitably robust. The multidentate ligand was designed to leave two metal coordination sites available for bidentate PNP binding. Substitution of THF ligands for PNP affords complexes that are six-coordinate. Treatment with [H(Et<sub>2</sub>O)<sub>2</sub>][BAr'<sub>4</sub>] leads to aryl or methyl ligand protonolysis. Subsequent addition of ethylene results in the catalytic formation of 1-octene and 1-hexene with high activities and low polymer production. Under the conditions investigated, activity and selectivity were comparable to those observed using CrCl<sub>3</sub> precatalysts with large excesses of MMAO. These catalyst features are important for industrial applications.

Further investigations yielded information about the diverse coordination chemistry of the bis(aryl) ether ligand, either as a bridge between two Cr(II) centers, or as a meridional ligand. An alternative strategy to stabilizing a Cr tris(aryl) complex used a tris(aryl)silane ligand. Ultimately, syntheses of new organochromium complexes in the +3 oxidation state must account for possible reductive or bimolecular decomposition, as well as dimerization of

intermediate halide species. The complexes reported in this chapter proved useful for more detailed mechanistic (Chapter 3) and spectroscopic (Chapter 5) studies.

## Experimental

**General Considerations.** All synthetic procedures containing chromium were performed in a nitrogen-atmosphere glove box or in sealed containers under a stream of nitrogen gas. All glassware was oven-dried and kept under active vacuum prior to use. Diethyl ether, tetrahydrofuran (THF), toluene, and pentane solvents were purified by sparging with nitrogen and then passing through a column of activated A2 alumina into sealed containers, degassed under active vacuum and stored over activated molecular sieves prior to use.  $C_6D_6$  (Cambridge Isotope Laboratories) and 1,4-dioxane were dried over Na/benzophenone, vacuum distilled, and kept over activated molecular sieves prior to use. Chlorobenzene was distilled from  $CaH_2$ , stored over activated molecular sieves for at least 24 hours, and filtered through activated alumina directly before use. Chlorobenzene- $d_5$  (from Acros Organics) was degassed using three freeze-pump-thaw cycles and stored over molecular sieves prior to use. M-MAO 3A was purchased from AkzoNobel as a 7% w/w Al solution in heptane. Ethylene gas was purchased at polymer purity (99.9%) from Matheson, and was dried by passage through two 1L Swagelok steel columns packed with 3Å activated molecular sieves and Mn(II) oxide on vermiculite.<sup>18</sup>  $CrCl_3(THF)_3$  was synthesized according to the literature procedure, using  $CrCl_3$  (anhydrous) purchased from Strem.<sup>19</sup> The synthesis of  $^{iPr}PNP$ ,  $^{tol}PNP$ , and  $[H(Et_2O)_2][BAR'_4]$  have been previously reported.<sup>20</sup>  $CrPh_3(THF)_3$  and bis(2-bromobenzyl)ether were synthesized according to the reported literature procedures.<sup>9b,21</sup>  $Cr(p-tol)Cl_2(THF)_3$  was synthesized according to the literature procedure,<sup>22</sup> and  $Cr(Me)Cl_2(THF)_3$  was synthesized according to a modification of this procedure using

MeMgBr. NMR spectra were recorded on a Varian 300 MHz or 400 MHz Spectrometer. Gas chromatography (GC) was performed on an Agilent 6890A instrument using a DB-1 capillary column (10 m length, 0.10 mm diameter, 0.40  $\mu\text{m}$  film) and a flame ionization detector. Gas chromatography/mass spectrometry (GC-MS) was performed on an Agilent 6890A instrument using a HP-5MS column (30 m length, 0.25 mm diameter, 0.50  $\mu\text{m}$  film) and an Agilent 5973N mass-selective EI detector.

**Preparation of  $\text{Mg}(\textit{o}\text{-C}_6\text{H}_4\text{CH}_2)_2\text{O}$ .** A solution of bis(2-bromobenzyl)ether was prepared in  $\text{Et}_2\text{O}$  (0.02 to 0.05 M). This was stirred in the presence of excess activated magnesium turnings for 12 to 18 h, until a yellow solution formed and a quenched aliquot indicated complete consumption of the starting material by GC/MS (pure dibenzylether). Then, the solution was decanted from the Mg turnings, and the volume was doubled by addition of THF. Subsequently, 1,4-dioxane (1 to 2 v/v%) was added, causing the precipitation of white solids (magnesium bromide salts). The yellow solution of  $\text{Mg}(\textit{o}\text{-C}_6\text{H}_4\text{CH}_2)_2\text{O}$  was filtered, using a small amount of  $\text{Et}_2\text{O}$  to rinse, and used directly in further reactions.

**Synthesis of  $\text{Cr}(\textit{o}\text{-C}_6\text{H}_4\text{CH}_2)_2\text{O}(\textit{p}\text{-tol})(\text{THF})_2$  (**1**).** Bis(aryl)ether magnesium reagent  $\text{Mg}(\textit{o}\text{-C}_6\text{H}_4\text{CH}_2)_2\text{O}$  (5.38 mmol) was prepared in 150 mL 1:1  $\text{Et}_2\text{O}$ :THF, with 2 mL 1,4-dioxane. This solution was added dropwise to a solution of  $\text{Cr}(\textit{p}\text{-tol})\text{Cl}_2(\text{THF})_3$  (2.32g, 5.38 mmol) dissolved in 60 mL 1:1  $\text{Et}_2\text{O}$ :THF, with 2 mL 1,4-dioxane over 30 min at  $-78^\circ\text{C}$ . The resulting green suspension was stirred at  $-78^\circ\text{C}$  for 1h, then warmed to  $0^\circ\text{C}$  over 2 h. The resulting dark red solution was allowed to warm to RT, stirring for 17 h. The dark red solution was filtered from white precipitate, and reduced in vacuo to 12 mL. To this, 24 mL pentane was added to precipitate bright red solids. These were dissolved in THF, from which red crystals of **1** were grown at  $-35^\circ\text{C}$  over several days; the product was dried under

vacuum after decanting the solvent (0.687 g, 26% yield). In  $C_6D_6$ :  $\mu_{eff} = 2.9(1) \mu_B$  (average of three measurements). In  $C_6D_6 + 100$  THF:  $\mu_{eff} = 3.8 \mu_B$ . Anal. Calcd. for  $C_{29}H_{35}CrO_3$ : C, 72.03; H, 7.30; N, 0.00. Found: C, 71.63; H, 7.32; N, 0.01.

**Synthesis of  $Cr((o-C_6H_4CH_2)_2O)(Me)(THF)_2$ . (2)** Bis(aryl)ether magnesium reagent  $Mg(o-C_6H_4CH_2)_2O$  (1.99 mmol) was prepared in 100 mL 1:1  $Et_2O$ :THF, with 1 mL 1,4-dioxane. This solution was added dropwise over 15 min to a  $-78^\circ C$  solution of  $Cr(Me)Cl_2(THF)_3$  (0.706 g, 1.99 mmol) dissolved in 40 mL 1:1  $Et_2O$ :THF, with 1.5 mL 1,4-dioxane. The resulting red/brown solution was stirred for a further 1 h, then warmed to RT over 15 h. The red solution was filtered from white solids, and reduced in vacuo to 12 mL. To this, 24 mL pentane was added to precipitate dark solids from the red solution. This mixture was filtered, and the solids were discarded. Dark red crystals were obtained by cooling the filtrate to  $-35^\circ C$  for two weeks, and were redissolved into THF for a second recrystallization. Red crystals of **2** were grown at  $-35^\circ C$  by diffusion of pentane into the THF filtrate; the product was obtained by decantation, and dried under vacuum (0.291 g, 36% yield). In  $C_6D_6$ :  $\mu_{eff} = 2.1 \mu_B$ . In  $C_6D_6 + 100$  THF:  $\mu_{eff} = 3.9 \mu_B$ . Anal. Calcd. for  $C_{23}H_{31}CrO_3$ : C, 67.79; H, 7.67; N, 0.00. Found: C, 67.80; H, 8.00; N, 0.07.

**Synthesis of  $(^{101}PNP)Cr((o-C_6H_4CH_2)_2O)(p-tol)$ . (3)** A solution of  $^{101}PNP$  (0.096 g, 0.20 mmol) in 3 mL  $C_6H_6$  was used to dissolve compound **1**, which was a dry red crystalline powder (0.098 g, 0.20 mmol). The resulting green solution was stirred for five minutes, then lyophilized down to a dry orange/brown powder. The crude product was dissolved in 2 mL toluene and layered with 12 mL pentane and cooled to  $-35^\circ C$  for 8 days. Brown microcrystalline **3** was obtained by decanting the supernatant, and the product was dried under vacuum (0.077 g, 0.094 mmol, 47% yield). Single, brown crystals of **3** suitable for XRD were grown by cooling a very dilute, green solution of crude **3** in pentane to  $35^\circ C$  (if

the solution was too concentrated, the product was observed to precipitate out within several minutes). In  $C_6D_6$ :  $\mu_{eff} = 3.8 \mu_B$ . Anal. Calcd. for  $C_{52}H_{46}CrNOP_2$ : C, 76.64; H, 5.69; N, 1.72. Found: C, 76.26; H, 5.81; N, 1.33.

**Synthesis of  $(^{101}PNP)Cr((o-C_6H_4CH_2)_2O)(Me)$ . (4)** A solution of  $^{101}PNP$  (0.091 g, 0.19 mmol) in 2 mL  $C_6H_6$  was used to dissolve compound **2**, which was a dry red/brown crystalline powder (0.078 g, 0.19 mmol). The resulting brown solution was stirred for ten minutes, then lyophilized down to a dry brown powder. The crude product was dissolved in 2 mL toluene and cooled to  $-35^\circ C$  for 2 weeks. The dark brown crystals of **4** were obtained by decantation and dried under vacuum (0.070 g, 0.095 mmol, 49% yield). The same procedure was used to obtain single crystals of **4** suitable for XRD. In  $C_6D_6$ :  $\mu_{eff} = 3.4 \mu_B$ . Anal. Calcd. for  $C_{46}H_{42}CrNOP_2$ : C, 74.79; H, 5.73; N, 1.90. Found: C, 75.31; H, 6.09; N, 1.31.

**Obtaining Crystals of  $CrCl((o-C_6H_4CH_2)_2O)(THF)_2$ ,  $(6 \cdot THF)$  and  $[CrCl((o-C_6H_4CH_2)_2O)(THF)]_2$ . ([6]<sub>2</sub>)** Bis(aryl)ether magnesium reagent  $Mg(o-C_6H_4CH_2)_2O$  (0.20 mmol) was prepared in 10 mL 1:1  $Et_2O:THF$ , with 0.25 mL 1,4-dioxane. This was added dropwise to a stirring suspension of  $CrCl_3(THF)_3$  (0.075 g, 0.20 mmol) in 5 mL THF. After 1 day, the brown solution was filtered from white solids, then reduced to dryness *in vacuo* to 0.085 g. The brown solid was redissolved in THF (1 mL) then stored at  $-35^\circ C$  with vapor diffusion of hexanes. After 1 day, some colorless salts were visible. The supernatant was decanted, then resubjected to the vapor diffusion. After two days, brown crystals were obtained, and single crystal XRD revealed them to contain one equivalent each of **6·THF** (monomer) and **[6]<sub>2</sub>** ( $\mu$ -Cl dimer, see Figure 8). Crystals of **6·THF** could be obtained by a similar synthetic procedure, and extracting the crude solids with a mixture of 3:1 pentane:THF and crystallizing the product from this mixture at  $-35^\circ C$ . The solids obtained

were redissolved in THF, then vapor diffusion of pentane in this solution at  $-35^{\circ}\text{C}$  was used to grow XRD-quality crystals of **6**·THF (see Figure 7). Due to the difficulty in separating **6**·THF and **[6]<sub>2</sub>** and/or forming either one selectively, bulk synthesis and characterization was not successful.

**Obtaining Crystals of  $[\text{Cr}_2((o\text{-C}_6\text{H}_4\text{CH}_2)_2\text{O})_2(1,4\text{-dioxane})]_n$ . (7)** Bis(aryl)ether magnesium reagent  $\text{Mg}(o\text{-C}_6\text{H}_4\text{CH}_2)_2\text{O}$  (0.24 mmol) was prepared in 8 mL 1:1  $\text{Et}_2\text{O}$ :THF, with 0.25 mL 1,4-dioxane. This was added dropwise to a stirring solution of  $\text{Cr}(p\text{-tol})\text{Cl}_2(\text{THF})_3$  (0.104 g, 0.24 mmol) in 5 mL THF that had been chilled to  $-35^{\circ}\text{C}$ . After stirring for 30 minutes at RT, the solution was reduced *in vacuo* to 5 mL. To the homogeneous dark red solution, 5 mL  $\text{Et}_2\text{O}$  and 0.25 mL 1,4-dioxane was added, causing the precipitation of white solids. After 20 minutes, the suspension was cooled to  $-35^{\circ}\text{C}$  over two days, then the suspension was reduced *in vacuo* to a dark orange residue. Hexanes (12 mL) was used to extract an orange solution from the brown solids, which were then rinsed with  $\text{Et}_2\text{O}$  (1 mL). The brown  $\text{Et}_2\text{O}$  solution was cooled to  $-35^{\circ}\text{C}$  yielding some crystals of **7**, the structure determined by XRD (see figure 9).

Separately,  $\text{Mg}(o\text{-C}_6\text{H}_4\text{CH}_2)_2\text{O}$  (0.15 mmol) was prepared in 6 mL 1:1  $\text{Et}_2\text{O}$ :THF. This was added dropwise to a stirring solution of  $\text{CrCl}_2(\text{THF})_2$  (0.040 g, 0.15 mmol) in 8 mL 1:1  $\text{Et}_2\text{O}$ :THF, with 0.25 mL 1,4-dioxane. Upon completion of addition, the Cr suspension converted to a dark green solution, and after 1 hr, white solids had started to precipitate. After 3 hr, a brown solution was filtered from white solids, and was reduced to dryness *in vacuo*. This was extracted with 3 mL  $\text{Et}_2\text{O}$ , and crystals of **7** were grown by cooling the solution to  $-35^{\circ}\text{C}$  (the unit cell determined from XRD matched the known structure).

**Obtaining Crystals of  $\text{Cr}((o\text{-C}_6\text{H}_4\text{CH}_2)_2\text{O})(p\text{-tol})(\text{dimethoxyethane})$ . (8)** Bis(aryl)ether magnesium reagent  $\text{Mg}(o\text{-C}_6\text{H}_4\text{CH}_2)_2\text{O}$  (0.22 mmol) was prepared in 4 mL

Et<sub>2</sub>O, then added dropwise to a stirring solution of Cr(*p*-tol)Cl<sub>2</sub>(THF)<sub>3</sub> (0.095 g, 0.22 mmol) in THF (5 mL). After completion of addition, 0.25 mL 1,4-dioxane was added. The dark suspension was then reduced *in vacuo* to an orange/brown residue. This was extracted with Et<sub>2</sub>O (5 mL) to separate a dark orange solution from gray salts. The Et<sub>2</sub>O solution was reduced to dryness *in vacuo* then triturated with additional Et<sub>2</sub>O to obtain 40 mg of red solid (crude **1**). Single crystals of **8** suitable for XRD were grown by cooling a dimethoxyethane solution of the residue to -35°C for several days.

**Synthesis of Cr((*o*-C<sub>6</sub>H<sub>4</sub>CH<sub>2</sub>)<sub>2</sub>O)(*p*-tol)(pyridine)<sub>2</sub>. (**9**)** To a solution of **1** (0.062 g, 0.13 mmol) in toluene (2 mL), pyridine (0.21 mL, 2.6 mmol) was added at RT. After several minutes, some bright red precipitate crashed out. After stirring for 15 h, the suspension was reduced to dryness *in vacuo*. The residue was redissolved in 2 mL toluene, then reduced to dryness again. The residue was again redissolved in 2 mL toluene, then the solution filtered from minimal solids and stored at -35°C for 1 day, yielding red crystals which were recovered by decanting the supernatant and drying under vacuum: 0.052 g (0.10 mmol, 77% yield).

**Obtaining Crystals of Cr((*o*-C<sub>6</sub>H<sub>4</sub>CH<sub>2</sub>)<sub>2</sub>O)(*p*-tol)(Ph<sub>2</sub>PMe)<sub>2</sub>. (**10**)** To a solution of **1** (0.017 g, 0.035 mmol) in toluene (1 mL), PPh<sub>2</sub>Me (0.007 g, 0.04 mmol) was added at RT. After stirring for 30 min, the brown solution was reduced to dryness *in vacuo*. The residue was partially dissolved in 1 mL toluene, then reduced to dryness again. The residue was again redissolved in 2 mL toluene, then the solution filtered from minimal solids and stored at -35°C for 1 day, with pentane in an outer vial to diffuse into the toluene solution. Small red crystals of **10** were observed after several days. The structure was determined by XRD (see figure 12).

**Synthesis of  $\text{CH}_3\text{Si}(\textit{o}\text{-BrC}_6\text{H}_4)_3$ . (12)** A stirring solution of 1,2-dibromobenzene (6.0 mL, 50 mmol) in 80 mL of 1:1 THF:Et<sub>2</sub>O was prepared in a three-neck flask, and cooled to -115°C for 15 min using an ethanol slush bath. Over fifteen minutes, <sup>n</sup>BuLi (20 mL in hexanes, 50 mmol) was added using a dropping addition funnel; care was taken to avoid quick addition, which would cause the temperature of the reaction to increase. The ethanol slush bath was carefully maintained by addition of liquid nitrogen over this time. To the resulting solution, neat MeSiCl<sub>3</sub> (1.95 mL, 16.6 mmol) was added via syringe over two minutes, then the mixture was removed from the cooling bath, and allowed to warm to room temperature. The solution became yellow, with precipitation of white solids as the mixture warmed. After 2 hr, 8 g of silica was added to the flask to quench the reaction. This mixture was reduced to dryness *in vacuo*, then 80 mL benzene was used to extract the residue. The benzene solution was subsequently filtered through a plug of silica. The filtrate was reduced to 6 g of a sticky yellow oil by rotary evaporation. This residue was further purified from numerous byproducts by silica gel column chromatography (eluent: 10% benzene in hexanes, R<sub>f</sub> = 0.5) and the product fractions were reduced to colorless solids by rotary evaporation. The product **12** could be obtained in 95% purity (A single impurity remained detectable by <sup>1</sup>H NMR and GC/MS) by recrystallization of these solids from ethyl acetate, yielding colorless blocks (0.922 g, 1.80 mmol, 11 % yield). <sup>1</sup>H NMR (399.8 MHz, 22°C, C<sub>6</sub>D<sub>6</sub>): δ 7.40 (d, J<sub>HH</sub> = 7.6 Hz, 3H), 7.37 (dd, J<sub>HH</sub> = 1.9 Hz, 7.3 Hz, 3H), 6.85 (t, J<sub>HH</sub> = 7.3 Hz, 3H), 6.78 (dt, J<sub>HH</sub> = 1.9 Hz, 7.6 Hz, 3H), 1.48 (s, 3H). <sup>13</sup>C NMR (100.5 MHz, 22°C, C<sub>6</sub>D<sub>6</sub>): δ 139.6, 137.0, 133.5, 131.8, 131.4, 126.8, 2.0. EI/MS (m/z): 511.

**Obtaining Crystals of  $\text{Cr}(\textit{o}\text{-C}_6\text{H}_4)_3\text{SiCH}_3(\text{THF})_3$ . (13)** In 3 mL THF,  $\text{CH}_3\text{Si}(\textit{o}\text{-BrC}_6\text{H}_4)_3$  (**12**) (0.025 g, 0.049 mmol) was stirred over excess Mg turnings with 3 equiv. LiCl until formation of the tris-Grignard (determined by GC/MS of a quenched aliquot). The

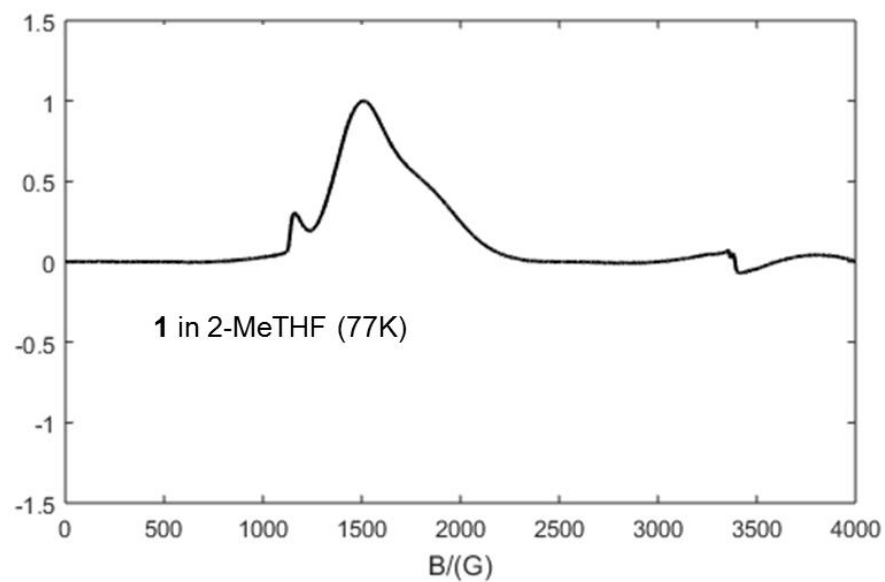
solution was filtered from Mg bromide salts which had precipitated. Then, it was added dropwise to a stirring suspension of  $\text{CrCl}_3(\text{THF})_3$  (0.018 g, 0.048 mmol) in 1 mL THF at RT. The resulting bright orange solution was reduced *in vacuo* to 2 mL, then 2 mL  $\text{Et}_2\text{O}$  was added, along with a few drops of 1,4-dioxane. After stirring for 45 min at RT, an orange solution was filtered from grey Mg salts. The filtrate was reduced *in vacuo* and triturated twice with pentane to obtain orange solids (0.022 g). Single crystals of **13** suitable for XRD were grown by vapor diffusion of pentane into a THF solution at  $-35^\circ\text{C}$ .

**Obtaining Crystals of  $(^{\text{iPr}}\text{PNP})\text{Cr}((\text{o-C}_6\text{H}_4)_3\text{SiCH}_3)$ . (**14**)** A solution of  $^{\text{iPr}}\text{PNP}$  (0.023 g, 0.54 mmol) in 2 mL  $\text{C}_6\text{H}_6$  was added to a vial containing crystals of **13** (0.029 g, 0.54 mmol). A brown supernatant formed over the crystals, which did not dissolve. About 0.5 mL THF was added to dissolve everything as a bright red solution. This was reduced to a dry red residue under vacuum. The solid was then redissolved using 1 mL toluene, and reduced *in vacuo* to dryness. This process was repeated three times with toluene, then twice with  $\text{C}_6\text{H}_6$ , eventually yielding a brown solid (instead of red). Again, toluene was used to dissolve the solid, and the solution reduced to dryness. It was triturated with pentane, then 1 mL toluene was added to the brown residue, at which point a green color was seen, attributable to the desired product. After trituration with pentane twice more, some  $\text{Et}_2\text{O}$  was used to dissolve some of the green residue. Upon cooling, and slow vapor diffusion of pentane into the  $\text{Et}_2\text{O}$  solution over several days, green crystals of **14** were obtained as blades. The structure was determined by XRD (see figure 18).

**Representative Procedure for Oligomerization Catalysis via Stoichiometric Activation of 1-4.** A mixture of **1** (4.0 mg, 0.0080 mmol) and  $^{\text{iPr}}\text{PNP}$  (3.8 mg, 0.0088 mmol) were dissolved in 1.0 mL PhCl. This was frozen in the glovebox cold well, and a 0.5 mL PhCl solution of  $[\text{H}(\text{Et}_2\text{O})_2][\text{BAR}'_4]$  (8.1 mg, 0.0080 mmol) was added dropwise to the

thawing solution. After ~30 seconds, the brown solution was diluted to 7.5 mL, then added to a prechilled Fischer-Porter reactor, causing the solution to freeze upon contacting the glass. The reactor was sealed, taken out of the glovebox, and stirred for 5 min in a water bath at 25 °C, then pressurized to 100 psig of ethylene, and stirred for 45 min at 25 °C. The reactor was then vented, and 0.1 mL methanol was added to quench the reaction mixture. The solution was used to dissolve 20 mg adamantane, filtered, and analyzed by GC/FID to quantify the oligomers vs. adamantane. It was also analyzed by GC/MS to identify other organic residues. Polymer was weighed on a tared glass fritted filter.

**Representative Procedure for Oligomerization Catalysis using  $\text{CrCl}_3(\text{THF})_3$  and MMAO.** A mixture of  $\text{CrCl}_3(\text{THF})_3$  (0.0040 g, 0.0080 mmol) and  $^{i\text{Pr}}\text{PNP}$  (3.8 mg, 0.0088 mmol) were dissolved in 6.15 mL PhCl. This was loaded into a glass Fischer-Porter reactor, and sealed in the glovebox. The reactor was taken out of the glovebox, and purged with ethylene at 30 psig for 60 seconds, during which time a solution of MMAO-3A (1.35 mL, 2.4 mmol) was added. The reactor was quickly sealed, and was pressurized to 100 psig of ethylene, and stirred for 45 min at 25 °C. The reactor was then vented, and 10 mL 1M HCl was added to quench the reaction. To the mixture, 20 mg adamantane was added, and the organic layer was separated, filtered, and analyzed by GC/FID to quantify the oligomers vs. adamantane. Polymer was weighed on a tared glass fritted filter.

**EPR and NMR Spectra.**

**Figure 20.** Continuous wave (cw) EPR spectrum of compound **1**. Temperature: 77K. Microwave frequency: 9.4 GHz.

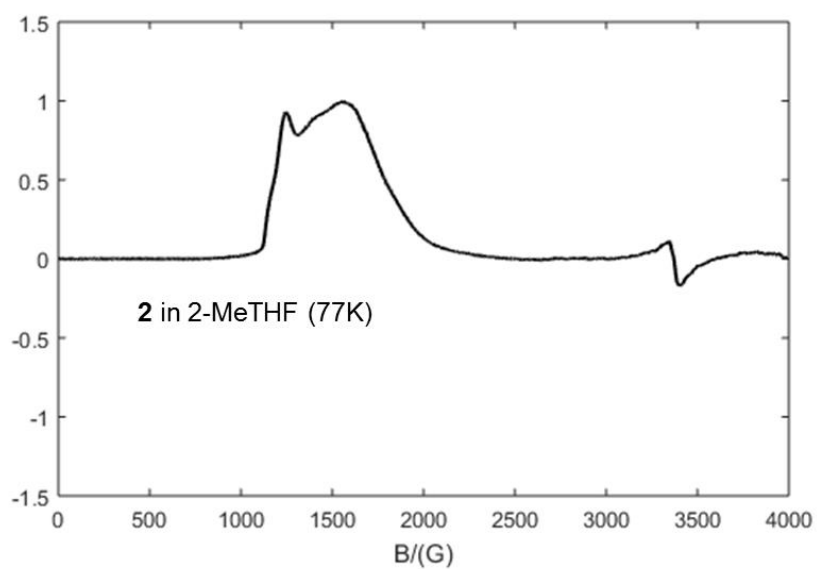


**Figure 21.** Continuous wave (cw) EPR spectrum of compound **2**. Temperature: 77K. Microwave frequency: 9.4 GHz.

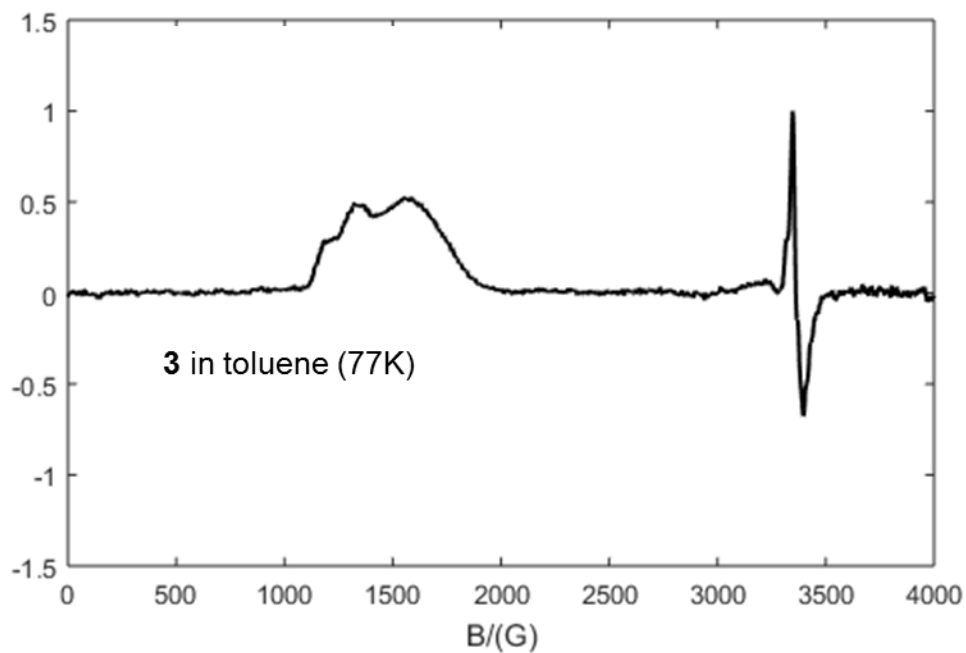


**Figure 22.** Continuous wave (cw) EPR spectrum of compound **3**. Temperature: 77K. Microwave frequency: 9.4 GHz.

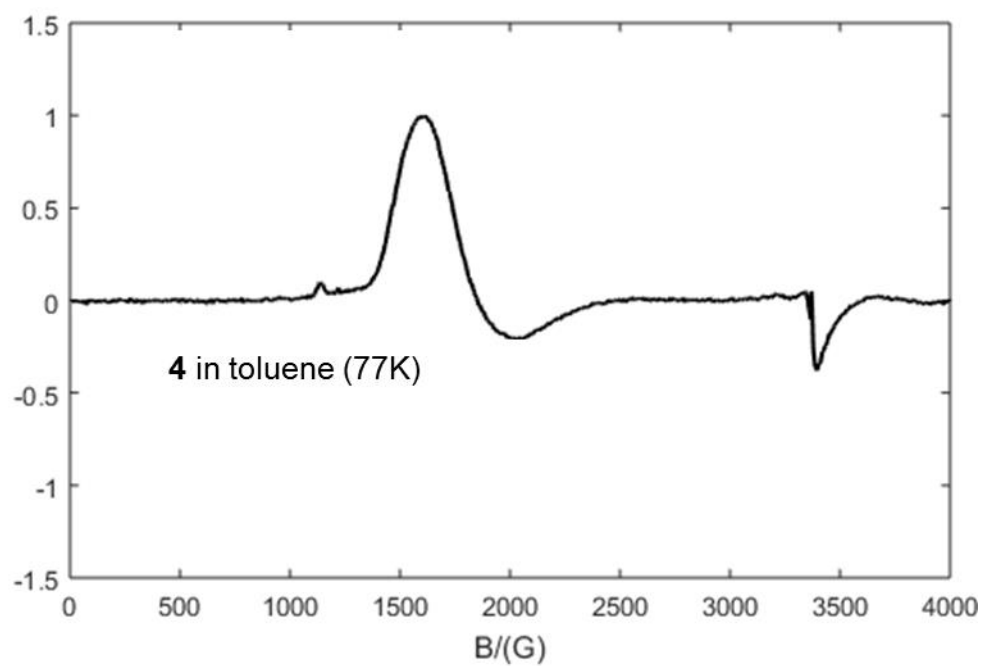


**Figure 23.** Continuous wave (cw) EPR spectrum of compound **4**. Temperature: 77K. Microwave frequency: 9.4 GHz.

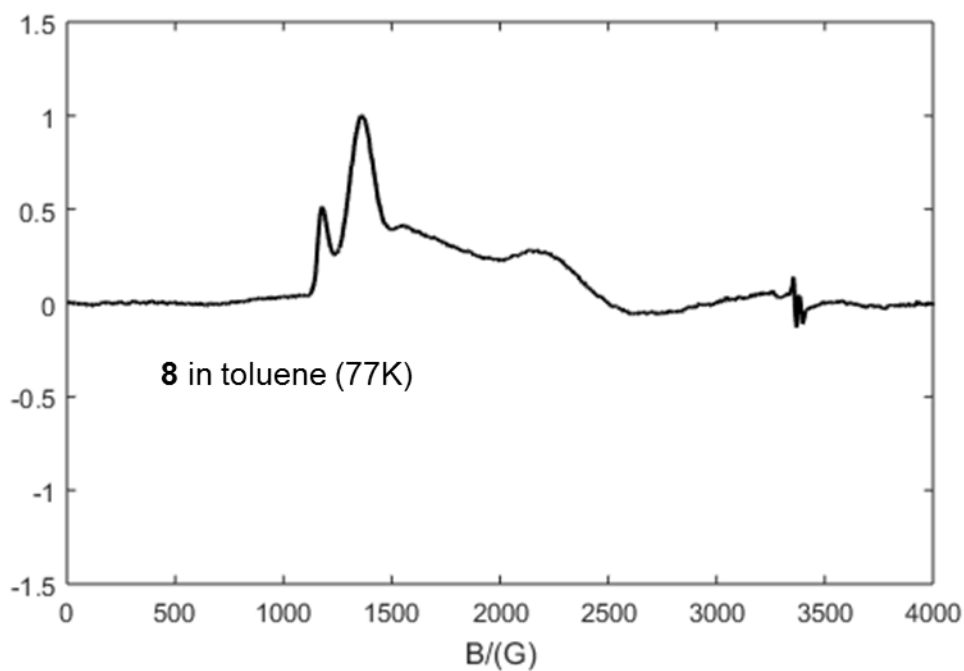


**Figure 24.** Continuous wave (cw) EPR spectrum of compound **8**. Temperature: 77K. Microwave frequency: 9.4 GHz.

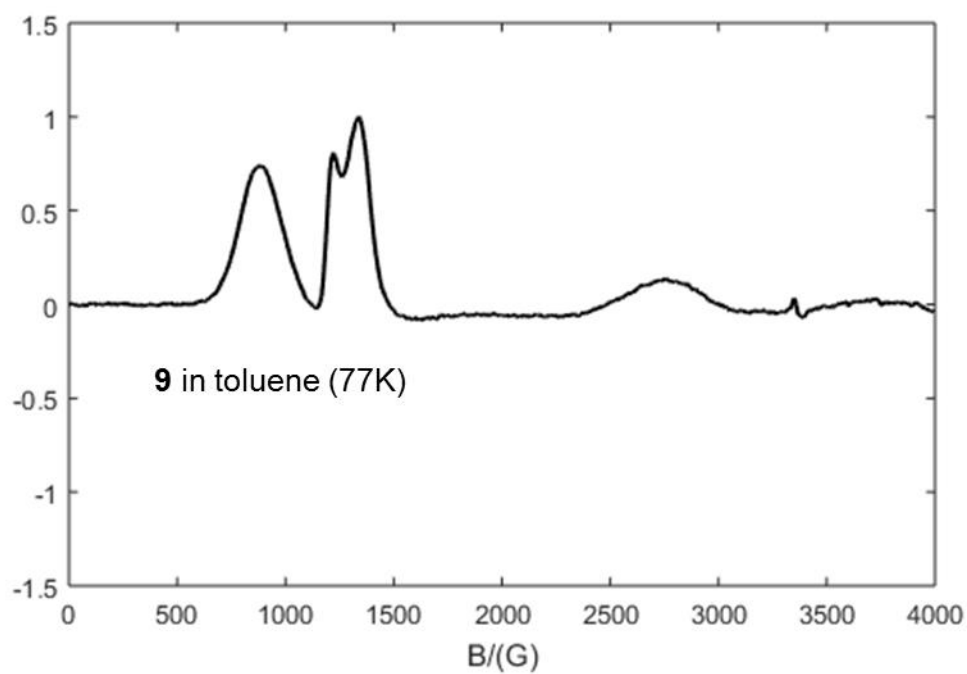


**Figure 25.** Continuous wave (cw) EPR spectrum of compound **9**. Temperature: 77K. Microwave frequency: 9.4 GHz.

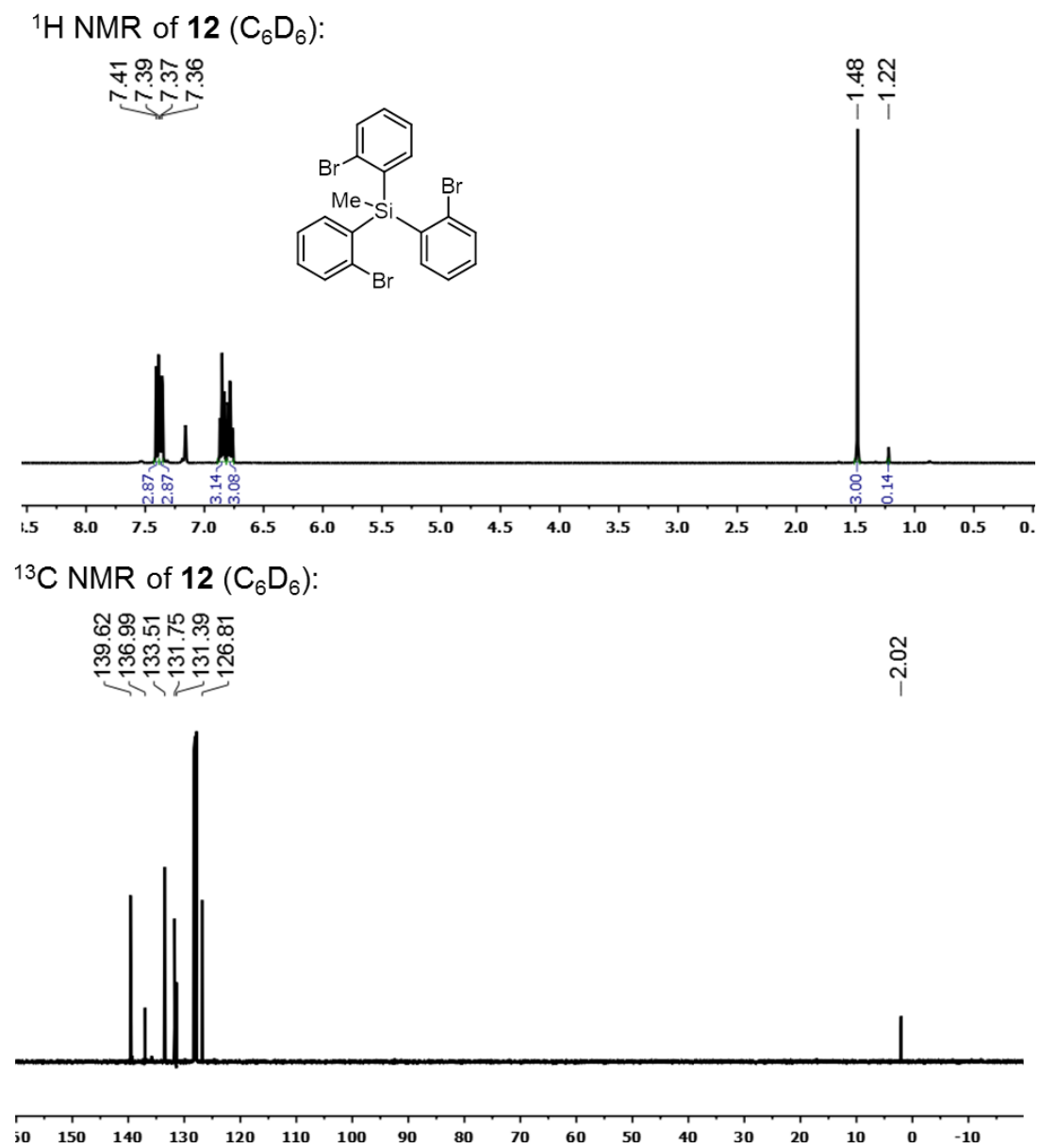


Figure 26.  $^1\text{H}$  and  $^{13}\text{C}$  NMR spectra of compound **12** ( $\text{C}_6\text{D}_6$ ).

**X-Ray Crystallography and Crystallographic Tables.** Suitable crystals of complexes **1**, **2**, **3**, and **4** were mounted on a nylon loop using Paratone oil, then placed on a diffractometer under a nitrogen stream. X-ray intensity data were collected on a Bruker APEXII CCD area detector or a Bruker D8 VENTURE Kappa Duo PHOTON 100 CMOS detector employing Mo-K $\alpha$  radiation ( $\lambda = 0.71073 \text{ \AA}$ ) or Cu-K $\alpha$  radiation ( $\lambda = 1.54178 \text{ \AA}$ ) at a temperature of 100 K. All diffractometer manipulations, including data collection, integration and scaling were carried out using the Bruker APEX3 software.<sup>23</sup> In APEX3, intensity data were absorption-corrected using SADABS, and space groups were determined on the basis of systematic absences and intensity statistics using XPREP. Using Olex2, the structures were solved using ShelXT and refined to convergence by full-matrix least squares minimization.<sup>24</sup> All non-hydrogen atoms were refined using anisotropic displacement parameters. Hydrogen atoms were placed in idealized positions and refined using a riding model. For complex **2**, the positional disorder of the carbon atoms for the aryl and THF ligands in two of the three molecules in the asymmetric unit was modeled using the PART instruction. Graphical representation of structures with 50% probability thermal ellipsoids were generated using Diamond 3 visualization software.<sup>25</sup>

Compound	1	2	3	4
CCDC	1562429	1562430	1562431	1562432
Empirical formula	C <sub>29</sub> H <sub>35</sub> CrO <sub>3</sub>	C <sub>23</sub> H <sub>31</sub> CrO <sub>3</sub>	C <sub>57</sub> H <sub>58</sub> CrNOP <sub>2</sub>	C <sub>56.5</sub> H <sub>54</sub> CrNOP <sub>2</sub>
Formula weight	483.57	407.48	886.98	876.94
Temperature/K	100.02	99.99	100.04	100.02
Crystal system	monoclinic	orthorhombic	monoclinic	monoclinic
Space group	<i>P2<sub>1</sub>/c</i>	<i>Pna2<sub>1</sub></i>	<i>P2<sub>1</sub>/n</i>	<i>P2<sub>1</sub></i>
a/Å	18.6763(14)	17.0687(6)	10.5738(7)	13.5452(5)
b/Å	17.5939(12)	26.5488(10)	18.1251(13)	14.5414(6)
c/Å	15.6720(11)	13.6540(6)	24.8864(17)	23.7385(10)
α/°	90	90	90	90
β/°	106.878(4)	90	101.934(5)	96.029(3)
γ/°	90	90	90	90
Volume/Å <sup>3</sup>	4927.8(6)	6187.4(4)	4666.4(6)	4649.8(3)
Z	8	12	4	4
ρ <sub>calc</sub> /cm <sup>3</sup>	1.304	1.312	1.263	1.253
μ/mm <sup>-1</sup>	0.492	0.574	2.974	2.981
F(000)	2056	2604	1876	1848
Crystal size/mm <sup>3</sup>	0.39 × 0.367 × 0.366	0.26 × 0.167 × 0.095	0.088 × 0.113 × 0.139	0.084 × 0.051 × 0.026
Radiation	MoKα (λ = 0.71073)	MoKα (λ = 0.71073)	CuKα (λ = 1.54178)	CuKα (λ = 1.54178)
2θ range for data collection/°	2.278 to 75.66	4.900 to 64.998	6.06 to 148.95	6.562 to 140.966
Index ranges	-31 ≤ h ≤ 31, -30 ≤ k ≤ 29, -26 ≤ l ≤ 26	-25 ≤ h ≤ 25, -40 ≤ k ≤ 33, -20 ≤ l ≤ 17	-13 ≤ h ≤ 13, -20 ≤ k ≤ 22, -26 ≤ l ≤ 30	-16 ≤ h ≤ 15, - 17 ≤ k ≤ 17, -28 ≤ l ≤ 28
Reflections collected	194220	76731	43912	48372
Independent reflections	25298 [R <sub>int</sub> = 0.0538, R <sub>sigma</sub> = 0.0379]	20045 [R <sub>int</sub> = 0.0744, R <sub>sigma</sub> = 0.1018]	9268 [R <sub>int</sub> = 0.2153, R <sub>sigma</sub> = 0.1812]	16960 [R <sub>int</sub> = 0.1637, R <sub>sigma</sub> = 0.1980]
Data/restraints/parameters	25298/0/597	20045/1/773	9268/0/503	16960/46/1080
Goodness-of-fit on F <sup>2</sup>	1.033	1.029	1.072	1.002
Final R indexes [I] ≥ 2σ (I)	R <sub>1</sub> = 0.0452, wR <sub>2</sub> = 0.1171	R <sub>1</sub> = 0.0741, wR <sub>2</sub> = 0.1643	R <sub>1</sub> = 0.1299, wR <sub>2</sub> = 0.2288	R <sub>1</sub> = 0.0866, wR <sub>2</sub> = 0.1785
Final R indexes [all data]	R <sub>1</sub> = 0.0734, wR <sub>2</sub> = 0.1339	R <sub>1</sub> = 0.1525, wR <sub>2</sub> = 0.1959	R <sub>1</sub> = 0.2107, wR <sub>2</sub> = 0.2638	R <sub>1</sub> = 0.1598, wR <sub>2</sub> = 0.2153
Largest diff. peak /hole / e Å <sup>-3</sup>	1.781/-0.607	1.350/-0.800	0.59/-0.754	0.532/-0.664

Compound	6·THF	6·THF/[6] <sub>2</sub>	7
Empirical formula	C <sub>22</sub> H <sub>27</sub> ClCrO <sub>3</sub>	C <sub>22</sub> H <sub>24</sub> ClCrO <sub>3</sub>	C <sub>32</sub> H <sub>32</sub> CrO <sub>4</sub>
Formula weight	426.60	423.86	584.57
Temperature/K	99.94	100.03	100.0
Crystal system	orthorhombic	triclinic	orthorhombic
Space group	<i>Pna</i> 2 <sub>1</sub>	<i>P</i> -1	<i>Pca</i> 2 <sub>1</sub>
a/Å	17.052(3)	10.4591(13)	16.9878(6)
b/Å	8.7786(12)	12.0117(15)	8.8091(3)
c/Å	13.5468(19)	17.295(2)	18.0665(6)
α/°	90	95.218(4)	90
β/°	90	105.395(4)	90
γ/°	90	96.170(3)	90
Volume/Å <sup>3</sup>	2027.9(5)	2066.4(5)	2703.6(2)
Z	4	4	4
ρ <sub>calc</sub> /cm <sup>3</sup>	1.397	1.362	1.436
μ/mm <sup>-1</sup>	0.715	0.701	0.840
F(000)	895	884	1216
Crystal size/mm <sup>3</sup>	—	—	—
Radiation	MoKα (λ = 0.71073)	MoKα (λ = 0.71073)	MoKα (λ = 0.71073)
2θ range for data collection/°	5.22 to 75.926	3.438 to 61.406	4.51 to 72.234
Index ranges	-29 ≤ h ≤ 28, -14 ≤ k ≤ 14, -22 ≤ l ≤ 22	-14 ≤ h ≤ 14, -17 ≤ k ≤ 16, -24 ≤ l ≤ 24	-28 ≤ h ≤ 28, -14 ≤ k ≤ 14, -29 ≤ l ≤ 29
Reflections collected	54548	55208	210221
Independent reflections	10307 [R <sub>int</sub> = 0.0729, R <sub>sigma</sub> = 0.0898]	11811 [R <sub>int</sub> = 0.1027, R <sub>sigma</sub> = 0.1288]	12378 [R <sub>int</sub> = 0.1287, R <sub>sigma</sub> = 0.0588]
Data/restraints/parameters	10307/52/270	11811/10/483	12378/1/343
Goodness-of-fit on F <sup>2</sup>	1.012	1.078	1.113
Final R indexes [I >= 2σ (I)]	R <sub>1</sub> = 0.0629, wR <sub>2</sub> = 0.1324	R <sub>1</sub> = 0.0887, wR <sub>2</sub> = 0.1984	R <sub>1</sub> = 0.0463, wR <sub>2</sub> = 0.0971
Final R indexes [all data]	R <sub>1</sub> = 0.1260, wR <sub>2</sub> = 0.1516	R <sub>1</sub> = 0.1780, wR <sub>2</sub> = 0.2373	R <sub>1</sub> = 0.0736, wR <sub>2</sub> = 0.1094
Largest diff. peak /hole / e Å <sup>-3</sup>	1.186/-0.571	1.408/-0.765	0.817/-0.949

Compound	8	9	10
Empirical formula	C <sub>25</sub> H <sub>29</sub> CrO <sub>3</sub>	C <sub>31</sub> H <sub>29</sub> CrN <sub>2</sub> O · C <sub>7</sub> H <sub>8</sub>	C <sub>47</sub> H <sub>45</sub> CrOP <sub>2</sub> · 2(C <sub>7</sub> H <sub>8</sub> )
Formula weight	429.48	589.69	923.03
Temperature/K	100.08	100.04	100.03
Crystal system	monoclinic	triclinic	monoclinic
Space group	<i>P</i> 2 <sub>1</sub> / <i>c</i>	<i>P</i> -1	<i>C</i> 2/ <i>c</i>
a/Å	15.9090(9)	10.701(1)	16.124(3)
b/Å	9.5449(6)	11.254(1)	12.648(3)
c/Å	13.8641(8)	13.704(1)	24.184(5)
α/°	90	67.513(4)	90
β/°	94.435(2)	80.070(4)	93.162(7)
γ/°	90	84.755(4)	90
Volume/Å <sup>3</sup>	2099.0(2)	1501.4(3)	4924.6(2)
Z	4	2	4
ρ <sub>calc</sub> /cm <sup>3</sup>	1.359	1.304	1.245
μ/mm <sup>-1</sup>	0.568	0.415	0.339
F(000)	908	622	1952
Crystal size/mm <sup>3</sup>	0.45 × 0.29 × 0.216	–	–
Radiation	MoKα (λ = 0.71073)	MoKα (λ = 0.71073)	MoKα (λ = 0.71073)
2θ range for data collection/°	5.136 to 72.626	5.172 to 72.932	4.376 to 66.266
Index ranges	-26 ≤ h ≤ 26, -15 ≤ k ≤ 15, -21 ≤ l ≤ 23	-17 ≤ h ≤ 17, -16 ≤ k ≤ 18, -21 ≤ l ≤ 22	-24 ≤ h ≤ 24, -19 ≤ k ≤ 18, -36 ≤ l ≤ 36
Reflections collected	90893	14351	61312
Independent reflections	10158 [R <sub>int</sub> = 0.0613, R <sub>sigma</sub> = 0.0471]	14351 [R <sub>int</sub> = –, R <sub>sigma</sub> = 0.0703]	8724 [R <sub>int</sub> = 0.1132, R <sub>sigma</sub> = 0.0706]
Data/restraints/parameters	10158/0/265	14351/0/382	8724/0/299
Goodness-of-fit on F <sup>2</sup>	1.074	1.102	1.079
Final R indexes [I >= 2σ (I)]	R <sub>1</sub> = 0.0500, wR <sub>2</sub> = 0.1241	R <sub>1</sub> = 0.0873, wR <sub>2</sub> = 0.2020	R <sub>1</sub> = 0.0538, wR <sub>2</sub> = 0.0930
Final R indexes [all data]	R <sub>1</sub> = 0.0789, wR <sub>2</sub> = 0.1366	R <sub>1</sub> = 0.1243, wR <sub>2</sub> = 0.2178	R <sub>1</sub> = 0.1205, wR <sub>2</sub> = 0.1395
Largest diff. peak/hole / e Å <sup>-3</sup>	1.276/-0.665	2.564/-1.005	0.576/-0.817

Compound	13	14	15
Empirical formula	C <sub>31</sub> H <sub>39</sub> CrO <sub>3</sub> Si	C <sub>46</sub> H <sub>42</sub> CrNP <sub>2</sub> Si · 3(C <sub>7</sub> H <sub>8</sub> )	C <sub>48</sub> H <sub>46</sub> CrNOP <sub>2</sub> · C <sub>7</sub> H <sub>8</sub>
Formula weight	539.71	1027.23	858.93
Temperature/K	100.03	99.96	100.0
Crystal system	trigonal	triclinic	monoclinic
Space group	<i>P</i> 31 <i>c</i>	<i>P</i> -1	<i>P</i> 2 <sub>1</sub> / <i>n</i>
a/Å	12.7078(7)	10.5479(8)	13.0775(10)
b/Å	12.7078(7)	13.5045(9)	21.5573(16)
c/Å	12.2915(7)	21.6261(15)	15.8504(11)
α/°	90	76.278(2)	90
β/°	90	78.533(2)	93.237(3)
γ/°	120	68.895(2)	90
Volume/Å <sup>3</sup>	1579.1(2)	2769.9(3)	4461.3(6)
Z	2	2	4
ρ <sub>calc</sub> /cm <sup>3</sup>	1.135	1.232	1.279
μ/mm <sup>-1</sup>	0.427	0.328	0.369
F(000)	574	1086	1812
Crystal size/mm <sup>3</sup>	0.209 × 0.204 × 0.162	0.29 × 0.07 × 0.04	–
Radiation	MoKα (λ = 0.71073)	MoKα (λ = 0.71073)	MoKα (λ = 0.71073)
2θ range for data collection/°	5.168 to 72.606	4.630 to 55.024	4.362 to 61.064
Index ranges	-21 ≤ h ≤ 21, -21 ≤ k ≤ 21, -18 ≤ l ≤ 18	-13 ≤ h ≤ 13, -17 ≤ k ≤ 17, -28 ≤ l ≤ 28	-16 ≤ h ≤ 18, -30 ≤ k ≤ 29, -19 ≤ l ≤ 22
Reflections collected	93004	126535	120982
Independent reflections	5119 [R <sub>int</sub> = 0.0794, R <sub>sigma</sub> = 0.0322]	12739 [R <sub>int</sub> = 0.0839, R <sub>sigma</sub> = 0.0511]	12639 [R <sub>int</sub> = 0.1389, R <sub>sigma</sub> = 0.1206]
Data/restraints/parameters	5119/1/135	12739/66/684	12639/0/545
Goodness-of-fit on F <sup>2</sup>	1.062	1.039	1.078
Final R indexes [I >= 2σ (I)]	R <sub>1</sub> = 0.0480, wR <sub>2</sub> = 0.1277	R <sub>1</sub> = 0.0506, wR <sub>2</sub> = 0.1017	R <sub>1</sub> = 0.0785, wR <sub>2</sub> = 0.1489
Final R indexes [all data]	R <sub>1</sub> = 0.0641, wR <sub>2</sub> = 0.1376	R <sub>1</sub> = 0.0812, wR <sub>2</sub> = 0.1123	R <sub>1</sub> = 0.1575, wR <sub>2</sub> = 0.1722
Largest diff. peak/hole / e Å <sup>-3</sup>	0.766/-0.623	0.586/-0.450	1.003/-0.817

**References.**

(1) (a) Olah, G. A.; Molnár, Á. "Oligomerization and Polymerization" In *Hydrocarbon Chemistry*; John Wiley & Sons, Inc.: 2003, p 723. (b) Lappin, G. R.; Nemeč, L. H.; Sauer, J. D.; Wagner, J. D. "Olefins, Higher" In *Kirk-Othmer Encyclopedia of Chemical Technology*; John Wiley & Sons, Inc.: 2000. (c) Skupinska, J. *Chem. Rev.* **1991**, *91*, 613.

(2) (a) van Leeuwen, P. W. N. M.; Clément, N. D.; Tschan, M. J. L. *Coord. Chem. Rev.* **2011**, *255*, 1499. (b) Baier, M. C.; Zuideveld, M. A.; Mecking, S. *Angew. Chem. Int. Ed.* **2014**, *53*, 9722. (c) Agapie, T. *Coord. Chem. Rev.* **2011**, *255*, 861. (d) McGuinness, D. S. *Chem. Rev.* **2011**, *111*, 2321. (e) Dixon, J. T.; Green, M. J.; Hess, F. M.; Morgan, D. H. *J. Organomet. Chem.* **2004**, *689*, 3641. (f) Wass, D. F. *Dalton Trans.* **2007**, 816.

(3) (a) Bollmann, A.; Blann, K.; Dixon, J. T.; Hess, F. M.; Killian, E.; Maumela, H.; McGuinness, D. S.; Morgan, D. H.; Neveling, A.; Otto, S.; Overett, M.; Slawin, A. M. Z.; Wasserscheid, P.; Kuhlmann, S. *J. Am. Chem. Soc.* **2004**, *126*, 14712. (b) Licciulli, S.; Thapa, I.; Albahily, K.; Korobkov, I.; Gambarotta, S.; Duchateau, R.; Chevalier, R.; Schuhen, K. *Angew. Chem. Int. Ed.* **2010**, *49*, 9225. (c) Shaikh, Y.; Albahily, K.; Sutcliffe, M.; Fomitcheva, V.; Gambarotta, S.; Korobkov, I.; Duchateau, R. *Angew. Chem. Int. Ed.* **2012**, *51*, 1366. (d) Shaikh, Y.; Gurnham, J.; Albahily, K.; Gambarotta, S.; Korobkov, I. *Organometallics* **2012**, *31*, 7427. (e) Zhang, L.; Meng, X.; Chen, Y.; Cao, C.; Jiang, T. *ChemCatChem* **2017**, *9*, 76.

(4) (a) Overett, M. J.; Blann, K.; Bollmann, A.; Dixon, J. T.; Hess, F.; Killian, E.; Maumela, H.; Morgan, D. H.; Neveling, A.; Otto, S. *Chem. Comm.* **2005**, 622. (b) Weng, Z.; Teo, S.; Andy Hor, T. S. *Dalton Trans.* **2007**, 3493. (c) McGuinness, D. S.; Overett, M.; Tooze, R. P.; Blann, K.; Dixon, J. T.; Slawin, A. M. Z. *Organometallics* **2007**, *26*, 1108. (d) McGuinness, D. S.; Rucklidge, A. J.; Tooze, R. P.; Slawin, A. M. Z. *Organometallics* **2007**, *26*, 2561. (e) Rucklidge, A. J.; McGuinness, D. S.; Tooze, R. P.; Slawin, A. M. Z.; Pelletier, J. D.

A.; Hanton, M. J.; Webb, P. B. *Organometallics* **2007**, *26*, 2782. (f) Killian, E.; Blann, K.; Bollmann, A.; Dixon, J. T.; Kuhlmann, S.; Maumela, M. C.; Maumela, H.; Morgan, D. H.; Nongodlwana, P.; Overett, M. J.; Pretorius, M.; Höfener, K.; Wasserscheid, P. *J. Mol. Catal. A: Chem.* **2007**, *270*, 214. (g) Blann, K.; Bollmann, A.; de Bod, H.; Dixon, J. T.; Killian, E.; Nongodlwana, P.; Maumela, M. C.; Maumela, H.; McConnell, A. E.; Morgan, D. H.; Overett, M. J.; Prétorius, M.; Kuhlmann, S.; Wasserscheid, P. *J. Catal.* **2007**, *249*, 244. (h) Kim, S.-K.; Kim, T.-J.; Chung, J.-H.; Hahn, T.-K.; Chae, S.-S.; Lee, H.-S.; Cheong, M.; Kang, S. O. *Organometallics* **2010**, *29*, 5805. (i) Overett, M. J.; Blann, K.; Bollmann, A.; Dixon, J. T.; Haasbroek, D.; Killian, E.; Maumela, H.; McGuinness, D. S.; Morgan, D. H. *J. Am. Chem. Soc.* **2005**, *127*, 10723. (j) Britovsek, G. J. P.; McGuinness, D. S.; Wierenga, T. S.; Young, C. T. *ACS Catal.* **2015**, *5*, 4152. (k) Lifschitz, A. M.; Hirscher, N. A.; Lee, H. B.; Buss, J. A.; Agapie, T. *Organometallics* **2017**, *36*, 1640. (l) Lee, D. H.; Kim, E. H.; Jeon, J. Y.; Park, S. H.; Jeong, M. S.; Kang, Y. Y.; Lee, J.; Lee, B. Y. *J. Organomet. Chem.* **2016**, *803*, 13.

(5) (a) MacMillan, S. N.; Lancaster, K. M. *ACS Catal.* **2017**, *7*, 1776. (b) Peitz, S.; Aluri, B. R.; Peulecke, N.; Müller, B. H.; Wöhl, A.; Müller, W.; Al-Hazmi, M. H.; Mosa, F. M.; Rosenthal, U. *Chem. Eur. J.* **2010**, *16*, 7670. (c) Rabeah, J.; Bauer, M.; Baumann, W.; McConnell, A. E. C.; Gabrielli, W. F.; Webb, P. B.; Selent, D.; Brückner, A. *ACS Catal.* **2012**, *3*, 95.

(6) Stennett, T. E.; Haddow, M. F.; Wass, D. F. *Organometallics* **2012**, *31*, 6960.

(7) (a) Monillas, W. H.; Young, J. F.; Yap, G. P. A.; Theopold, K. H. *Dalton Trans.* **2013**, *42*, 9198. (b) McGowan, K. P.; Abboud, K. A.; Veige, A. S. *Organometallics* **2011**, *30*, 4949. (c) Ronellenfitsch, M.; Wadepohl, H.; Enders, M. *Organometallics* **2014**, *33*, 5758. (d) Rozenel, S. S.; Chomitz, W. A.; Arnold, J. *Organometallics* **2009**, *28*, 6243. (e) Jabri, A.; Crewdson, P.; Gambarotta, S.; Korobkov, I.; Duchateau, R. *Organometallics* **2006**, *25*, 715. (f) Albahily, K.;

Fomitcheva, V.; Gambarotta, S.; Korobkov, I.; Murugesu, M.; Gorelsky, S. I. *J. Am. Chem. Soc.* **2011**, *133*, 6380. (g) Conde-Guadano, S.; Danopoulos, A. A.; Pattacini, R.; Hanton, M.; Tooze, R. P. *Organometallics* **2012**, *31*, 1643. (h) Kreisel, K. A.; Yap, G. P. A.; Theopold, K. H. *Organometallics* **2006**, *25*, 4670. (i) Ai, P.; Danopoulos, A. A.; Braunstein, P. *Organometallics* **2015**, *34*, 4109. (j) Schofer, S. J.; Day, M. W.; Henling, L. M.; Labinger, J. A.; Bercaw, J. E. *Organometallics* **2006**, *25*, 2743. (k) Agapie, T.; Schofer, S. J.; Labinger, J. A.; Bercaw, J. E. *J. Am. Chem. Soc.* **2004**, *126*, 1304. (l) Agapie, T.; Labinger, J. A.; Bercaw, J. E. *J. Am. Chem. Soc.* **2007**, *129*, 14281. (m) Liu, S.; Pattacini, R.; Braunstein, P. *Organometallics* **2011**, *30*, 3549.

(8) (a) Thapa, I.; Gambarotta, S.; Korobkov, I.; Duchateau, R.; Kulangara, S. V.; Chevalier, R. *Organometallics* **2010**, *29*, 4080. (b) Vidyaratne, I.; Nikiforov, G. B.; Gorelsky, S. I.; Gambarotta, S.; Duchateau, R.; Korobkov, I. *Angew. Chem. Int. Ed.* **2009**, *48*, 6552. (c) Albahily, K.; Fomitcheva, V.; Shaikh, Y.; Sebastiao, E.; Gorelsky, S. I.; Gambarotta, S.; Korobkov, I.; Duchateau, R. *Organometallics* **2011**, *30*, 4201.

(9) (a) Danopoulos, A. A.; Monakhov, K. Y.; Robert, V.; Braunstein, P.; Pattacini, R.; Conde-Guadano, S.; Hanton, M.; Tooze, R. P. *Organometallics* **2013**, *32*, 1842. (b) Herwig, W.; Zeiss, H. *J. Am. Chem. Soc.* **1959**, *81*, 4798. (c) Khan, S. I.; Bau, R. *Organometallics* **1983**, *2*, 1896. (d) Theopold, K. H. *Acc. Chem. Res.* **1990**, *23*, 263.

(10) (a) MacLeod, K. C.; Patrick, B. O.; Smith, K. M. *Organometallics* **2012**, *31*, 6681. (b) Edema, J. J. H.; Gambarotta, S.; Meetsma, A.; Spek, A. L. *Organometallics* **1992**, *11*, 2452. (c) Manzer, L. E. *J. Organomet. Chem.* **1977**, *135*, C6. (d) Cotton, F. A.; Mott, G. N. *Organometallics* **1982**, *1*, 38. (e) Alonso, P. J.; Forniés, J.; García-Monforte, M. A.; Martín, A.; Menjón, B.; Rillo, C. J. *Organomet. Chem.* **2007**, *692*, 3236. (f) Daly, J. J.; Sanz, F.; Sneeden, R. P. A.; Zeiss, H. H. *Helv. Chim. Acta* **1974**, *57*, 1863.

- (11) Kim, E. H.; Lee, H. M.; Jeong, M. S.; Ryu, J. Y.; Lee, J.; Lee, B. Y. *ACS Omega* **2017**, *2*, 765.
- (12) Hartwig, J. F. In *Organotransition Metal Chemistry: from Bonding to Catalysis*; University Science Books: 2010, p 321.
- (13) (a) Aoki, T.; Furusaki, A.; Tomiie, Y.; Ono, K.; Tanaka, K. *Bulletin of the Chemical Society of Japan* **1969**, *42*, 545. (b) Angermund, K.; Doehring, A.; Jolly, P. W.; Krueger, C.; Romao, C. C. *Organometallics* **1986**, *5*, 1268.
- (14) Mattamana, S. P.; Poli, R. *Organometallics* **1997**, *16*, 2427.
- (15) Fryzuk, M. D.; Leznoff, D. B.; Rettig, S. J. *Organometallics* **1997**, *16*, 5116.
- (16) Schneider, S.; Filippou, A. C. *Inorg. Chem.* **2001**, *40*, 4674.
- (17) Piller, F. M.; Appukkuttan, P.; Gavryushin, A.; Helm, M.; Knochel, P. *Angewandte Chemie International Edition* **2008**, *47*, 6802.
- (18) Brown, T. L.; Dickerhoof, D. W.; Bafus, D. A.; Morgan, G. L. *Review of Scientific Instruments* **1962**, *33*, 491.
- (19) Herwig, W.; Zeiss, H. *The Journal of Organic Chemistry* **1958**, *23*, 1404.
- (20) (a) Elowe, P. R.; McCann, C.; Pringle, P. G.; Spitzmesser, S. K.; Bercaw, J. E. *Organometallics* **2006**, *25*, 5255. (b) Jiang, T.; Zhang, S.; Jiang, X.; Yang, C.; Niu, B.; Ning, Y. *J. Mol. Catal. A: Chem.* **2008**, *279*, 90. (c) Brookhart, M.; Grant, B.; Volpe, A. F. *Organometallics* **1992**, *11*, 3920.
- (21) Chang, V. H. T.; Corey, J. Y. *J. Organomet. Chem.* **1980**, *190*, 217.
- (22) Zeiss, H. H.; Sneed, R. P. A. *Angew. Chem. Int. Ed. in English* **1967**, *6*, 435.
- (23) Bruker APEX3; Bruker AXS Inc.: Madison, Wisconsin, USA, 2012.

(24) (a) Dolomanov, O. V.; Bourhis, L. J.; Gildea, R. J.; Howard, J. A. K.; Puschmann, H. *Journal of Applied Crystallography* **2009**, *42*, 339. (b) Sheldrick, G. *Acta Crystallographica Section A* **2015**, *71*, 3.

(25) Putz, H.; Brandenburg, K. *Diamond - Crystal and Molecular Structure Visualization* Bonn, Germany.

## Chapter 3

Isotopic Labelling in Ethylene Oligomerization: Addressing the Issue of 1-  
Octene vs. 1-Hexene Selectivity

Adapted from

*Dalton Transactions*, **2019**, 48, pp 40-44

with permission from the Royal Society of Chemistry.

**Abstract.**

The selectivity-determining mechanistic steps of ethylene tetramerization and trimerization are evaluated in light of isotopic labeling experiments. We offer a new mechanistic proposal, based upon a shared chromacycloheptane intermediate rather than C-C coupling of chromacyclopentanes or Cr speciation into independent trimerization and tetramerization catalysts, that is consistent with the data, including observed upper limits on 1-octene selectivity.

## Introduction.

Despite extensive study of selective ethylene tetramerization with Cr(III)/diphosphinoamine (PNP) precatalysts activated by alkylaluminum species such as modified methylaluminoxane (MMAO), no system has been reported to match the selectivity of analogous ethylene trimerization catalysts.<sup>1</sup> The best performance is limited to around 75% selectivity for 1-octene, even at high ethylene pressures.<sup>2</sup> With 1-hexene as the major co-product, the origin of tetramerization vs. trimerization selectivity remains unclear, and further insight is necessary for future catalyst design. A metallacyclic mechanism has been established for both Cr-based trimerization<sup>3</sup> and tetramerization<sup>4</sup> catalysts by analysis of the products from a mixture of C<sub>2</sub>H<sub>4</sub> and C<sub>2</sub>D<sub>4</sub> gases. Catalyst design features such as ligand sterics have been studied to address effects on selectivity,<sup>5</sup> but it has remained unclear which mechanistic steps are affected. Specific mechanistic details determining 1-octene selectivity have not been experimentally elucidated, but the options can be distilled into three classes:

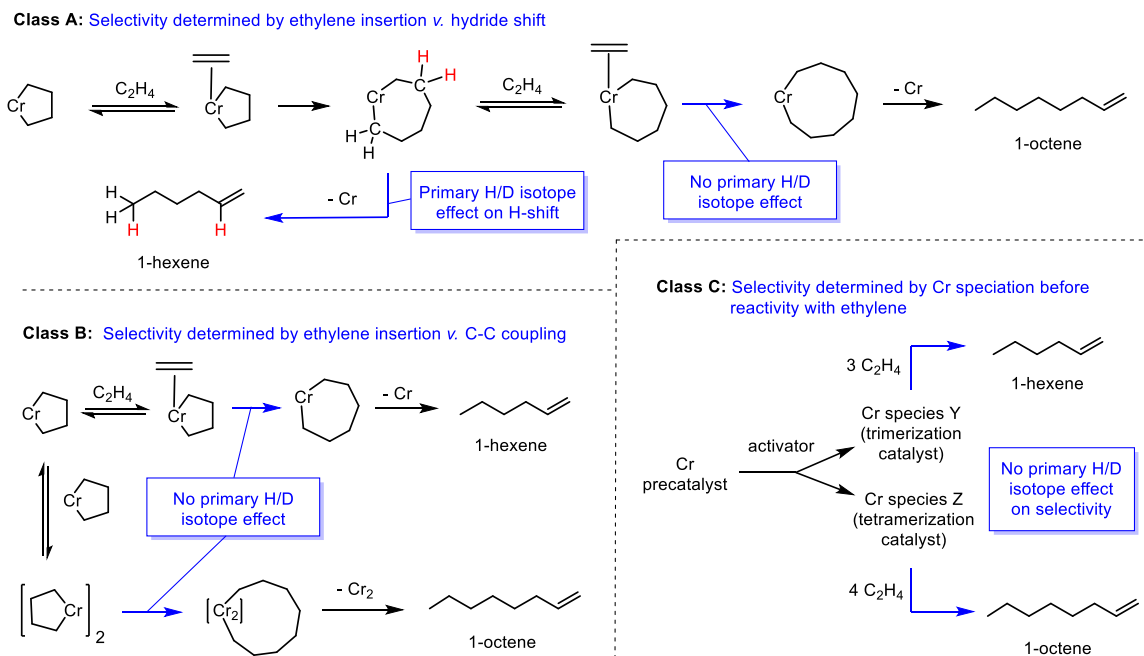
A. Formation of both 1-hexene and 1-octene proceeds via a common chromacycloheptane intermediate (Scheme 1, top); selectivity is governed by the relative rates of ethylene insertion and 1-hexene elimination from that intermediate.

B. A dinuclear species formed from two chromacyclopentane intermediates leads to C-C coupling and formation of 1-octene, whereas only 1-hexene is produced from a chromacycloheptane species (Scheme 1, bottom left).<sup>6</sup>

C. Two distinct catalysts are formed, each being selective for either 1-hexene or 1-octene. Overall selectivity is determined by the speciation of Cr following activation via MMAO and relative activities of the two catalysts (Scheme 1, bottom right).

Computational studies aimed at explaining ethylene tetramerization selectivity have focused on a class A mechanism;<sup>7</sup> however, no direct experimental evidence ruling out

**Scheme 1.** Different mechanistic proposals explaining 1-octene selectivity relative to 1-hexene are organized into three classes: A, B, or C.



classes B or C has yet been put forward. Ligand design strategies directed towards the goal of inducing Cr catalyst dimerization (class B) have been reported.<sup>6,8</sup> Class C has not been specifically addressed in the literature to our knowledge, but cannot be disregarded a priori considering the complicated nature of typical activation methods<sup>9</sup> and PNP ligand architectures.<sup>10</sup>

We have employed isotopic labelling mechanistic tests<sup>3-4</sup> to gain new mechanistic insight in this study. Previously, oligomerization of a mixture of  $C_2H_4/C_2D_4$  using a catalyst capable of ethylene tetramerization was found to give differential incorporation of  $C_2H_4$  vs.  $C_2D_4$  in 1-hexene and 1-octene, indicating that the selectivity between 1-hexene and 1-octene is subject to an isotope effect.<sup>4</sup> The result was interpreted in terms of secondary KIEs in chromacyclopentane formation, the presumed rate-determining step.<sup>4</sup> Although a KIE on ethylene oxidative coupling could lead to a difference in isotopic composition between 1-

hexene and 1-octene, we suspected that secondary KIEs were not sufficient to explain the magnitude of this effect. As the observation of this isotope effect may be relevant to the selectivity issue, we felt a more detailed exploration was warranted.

## Results and Discussion.

Co-oligomerization of  $C_2H_4$  and  $C_2D_4$  was carried out using two catalysts that lead to substantial formation of both 1-octene and 1-hexene. One was generated by activation with excess MMAO of a mixture of  $CrCl_3(THF)_3$  and PNP ligand  $(Ph_2P)_2N(i-Pr)$  (**1**); the other by stoichiometric activation with acid of  $Cr(CH_3)[(C_6H_4CH_2)_2O][(Ph_2P)_2N(p-tolyl)]$  (**2**, see Figure 1). Oligomeric product isotopologues were quantified by GC/MS as in previous studies (see Experimental Section for details).<sup>3,4,11</sup>

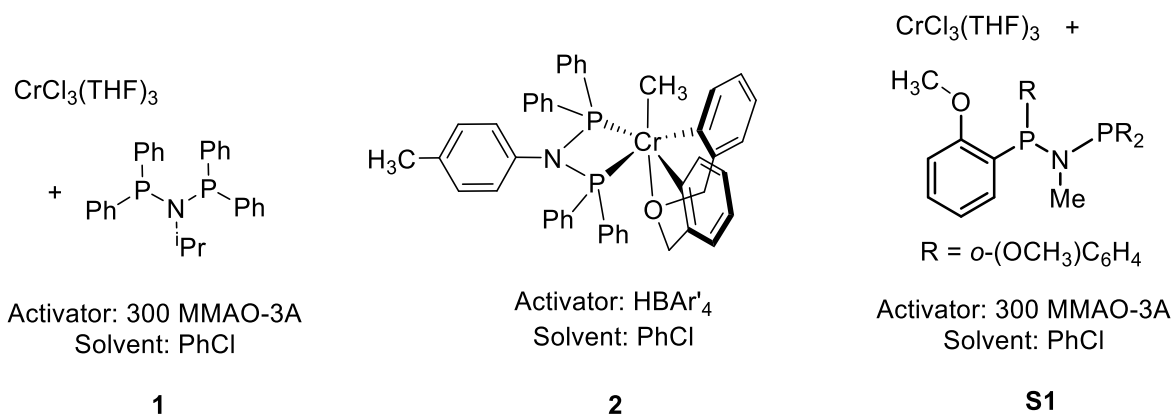


**Figure 1.** Catalyst **1** is formed by the addition of 300 equiv. MMAO-3A to a mixture of  $CrCl_3(THF)_3$  and  $iPr$ PNP. Catalyst **2** is formed by protonolysis of a PNP-ligated  $Cr$  tris(hydrocarbyl) precatalyst.<sup>18</sup> Catalyst **S1** was used as a 1-hexene selective control.

As previously reported, both oligomers show  $m/z$  values that are multiples of four for the major isotopologues (112, 116, 120, 124, 128 for 1-octene; 84, 88, 92, 96 for 1-hexene), consistent with a metallacyclic mechanism. Visual inspection of the MS data (shown in Figure 2) reveals that the 1-octene fraction is enriched in deuterium relative to the 1-

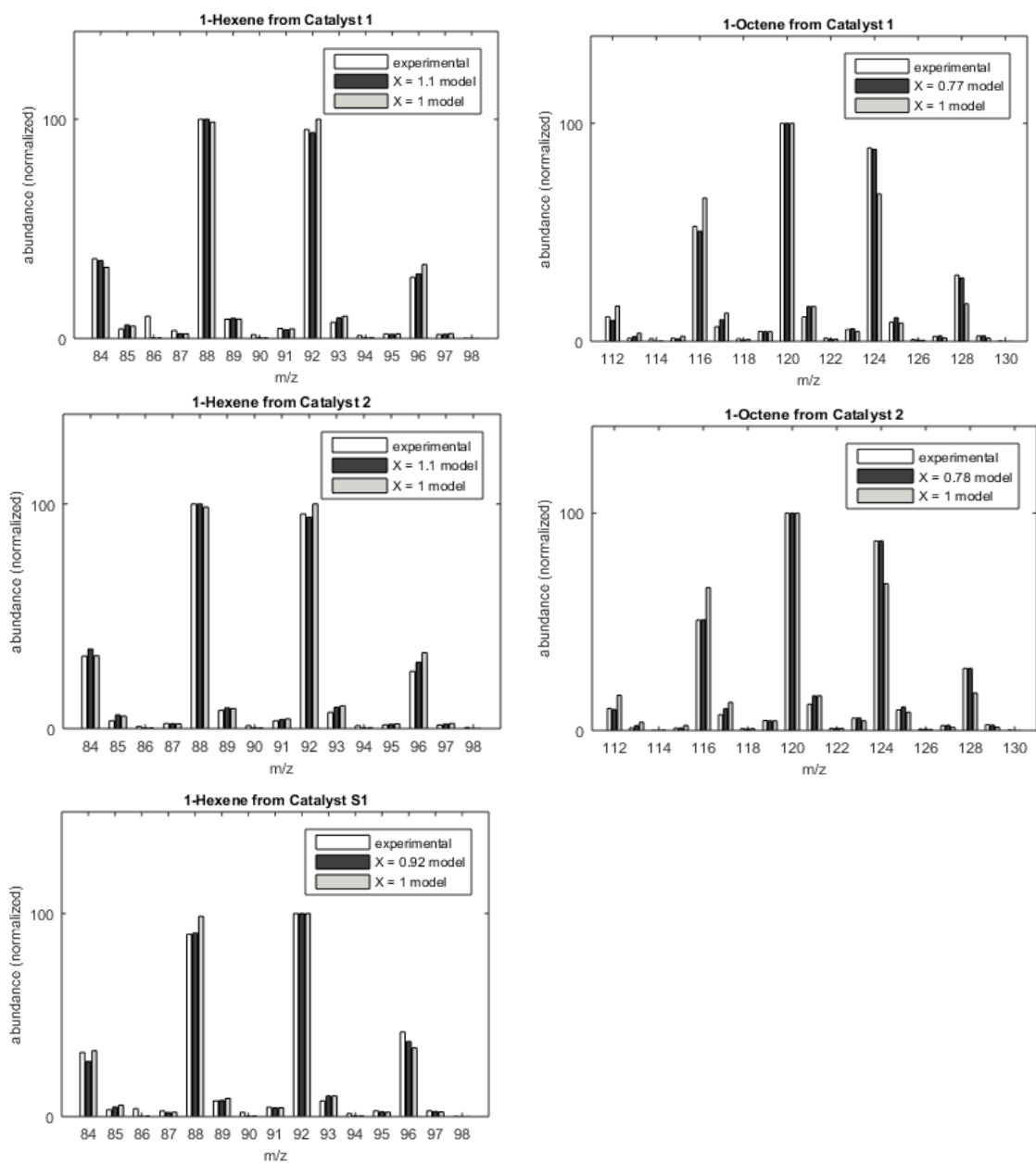


**Figure 2.** Isotopologue distributions of 1-hexene and 1-octene from catalyst **1** (top), and catalyst **2** (middle), as well as the isotopologue distribution from trimerization-selective **S1** (bottom).

hexene fraction. The MS data was modelled to determine the H:D ratio of each oligomer (details in Experimental section) and found to be the same within experimental uncertainty for both catalysts **1** and **2**. The H:D ratio ( $X$ ) is 1.1 for 1-hexene and 0.77 for 1-octene in catalysis using **1**, and  $X_{\text{hexene}} = 1.1$ ,  $X_{\text{octene}} = 0.78$  with **2**. These values correspond to overall incorporation of 56-57% D in 1-octene and 48% D in 1-hexene, from a starting gas mixture of (nominally) 50% D. Clearly, there is a preference for deuterons to incorporate in 1-octene relative to 1-hexene. This suggests a normal KIE in a step leading to 1-hexene (or, conceivably, an inverse KIE in a step leading to 1-octene formation; or even both).<sup>12</sup> This is consistent with the observation made by Overett and coworkers.<sup>4</sup> The  $X_{\text{hexene}}$  (2.5) and  $X_{\text{octene}}$  values (1.9) obtained by Overett and coworkers were much higher than their  $X_{\text{ethylene}}$  ( $\approx 1.3$ ),<sup>4</sup> but we do not see such a discrepancy. Most reassuringly, the ratio of  $X_{\text{hexene}}$  to  $X_{\text{octene}}$  in both of our studies is similar (1.3 & 1.4), confirming the reproducibility of this observation.

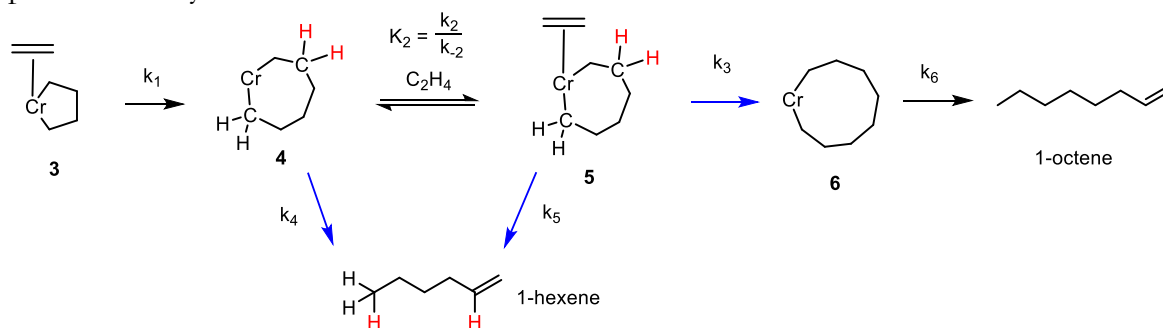
In mechanisms of class A, selectivity between 1-hexene and 1-octene is determined by the relative rates of a C-H bond cleaving step (either hydride-shift or  $\beta$ -H elimination followed by reductive elimination) leading to olefin elimination vs. ethylene insertion. The former is expected to exhibit a normal H/D isotope effect, which would be consistent with the experimental observations.<sup>3b</sup>

In mechanisms of class B, selectivity is determined by relative rates of C-C coupling of metallacyclopentanes or steps leading up to C-C coupling versus ethylene insertion. Neither involves formation or cleavage of a C-H or Cr-H bond, and hence no primary H/D KIE is expected. It is worth noting that selectivity in class B mechanisms could be affected by Cr concentration, as one of the competing pathways involves coupling of two Cr species. Selective ethylene tetramerization catalysts can be generated under quite dilute conditions;<sup>1a,1b,4</sup> which may suggest such mechanisms are not operative, although it is

conceivable that a dinuclear or multinuclear Cr species could be the active species for catalysis via mechanism class A, as precatalysts are commonly Cr dinuclear species,<sup>1a</sup> and dimerization of Cr complexes is well established.<sup>13</sup>

In mechanisms of class C, selectivity is determined by catalyst speciation resulting from precatalyst activation and/or subsequent initiation steps. Previous work using methylaluminoxane activation has shown that an active trimerization catalyst species comprises only a small fraction of the total Cr content.<sup>9c</sup> A selectivity explanation based on Class C would mean that two of these species (Y and Z) are separately responsible for 1-hexene and 1-octene formation; but if that were the only factor, both product isotopologue distributions should be equally representative of the starting gas mixtures, inconsistent with our experimental data. Although secondary isotope effects may be operable (e.g. on ethylene oxidative coupling) the magnitude of these effects would likely not be different between species Y and Z. Having more than one active species remains conceivable; for example, there could be one highly selective trimerization catalyst along with a second that produces a mixture of trimers and tetramers via a class A mechanism. Such a scenario seems unlikely since the same results are obtained from both **1** and **2**, which are prepared by different routes, but cannot be ruled out conclusively.

**Scheme 2.** A new mechanistic proposal (mechanism A1) in class A. This is consistent with the isotope effect data and explains the limit to 1-octene selectivity in high-pressure catalysis.



Overall, the results of the oligomerization of a mixture of  $C_2H_4/C_2D_4$  appear most consistent with mechanisms in class A: those involving a common chromacycloheptane intermediate along the path to form 1-hexene and 1-octene. As remarked above, several theoretical studies have investigated Cr-based ethylene tetramerization catalysis assuming mechanisms in class A,<sup>7</sup> but have not provided a commonly accepted explanation for why 1-octene selectivity is limited to  $\approx 75\%$  even under increased ethylene pressures.<sup>1a,2e,7a</sup> Since the 1-octene:1-hexene ratio shows some dependence on ethylene pressure, achieving higher selectivity is likely possible under certain conditions. But pressure increases have not resulted in a commensurate shift in the 1-octene:1-hexene ratio.<sup>2e,7a</sup> To rationalize this, we propose the specific mechanism A1 in Scheme 2, which includes two pathways for 1-hexene formation: one via elimination from **4**, the other via elimination from **5**. McGuinness, Britovsek and coworkers have considered the equilibrium between **4** and **5**, but computationally ruled out a two-step process (starting with hydride migration to the ethylene ligand) leading to 1-hexene from **5**.<sup>7a</sup> In a subsequent computational study, direct 1-hexene formation from **5** was discussed, but not incorporated into a general mechanistic proposal.<sup>7b</sup> According to mechanism A1, at high pressures of ethylene,  $[5] \gg [4]$  and 1-hexene is formed predominantly from **5** (assuming  $k_4$  is not very much greater than  $k_5$ ). Then the equation for the selectivity ratio, 1-octene:1-hexene (see Experimental section for derivation), reduces to:

$$\frac{1\text{-octene}}{1\text{-hexene}} = \frac{k_3}{k_5} \quad (1)$$

which is independent of ethylene pressure. Thus this mechanism can account for the experimentally observed (to date) limit to tetramerization selectivity.

Mechanisms in class A carry a further important and testable implication: oligomerization of pure  $C_2H_4$  or  $C_2D_4$  in separate experiments should give different 1-

octene:1-hexene ratios, and furthermore that difference should be quantitatively related to the primary kinetic isotope effect on hydride shift (or  $\beta$ -H elimination). Assuming saturation in ethylene, as above, we get the following equation for the selectivity ratios with the two isotopologous ethylenes:

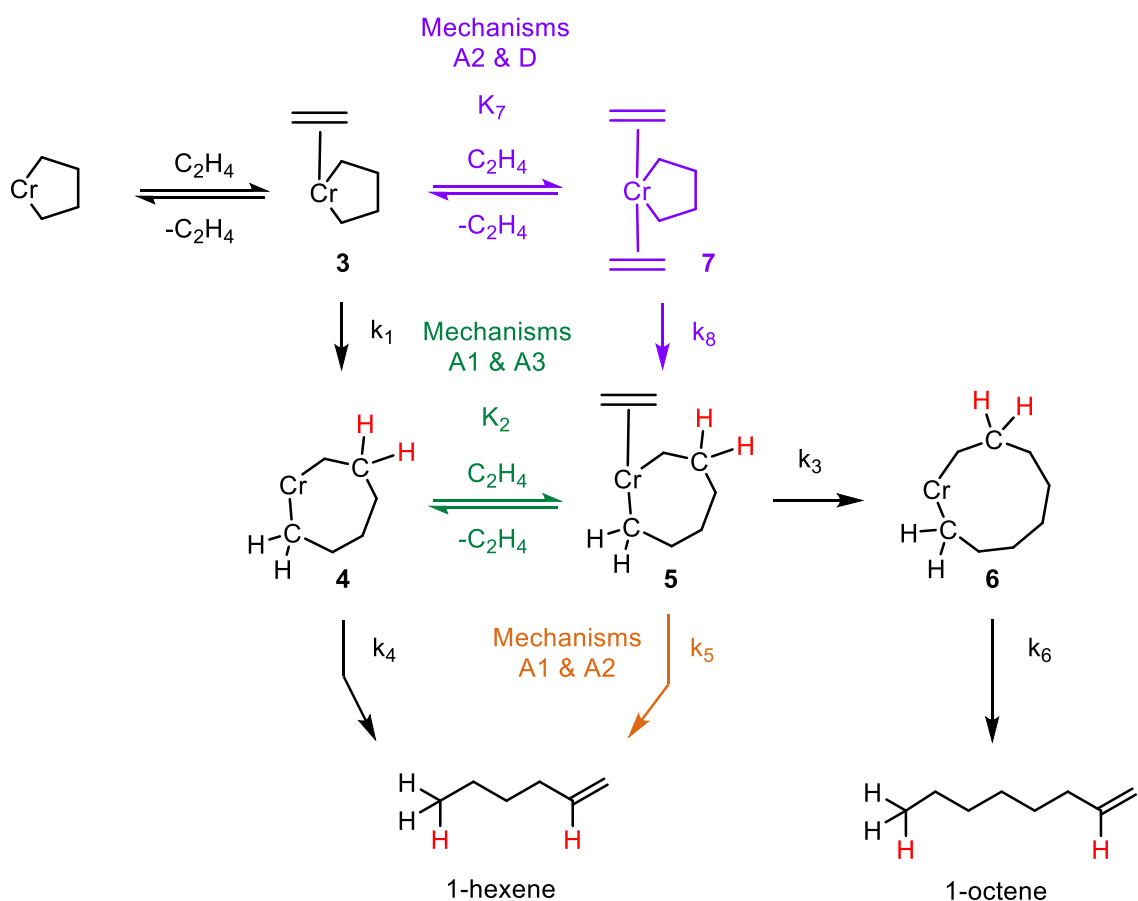
$$\frac{k_{5H}}{k_{5D}} = \frac{\frac{1\text{-octene(D)}}{1\text{-hexene(D)}}}{\frac{1\text{-octene(H)}}{1\text{-hexene(H)}}} \quad (2)$$

Due to the use of isotopically-labelled gas, we could not utilize industrially-relevant high pressures (450-600 psi), and saturation kinetics may not be operable; however, equation (2) remains valid if mechanism A1 is operable and KIE-4 = KIE-5, regardless of the relative values of [4] and [5] (see Experimental section for derivations).

**Mechanism A1 and its Variants (A2, A3, and D):** Variants of mechanism A1 (A2, A3, and D) are discussed here with regard to their consistency with both a primary H/D KIE and the typical 1-octene selectivity limits. Two of these are based on an alternative scenario proposed by McGuinness, Britovsek, and coworkers,<sup>7a-c</sup> wherein a second ethylene binds reversibly to **3** forming species **7**, as shown in Scheme 3. Subsequent migratory insertion of the ethylene ligand in **7** leads to **5**; **4** and **5** do not interconvert in those cases.

In mechanisms A1 and A3, ethylene insertion in **3** is very rapid relative to additional binding of ethylene ( $k_1 \gg k_7$ ). So,  $K_2$  governs a fast pre-equilibrium between **4** and **5**, such that  $k_2, k_{-2} \gg k_3, k_4, k_5$ . In mechanisms A2 and D, ethylene insertion in **3** and **7** is slow relative to ethylene coordination/dissociation ( $k_1, k_8 \ll k_7, k_{-7}$ ) and reactions from **4** and **5** are fast ( $k_3, k_4, k_5 \gg k_2, k_{-2}$ ). In mechanisms A1 and A2, the step leading to 1-hexene from **5** is included, whereas mechanisms A3 and D exclude that step. Mechanism D is not technically a class A mechanism (hence its label) as we have defined it, since 1-hexene and 1-

**Scheme 3.** Mechanism A1 and its variations (A2, A3, and D). See Experimental section for explicit outline of each individual proposed mechanism.



octene are not both formed via a common chromacycloheptane intermediate; hence selectivity in mechanism D is not expected to depend on a primary H/D KIE. Selectivities in mechanisms A1, A2, and A3 all do rely on a primary H/D KIE. However, the value of this KIE cannot be determined from our experiments if mechanism A2 is operable, and saturation kinetics are not (the derivation is shown in the Experimental section). Therefore, mechanisms A1, A2, and A3 are consistent with all our experimental data. Only for mechanisms A1 and A3 is equation (2) valid for all ethylene concentrations.

Ethylene oligomerization was performed in three separate trials using catalyst **2**, at  $\approx 100$  psi  $C_2H_4$  or  $C_2D_4$  initial pressure, in a sealed thick-walled glass vessel. The 1-octene:1-hexene

selectivity ratios for all three trials were averaged (Table 1); the ratio of those ratios is  $2.4 \pm 0.3$ , which (based on the built-in assumptions) gives us the value of  $\text{KIE-4} = \text{KIE-5}$ . If consideration of cyclic  $\text{C}_6$  coproducts is made, then the KIE may be as high as  $3.0 \pm 0.3$  (see Experimental section for details). These values are consistent with a primary H/D isotope effect, and are close to a reported value for ethylene trimerization ( $3.1 \pm 0.1$ ),<sup>3b</sup> providing strong further support for a class A mechanism. (Mechanisms in class A are discussed above with regard to their consistency with both a primary H/D KIE and the typical 1-octene selectivity limits.) This result is inconsistent with mechanisms in class B. While mechanisms in class C are not ruled out per se (there could be an H/D isotope effect on catalyst initiation or speciation), they are incompatible with the mixed-gas experiments (vide supra). Finally, the notion that the most significant KIE (regardless of its magnitude) originates in ethylene oxidative coupling is ruled out by the selectivity difference in the use of pure  $\text{C}_2\text{H}_4$  vs. pure  $\text{C}_2\text{D}_4$ . Oxidative coupling leads to both 1-hexene and 1-octene in all mechanistic proposals, so a KIE on that step would not lead to a difference in selectivity for  $\text{C}_2\text{H}_4$  vs.  $\text{C}_2\text{D}_4$ .

**Table 1.** Results from oligomerization of pure  $\text{C}_2\text{H}_4$  or pure  $\text{C}_2\text{D}_4$  using catalyst **2**.

<b>Gas</b>	<b>Productivity (g/g Cr)</b>	<b>1-C<sub>6</sub> (mol %)</b>	<b>1-C<sub>8</sub> (mol %)</b>	<b>1-octene: 1-hexene</b>
$\text{C}_2\text{H}_4$	$180 \pm 10$	$42 \pm 3$	$43 \pm 3$	$1.0 \pm 0.1$
$\text{C}_2\text{D}_4$	$160 \pm 10$	$28 \pm 1$	$69 \pm 1$	$2.4 \pm 0.2$

## Conclusion.

We have presented experimental evidence for a primary H/D kinetic isotope effect on the selectivity between 1-octene and 1-hexene in Cr-catalyzed ethylene oligomerization. Such a KIE on product selectivity rules out several proposals for 1-octene formation: C-C

coupling of chromacyclopentanes or speciation of Cr into separately selective tetramerization and trimerization catalysts. Mechanisms displaying chromacycloheptanes as common intermediates are supported by our isotopic labelling experiments, and involve H-transfer at the branching point that determines selectivity.

## Experimental.

**General Considerations.** All glassware was oven-dried and kept under active vacuum prior to use. Chlorobenzene was distilled from  $\text{CaH}_2$ , stored over activated molecular sieves for at least 24 hours, and filtered through activated alumina directly before use. M-MAO 3A was purchased from AkzoNobel as a 7% w/w Al solution in heptane. Ethylene- $\text{H}_4$  gas was purchased from Sigma-Aldrich (99.99%) in a lecture bottle and immediately before use in catalysis was thawed under static vacuum from its condensed state in a cooled trap using high vacuum line techniques. Ethylene- $\text{D}_4$  gas was purchased from Cambridge Isotope Laboratories (98%-D) in a lecture bottle, and stored in a glass storage bulb under partial vacuum over dried, methylaluminoxane-treated silica (prepared using a similar procedure to that described by Bercaw and coworkers<sup>14</sup>) to remove traces of moisture. Immediately before use in catalysis, the ethylene- $\text{D}_4$  was thawed under static vacuum from its condensed state using high vacuum line techniques.  $\text{CrCl}_3(\text{THF})_3$  was synthesized according to the literature procedure, using  $\text{CrCl}_3$  (anhydrous) purchased from Strem.<sup>15</sup> The synthesis of  $^{i\text{Pr}}\text{PNP}$ ,  $\text{PNP}^{(\text{OMe})4}$ ,  $[\text{H}(\text{Et}_2\text{O})_2][\text{BAr}'_4]$ , and  $(^{101}\text{PNP})\text{Cr}((o\text{-C}_6\text{H}_4\text{CH}_2)_2\text{O})(\text{Me})$  have been previously reported.<sup>1g,2a,16</sup> Gas chromatography (GC) was performed on an Agilent 6890A instrument using a DB-1 capillary column (10 m length, 0.10 mm diameter, 0.40  $\mu\text{m}$  film) and a flame ionization detector. Gas chromatography/mass spectrometry (GC-MS)

was performed on an Agilent 6890A instrument using a HP-5MS column (30 m length, 0.25 mm diameter, 0.50  $\mu\text{m}$  film) and an Agilent 5973N mass-selective EI detector.

**Oligomerization Catalysis Using 1:1  $\text{C}_2\text{H}_4:\text{C}_2\text{D}_4$ .** For catalyst **1**, a 1.2 mL mixture of  $\text{CrCl}_3(\text{THF})_3$  (1.6 mM concentration) and  $^{i\text{Pr}}\text{PNP}$  (1.7 mM concentration) in PhCl was added to a thick-walled 8 mL glass Schlenk tube equipped with a stirbar in a nitrogen-filled glovebox. The solution was frozen in the cold well, then a 0.32 mL solution of MMAO-3A (300 equiv. Al relative to Cr) was layered on top. The Schlenk tube was sealed with a Kontes pin, then taken to the high-vacuum line and degassed using three freeze-pump-thaw cycles, resulting in an activated Cr solution with  $[\text{Cr}] = 1.3 \text{ mM}$ .

For catalyst **2**, a 1.0 mL solution of  $(^{o\text{l}}\text{PNP})\text{Cr}((\text{o-C}_6\text{H}_4\text{CH}_2)_2\text{O})(\text{Me})$  (1.9 mM concentration) was prepared in a vial equipped with a stirbar in a nitrogen-filled glovebox. This solution was frozen in the cold well, then a 0.5 mL solution of  $[\text{H}(\text{Et}_2\text{O})_2][\text{BAR}'_4]$  (1 equiv., 3.8 mM concentration) was added to the thawing solution. Upon warming to room temperature, the mixture was transferred to a thick-walled 8 mL glass Schlenk tube, along with the stirbar. The Schlenk tube was sealed with a Kontes pin, then taken to the high-vacuum line and degassed using three freeze-pump-thaw cycles, resulting in an activated Cr solution with  $[\text{Cr}] = 1.3 \text{ mM}$ .

For catalyst **S1** (known to be selective for trimerization only), a 1.2 mL mixture of  $\text{CrCl}_3(\text{THF})_3$  (1.6 mM concentration) and  $\text{PNP}^{(\text{OMe})_4}$  (1.7 mM concentration) in PhCl was added to a thick-walled 8 mL glass Schlenk tube equipped with a stirbar in a nitrogen-filled glovebox. The solution was frozen in the cold well, then a 0.32 mL solution of MMAO-3A (300 equiv. Al/Cr) was layered on top. The Schlenk tube was sealed with a Kontes pin, then taken to the high-vacuum line and degassed using three freeze-pump-thaw cycles, resulting in an activated Cr solution with  $[\text{Cr}] = 1.3 \text{ mM}$ .

For catalysis using **1**, **2**, or **S1**,  $C_2H_4$  and  $C_2D_4$  gas were independently measured in a calibrated glass bulb under partial vacuum, using high-vacuum line techniques. The gases were then mixed in a separate bulb, then condensed into the glass Schlenk tube containing a solution of the activated Cr species ( $[Cr] = 1.3 \text{ mM}$ ), and the tube was sealed with a Kontes pin. Approximately 1100 total equivalents of ethylene were added to the tube in this manner. After thawing the tube in a room temperature water bath, and allowing the solution to stir for 5 minutes, the reaction was cooled to  $-78^\circ\text{C}$ , to freeze the chlorobenzene solvent. The tube was degassed using two freeze-pump-thaw cycles, then back-filled with argon. Next, the solution was quenched using 0.1 mL methanol (for the reactions using MMAO activation, acetone was used to dilute the suspension that formed upon quenching). A weighed amount of adamantane dissolved in acetone was added to the resulting quenched solution (or suspension, for catalysis with MMAO), which was filtered and analyzed by GC/FID to quantify the oligomers vs. adamantane. An appropriately diluted solution was analyzed by GC/MS to quantify the isotopologues of 1-hexene and 1-octene which were produced. Isotopologues of each oligomer co-eluted on the GC with only slightly shifted retention times. Therefore, quantitation of each isotopologue was achieved by recording the abundance of the parent ions detected by the MS analyzer across the full breadth of the signal in the GC trace. Figure 2 shows the isotopologue distributions for 1-hexene and 1-octene from catalysis using **1**, **2**, and **S1**.

**MS Experimental and Modelled Data from the Mixed Gas Experiments.** The experimental isotopologue abundances for each fraction (1-hexene or 1-octene) are modelled according to the procedure outlined by Overett and coworkers. The ratios of  $C_2H_4:C_2D_4$  (or simply H:D) incorporated into each fraction, “X”, can be determined thereby, and are given in Table 2. Figure 2 shows the experimental data, the best-fit model, and the  $X = 1$  model

(for comparison) for fractions of products obtained from catalysts **1**, **2**, and **S1**. It is notable that  $X_{1\text{-hexene}}$  from **S1** is not 1.0, but 0.92. This could be a result of error in the individual measurement of  $C_2H_4$  &  $C_2D_4$  gases or due to a secondary isotope effect on ethylene binding, oxidative coupling, or migratory insertion, whereby deuterated olefins react faster than non-deuterated olefins. If such a secondary isotope effect is operating, it could affect our calculated results, but the qualitative conclusions would remain valid, as both fractions (1-hexene and 1-octene) should be influenced similarly by such a KIE regardless of which class of mechanisms is considered.

**Table 2.** H:D isotope ratios in the products from catalysts **1**, **2**, and **S1**

Catalyst	$X_{\text{hexene}}$	$X_{\text{octene}}$
<b>1</b>	1.1	0.77
<b>2</b>	1.1	0.78
<b>S1</b>	0.92	--

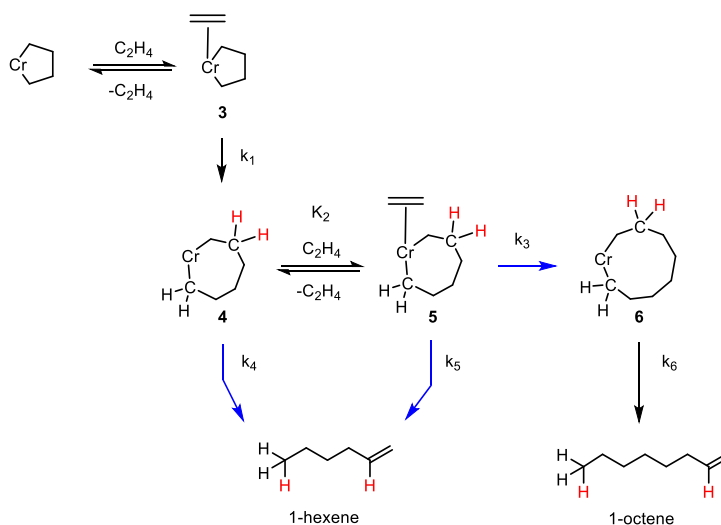
**Oligomerization Catalysis Using Pure  $C_2H_4$  or Pure  $C_2D_4$ .** A solution of catalyst **2** ( $[Cr] = 1.3$  mM) was prepared and degassed in the Schlenk tube as described in the sections above. The same batch of activated Cr solution was divided for use in separate experiments using  $C_2H_4$  and  $C_2D_4$ , to control for variability in the precatalyst activation process. Ethylene gas (approximately 1100 equivalents relative to Cr) was condensed into each Schlenk tube using high vacuum line techniques. The Schlenk tubes were sealed, and the frozen mixtures were thawed in a room temperature water bath for one minute. Then, the solutions were cooled to  $-78^\circ C$ , to freeze the chlorobenzene solvent. The tubes were degassed using two freeze-pump-thaw cycles, then back-filled with argon. Next, the solutions were quenched using 0.1 mL methanol. Weighed amounts of adamantane were dissolved in acetone and were added to the resulting quenched solutions, which were filtered and analyzed by

GC/FID to quantify the oligomers vs. adamantane. Results are shown in Table 3; it can be seen that reproducibility in terms of overall activity (as measured by the total weight of products per weight of Cr) and product distribution is quite good.

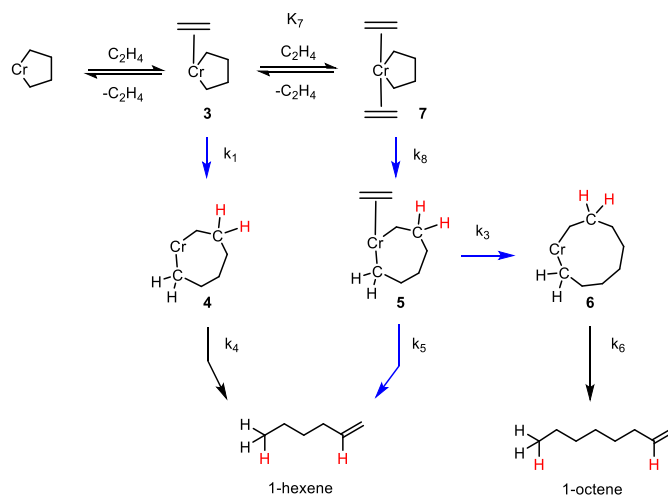
**Table 3.** Oligomeric products from C<sub>2</sub>H<sub>4</sub> and C<sub>2</sub>D<sub>4</sub> using catalyst **2**

Entry	Gas	Yield (g)	g/g Cr	equiv. C <sub>2</sub> H <sub>4</sub> in products	mol % 1-hexene	mol % 1-octene	mol % cyclic C <sub>6</sub>	1-octene: 1-hexene
1	C <sub>2</sub> H <sub>4</sub>	0.017	160	290	41%	44%	15%	1.07
2	C <sub>2</sub> H <sub>4</sub>	0.020	190	350	40%	45%	15%	1.13
3	C <sub>2</sub> H <sub>4</sub>	0.018	180	340	46%	39%	15%	0.85
Average		0.018	180	330	42%	43%	15%	1.02
Std Dev		0.001	10	30	3%	3%	0%	0.12
4	C <sub>2</sub> D <sub>4</sub>	0.018	170	320	30%	67%	2.5%	2.23
5	C <sub>2</sub> D <sub>4</sub>	0.015	160	290	27%	70%	2.9%	2.59
6	C <sub>2</sub> D <sub>4</sub>	0.014	140	260	28%	69%	2.3%	2.46
Average		0.016	160	290	28%	69%	2.6%	2.43
Std Dev		0.002	10	30	1%	1%	0.2%	0.15
Ratio								2.39
Error								0.32

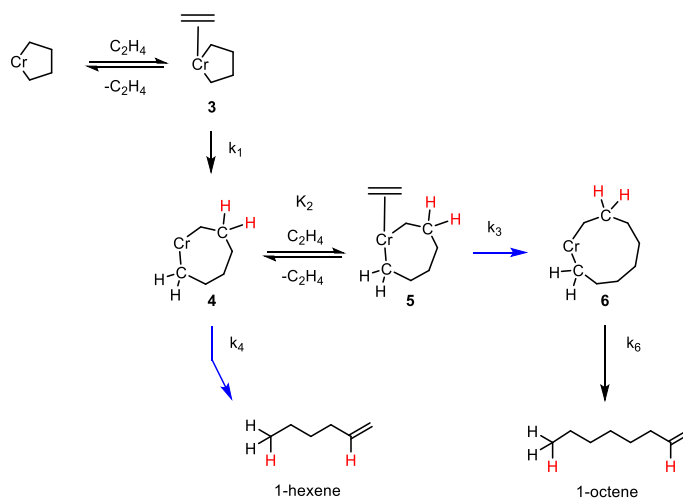
**Scheme 4.** Mechanism A1, which is operable when metallacycle expansion from **3** is rapid relative to further ethylene binding (distinguishing this from Mechanisms A2 or D). Also, 1-hexene is formed from both **4** and **5** (distinguishing this from Mechanism A3).



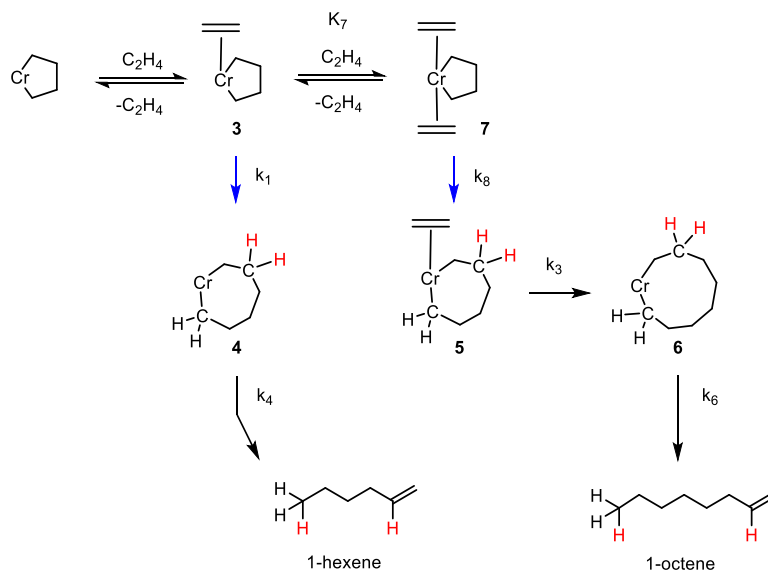
**Scheme 5.** Mechanism A2, which is operable when metallacycle expansion from **3** or **7** is slow relative to further ethylene binding/dissociation. Reactivity from **4** or **5** (via 1-hexene elimination or metallacycle expansion) is rapid relative to ethylene binding or dissociation (distinguishing this from mechanisms A1 or A3). Also, 1-hexene is formed from both **4** and **5** (distinguishing this from Mechanism D).



**Scheme 6.** Mechanism A3, which is operable when metallacycle expansion from **3** is rapid relative to further ethylene binding (distinguishing this from Mechanisms A2 or D). Also, 1-hexene is not formed from **5** (distinguishing this from Mechanism A1).



**Scheme 7.** Mechanism D, which is operable when metallacycle expansion from **3** or **7** is slow relative to further ethylene binding/dissociation. Reactivity from **4** or **5** (via 1-hexene elimination or metallacycle expansion) is rapid relative to ethylene binding or dissociation (distinguishing this from mechanisms A1 or A3). Also, 1-hexene is not formed from **5** (distinguishing this from Mechanism A2).



### Analysis of Mechanisms A1, A2, A3, and D.

For Mechanism A1, the selectivity for 1-octene (relative to 1-hexene) is given according to:

$$\text{rate (1-octene)} = \frac{k_2 k_3 [\mathbf{4}] [\text{C}_2\text{H}_4]}{k_{-2}} \quad (1)$$

$$\text{rate (1-hexene)} = k_4 [\mathbf{4}] + \frac{k_2 k_5 [\mathbf{4}] [\text{C}_2\text{H}_4]}{k_{-2}} \quad (2)$$

$$\frac{\text{rate (1-octene)}}{\text{rate (1-hexene)}} = \frac{\frac{k_2 k_3 [\text{C}_2\text{H}_4]}{k_{-2}}}{k_4 + \frac{k_2 k_5 [\text{C}_2\text{H}_4]}{k_{-2}}} \quad (3)$$

If under saturation kinetics,  $\frac{k_2 k_5 [\text{C}_2\text{H}_4]}{k_{-2}} \gg k_4$ , then:

$$\frac{\text{rate (1-octene)}}{\text{rate (1-hexene)}} = \frac{\frac{k_2 k_3 [\text{C}_2\text{H}_4]}{k_{-2}}}{\frac{k_2 k_5 [\text{C}_2\text{H}_4]}{k_{-2}}} = \frac{k_3}{k_5} \quad (4)$$

Using equation 4 (under the saturation kinetics approximation), and assuming no isotope effect on metallacycle expansion ( $k_3$ ) it can easily be seen that:

$$\frac{\frac{1\text{-octene(D)}}{1\text{-hexene(D)}}}{\frac{1\text{-octene(H)}}{1\text{-hexene(H)}}} = \frac{\frac{\text{rate } 1\text{-octene (D)}}{\text{rate } 1\text{-hexene (D)}}}{\frac{\text{rate } 1\text{-octene (H)}}{\text{rate } 1\text{-hexene (H)}}} = \frac{\frac{k_{3D}}{k_{5D}}}{\frac{k_{3H}}{k_{5H}}} = \frac{k_{5H}}{k_{5D}} \quad (5)$$

If saturation kinetics are not operable, the derivation is as follows. Assuming no isotope effect on metallacycle expansion ( $k_{3H} = k_{3D}$ ), ethylene binding or dissociation ( $K_{2H} = K_{2D}$ ), or ethylene concentration ( $[C_2D_4] = [C_2H_4]$ ), the relative ratios of 1-octene to 1-hexene from  $C_2D_4$  and  $C_2H_4$  give the following relation, using equation 3:

$$\frac{\frac{1\text{-octene(D)}}{1\text{-hexene(D)}}}{\frac{1\text{-octene(H)}}{1\text{-hexene(H)}}} = \frac{k_{4H} + \frac{k_{2H}k_{5H}[C_2H_4]}{k_{-2H}}}{k_{4D} + \frac{k_{2D}k_{5D}[C_2D_4]}{k_{-2D}}} \quad (6)$$

Which, when KIE-4 = KIE-5:

$$\frac{k_{4H}}{k_{4D}} = \frac{k_{5H}}{k_{5D}} \quad (7)$$

And because  $[C_2D_4] = [C_2H_4]$ ,  $K_{2H} = K_{2D}$ , by expanding equation 6 and inserting rearranged equation 7:

$$\frac{\frac{1\text{-octene(D)}}{1\text{-hexene(D)}}}{\frac{1\text{-octene(H)}}{1\text{-hexene(H)}}} = \frac{k_{5H} \left( \frac{k_{4H}}{k_{5H}} + \frac{k_{2H}[C_2H_4]}{k_{-2H}} \right)}{k_{5D} \left( \frac{k_{4D}}{k_{5D}} + \frac{k_{2D}[C_2D_4]}{k_{-2D}} \right)} = \frac{k_{5H}}{k_{5D}} \quad (8)$$

For Mechanism A2, the selectivity for 1-octene (relative to 1-hexene) is given according to:

$$\text{rate (1-octene)} = \frac{k_7 k_8 k_3 [\mathbf{3}] [C_2H_4]}{k_{-7}(k_3 + k_5)} \quad (9)$$

$$\text{rate (1-hexene)} = k_1 [\mathbf{3}] + \frac{k_7 k_8 k_5 [\mathbf{3}] [C_2H_4]}{k_{-7}(k_3 + k_5)} \quad (10)$$

$$\frac{\text{rate (1-octene)}}{\text{rate (1-hexene)}} = \frac{\frac{k_7 k_8 k_3 [C_2H_4]}{k_{-7}(k_3 + k_5)}}{k_1 + \frac{k_7 k_8 k_5 [C_2H_4]}{k_{-7}(k_3 + k_5)}} \quad (11)$$

If under saturation kinetics,  $\frac{k_7 k_8 k_5 [C_2H_4]}{k_{-7}(k_3 + k_5)} \gg k_1$ , then:

$$\frac{\text{rate (1-octene)}}{\text{rate (1-hexene)}} = \frac{\frac{k_7 k_8 k_3 [C_2 H_4]}{k_{-7}(k_3 + k_5)}}{\frac{k_7 k_8 k_5 [C_2 H_4]}{k_{-7}(k_3 + k_5)}} = \frac{k_3}{k_5} \quad (12)$$

So, under the saturation kinetics approximation, equation 12 can be used to derive equation 5, as was done for the analysis of mechanism A1.

If saturation kinetics are not operable, and assuming no isotope effect on metallacycle expansion ( $k_{3H} = k_{3D}$ ,  $k_{8H} = k_{8D}$ ), ethylene binding or dissociation ( $K_{7H} = K_{7D}$ ), or ethylene concentration ( $[C_2 D_4] = [C_2 H_4]$ ), the relative ratios of 1-octene to 1-hexene from  $C_2 D_4$  and  $C_2 H_4$  give the following relation, using equation 11:

$$\frac{\frac{1\text{-octene(D)}}{1\text{-hexene(D)}}}{\frac{1\text{-octene(H)}}{1\text{-hexene(H)}}} = \frac{\frac{\text{rate } 1\text{-octene (D)}}{\text{rate } 1\text{-hexene (D)}}}{\frac{\text{rate } 1\text{-octene (H)}}{\text{rate } 1\text{-hexene (H)}}} = \frac{k_{1H}k_{3H} + k_{1H}k_{5H} + \frac{k_{8H}k_{7H}k_{5H}[C_2 H_4]}{k_{-7H}}}{k_{1D}k_{3D} + k_{1D}k_{5D} + \frac{k_{8D}k_{7D}k_{5D}[C_2 D_4]}{k_{-7D}}} \quad (13)$$

So, in mechanism A2, the H/D KIE of the step leading to elimination of 1-hexene can only be obtained *if*  $[7] \gg [3]$  that is, in the case of saturation kinetics.

For Mechanism A3, the selectivity for 1-octene (relative to 1-hexene) is given according to:

$$\text{rate (1-octene)} = \frac{k_2 k_3 [4] [C_2 H_4]}{k_{-2}} \quad (14)$$

$$\text{rate (1-hexene)} = k_4 [4] \quad (15)$$

$$\frac{\text{rate (1-octene)}}{\text{rate (1-hexene)}} = \frac{\frac{k_2 k_3 [C_2 H_4]}{k_{-2}}}{k_4} \quad (16)$$

So,

$$\frac{\text{rate (1-octene)}}{\text{rate (1-hexene)}} = \frac{k_2 k_3 [C_2 H_4]}{k_{-2} k_4} \quad (17)$$

And, the relative ratios of 1-octene to 1-hexene from  $C_2 D_4$  and  $C_2 H_4$  give the following relation:

$$\frac{\frac{1\text{-octene(D)}}{1\text{-hexene(D)}}}{\frac{1\text{-octene(H)}}{1\text{-hexene(H)}}} = \frac{\frac{\text{rate } 1\text{-octene (D)}}{\text{rate } 1\text{-hexene (D)}}}{\frac{\text{rate } 1\text{-octene (H)}}{\text{rate } 1\text{-hexene (H)}}} = \frac{k_{4H} \frac{k_{2D} k_{3D} [C_2 D_4]}{k_{-2D}}}{k_{4D} \frac{k_{2H} k_{3H} [C_2 H_4]}{k_{-2H}}} \quad (18)$$

And, if there is no isotope effect on ethylene binding or dissociation, metallacycle expansion, or on ethylene concentration  $K_{2H} = K_{2D}$ ,  $k_{3H} = k_{3D}$ , and  $[C_2D_4] = [C_2H_4]$ :

$$\frac{\frac{1\text{-octene(D)}}{1\text{-hexene(D)}}}{\frac{1\text{-octene(H)}}{1\text{-hexene(H)}}} = \frac{k_{4H}}{k_{4D}} \quad (19)$$

For Mechanism D, the selectivity for 1-octene (relative to 1-hexene) is given according to:

$$\text{rate (1-octene)} = \frac{k_7 k_8 [3] [C_2H_4]}{k_{-7}} \quad (20)$$

$$\text{rate (1-hexene)} = k_1 [3] \quad (21)$$

$$\frac{\text{rate (1-octene)}}{\text{rate (1-hexene)}} = \frac{k_7 k_8 [C_2H_4]}{k_1} \quad (22)$$

The selectivity in mechanism D is not governed by any step exhibiting a primary H/D KIE.

**Considering 1-Hexene Formation From  $\beta$ -H Elimination v. Hydride Shift (Or Both).** Heretofore we have simplified the analysis by not considering the formation of cyclic  $C_6$ 's. However, it can be seen from Table S2 that there is a significant isotope effect on the production of these two species (methylcyclopentane and methylenecyclopentane). Previous proposals have invoked  $\beta$ -H elimination from chromacycloheptanes (like **5**) as leading to these products (see Scheme 8). Of course, 1-hexene may be derived from this pathway, instead of from hydride shift. Or, 1-hexene may be derived from both. To account for cyclic  $C_6$  production, both  $k_9$  and  $k_{10}$  must be appreciable. The pertinent scenarios, and their effect on the KIE measurement, are outlined below:

Case 1:  $k_5$  is negligible but  $k_{11}$  is appreciable (1-hexene is only derived from a  $\beta$ -H elimination):

$$\frac{\frac{1\text{-octene(D)}}{1\text{-hexene(D)+cyclics(D)}}}{\frac{1\text{-octene(H)}}{1\text{-hexene(H)+cyclics(H)}}} = \frac{k_{9H}}{k_{9D}} = 3.0 \pm 0.3 \quad (23)$$

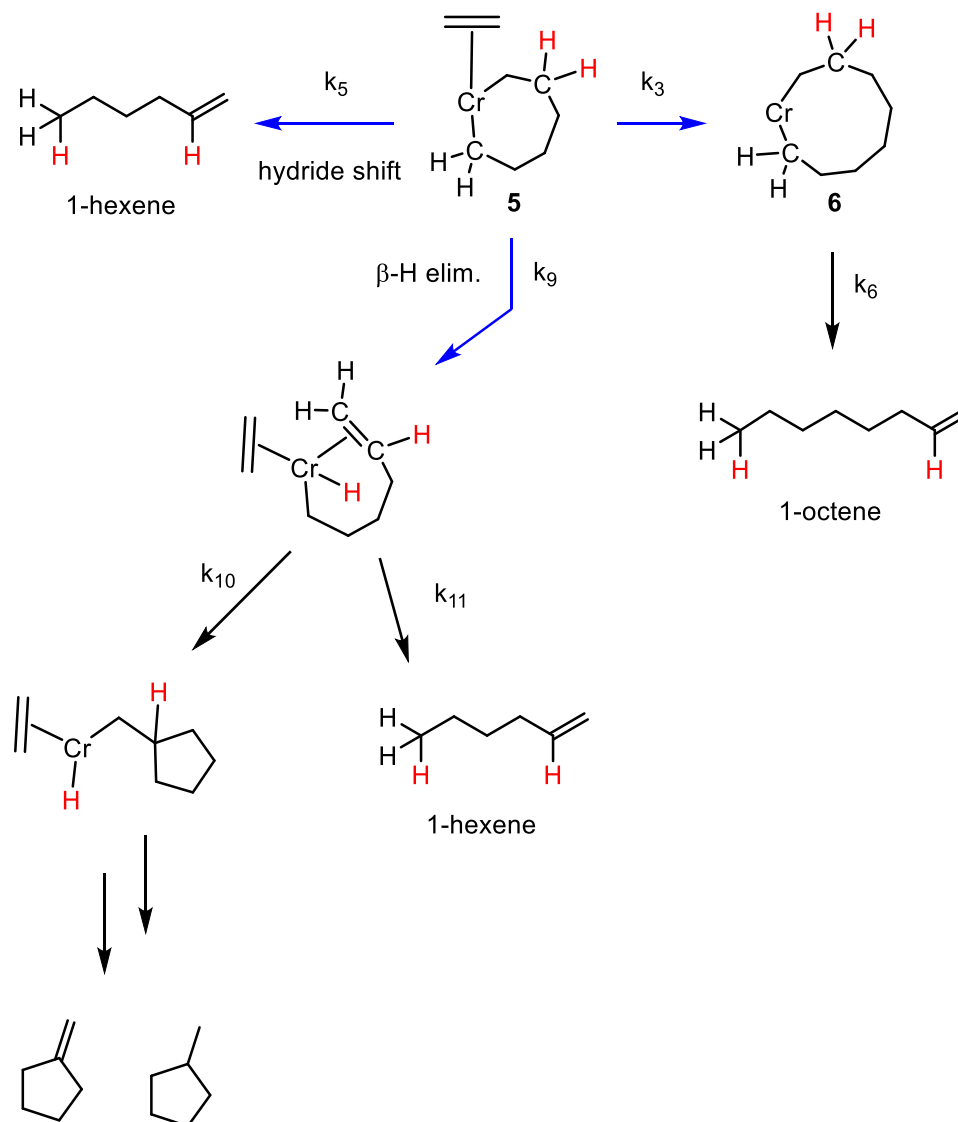
Case 2:  $k_{11}$  is negligible but  $k_5$  is appreciable (1-hexene is only derived from a hydride shift; this is the simplification used in the preceding sections):

$$\frac{\frac{1\text{-octene(D)}}{1\text{-hexene(D)}}}{\frac{1\text{-octene(H)}}{1\text{-hexene(H)}}} = \frac{k_{5H}}{k_{5D}} = 2.4 \pm 0.3 \quad (24)$$

Case 3: neither  $k_5$  nor  $k_{11}$  is negligible (1-hexene is derived from both pathways):

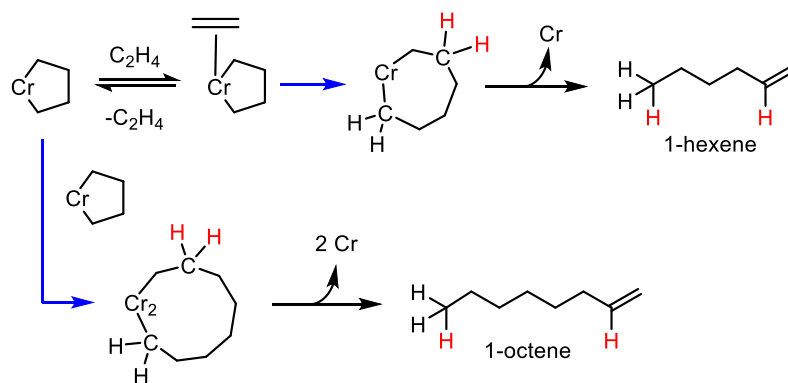
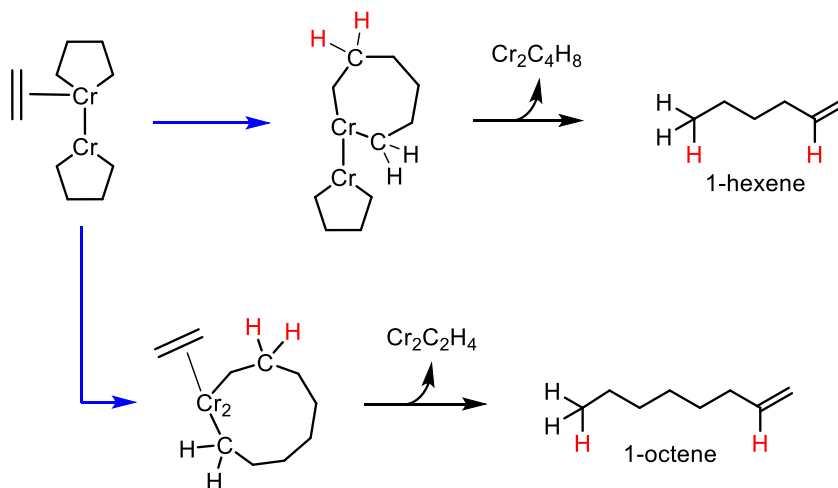
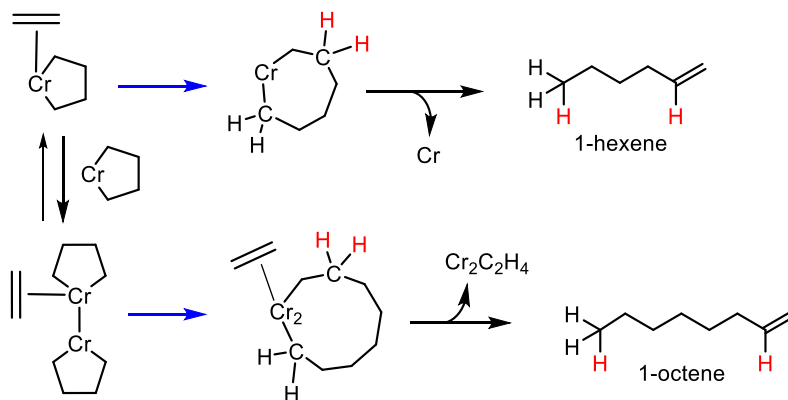
$$\frac{\frac{1\text{-octene(D)}}{1\text{-hexene(D)+cyclics(D)}}}{\frac{1\text{-octene(H)}}{1\text{-hexene(H)+cyclics(H)}}} = \frac{k_{5H} + k_{9H}}{k_{5D} + k_{9D}} = 3.0 \pm 0.3 \quad (25)$$

**Scheme 8.** Pathways to form the cyclic  $C_6$  products should start with  $\beta$ -H elimination (governed by  $k_9$ ). 1-Hexene may or may not be derived from this pathway.



### Mechanisms in Class B.

**Scheme 9.** Example mechanisms in class B, wherein 1-octene selectivity (relative to 1-hexene) is determined by the relative rate of C-C coupling versus ethylene insertion.



**References.**

- (1) (a) Bollmann, A.; Blann, K.; Dixon, J. T.; Hess, F. M.; Killian, E.; Maumela, H.; McGuinness, D. S.; Morgan, D. H.; Neveling, A.; Otto, S.; Overett, M.; Slawin, A. M. Z.; Wasserscheid, P.; Kuhlmann, S. *J. Am. Chem. Soc.* **2004**, *126*, 14712. (b) Kim, E. H.; Lee, H. M.; Jeong, M. S.; Ryu, J. Y.; Lee, J.; Lee, B. Y. *ACS Omega* **2017**, *2*, 765. (c) Brückner, A.; Jabor, J. K.; McConnell, A. E. C.; Webb, P. B. *Organometallics* **2008**, *27*, 3849. (d) Rabeah, J.; Bauer, M.; Baumann, W.; McConnell, A. E. C.; Gabrielli, W. F.; Webb, P. B.; Selent, D.; Brückner, A. *ACS Catal.* **2012**, *3*, 95. (e) Stennett, T. E.; Haddow, M. F.; Wass, D. F. *Organometallics* **2012**, *31*, 6960. (f) Bartlett, S. A.; Moulin, J.; Tromp, M.; Reid, G.; Dent, A. J.; Cîbin, G.; McGuinness, D. S.; Evans, J. *Catal. Sci. Technol.* **2016**, *6*, 6237. (g) Hirscher, N. A.; Agapie, T. *Organometallics* **2017**, *36*, 4107. (h) McGuinness, D. S. *Chem. Rev.* **2011**, *111*, 2321. (i) Agapie, T. *Coord. Chem. Rev.* **2011**, *255*, 861. (j) Wass, D. F. *Dalton Trans.* **2007**, 816. (k) Dixon, J. T.; Green, M. J.; Hess, F. M.; Morgan, D. H. *J. Organomet. Chem.* **2004**, *689*, 3641.
- (2) (a) Overett, M. J.; Blann, K.; Bollmann, A.; Dixon, J. T.; Hess, F.; Killian, E.; Maumela, H.; Morgan, D. H.; Neveling, A.; Otto, S. *Chem. Commun.* **2005**, 622. (b) Weng, Z.; Teo, S.; Andy Hor, T. S. *Dalton Trans.* **2007**, 3493. (c) Blann, K.; Bollmann, A.; de Bod, H.; Dixon, J. T.; Killian, E.; Nongodlwana, P.; Maumela, M. C.; Maumela, H.; McConnell, A. E.; Morgan, D. H.; Overett, M. J.; Prétorius, M.; Kuhlmann, S.; Wasserscheid, P. *J. Catal.* **2007**, *249*, 244. (d) Overett, M. J.; Blann, K.; Bollmann, A.; de Villiers, R.; Dixon, J. T.; Killian, E.; Maumela, M. C.; Maumela, H.; McGuinness, D. S.; Morgan, D. H.; Rucklidge, A.; Slawin, A. M. Z. *J. Mol. Catal. A: Chem* **2008**, *283*, 114. (e) Kuhlmann, S.; Dixon, J. T.; Haumann, M.; Morgan, D. H.; Ofili, J.; Spuhl, O.; Taccardi, N.; Wasserscheid, P. *Adv. Synth. Catal.* **2006**, *348*, 1200.

(3) (a) Agapie, T.; Schofer, S. J.; Labinger, J. A.; Bercaw, J. E. *J. Am. Chem. Soc.* **2004**, *126*, 1304. (b) Agapie, T.; Labinger, J. A.; Bercaw, J. E. *J. Am. Chem. Soc.* **2007**, *129*, 14281.

(4) Overett, M. J.; Blann, K.; Bollmann, A.; Dixon, J. T.; Haasbroek, D.; Killian, E.; Maumela, H.; McGuinness, D. S.; Morgan, D. H. *J. Am. Chem. Soc.* **2005**, *127*, 10723.

(5) Cloete, N.; Visser, H. G.; Engelbrecht, I.; Overett, M. J.; Gabrielli, W. F.; Roodt, A. *Inorg. Chem.* **2013**, *52*, 2268.

(6) Peitz, S.; Aluri, B. R.; Peulecke, N.; Müller, B. H.; Wöhl, A.; Müller, W.; Al-Hazmi, M. H.; Mosa, F. M.; Rosenthal, U. *Chem. Eur. J.* **2010**, *16*, 7670.

(7) (a) Britovsek, G. J. P.; McGuinness, D. S.; Wierenga, T. S.; Young, C. T. *ACS Catal.* **2015**, *5*, 4152. (b) Britovsek, G. J. P.; McGuinness, D. S. *Chem. Eur. J.* **2016**, *22*, 16891. (c) Britovsek, G. J. P.; McGuinness, D. S.; Tomov, A. K. *Catal. Sci. Technol.* **2016**, *6*, 8234. (d) Kwon, D.-H.; Fuller, J. T.; Kilgore, U. J.; Sydora, O. L.; Bischof, S. M.; Ess, D. H. *ACS Catal.* **2018**, 1138.

(8) (a) Licciulli, S.; Thapa, I.; Albahily, K.; Korobkov, I.; Gambarotta, S.; Duchateau, R.; Chevalier, R.; Schuhen, K. *Angew. Chem. Int. Ed.* **2010**, *49*, 9225. (b) Shaikh, Y.; Albahily, K.; Sutcliffe, M.; Fomitcheva, V.; Gambarotta, S.; Korobkov, I.; Duchateau, R. *Angew. Chem. Int. Ed.* **2012**, *51*, 1366. (c) Kim, Y. A.; Oh, S. J.; Cho, S.; Son, K.-s. *Macromolecular Research* **2018**, *26*, 341.

(9) (a) McGuinness, D. S.; Overett, M.; Tooze, R. P.; Blann, K.; Dixon, J. T.; Slawin, A. M. Z. *Organometallics* **2007**, *26*, 1108. (b) McGuinness, D. S.; Rucklidge, A. J.; Tooze, R. P.; Slawin, A. M. Z. *Organometallics* **2007**, *26*, 2561. (c) Do, L. H.; Labinger, J. A.; Bercaw, J. E. *ACS Catal.* **2013**, *3*, 2582.

(10) (a) Teo, S.; Weng, Z.; Hor, T. S. A. *Organometallics* **2008**, *27*, 4188. (b) Fliedel, C.; Ghisolfi, A.; Braunstein, P. *Chem. Rev.* **2016**, *116*, 9237. (c) Lifschitz, A. M.; Hirscher, N. A.;

Lee, H. B.; Buss, J. A.; Agapie, T. *Organometallics* **2017**, *36*, 1640. (d) Haddow, M. F.; Jaltai, J.; Hanton, M.; Pringle, P. G.; Rush, L. E.; Sparkes, H. A.; Woodall, C. H. *Dalton Trans.* **2016**, *45*, 2294.

(11) (a) Tomov, A. K.; Gibson, V. C.; Britovsek, G. J. P.; Long, R. J.; van Meurs, M.; Jones, D. J.; Tellmann, K. P.; Chirinos, J. J. *Organometallics* **2009**, *28*, 7033. (b) Suttill, J. A.; McGuinness, D. S. *Organometallics* **2012**, *31*, 7004. (c) Sattler, A.; Labinger, J. A.; Bercaw, J. E. *Organometallics* **2013**, *32*, 6899.

(12) Gómez-Gallego, M.; Sierra, M. A. *Chem. Rev.* **2011**, *111*, 4857.

(13) (a) Heintz, R. A.; Leelasubcharoen, S.; Liable-Sands, L. M.; Rheingold, A. L.; Theopold, K. H. *Organometallics* **1998**, *17*, 5477. (b) Noh, S. K.; Sendlinger, S. C.; Janiak, C.; Theopold, K. H. *Journal of the American Chemical Society* **1989**, *111*, 9127. (c) Zhang, J.; Li, A.; Hor, T. S. A. *Organometallics* **2009**, *28*, 2935.

(14) Sattler, A.; Aluthge, D. C.; Winkler, J. R.; Labinger, J. A.; Bercaw, J. E. *ACS Catalysis* **2016**, *6*, 19.

(15) Herwig, W.; Zeiss, H. *The Journal of Organic Chemistry* **1958**, *23*, 1404.

(16) (a) Elowe, P. R.; McCann, C.; Pringle, P. G.; Spitzmesser, S. K.; Bercaw, J. E. *Organometallics* **2006**, *25*, 5255. (b) Brookhart, M.; Grant, B.; Volpe, A. F. *Organometallics* **1992**, *11*, 3920.

## Chapter 4

### Robust Chromium Precursors for Catalysis: Isolation and Structure of a Single-Component Ethylene Tetramerization Precatalyst

Reprinted with permission from:

*Journal of the American Chemical Society*, **2019**, 141 (14), pp 6022-6029

Copyright 2019 American Chemical Society

**Abstract.**

We have introduced a new class of stable organometallic Cr reagents (compounds **1–4**) that are readily prepared, yet reactive enough to serve as precursors. They were used for ethylene tetramerization catalysis following stoichiometric activation by in situ protonation. This study highlights the importance of balancing stability with reactivity in generating an organometallic precursor that is useful in catalysis. Moreover, precursor **4** allowed for the isolation and crystallographic characterization of a room-temperature stable cationic species,  $(\text{PNP})\text{CrR}_2^+$  ( $\text{R} = o\text{-C}_6\text{H}_4(\text{CH}_2)_2\text{OMe}$ ,  $\text{PNP} = {}^i\text{PrN}(\text{PPh}_2)_2$ ). This complex (**5**) may be used as a single component precatalyst, without any alkylaluminum reagents. This result provides an unprecedented level of insight into the kind of structures that must be produced from more complicated activation processes.

## Introduction.

Chromium catalysis has not yet experienced a renaissance quite like other first row transition metals.<sup>1</sup> Recent development of low-valent Cr catalysis in organic methodology has renewed interest in reactive Cr  $\sigma$ -aryl complexes.<sup>2</sup> The necessity for suitable and well-defined organometallic precursors has been appreciated in the context of iron and nickel catalysis.<sup>3</sup> Anionic (e.g., aryl,  $\beta$ -diketiminate, or cyclopentadienyl) ligands have proven useful entries for Cr chemistry.<sup>4</sup> However, the selection of chromium hydrocarbyl precursors is very limited (*vide infra*), which may hinder new methodology development.

Chromium has been uniquely demonstrated to serve as a catalyst for ethylene tetramerization, although a completely selective catalyst has remained elusive.<sup>5</sup> Significant efforts have identified ligands<sup>6</sup> and cocatalysts<sup>7</sup> to support ethylene tetramerization, but the pool of Cr precursors has remained small (Figure 1a). These are typically Cr(III) or Cr(II) salts: Cr(acac)<sub>3</sub>,<sup>8</sup> Cr(ethylhexanoate)<sub>3</sub>,<sup>9</sup> CrCl<sub>3</sub>(THF)<sub>3</sub>,<sup>10</sup> and CrCl<sub>2</sub>(THF)<sub>2</sub> (acac = acetylacetonate, THF = tetrahydrofuran).<sup>11</sup> To generate a catalytically active species *in situ*, these precursors are typically mixed with alkylaluminum cocatalysts such as modified methylaluminoxane (MMAO) in the presence of an auxiliary ligand. The need for harsh activation processes, in terms of high excess and reactivity of Al additives, has impeded rational improvements to catalysis. More problematically, the paramagnetism of relevant Cr intermediates has limited insight into their structure.<sup>12</sup>

Currently, there are few Cr precatalysts that can be activated by milder methods (or that are self-activating). In several studies for ethylene trimerization<sup>13</sup> and in our recent report for ethylene tetramerization,<sup>14</sup> catalysis was achieved without excess of alkyl aluminum reagents. These and related studies have relied on the isolation of Cr multiaryl or multialkyl

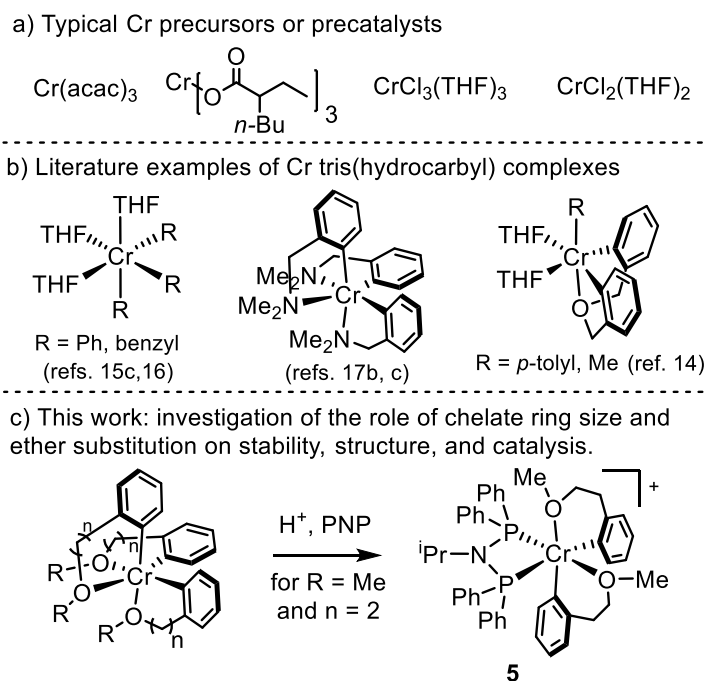
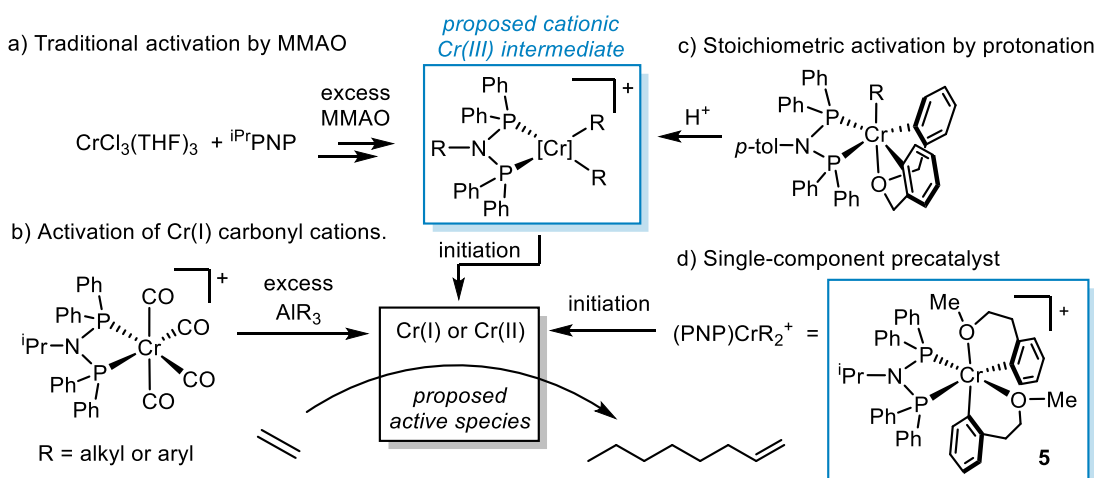


**Figure 1.** (a) Typical Cr<sup>III</sup> or Cr<sup>II</sup> precursors or precatalysts, (b) examples of Cr tris(hydrocarbyl) complexes, and (c) this work.

**Scheme 1.** (a) Activation of CrCl<sub>3</sub>-based precatalysts with MMAO, leading to a reduced active species, (b) activation of Cr(I) carbonyl precatalysts with AlR<sub>3</sub>, also leading to a reduced active species, (c) stoichiometric activation by protonation, and (d) a single-component (PNP)CrR<sub>2</sub><sup>+</sup> precatalyst.



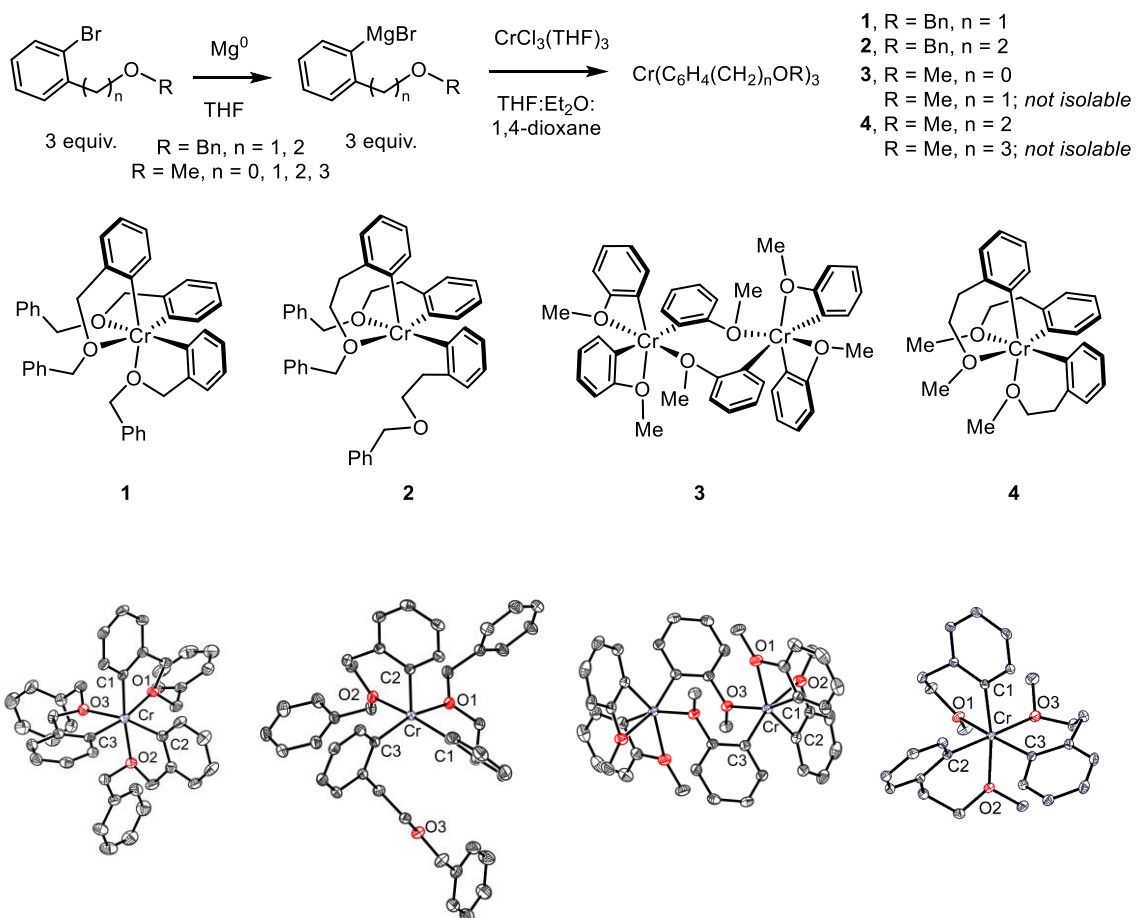
complexes.<sup>15</sup> The scarcity of examples of “prealkylated” Cr precursors is likely related to the instability of  $\text{CrPh}_3(\text{THF})_3$  and its derivatives.<sup>13b,15a,16</sup> The precursor  $\text{CrBn}_3(\text{THF})_3$  (Bn = benzyl) has been reported but is also highly unstable.<sup>15c</sup> To stabilize Cr–aryl or Cr–alkyl species, chelating ligands have been used in rare cases (see examples in Figure 1b).<sup>14,17</sup> However, this strategy has only recently been implemented in chromium catalysis.<sup>14,17g</sup>

Herein, we report the synthesis of a series of Cr(III) tris(aryl) complexes stabilized by the binding of pendant ethers (Figure 1c). We demonstrate the stability of these complexes, attributable to this chelate effect. Furthermore, these complexes are investigated as precatalysts for ethylene tetramerization following activation with a Brønsted acid in the presence of a diphosphinoamine (PNP) supporting ligand (i.e., stoichiometric activation). Previous studies have suggested that a cationic Cr(III) complex is the product of stoichiometric activation, which is followed by initiation via ethylene insertion, H-transfer, and reductive elimination to generate a Cr(I) active species.<sup>13a,13b,14</sup> The same type of active species is presumed following activation by alkylaluminum reagents (Scheme 1a), although the involvement of Cr(II) species has not been experimentally ruled out.<sup>12</sup> Although precursor Cr(I) cations may be stabilized by carbonyl ligands, such complexes still require activation by alkylaluminum reagents (Scheme 1b).<sup>18</sup> Our previous report detailed the first example of activation by protonation (Scheme 1c).<sup>14</sup> To our knowledge, no cationic Cr(III) species has yet been isolated and shown to be a viable single-component precatalyst for ethylene tetramerization. Therefore, the identity of the activated Cr species has never been directly established. We demonstrate that by first developing a route to robust but still reactive Cr tris-(hydrocarbyl) precursors, an activated complex,  $(\text{PNP})\text{CrR}_2^+$ , can be isolated and crystallographically characterized (Scheme 1d).

## Results and Discussion.

**Synthesis of Cr Tris(aryl) Complexes (1–4) Stabilized by Ether Chelation.** A general procedure for the synthesis of complexes **1–4** was developed (Scheme 2). An amount of 3 equiv. of each aryl bromide was converted to the corresponding aryl Grignard reagent by stirring over Mg turnings. The Grignard solutions were used directly in the arylation of  $\text{CrCl}_3(\text{THF})_3$ . After filtering away Mg salts, the Cr products could be obtained, typically by precipitation (see Experimental Section for specific workup procedures). In contrast, isolation of the methyl ether-stabilized Cr complex with a single methylene linker in the chelate ( $\text{R} = \text{Me}$ ,  $n = 1$ ) was not successful. The obtained solid residue was completely insoluble in THF or DCM, suggesting that the desired product converted to oligomeric or polymeric forms, possibly due to association of Mg salts. Additionally, although the desired methyl ether-stabilized Cr complex with three methylene linkers in the chelate ( $\text{R} = \text{Me}$ ,  $n = 3$ ) appeared to have been generated in situ, it decomposed in solution at room temperature: the aryl–aryl reductive elimination product was observed by GC/MS in quenched aliquots of this reaction. These changes in reactivity highlight the importance of the chelate ring size and ether substituents in the stabilization of the Cr tris(aryl) complexes.

**Structural Characterization of Complexes 1–4.** Single crystals were obtained of complexes **1**, **2**, **3**, and **4**, allowing for structural determination by XRD (Figure 2). Among this series, some structural diversity was observed. For **1** and **4**, XRD confirmed the expected geometry of the products as six-coordinate Cr complexes, where each aryl ligand was bidentate due its chelating ether functionality. Complex **2** was determined to be a five-coordinate, square pyramidal complex, where one of the three ether donors was not coordinated to Cr. For **3**, a dimeric structure was revealed by XRD, wherein one of the three aryl ligands bridges two Cr centers, binding through the aryl donor to one Cr center, and the

**Scheme 2.** General synthetic scheme for complexes **1-4**.**Figure 2.** From left to right, solid-state structures of compounds **1**, **2**, **3** and **4**. Thermal ellipsoids are displayed at the 50% probability level. Solvent molecules and hydrogen atoms are omitted for clarity.**Table 1.** Selected bond lengths and angles for compounds **1-5**.

Compound	Bond Lengths (Å)						Bond Angles (°)		
	Cr-O1	Cr-O2	Cr-O3	Cr-C1	Cr-C2	Cr-C3	O1-Cr-C1	O2-Cr-C2	O3-Cr-C3
1	2.152(2)	2.176(2)	2.139(2)	2.038(2)	2.040(3)	2.039(3)	79.69(9)	79.81(9)	79.68(9)
2	2.1529(8)	2.1893(7)	n/a <sup>a</sup>	2.050(1)	2.037(1)	2.067(1)	86.41(4)	90.67(3)	n/a <sup>a</sup>
3	2.230(2)	2.293(2)	2.138(1)	2.032(2)	2.034(2)	2.040(2)	64.81(7)	63.63(7)	93.41(7) <sup>b</sup>
4	2.2059(9)	2.1963(8)	2.1844(8)	2.104(1)	2.081(1)	2.079(1)	88.75(4)	88.05(4)	88.32(4)
5	2.181(1)	2.108(1)	n/a	2.056(2)	2.072(2)	n/a	90.39(6)	88.02(6)	n/a

ether donor to the other. Under different crystallization conditions (using THF instead of DCM), different crystals were obtained; the XRD analysis revealed a six-coordinate, monomeric Cr center (**3'**). In **3'**, one of the ether donors has dissociated from Cr, and a THF ligand was bound in its place. Clearly, the chelate forming a four-membered ring (in **3**) is less favored than the five- and six-membered ring examples (in **1**, **2**, and **4**). An ether donor in **3** prefers either to dissociate in preference to THF or to bridge to another metal center. Nevertheless, the four-membered chelate stabilizes the aryl ligand against reductive elimination relative to the example with the seven-membered ring.

Although there were notable differences in the structural arrangement about Cr based on chelate ring size and ether substitution, there are not drastic differences in the bond metrics among the series. However, it can be seen that **4** exhibits the longest Cr–C bonds, by at least 0.03 Å on average (Table 1). This is likely due to it having the largest chelate ring size of the six-coordinate Cr examples. Complex **4** also exhibits relatively long Cr–O bonds, at least 0.02 Å longer than in **1** and **2**. However, **3** exhibits the longest Cr–O bonds (excluding the oxygen from the bridging ligand) by 0.06 Å on average. The strained four-membered chelate ring decreases the ability of the ether moiety to bind to Cr. Its propensity to dissociate and/or bind to a different Cr center is further evidence of this. Finally, the O–Cr–C angle (the “bite angle” of the aryether ligands) is close to 90° for **2** and **4**, where a six-membered chelate ring is present. Expectedly, a corresponding decrease in the bite angle is seen as the chelate ring size decreases to five (80° in **1**) or four (64° in **3**).

**Stability of Complexes 1–4.** For use as catalytic or synthetic precursors, Cr multiaryl complexes should exhibit stability in noncoordinating solvents. The commonly used  $\text{CrPh}_3(\text{THF})_3$  is isolable from its synthesis by recrystallization from THF, but its instability in less-coordinating solvents (e.g., diethyl ether or toluene) is well-documented.<sup>16a</sup> For example,

within seconds of adding diethyl ether or toluene to  $\text{CrPh}_3(\text{THF})_3$ , conversion to brown precipitate is observed, in the absence of excess amounts of a coordinating ligand such as THF. The decomposition pathway involves reductive elimination to generate biphenyl.<sup>16a</sup> For comparison, the stability of complexes **1–4** was tested in dried, degassed toluene solution (4 mM) in sealed cuvettes. Over 24 h at room temperature, no changes to the UV/vis absorption spectra were observed for complexes **1**, **2**, and **4**; quenched aliquots analyzed by GC/MS showed no decomposition by aryl–aryl reductive elimination over this time. Compound **3** decomposed slowly over 24 h in toluene at room temperature (a 23% decrease in absorption at 534 nm); dark precipitate was observed from the red solution ( $\lambda$ : 444 nm, 534 nm); reductive elimination was observed by GC/MS. Unsurprisingly, these compounds were not stable in solution upon exposure to air. Clearly, the presence of ether chelation in ring sizes of five or six stabilized the Cr-aryl motif dramatically. With a chelate ring size of four (in complex **3**) or with a combination of chelated and nonchelated aryl ligands (as noted in our previous report),<sup>14</sup> a lesser degree of stabilization is imposed, although these examples are still more robust than  $\text{CrPh}_3(\text{THF})_3$ .

**Catalytic Utility of Cr Tris(aryl) Complexes 1–4.** The utility of the Cr complexes reported herein as precursors in catalysis was investigated in the context of selective ethylene tetramerization. Due to structural similarities to previously reported Cr multiaryl complexes, we expected these to be successfully activated by protonation with  $\text{HBAr}'_4$  in the presence of a PNP ligand.<sup>13a,13b,14</sup> Using this process, all complexes investigated led to some productivity in the absence of alkylaluminum activators; however, **4** was particularly active (see Table 2). We propose that the differences in productivity are related to the initiation rates (leading to a reduced Cr active species). All of these Cr tris(hydrocarbyl) precursors are expected to generate, upon protonation in the presence of PNP ligands, cationic (PNP)Cr-bis(aryl)

species capable of catalysis. The difference in performance is likely related to how the initiation rate is affected by the chelate ring size and substituent on the ether donor. Complex **4** has relatively long Cr–C and Cr–O bonds compared to the other precursors (*vide supra*), a possible explanation for faster initiation. Importantly, we found that a known Cr tris(aryl) precursor (**6**, Cr(o-(Et<sub>2</sub>NCH<sub>2</sub>)-C<sub>6</sub>H<sub>4</sub>)<sub>3</sub>)<sup>19</sup> stabilized by pendant amines was not a viable precatalyst. No oligomers were observed following stoichiometric activation of **6**. Likely, the amine donor chelates too strongly to Cr, preventing catalyst formation in terms of efficient protonation, coordination by PNP, or subsequent initiation steps. This difference in behavior highlights the necessary balance between stability and reactivity in these Cr precursors. While stability is desirable in a versatile precursor, sufficient reactivity is still necessary for catalytic utility. The ether chelates employed here satisfy both requirements.

**Synthesis and Structural Characterization of 5.** The ability of ligands relevant to catalysis to displace the chelating donors in **1–4** was investigated, but no evidence of a reaction was observed at room temperature, even with bis(diphenylphosphino)benzene (tracked by EPR or UV/vis spectroscopy). Nevertheless, PNP must bind to Cr after the protonolysis of an aryl group in order to generate active catalysts as demonstrated in Table 2. Therefore, the isolation of the cationic complex was targeted. Addition of [H(OEt<sub>2</sub>)<sub>2</sub>][BAr'<sub>4</sub>] (Ar' = 3,5-(CF<sub>3</sub>)<sub>2</sub>-C<sub>6</sub>H<sub>3</sub>) to a mixture of (iPr)N(PPh<sub>2</sub>)<sub>2</sub> (<sup>iPr</sup>PNP) and **4** results in a color change from orange to green. The product was isolated as a green powder and was proposed to have the formulation of [(<sup>iPr</sup>PNP)Cr(o-(CH<sub>3</sub>O(CH<sub>2</sub>)<sub>2</sub>)-C<sub>6</sub>H<sub>4</sub>)<sub>2</sub>][BAr'<sub>4</sub>] (**5**, Figure 3). This corresponds to protonation of one aryl ligand (releasing 2-methoxyethylbenzene) and binding of <sup>iPr</sup>PNP to Cr. This solid could be used directly in catalysis simply by dissolving it in chlorobenzene and adding ethylene (*vide infra*). This product (**5**) was not readily amenable to crystallization due to its propensity to form oils. However, suitable single crystals of **5**

**Table 2.** Comparison of ethylene oligomerization catalysis using Cr complexes **1-6**. No alkyl aluminum activators were used in these trials (entries 1-6). A comparison is made with MMAO-activated  $\text{CrCl}_3(\text{THF})_3$  (entry 7).

Entry	Cr Source <sup>a</sup>	Productivity (g/g of Cr)	PE <sup>b,c</sup>	C <sub>6</sub> <sup>c</sup>	1-C <sub>8</sub> <sup>c</sup>	C <sub>10</sub> -C <sub>14</sub> <sup>c</sup>	% 1-C <sub>6</sub> in C <sub>6</sub> <sup>c</sup>	1-octene: 1-hexene <sup>d</sup>
1	<b>1</b>	12	0	42	58	0	94	1.1
2	<b>2</b>	62	0	42	58	0	91	1.1
3	<b>3</b>	34	0	72	26	2	98	0.28
4	<b>4</b>	1500	0	48	45	7	92	0.77
5	<b>5</b>	3400	< 1	47	38	15	93	0.64
6	<b>6</b>	0	0	—	—	—	—	—
7 <sup>e</sup>	$\text{CrCl}_3(\text{THF})_3$	5200	< 1	43	41	16	0.89	0.80

Reaction vessel: glass Fisher-Porter bottle.  $[\text{Cr}] = 1 \text{ mM}$ , Solvent: 7.5 mL PhCl. Pressure: 100 psig  $\text{C}_2\text{H}_4$ . Temperature: 25°C. Reaction time: 45 min. <sup>a</sup>Complexes **1-4**, & **6** were activated with 1.0 equiv.  $\text{HBAr}'_4$  in the presence of 1.1 equiv. <sup>i</sup>PrPNP. <sup>b</sup> PE = polyethylene. <sup>c</sup> Wt% (total). <sup>d</sup> Molar ratio. <sup>e</sup> Result from ref. 14: 300 equivalents of MMAO were added in the presence of 1.1 equiv. <sup>i</sup>PrPNP; other conditions are the same.

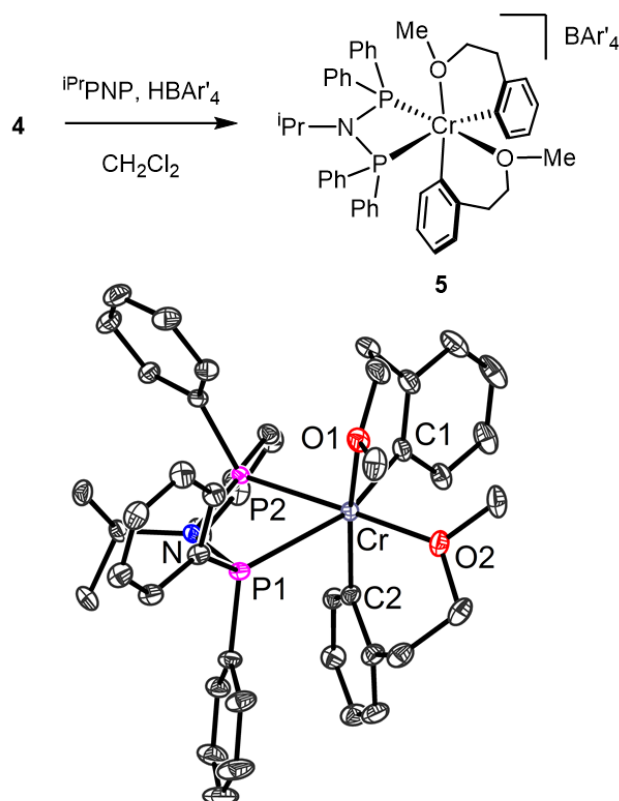


**Figure 3.** Top: Synthesis of complex **5**. Bottom: Solid-state structure of complex **5**. Thermal ellipsoids are displayed at the 50% probability level. Solvent of crystallization ( $\text{CH}_2\text{Cl}_2$ ),  $\text{BAr}'_4$  anion, and hydrogen atoms omitted for clarity.

were obtained from DCM. The expected structure was confirmed by XRD: six-coordinate, cationic Cr with two aryether ligands and one PNP ligand bound (Figure 3).

The stability of compound **5** in toluene was checked to evaluate that it is practically useful. No changes to the UV/vis absorption spectra were observed in toluene solution for at least 24 h at room temperature, which is very notable given the scarcity of Cr-hydrocarbyl cationic species.<sup>15b,20</sup>

Indeed, compound **5** is a particularly uncommon example of an isolated Cr-hydrocarbyl cation in the context of ethylene oligomerization catalysis. Although related cationic complexes have in some cases been structurally characterized,<sup>12b,18,21</sup> to our knowledge they are not catalytically active without alkylaluminum-based cocatalysts. None of the referenced examples maintain salient features present in **5**, which is free of halide or carbonyl ligands, has a single PNP ligand, and has a noncoordinating anion. Because of these features, compound **5** is poised to generate the catalytically active species simply upon addition of ethylene.

**Use of Pre-“Activated” Cr Complex 5 in Catalysis.** We found that **5** was a single-component precatalyst for ethylene tetramerization. Following dissolution of **5** in chlorobenzene, addition of ethylene in a high-pressure reaction vessel led to formation of 1-hexene and 1-octene, similar to catalytic trials following stoichiometric activation of **4** (see Table 2, entry 5). Remarkably, the catalytic productivity and 1-octene selectivity are comparable to when  $\text{CrCl}_3(\text{THF})_3$  is activated with 300 equiv of MMAO (Table 2, entry 7). The direct utility of **5** is advantageous since no weighing or premixing of multiple components is necessary prior to loading the reactor. In a traditional activation scheme, the PNP ligand, Cr precursor, and MMAO solution must all be meticulously prepared and combined. It has been reported that MMAO-activation leads to Cr species that are unstable

and in which multiple species are detectable by UV/vis and EPR spectroscopy.<sup>12c</sup> Because **5** is reasonably stable at room temperature, these complications regarding catalyst preparation and activation have been completely removed. Fundamentally, this catalytic result also bolsters the assertion that a cationic (PNP)Cr dialkyl complex is the relevant product of traditional MMAO-activation leading to the Cr active species.

### **Conclusion.**

A high degree of stability is imparted to the Cr tris(aryl) motif by the addition of pendant ether donors. However, these precursors (**1–4**) remain reactive enough for catalytic use in ethylene tetramerization. Differences in stability and reactivity were observed among the series of ether-stabilized Cr precursors. In particular, one example (**4**) not only led to higher productivity in ethylene tetramerization catalysis but also was a useful synthon for a cationic Cr complex (**5**). This example (**5**) is the first single-component precatalyst for ethylene tetramerization and is a rare example of a structurally characterized Cr  $\sigma$ -aryl cationic species. Complex **5** exemplifies structural features required for an “activated” Cr species, eliminating speculation as to the role of MMAO as an activator in typical catalytic processes. Compound **5** represents a unique example of a well-defined and structurally characterized (PNP)CrR<sub>2</sub><sup>+</sup> activated species, typically produced from MMAO-activation of CrX<sub>3</sub>-based (X = Cl or acac) precatalysts. Analogous methodologies are expected to be fruitful for other Cr catalytic systems, using the precursors reported here.

## Experimental.

**General Information.** All synthetic procedures containing chromium were performed in a nitrogen-atmosphere glove box or in sealed containers under a stream of nitrogen gas. All glassware was oven-dried and kept under active vacuum prior to use. Diethyl ether, tetrahydrofuran (THF), toluene, dichloromethane (DCM), hexanes, and pentane solvents were purified by sparging with nitrogen and then passing through a column of activated A2 alumina into sealed containers, degassed under active vacuum, and stored over activated molecular sieves prior to use. 1,4-Dioxane was dried over Na/benzophenone, vacuum distilled, and kept over activated molecular sieves prior to use. Chlorobenzene was distilled from CaH<sub>2</sub>, stored over activated molecular sieves for at least 24 hours, and filtered through activated alumina directly before use. CD<sub>2</sub>Cl<sub>2</sub> (Cambridge Isotope Laboratories) was distilled from CaH<sub>2</sub> and kept over activated molecular sieves prior to use. M-MAO 3A was purchased from AkzoNobel as a 7% w/w Al solution in heptane. Ethylene gas was purchased at polymer purity (99.9%) from Matheson, and was dried by passage through two 1L Swagelok steel columns packed with 3Å activated molecular sieves and Mn(II) oxide on vermiculite.<sup>22</sup> CrCl<sub>3</sub>(THF)<sub>3</sub> was synthesized according to the literature procedure, using CrCl<sub>3</sub> (anhydrous) purchased from Strem.<sup>10a</sup> The synthesis of <sup>iPr</sup>PNP, and [H(Et<sub>2</sub>O)<sub>2</sub>][BAr'<sub>4</sub>] have been previously reported.<sup>6b,23</sup> 2-Bromoanisole was purchased from Sigma-Aldrich and distilled before use. The other ether-based aryl bromides were synthesized by methylation or benzylation of the corresponding alcohols, according to the literature procedures,<sup>24</sup> and dried under vacuum before use. N-(2-bromobenzyl)-N-ethylethanamine was synthesized as reported.<sup>25</sup> Paramagnetic susceptibility values ( $\mu_{\text{eff}}$ ) were determined by NMR (Evans' method).<sup>26</sup> Evans' method was performed by dissolving the compound in CD<sub>2</sub>Cl<sub>2</sub> solvent (with added protio solvent as the reference). The NMR tube contained a capillary insert with

blank  $\text{CD}_2\text{Cl}_2:\text{CH}_2\text{Cl}_2$  of the same composition inside. NMR spectra were recorded on a Varian 300 MHz or 400 MHz Spectrometer. UV/Vis spectra were obtained on a Varian Cary Bio 50 spectrophotometer. EPR spectra were obtained by freezing 1:1 toluene:dichloromethane solutions of  $[\text{Cr}] = 4 \text{ mM}$ , using a Bruker EMX spectrometer. Elemental analysis was performed using a PerkinElmer 2400 Series II CHN Elemental Analyzer. Gas chromatography (GC) was performed on an Agilent 6890A instrument using a DB-1 capillary column (10 m length, 0.10 mm diameter, 0.40  $\mu\text{m}$  film) and a flame ionization detector. Gas chromatography/mass spectrometry (GC-MS) was performed on an Agilent 6890A instrument using a HP-5MS column (30 m length, 0.25 mm diameter, 0.50  $\mu\text{m}$  film) and an Agilent 5973N mass-selective EI detector.

**$\text{Cr}(\sigma\text{-}(\text{C}_6\text{H}_5\text{CH}_2\text{OCH}_2)\text{-C}_6\text{H}_4)_3$  (1).** A solution of 1-((benzyloxy)methyl)-2-bromobenzene (0.930 g, 3.36 mmol) in 20 mL THF was stirred over excess activated Mg turnings at room temperature. After several hours, Grignard formation was complete. The solution was filtered through glass wool, away from excess Mg. It was added dropwise over ten minutes to a thawing 20 mL THF suspension of  $\text{CrCl}_3(\text{THF})_3$  (0.420 g, 1.12 mmol). The resulting brown, homogeneous solution was warmed to RT over 90 minutes, then diluted to 80 mL with  $\text{Et}_2\text{O}$ . Next, 0.8 mL 1,4-dioxane was added; the solution continued to stir at RT for 20 h. The resulting brown solution was filtered through Celite, away from pale, yellow solids. These solids were rinsed into a separate flask using 20 mL DCM, to obtain a yellow-orange solution from insoluble, gray solids. This filtrate was reduced *in vacuo* to a yellow powder (0.265 g, 0.411 mmol, 37% yield). Yellow single crystals suitable for XRD were grown by cooling a diethylether solution of **1** to  $-40^\circ\text{C}$  for several days.  $\mu_{\text{eff}} = 4.0(2) \mu_{\text{B}}$  (average of three measurements).  $^1\text{H}$  NMR (400 MHz,  $\text{CD}_2\text{Cl}_2$ )  $\delta$  (ppm): 26.6 (br), 11.7 (br), 7.6 (br), 7.3 (br). UV-vis [THF;  $\lambda$ , nm ( $\epsilon$ ,  $\text{M}^{-1} \text{cm}^{-1}$ ): 244 ( $3.9 \times 10^4$ ), 314 ( $1.1 \times 10^3$ ), 388 ( $3.6 \times$

$10^3$ ), 458 ( $3.4 \times 10^3$ ). Anal. Calcd. for  $C_{42}H_{39}CrO_3$ : C, 78.36; H, 6.11; N, 0.0. Found: C, 78.18; H, 6.14; N, 0.0.

**Cr(*o*-( $C_6H_5CH_2O(CH_2)_2$ )- $C_6H_4$ )<sub>3</sub> (2).** A solution of 1-((benzyloxy)ethyl)-2-bromobenzene (1.81 g, 6.22 mmol) in 10 mL THF was stirred over excess activated Mg turnings at room temperature. After several hours, Grignard formation was complete. The solution was filtered through glass wool, away from excess Mg, and diluted to 25 mL with THF. The solution was added dropwise over ten minutes to a thawing 10 mL THF suspension of  $CrCl_3(THF)_3$  (0.778 g, 2.08 mmol). The resulting green, homogeneous solution was warmed to RT over 2 hours, then diluted to 70 mL with  $Et_2O$ . Next, 1.2 mL 1,4-dioxane was added; the solution continued to stir at RT for 24 h. The resulting green solution was filtered through Celite, away from white solids. This filtrate was reduced *in vacuo* to a green sticky residue, which was redissolved in 5 mL toluene. This toluene solution was stirred vigorously, and 25 mL pentane was added to precipitate reddish powder amongst a sticky, dark green residue. The red powder was collected, and the green residue was redissolved in toluene, and pentane was added in like fashion to precipitate more red powder. These two fractions were combined to give 750 mg of red power, redissolved in 20 mL toluene to give a green solution, and rinsed from white solids (presumably magnesium salts). This green solution was reduced *in vacuo* to a green powder (0.613 g, 0.895 mmol, 43% yield). Green single crystals were grown by slow concentration of a toluene solution of **2** under vacuum.  $\mu_{eff} = 3.9 \mu_B$ .  $^1H$  NMR (400 MHz,  $CD_2Cl_2$ )  $\delta$  (ppm): 25.1 (br), 14.9 (br), 7.5 (br), 7.3 (br), 2.4 (s), -17.0 (br). UV-vis [THF;  $\lambda$ , nm ( $\epsilon$ ,  $M^{-1} cm^{-1}$ ): 259 ( $1.9 \times 10^4$ ), 359 ( $6.1 \times 10^3$ ), 404 ( $2.9 \times 10^3$ ), 481 ( $1.5 \times 10^3$ ). Anal. Calcd. for  $C_{45}H_{45}CrO_3$ : C, 78.81; H, 6.61; N, 0.0. Found: C, 79.03; H, 6.70; N, 0.0.

**Cr(*o*-(CH<sub>3</sub>O)-C<sub>6</sub>H<sub>4</sub>)<sub>3</sub> (3).** A solution of 2-bromoanisole (1.863 g, 9.96 mmol) in 20 mL THF was stirred over excess activated Mg turnings at room temperature. After several hours, Grignard formation was complete. The solution was filtered through glass wool, away from excess Mg. It was added dropwise over five minutes to a thawing 30 mL THF suspension of CrCl<sub>3</sub>(THF)<sub>3</sub> (1.244 g, 3.32 mmol). A homogeneous, dark red solution resulted after warming to RT over three hours. The solution was diluted to 100 mL with Et<sub>2</sub>O, and 3 mL 1,4-dioxane was added, causing formation of some precipitate. After stirring at RT for 14 hours, a red solution was filtered from light solids using Celite. The filtrate was reduced *in vacuo* to red, flaky solids, which were redissolved in 10 mL DCM. The red solution was filtered through glass wool from minimal grey solids, layered with 10 mL hexanes, and stored for 6 days at -40°C. Then, the cold supernatant was decanted from ~50 mg red solids, and reduced *in vacuo* to 12 mL, causing additional precipitation. This suspension was stored at -40°C for another day. The supernatant was then decanted from red solids, which were dried *in vacuo* (0.748 g). Satisfactory elemental analysis could not be obtained, possibly due to remaining magnesium salts. Single crystals suitable for XRD could be obtained by vapor diffusion of pentane into a DCM solution at -40°C.

**Cr(*o*-(CH<sub>3</sub>O(CH<sub>2</sub>)<sub>2</sub>)-C<sub>6</sub>H<sub>4</sub>)<sub>3</sub> (4).** A solution of 1-bromo-2-(2-methoxyethyl)benzene (1.356 g, 6.31 mmol) in 20 mL THF was stirred over excess activated Mg turnings at room temperature. After several hours, Grignard formation was complete. The solution was filtered through glass wool, away from excess Mg. It was added dropwise over fifteen minutes to a thawing 30 mL THF suspension of CrCl<sub>3</sub>(THF)<sub>3</sub> (0.791 g, 2.11 mmol). The resulting dark red, homogeneous solution was warmed to RT over three hours, then diluted to 100 mL with Et<sub>2</sub>O. Next, 1.2 mL 1,4-dioxane was added, resulting in a suspension of red solids, which was stirred at RT for 20 h. The resulting suspension was filtered, collecting red

solids on a Celite filter cake. These solids were rinsed into a separate flask using 40 mL DCM. This red DCM solution was reduced *in vacuo* to yield the product as a red powder (0.192 g, 0.419 mmol, 20% yield). Single crystals suitable for XRD were grown by vapor diffusion of pentane into a THF solution of **4** at  $-40^{\circ}\text{C}$ .  $\mu_{\text{eff}} = 3.8 \mu_{\text{B}}$ .  $^1\text{H}$  NMR (400 MHz,  $\text{CD}_2\text{Cl}_2$ )  $\delta$  (ppm): 23.2 (br), 17.4 (br), -14.9 (br). UV-vis [THF;  $\lambda$ , nm ( $\epsilon$ ,  $\text{M}^{-1} \text{cm}^{-1}$ ): 256 ( $2.7 \times 10^4$ ), 371 ( $9.9 \times 10^3$ ), 416 ( $5.0 \times 10^3$ ), 602 ( $1.5 \times 10^3$ ). Anal. Calcd. for  $\text{C}_{27}\text{H}_{33}\text{CrO}_3$ : C, 70.88; H, 7.27; N, 0.0. Found: C, 70.63; H, 7.37; N, 0.19.

**[( $^{\text{Pr}}$ PNP)Cr( $\alpha$ -( $\text{CH}_3\text{O}(\text{CH}_2)_2$ )- $\text{C}_6\text{H}_4$ ) $_2$ ][ $\text{BAr}'_4$ ] (**5**). A solution of **4** (0.145 g, 0.317 mmol) and  $^{\text{Pr}}$ PNP (0.135 g, 0.316 mmol) was prepared in 4 mL DCM. To the room temperature orange solution, a 4 mL DCM solution of  $\text{HBAr}'_4$  (0.320 g, 0.316 mmol) was added dropwise over five minutes. Upon completion of addition, a dark green solution was obtained. After 20 min, the solution was reduced to a sticky green solid under vacuum; the dry residue was further dried under vacuum for several hours. The residue was dissolved in minimal DCM ( $\approx 1$  mL). Hexanes was added in portions to the thick, vigorously stirring solution, causing some oiling, then eventual precipitation of dry green solids. These green solids were isolated by decanting the supernatant and reducing further under vacuum to complete dryness (0.480 g, 0.298 mmol 94% yield). Single crystals suitable for XRD were grown in  $\approx 1$  day by slow evaporation of a DCM solution into hexamethyldisiloxane (HMDSO) at room temperature.  $\mu_{\text{eff}} = 3.6 \mu_{\text{B}}$ .  $^1\text{H}$  NMR (400 MHz,  $\text{CD}_2\text{Cl}_2$ )  $\delta$  (ppm): 28.4 (br), 25.6 (br), 12.7 (br), 9.7 (br), 7.8 (s, aryl-*H* on  $\text{BAr}'_4$ ), 7.6 (s, aryl-*H* on  $\text{BAr}'_4$ ), 6.9 (br), 2.9 (br), 0.2 (br), -0.6 (br), -9.3 (br), -17.6 (br).  $^{19}\text{F}$  NMR (376 MHz,  $\text{CD}_2\text{Cl}_2$ )  $\delta$  (ppm): -62.7 (s).  $^{31}\text{P}$  NMR (162 MHz,  $\text{CD}_2\text{Cl}_2$ )  $\delta$  (ppm): *silent*. UV-vis [DCM;  $\lambda$ , nm ( $\epsilon$ ,  $\text{M}^{-1} \text{cm}^{-1}$ ): 619 ( $2.3 \times 10^3$ ). Anal. Calcd. for  $\text{C}_{77}\text{H}_{61}\text{BCrF}_{24}\text{NO}_2\text{P}_2$ : C, 57.34; H, 3.81; N, 0.87. Found: C, 57.36; H, 3.99; N, 0.92.**

**Cr(*o*-(Et<sub>2</sub>NCH<sub>2</sub>)-C<sub>6</sub>H<sub>4</sub>)<sub>3</sub> (6).** This has been described previously,<sup>19</sup> and is related to the dimethylamino-substituted version.<sup>17b,17c</sup> Our synthesis is as follows: N-(2-bromobenzyl)-N-ethylethanamine (0.288 g, 1.20 mmol) in 4 mL THF was stirred over excess activated Mg turnings at room temperature. After several hours, Grignard formation was complete. The solution was filtered through glass wool, away from excess Mg. It was added dropwise over a few minutes to a thawing 4 mL THF suspension of CrCl<sub>3</sub>(THF)<sub>3</sub> (0.149 g, 0.398 mmol). The resulting dark solution was warmed to RT over two hours, then diluted to 16 mL with Et<sub>2</sub>O. Next, 0.5 mL 1,4-dioxane was added, resulting in the precipitation of white solids. After stirring for 18 hr, the dark solution was filtered through Celite, and the filtrate reduced *in vacuo* to obtain red crystals amongst a sticky brown residue. This mixture was rinsed with minimal hexanes, then Et<sub>2</sub>O, decanting the brown washes from the red crystals. Anal. Calcd. for C<sub>34</sub>H<sub>51</sub>CrN<sub>3</sub>: C, 73.57; H, 8.98; N, 7.80. Found: C, 73.52; H, 9.18; N, 7.70.

**Oligomerization Catalysis.** Complexes **1-4** and **6** were activated as follows: the Cr complex (8.0 μmol) and <sup>iPr</sup>PNP (8.8 μmol) were dissolved in 1.0 mL PhCl in a 20 mL vial in the glovebox. To the stirring, room temperature solution, HBAr'<sub>4</sub> (8.0 μmol) dissolved in 0.5 mL PhCl was added dropwise over one minute. For most examples, a color change rapidly occurred. Quickly, the solution was diluted to 7.5 mL by addition of PhCl, and then transferred to a glass Fisher-Porter bottle equipped with a stir bar (for experiments at 100 psi). The reactor was sealed, and taken out of the glovebox to the high-pressure setup, and placed in a water bath at 25 °C. The gas line was evacuated, then backfilled with ethylene gas. The line was pressurized to 100 psig with ethylene, and then opened to the reactor. The pressurized solution was stirred for 45 min. After this time, the reactor was vented, and 0.1 mL methanol was added to quench the mixture. Adamantane was added to the solution as a

reference compound, which was then filtered and analyzed by GC/FID to quantify the oligomers. Polymer was weighed on a tared glass fritted filter.

For catalysis using **5**, it was weighed in the glovebox (14.5 mg, 9.0  $\mu\text{mol}$ ), then dissolved in 7.5 mL PhCl. This solution was transferred to the reactor and pressurized as described above.

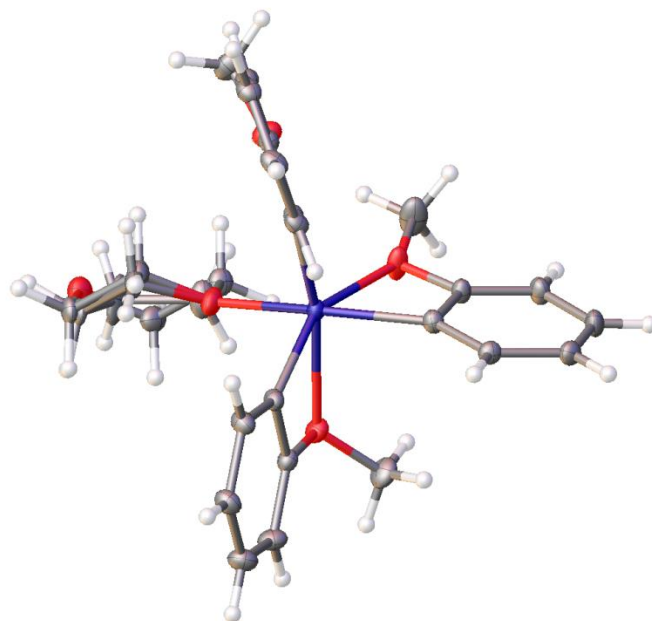
**X-Ray Crystallography and Crystallographic Tables.** Suitable crystals of complexes **1**, **2**, **3**, **3'**, **4**, and **5** were mounted on a nylon loop using Paratone oil, then placed on a diffractometer under a nitrogen stream. X-ray intensity data were collected on a Bruker APEXII CCD area detector or a Bruker D8 VENTURE Kappa Duo PHOTON 100 CMOS detector employing Mo-K $\alpha$  radiation ( $\lambda = 0.71073 \text{ \AA}$ ) or Cu-K $\alpha$  radiation ( $\lambda = 1.54178 \text{ \AA}$ ) at a temperature of 100 K. All diffractometer manipulations, including data collection, integration and scaling were carried out using the Bruker APEX3 software<sup>27</sup> In APEX3, intensity data were absorption-corrected using SADABS, and space groups were determined on the basis of systematic absences and intensity statistics using XPREP. Using Olex2, the structures were solved using ShelXT and refined to convergence by full-matrix least squares minimization.<sup>28</sup> All non-hydrogen atoms were refined using anisotropic displacement parameters. Hydrogen atoms were placed in idealized positions and refined using a riding model. In complex **3**, solvent disorder from a combination of 3.4 CH<sub>2</sub>Cl<sub>2</sub> and/or pentane molecules (42 electrons each) was treated by SQUEEZE/PLATON. Crystals of complex **3'** were obtained by the same route as complex **3**, but THF was the solvent of crystallization, rather than CH<sub>2</sub>Cl<sub>2</sub>; the molecular structure is shown in Figure 4. In complex **3'**, the disorder in the ethereal ligand bound to Cr was modeled as a mixture of THF and 1,4-dioxane using the PART instruction (1,4-dioxane was also used in the synthetic protocol) and C-C bond distance constraints and restraints. For complex **5**, the disorder in five of the eight CF<sub>3</sub>

groups of the  $\text{BAr}'_4$  anion was modeled using the PART instruction and bond distance and anisotropic displacement parameter restraints. In complex **5**, the  $\text{CH}_2\text{Cl}_2$  solvent disorder was modeled using the EQIV instruction, placing half of a molecule of  $\text{CH}_2\text{Cl}_2$  in the asymmetric unit. Graphical representations of structures with 50% probability thermal ellipsoids were generated using Diamond 3 visualization software.<sup>29</sup>

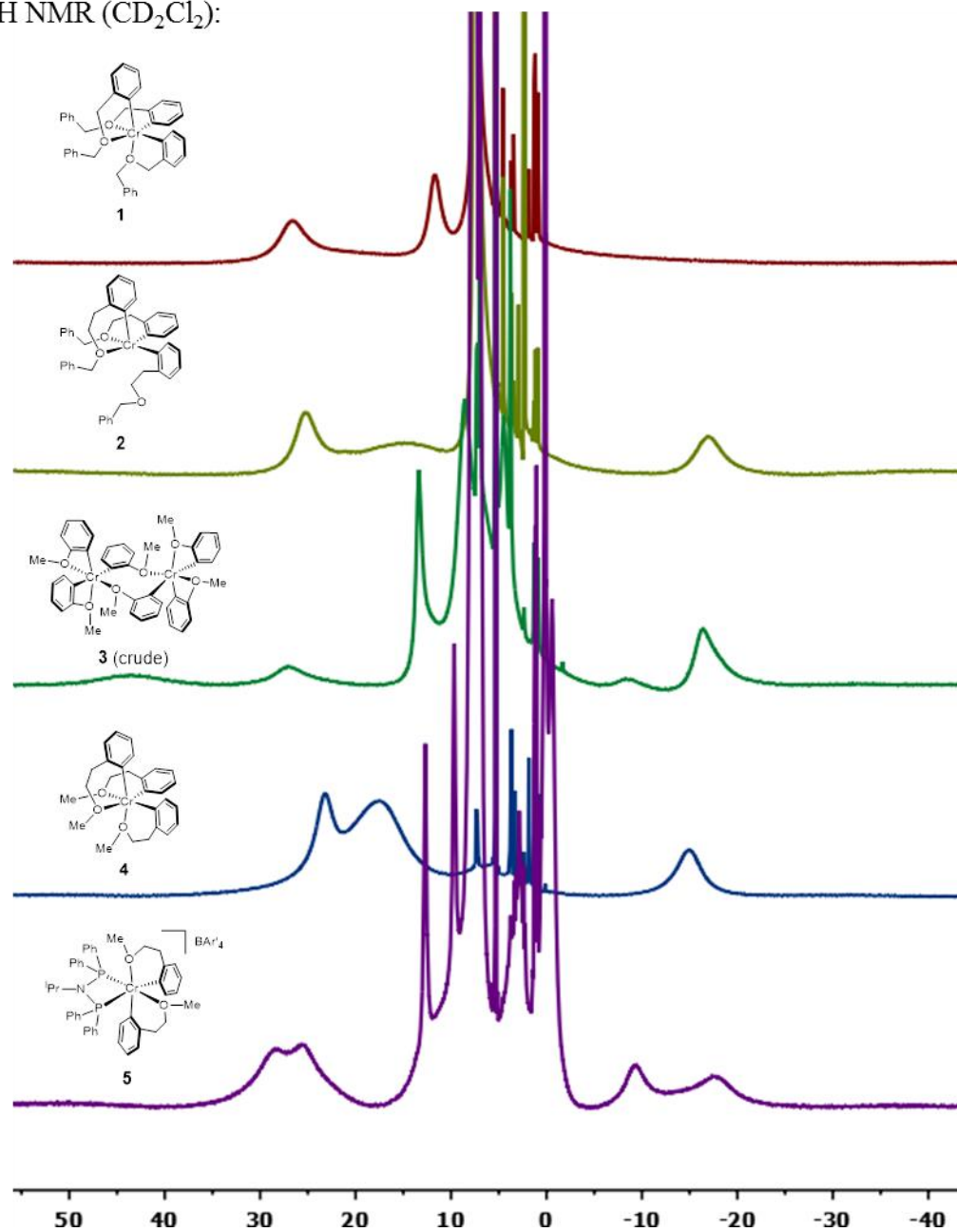
Compound	1	2
CCDC	1895679	1895680
Empirical formula	C <sub>42</sub> H <sub>39</sub> CrO <sub>3</sub>	C <sub>45</sub> H <sub>45</sub> CrO <sub>3</sub>
Formula weight	643.73	685.81
Temperature/K	99.97	99.99
Crystal system	triclinic	monoclinic
Space group	P-1	P2 <sub>1</sub> /c
a/Å	10.7286(4)	11.5802(10)
b/Å	11.7519(4)	15.8845(12)
c/Å	15.0753(5)	20.0281(17)
α/°	95.481(2)	90
β/°	102.260(2)	103.123(3)
γ/°	115.318(2)	90
Volume/Å <sup>3</sup>	1641.19(11)	3587.9(5)
Z	2	4
ρ <sub>calc</sub> /cm <sup>3</sup>	1.303	1.270
μ/mm <sup>-1</sup>	3.170	0.359
F(000)	678	1452
Crystal size/mm <sup>3</sup>	0.166 × 0.14 × 0.086	0.314 × 0.245 × 0.22
Radiation	CuKα (λ = 1.54178)	MoKα (λ = 0.71073)
2θ range for data collection/°	6.14 to 136.72	4.902 to 72.626
Index ranges	-12 ≤ h ≤ 12, -14 ≤ k ≤ 14, -18 ≤ l ≤ 18	-19 ≤ h ≤ 19, -26 ≤ k ≤ 26, -33 ≤ l ≤ 33
Reflections collected	44667	210362
Independent reflections	6047 [R <sub>int</sub> = 0.0679, R <sub>sigma</sub> = 0.0454]	17385 [R <sub>int</sub> = 0.0701, R <sub>sigma</sub> = 0.0305]
Data/restraints/parameters	6047/0/415	17385/0/442
Goodness-of-fit on F <sup>2</sup>	1.041	1.059
Final R indexes [I ≥ 2σ (I)]	R <sub>1</sub> = 0.0493, wR <sub>2</sub> = 0.0983	R <sub>1</sub> = 0.0409, wR <sub>2</sub> = 0.1106
Final R indexes [all data]	R <sub>1</sub> = 0.0685, wR <sub>2</sub> = 0.1061	R <sub>1</sub> = 0.0594, wR <sub>2</sub> = 0.1225
Largest diff. peak/hole / e Å <sup>-3</sup>	0.300/-0.472	0.703/-0.619

Compound	<b>3</b>	<b>3'</b>
CCDC	1895681	1895682
Empirical formula	C <sub>21</sub> H <sub>21</sub> CrO <sub>3</sub>	C <sub>25</sub> H <sub>29</sub> CrO <sub>4.58</sub>
Formula weight	373.38	454.80
Temperature/K	100.0	100.05
Crystal system	triclinic	monoclinic
Space group	P-1	Cc
a/Å	12.0150(16)	20.0935(10)
b/Å	12.4851(16)	11.1921(6)
c/Å	15.1703(19)	10.9889(5)
$\alpha$ /°	75.513(5)	90
$\beta$ /°	87.541(5)	116.859(2)
$\gamma$ /°	80.203(5)	90
Volume/Å <sup>3</sup>	2171.2(5)	2204.68(19)
Z	4	4
$\rho_{\text{calc}}/\text{cm}^3$	1.142	1.370
$\mu/\text{mm}^{-1}$	0.540	0.551
F(000)	780	959
Crystal size/mm <sup>3</sup>	0.252 × 0.179 × 0.125	0.406 × 0.168 × 0.108
Radiation	MoK $\alpha$ ( $\lambda$ = 0.71073)	MoK $\alpha$ ( $\lambda$ = 0.71073)
2 $\theta$ range for data collection/°	4.42 to 66.342	6.650 to 72.734
Index ranges	-17 ≤ h ≤ 18, -19 ≤ k ≤ 19, -23 ≤ l ≤ 22	-33 ≤ h ≤ 33, -18 ≤ k ≤ 18, -18 ≤ l ≤ 18
Reflections collected	102156	60629
Independent reflections	14945 [R <sub>int</sub> = 0.0687, R <sub>sigma</sub> = 0.0569]	10655 [R <sub>int</sub> = 0.0585, R <sub>sigma</sub> = 0.0405]
Data/restraints/parameters	14945/0/457	10655/10/320
Goodness-of-fit on F <sup>2</sup>	1.039	1.028
Final R indexes [I ≥ 2 $\sigma$ (I)]	R <sub>1</sub> = 0.0610, wR <sub>2</sub> = 0.1147	R <sub>1</sub> = 0.0310, wR <sub>2</sub> = 0.0730
Final R indexes [all data]	R <sub>1</sub> = 0.0897, wR <sub>2</sub> = 0.1247	R <sub>1</sub> = 0.0366, wR <sub>2</sub> = 0.0750
Largest diff. peak/hole / e Å <sup>-3</sup>	0.696/-0.613	0.667/-0.493

Compound	4	5
CCDC	1895683	1895684
Empirical formula	C <sub>27</sub> H <sub>33</sub> CrO <sub>3</sub>	C <sub>77.5</sub> H <sub>62</sub> BClCrF <sub>24</sub> NO <sub>2</sub> P <sub>2</sub>
Formula weight	457.53	1655.48
Temperature/K	100.09	100.01
Crystal system	monoclinic	triclinic
Space group	P2 <sub>1</sub> /n	P-1
a/Å	8.3974(4)	12.9268(7)
b/Å	22.6187(10)	16.7595(10)
c/Å	12.1007(5)	18.9950(9)
α/°	90	104.445(2)
β/°	92.754(2)	96.510(2)
γ/°	90	107.746(2)
Volume/Å <sup>3</sup>	2295.73(18)	3714.6(4)
Z	4	2
ρ <sub>calc</sub> /cm <sup>3</sup>	1.324	1.48
μ/mm <sup>-1</sup>	0.524	0.341
F(000)	972	1684
Crystal size/mm <sup>3</sup>	0.198 × 0.143 × 0.133	0.2 × 0.15 × 0.1
Radiation	MoKα (λ = 0.71073)	MoKα (λ = 0.71073)
2θ range for data collection/°	5.778 to 72.716	4.526 to 67.496
Index ranges	-13 ≤ h ≤ 13, -37 ≤ k ≤ 37, -19 ≤ l ≤ 20	-20 ≤ h ≤ 20, -26 ≤ k ≤ 25, -29 ≤ l ≤ 29
Reflections collected	87691	199425
Independent reflections	11083 [R <sub>int</sub> = 0.0548, R <sub>sigma</sub> = 0.0363]	29673 [R <sub>int</sub> = 0.0508, R <sub>sigma</sub> = 0.0379]
Data/restraints/parameters	11083/0/283	29673/369/1135
Goodness-of-fit on F <sup>2</sup>	1.065	1.100
Final R indexes [I ≥ 2σ (I)]	R <sub>1</sub> = 0.0444, wR <sub>2</sub> = 0.0987	R <sub>1</sub> = 0.0621, wR <sub>2</sub> = 0.1413
Final R indexes [all data]	R <sub>1</sub> = 0.0631, wR <sub>2</sub> = 0.1056	R <sub>1</sub> = 0.0808, wR <sub>2</sub> = 0.1500
Largest diff. peak/hole / e Å <sup>-3</sup>	1.357/-0.488	1.197/-2.170



**Figure 4.** Solid-state structure of complex **3'**, which is obtained by following the synthetic protocol for **3**, yet growing crystals in THF. The coordinated ethereal ligand is modeled as a mixture of THF/1,4-dioxane (1,4-dioxane is used in the synthesis of **3/3'**).

$^1\text{H}$  NMR ( $\text{CD}_2\text{Cl}_2$ ):

**Figure 5.** Paramagnetic  $^1\text{H}$  NMR spectra. Each sample is prepared in  $\text{CD}_2\text{Cl}_2$  with  $[\text{Cr}] \approx 100$  mM.

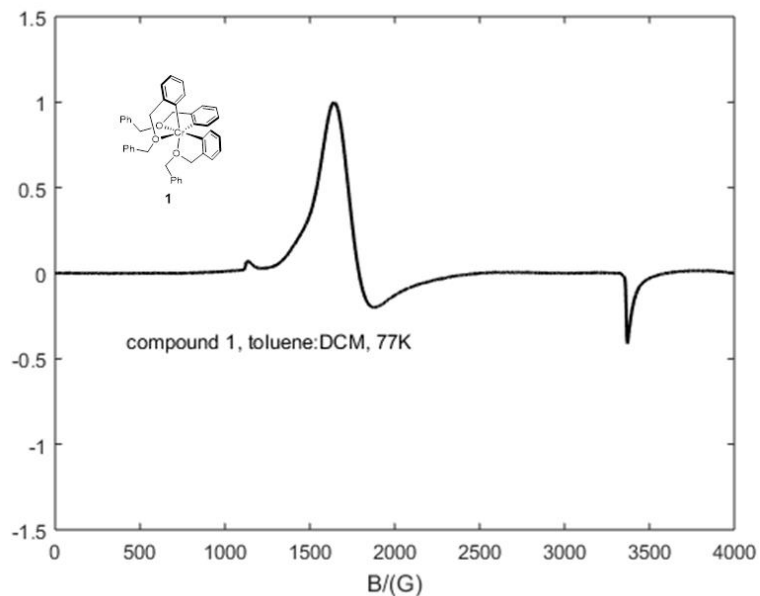


**Figure 6.** Continuous wave (cw) EPR spectrum of compound **1**. Temperature: 77K. Microwave frequency: 9.4 GHz. Microwave power: 6.4 mW. Modulation frequency: 100 kHz. Modulation amplitude: 4.0 G.

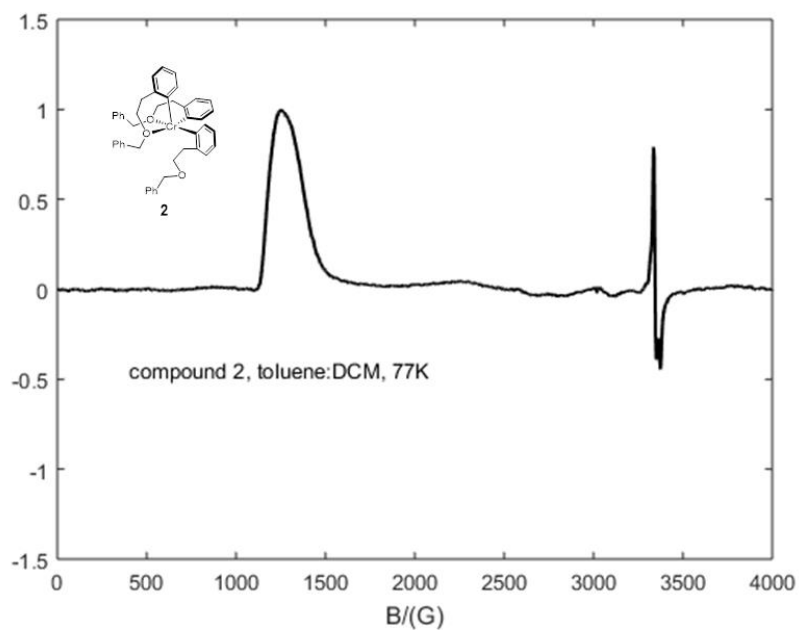


**Figure 7.** Continuous wave (cw) EPR spectrum of compound **2**. Temperature: 77K. Microwave frequency: 9.4 GHz. Microwave power: 6.4 mW. Modulation frequency: 100 kHz. Modulation amplitude: 4.0 G.

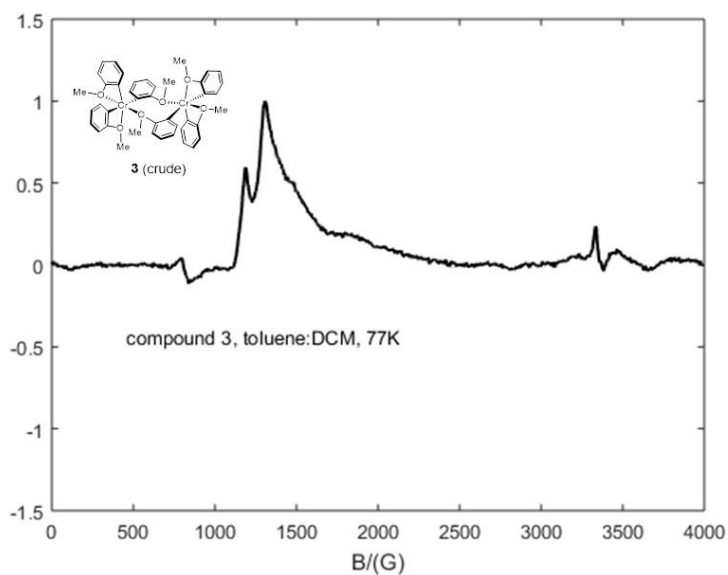


**Figure 8.** Continuous wave (cw) EPR spectrum of compound **3**. Temperature: 77K. Microwave frequency: 9.4 GHz. Microwave power: 6.4 mW. Modulation frequency: 100 kHz. Modulation amplitude: 4.0 G.

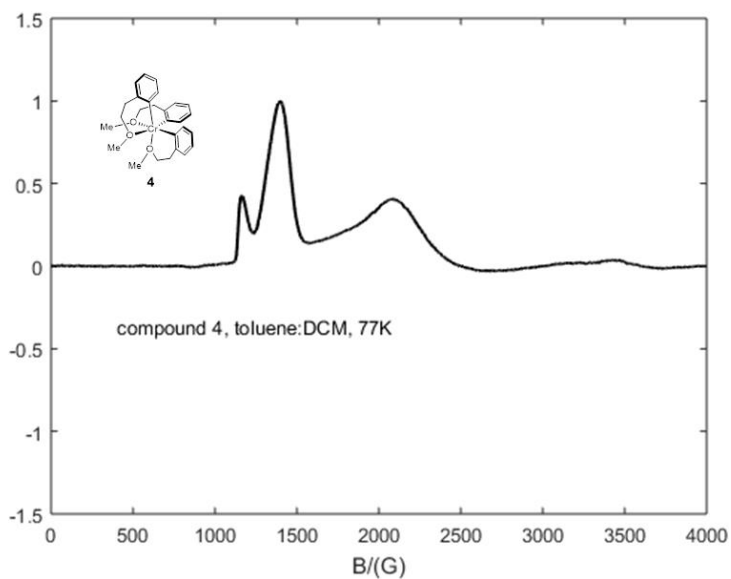


**Figure 9.** Continuous wave (cw) EPR spectrum of compound **4**. Temperature: 77K. Microwave frequency: 9.4 GHz. Microwave power: 6.4 mW. Modulation frequency: 100 kHz. Modulation amplitude: 4.0 G.

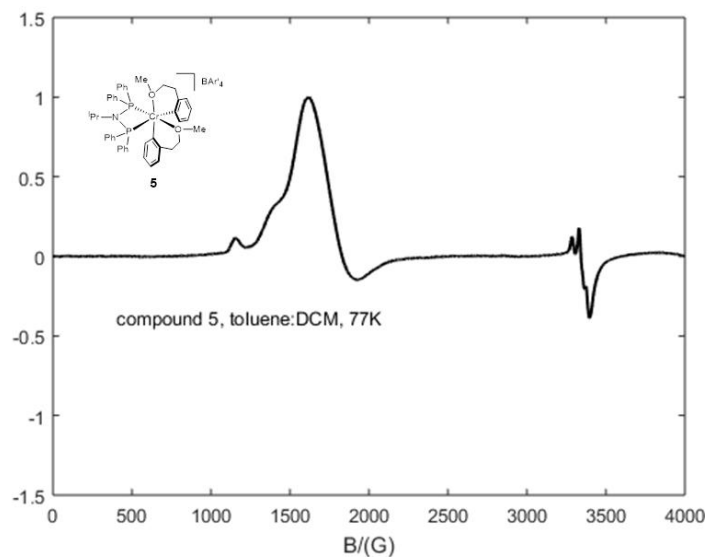


**Figure 10.** Continuous wave (cw) EPR spectrum of compound **5**. Temperature: 77K. Microwave frequency: 9.4 GHz. Microwave power: 6.4 mW. Modulation frequency: 100 kHz. Modulation amplitude: 4.0 G.

## References.

- (1) Chirik, P.; Morris, R. *Acc. Chem. Res.* **2015**, *48*, 2495.
- (2) (a) Steib, A. K.; Kuzmina, O. M.; Fernandez, S.; Flubacher, D.; Knochel, P. *J. Am. Chem. Soc.* **2013**, *135*, 15346. (b) Cong, X.; Tang, H.; Zeng, X. *J. Am. Chem. Soc.* **2015**, *137*, 14367. (c) Cong, X.; Fan, F.; Ma, P.; Luo, M.; Chen, H.; Zeng, X. *J. Am. Chem. Soc.* **2017**, *139*, 15182. (d) Tang, J.; Liu, P.; Zeng, X. *Chem. Comm.* **2018**, *54*, 9325. (e) Chen, C.; Liu, P.; Luo, M.; Zeng, X. *ACS Catal.* **2018**, *8*, 5864. (f) Schiwiek, C. H.; Vasilenko, V.; Wadepohl, H.; Gade, L. H. *Chem. Comm.* **2018**, *54*, 9139.
- (3) (a) Wu, J. Y.; Stanzl, B. N.; Ritter, T. *J. Am. Chem. Soc.* **2010**, *132*, 13214. (b) García Mancheño, O. *Angew. Chem. Int. Ed.* **2011**, *50*, 2216. (c) Hazari, N.; Melvin, P. R.; Beromi, M. *Nat. Rev. Chem.* **2017**, *1*, 0025.
- (4) (a) Monillas, W. H.; Yap, G. P. A.; MacAdams, L. A.; Theopold, K. H. *J. Am. Chem. Soc.* **2007**, *129*, 8090. (b) Monillas, W. H.; Yap, G. P. A.; Theopold, K. H. *Inorg. Chim. Acta*

**2011**, 369, 103. (c) Akturk, E. S.; Yap, G. P. A.; Theopold, K. H. *Chem. Comm.* **2015**, 51, 15402. (d) MacLeod, K. C.; Conway, J. L.; Patrick, B. O.; Smith, K. M. *J. Am. Chem. Soc.* **2010**, 132, 17325. (e) Emrich, R.; Heinemann, O.; Jolly, P. W.; Krüger, C.; Verhovnik, G. P. *J. Organometallics* **1997**, 16, 1511. (f) Rozenel, S. S.; Chomitz, W. A.; Arnold, J. *Organometallics* **2009**, 28, 6243. (g) Albahily, K.; Shaikh, Y.; Sebastiao, E.; Gambarotta, S.; Korobkov, I.; Gorelsky, S. I. *J. Am. Chem. Soc.* **2011**, 133, 6388. (h) Wolf, R.; Brynda, M.; Ni, C.; Long, G. J.; Power, P. P. *J. Am. Chem. Soc.* **2007**, 129, 6076. (i) Boynton, J. N.; Summerscales, O. T.; Grandjean, F.; Long, G. J.; Fettingner, J. C.; Power, P. P. *Organometallics* **2012**, 31, 8556.

(5) (a) Bollmann, A.; Blann, K.; Dixon, J. T.; Hess, F. M.; Killian, E.; Maumela, H.; McGuinness, D. S.; Morgan, D. H.; Neveling, A.; Otto, S.; Overett, M.; Slawin, A. M. Z.; Wasserscheid, P.; Kuhlmann, S. *J. Am. Chem. Soc.* **2004**, 126, 14712. (b) Dixon, J. T.; Green, M. J.; Hess, F. M.; Morgan, D. H. *J. Organomet. Chem.* **2004**, 689, 3641. (c) Overett, M. J.; Blann, K.; Bollmann, A.; Dixon, J. T.; Haasbroek, D.; Killian, E.; Maumela, H.; McGuinness, D. S.; Morgan, D. H. *J. Am. Chem. Soc.* **2005**, 127, 10723. (d) Wass, D. F. *Dalton Trans.* **2007**, 816. (e) McGuinness, D. S. *Chem. Rev.* **2011**, 111, 2321. (f) Agapie, T. *Coord. Chem. Rev.* **2011**, 255, 861. (g) van Leeuwen, P. W. N. M.; Clément, N. D.; Tschan, M. J. L. *Coord. Chem. Rev.* **2011**, 255, 1499.

(6) (a) Overett, M. J.; Blann, K.; Bollmann, A.; Dixon, J. T.; Hess, F.; Killian, E.; Maumela, H.; Morgan, D. H.; Neveling, A.; Otto, S. *Chem. Comm.* **2005**, 622. (b) Elowe, P. R.; McCann, C.; Pringle, P. G.; Spitzmesser, S. K.; Bercaw, J. E. *Organometallics* **2006**, 25, 5255. (c) Blann, K.; Bollmann, A.; de Bod, H.; Dixon, J. T.; Killian, E.; Nongodlwana, P.; Maumela, M. C.; Maumela, H.; McConnell, A. E.; Morgan, D. H.; Overett, M. J.; Prétorius, M.; Kuhlmann, S.; Wasserscheid, P. *J. Catal.* **2007**, 249, 244. (d) Killian, E.; Blann, K.; Bollmann, A.; Dixon, J. T.; Kuhlmann, S.; Maumela, M. C.; Maumela, H.; Morgan, D. H.;

Nongodlwana, P.; Overett, M. J.; Pretorius, M.; Höfener, K.; Wasserscheid, P. *J. Mol. Catal. A: Chem.* **2007**, *270*, 214. (e) Weng, Z.; Teo, S.; Andy Hor, T. S. *Dalton Trans.* **2007**, 3493. (f) Overett, M. J.; Blann, K.; Bollmann, A.; de Villiers, R.; Dixon, J. T.; Killian, E.; Maumela, M. C.; Maumela, H.; McGuinness, D. S.; Morgan, D. H.; Rucklidge, A.; Slawin, A. M. Z. *J. Mol. Catal. A: Chem.* **2008**, *283*, 114. (g) Licciulli, S.; Thapa, I.; Albahily, K.; Korobkov, I.; Gambarotta, S.; Duchateau, R.; Chevalier, R.; Schuhen, K. *Angew. Chem. Int. Ed.* **2010**, *49*, 9225. (h) Shaikh, Y.; Albahily, K.; Sutcliffe, M.; Fomitcheva, V.; Gambarotta, S.; Korobkov, I.; Duchateau, R. *Angew. Chem. Int. Ed.* **2012**, *51*, 1366. (i) Newland, R. J.; Smith, A.; Smith, D. M.; Fey, N.; Hanton, M. J.; Mansell, S. M. *Organometallics* **2018**, *37*, 1062.

(7) (a) McGuinness, D. S.; Overett, M.; Tooze, R. P.; Blann, K.; Dixon, J. T.; Slawin, A. M. Z. *Organometallics* **2007**, *26*, 1108. (b) McGuinness, D. S.; Rucklidge, A. J.; Tooze, R. P.; Slawin, A. M. Z. *Organometallics* **2007**, *26*, 2561.

(8) Fernelius, W. C., Blanch, J. E., Bryant, B.E., Terada, K., Drago, R. S. and Stille, J. K. "Chromium(III) Acetylacetonate" In *Inorganic Syntheses* 2007.

(9) Sydora, O. L.; Hart, R. T.; Eckert, N. A.; Martinez Baez, E.; Clark, A. E.; Benmore, C. J. *Dalton Trans.* **2018**, *47*, 4790.

(10) (a) Herwig, W.; Zeiss, H. *The Journal of Organic Chemistry* **1958**, *23*, 1404. (b) Jeon, J. Y.; Park, J. H.; Park, D. S.; Park, S. Y.; Lee, C. S.; Go, M. J.; Lee, J.; Lee, B. Y. *Inorg. Chem. Commun.* **2014**, *44*, 148.

(11) (a) Kern, R. J. *J. Inorg. Nucl. Chem.* **1962**, *24*, 1105. (b) Crochet, A.; Brog, J.-P.; Fromm, K. M. *Cryst. Growth Des.* **2016**, *16*, 189.

(12) (a) Rabeah, J.; Bauer, M.; Baumann, W.; McConnell, A. E. C.; Gabrielli, W. F.; Webb, P. B.; Selent, D.; Brückner, A. *ACS Catal.* **2012**, *3*, 95. (b) Stennett, T. E.; Haddow, M. F.; Wass, D. F. *Organometallics* **2012**, *31*, 6960. (c) Do, L. H.; Labinger, J. A.; Bercaw, J. E.

*ACS Catal.* **2013**, *3*, 2582. (d) Bartlett, S. A.; Moulin, J.; Tromp, M.; Reid, G.; Dent, A. J.; Cibin, G.; McGuinness, D. S.; Evans, J. *Catal. Sci. Technol.* **2016**, *6*, 6237.

(13) (a) Agapie, T.; Schofer, S. J.; Labinger, J. A.; Bercaw, J. E. *J. Am. Chem. Soc.* **2004**, *126*, 1304. (b) Schofer, S. J.; Day, M. W.; Henling, L. M.; Labinger, J. A.; Bercaw, J. E. *Organometallics* **2006**, *25*, 2743. (c) Vidyaratne, I.; Nikiforov, G. B.; Gorelsky, S. I.; Gambarotta, S.; Duchateau, R.; Korobkov, I. *Angew. Chem. Int. Ed.* **2009**, *48*, 6552. (d) Albahily, K.; Fomitcheva, V.; Gambarotta, S.; Korobkov, I.; Murugesu, M.; Gorelsky, S. I. *J. Am. Chem. Soc.* **2011**, *133*, 6380. (e) Monillas, W. H.; Young, J. F.; Yap, G. P. A.; Theopold, K. H. *Dalton Trans.* **2013**, *42*, 9198. (f) Jabri, A.; Mason, C. B.; Sim, Y.; Gambarotta, S.; Burchell, T. J.; Duchateau, R. *Angew. Chem. Int. Ed.* **2008**, *47*, 9717.

(14) Hirscher, N. A.; Agapie, T. *Organometallics* **2017**, *36*, 4107.

(15) (a) Kreisel, K. A.; Yap, G. P. A.; Theopold, K. H. *Organometallics* **2006**, *25*, 4670. (b) Conde-Guadano, S.; Danopoulos, A. A.; Pattacini, R.; Hanton, M.; Tooze, R. P. *Organometallics* **2012**, *31*, 1643. (c) Danopoulos, A. A.; Monakhov, K. Y.; Robert, V.; Braunstein, P.; Pattacini, R.; Conde-Guadano, S.; Hanton, M.; Tooze, R. P. *Organometallics* **2013**, *32*, 1842. (d) Ronellenfitsch, M.; Wadepohl, H.; Enders, M. *Organometallics* **2014**, *33*, 5758. (e) Ai, P.; Danopoulos, A. A.; Braunstein, P. *Organometallics* **2015**, *34*, 4109.

(16) (a) Herwig, W.; Zeiss, H. *J. Am. Chem. Soc.* **1959**, *81*, 4798. (b) Khan, S. I.; Bau, R. *Organometallics* **1983**, *2*, 1896.

(17) (a) Manzer, L. E. *J. Organomet. Chem.* **1977**, *135*, C6. (b) Manzer, L. E. *J. Am. Chem. Soc.* **1978**, *100*, 8068. (c) Cotton, F. A.; Mott, G. N. *Organometallics* **1982**, *1*, 38. (d) Edema, J. J. H.; Gambarotta, S.; Meetsma, A.; Spek, A. L. *Organometallics* **1992**, *11*, 2452. (e) Hao, S.; Song, J.-I.; Berno, P.; Gambarotta, S. *Organometallics* **1994**, *13*, 1326. (f) Daly, J. J.; Sanz, F.; Sneed, R. P. A.; Zeiss, H. H. *Helv. Chim. Acta* **1974**, *57*, 1863. (g) Kim, E. H.; Lee, H. M.; Jeong, M.

S.; Ryu, J. Y.; Lee, J.; Lee, B. Y. *ACS Omega* **2017**, *2*, 765. (h) MacLeod, K. C.; Patrick, B. O.; Smith, K. M. *Organometallics* **2012**, *31*, 6681. (i) McGowan, K. P.; Abboud, K. A.; Veige, A. S. *Organometallics* **2011**, *30*, 4949. (j) O'Reilly, M. E.; Del Castillo, T. J.; Falkowski, J. M.; Ramachandran, V.; Pati, M.; Correia, M. C.; Abboud, K. A.; Dalal, N. S.; Richardson, D. E.; Veige, A. S. *J. Am. Chem. Soc.* **2011**, *133*, 13661.

(18) (a) Bowen, L. E.; Haddow, M. F.; Orpen, A. G.; Wass, D. F. *Dalton Trans.* **2007**, 1160. (b) Rucklidge, A. J.; McGuinness, D. S.; Tooze, R. P.; Slawin, A. M. Z.; Pelletier, J. D. A.; Hanton, M. J.; Webb, P. B. *Organometallics* **2007**, *26*, 2782.

(19) Bähr, G.; Zohm, H. *Angew. Chem.* **1963**, *75*, 94.

(20) (a) Robertson, N. J.; Carney, M. J.; Halfen, J. A. *Inorg. Chem.* **2003**, *42*, 6876. (b) Rogers, J. S.; Bu, X.; Bazan, G. C. *J. Am. Chem. Soc.* **2000**, *122*, 730. (c) MacAdams, L. A.; Buffone, G. P.; Incarvito, C. D.; Rheingold, A. L.; Theopold, K. H. *J. Am. Chem. Soc.* **2005**, *127*, 1082. (d) Thomas, B. J.; Noh, S. K.; Schulte, G. K.; Sendlinger, S. C.; Theopold, K. H. *J. Am. Chem. Soc.* **1991**, *113*, 893.

(21) (a) Jabri, A.; Crewdson, P.; Gambarotta, S.; Korobkov, I.; Duchateau, R. *Organometallics* **2006**, *25*, 715. (b) Lifschitz, A. M.; Hirscher, N. A.; Lee, H. B.; Buss, J. A.; Agapie, T. *Organometallics* **2017**, *36*, 1640. (c) Alzamy, A.; Gambarotta, S.; Korobkov, I. *Organometallics* **2013**, *32*, 7107. (d) Alzamy, A.; Gambarotta, S.; Korobkov, I. *Organometallics* **2013**, *32*, 7204. (e) Liu, S.; Pattacini, R.; Braunstein, P. *Organometallics* **2011**, *30*, 3549.

(22) Brown, T. L.; Dickerhoof, D. W.; Bafus, D. A.; Morgan, G. L. *Review of Scientific Instruments* **1962**, *33*, 491.

(23) Brookhart, M.; Grant, B.; Volpe, A. F. *Organometallics* **1992**, *11*, 3920.

(24) (a) Bos, M. E.; Wulff, W. D.; Miller, R. A.; Chamberlin, S.; Brandvold, T. A. *J. Am. Chem. Soc.* **1991**, *113*, 9293. (b) Zhang, A.; RajanBabu, T. V. *J. Am. Chem. Soc.* **2006**, *128*, 54.

(c) Reich, H. J.; Goldenberg, W. S.; Sanders, A. W.; Jantzi, K. L.; Tzschucke, C. C. *J. Am. Chem. Soc.* **2003**, *125*, 3509.

(25) Wehman-Ooyevaar, I. C. M.; Luitwieler, I. F.; Vatter, K.; Grove, D. M.; Smeets, W. J. J.; Horn, E.; Spek, A. L.; Koten, G. v. *Inorg. Chim. Acta* **1996**, *252*, 55.

(26) (a) Evans, D. F. *Journal of the Chemical Society (Resumed)* **1959**, 2003. (b) Piguët, C. *Journal of Chemical Education* **1997**, *74*, 815.

(27) Bruker APEX3; Bruker AXS Inc.: Madison, Wisconsin, USA, 2012.

(28) (a) Dolomanov, O. V.; Bourhis, L. J.; Gildea, R. J.; Howard, J. A. K.; Puschmann, H. *Journal of Applied Crystallography* **2009**, *42*, 339. (b) Sheldrick, G. *Acta Crystallographica Section A* **2015**, *71*, 3.

(29) Putz, H.; Brandenburg, K. *Diamond - Crystal and Molecular Structure Visualization* Bonn, Germany.

## Chapter 5

Structural Determination of Cr-Hydrocarbyl Species via Pulse EPR in the  
Study of Ethylene Tetramerization Catalysis

Reprinted with permission from:

*Organometallics* **Article ASAP** DOI: 10.1021/acs.organomet.0c00521

Copyright 2020 American Chemical Society

**Abstract.**

A chromium-methyl precatalyst for ethylene tetramerization (**1-h<sub>3</sub>**) has been investigated by CW- and pulse EPR spectroscopies. Using a synthesized Cr-CD<sub>3</sub> (**1-d<sub>3</sub>**) isotopologue, the presence of this methyl ligand was confirmed to remain bound to Cr in solution, by detection of <sup>2</sup>H couplings in X-band hyperfine sublevel correlation (HYSCORE) spectroscopy. Furthermore, the product of Cr-CD<sub>3</sub> protonolysis maintained spectroscopic features in HYSCORE attributable to this CD<sub>3</sub> group. Additionally, the pulse EPR characterization of an S = 1/2 Cr(I) species generated from this precatalyst during catalytic reaction with ethylene is reported. This is the first direct observation of hydrocarbyl ligands on Cr using pulse EPR methods.

## Introduction.

The development of catalysis using first-row metals is very desirable from a cost and sustainability perspective. The associated challenge is that mechanistic and synthetic studies required to develop these catalysts are often complicated by the paramagnetism of first-row metal complexes.<sup>1</sup> Nuclear magnetic resonance (NMR) spectroscopy is much less suited for the structural elucidation of paramagnetic species than diamagnetic ones due to the significant broadening induced by the paramagnetic metal center.<sup>2</sup> Electron paramagnetic resonance (EPR) spectroscopy, as commonly employed in a continuous wave (CW) setup, also does not provide a high degree of information regarding chemical structure.<sup>3</sup> To develop open-shell catalysts based on first-row metals, pulse EPR must become more widely applied in synthetic chemistry.<sup>4</sup>

Chromium catalysts are used in the selective production of  $\alpha$ -olefins (1-hexene and 1-octene) by ethylene oligomerization.<sup>5</sup> To study the chromium catalyst speciation in a variety of oligomerization systems, EPR spectroscopic methods have been employed.<sup>6</sup> Conclusions from these studies have been based primarily on the spectroscopic signature of spin-active species observed *in situ* following both precatalyst activation or reactions with ethylene.

All of these studies implemented large excesses of alkyl aluminum activators, as is typically required for all ethylene tetramerization catalysis, until a recent report from our group (work described in Chapter 2). These activation processes complicate the interpretation of spectroscopic results due to the dynamism of Cr speciation *in situ*.<sup>6c</sup> Furthermore, the EPR methods employed on these systems in the past have largely been limited to continuous wave (CW) spectroscopy, which provides little information regarding the specific coordination sphere of Cr, as these spectra are typically dominated by the zero

field splitting (zfs) interaction between the 3 unpaired electrons in Cr(III) species, or inhomogeneous broadening in Cr(I) species.

Herein, we apply pulse EPR techniques to the *in situ* characterization of Cr precatalysts activated by protonation. Using hyperfine sublevel correlation spectroscopy (HYSCORE), the direct detection of an isotopically-labelled Cr-methyl (Cr-CD<sub>3</sub>) moiety is achieved by measurement of deuterium hyperfine couplings to the paramagnetic Cr(III) center. Deuterium hyperfine features associated with this CD<sub>3</sub> moiety are retained in the product of activation via protonation, indicating that this ligand remains bound upon activation for ethylene oligomerization. This provides structural information of an activated precatalyst for ethylene tetramerization. This method was also applied to a freeze-quenched sample following addition of ethylene. To our knowledge, these are the first measurements of deuterium HYSCORE spectroscopy performed on any synthetic organometallic chromium species.

## Results and Discussion.

Chromium-PNP bis(aryl)ether complex **1** (i.e. **1-h<sub>3</sub>**) was previously structurally characterized via single-crystal X-ray diffraction (XRD) and demonstrated to be a competent precatalyst for ethylene tetramerization following activation by protonation (Chapter 2). The frozen solution CW EPR spectrum for **1** is displayed in Figure 1. The spectrum is characteristic of a high-spin Cr(III) center ( $S = 3/2$ ). Because of its instability, the protonated product (**2** and/or **3**) could not be isolated as a solid for structural characterization. Chapter 4 highlighted the importance of coordinative saturation to stabilize a PNP Cr(III) diaryl cationic species (**4** in Figure 1). Precatalyst **1** has the advantage over **4** in that its protonation leads to a cationic species that reacts readily with ethylene at low

pressures ( $\approx 1$  atm). Presumably due to slow initiation (attributable to the coordinative saturation), the UV/Vis or EPR spectra of **4** do not change upon exposure to 1 atm  $C_2H_4$  at room temperature (RT). At higher pressures of  $C_2H_4$  (100 psi), catalysis is achieved using **4** at RT; it is likely that a more substantial fraction of **4** initiates under those conditions (Chapter 4 and Appendix 2). Because of the relatively fast initiation, **1** was used successfully in a mechanistic study of catalysis using  $C_2D_4$  gas (Chapter 3). Therefore, the coordinatively-unsaturated protonation products of **1** were suited for spectroscopic studies of catalysis using EPR. The final advantage of the precatalyst **1** is that the methyl ligand provides a handle for isotopic labelling ( $CD_3$ ) for detection via pulse EPR experiments.

**Scheme 1.** Protonation of **1-h<sub>3</sub>** (or isotopically-labelled **1-d<sub>3</sub>**) is expected to lead to a mixture of **2-h<sub>3</sub>** (or **2-d<sub>3</sub>**) and **3**.

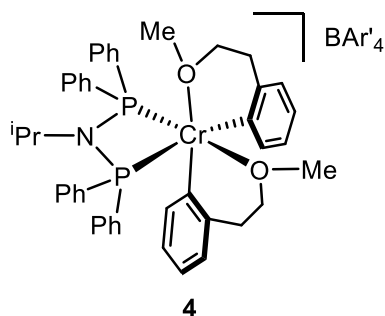
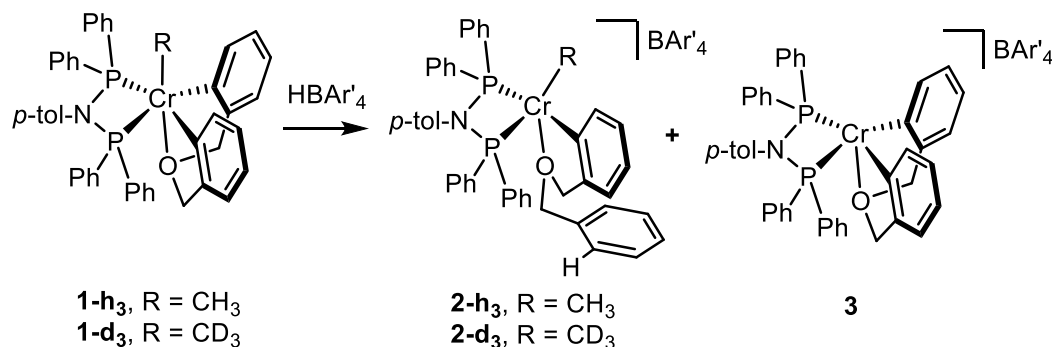


**Figure 1.** Single-component catalyst (discussed in Chapter 4).

**Preparation of an Isotopically-Labelled Cr(III) Methyl Cationic Species.** In order to provide specific structural details about the precatalyst **1** (**1-h<sub>3</sub>** from hereon) and its activation product, the deuterium isotopologue was made: **1-d<sub>3</sub>**. The frozen solution cw EPR spectrum of **1-d<sub>3</sub>** is nearly identical to that of **1-h<sub>3</sub>** (Figure 21 in Experimental section). The broadness of the spectra due to the zero-field splitting interaction is expected to preclude any resolution of hyperfine coupling to H or D on the methyl ligand. The C-H and C-D stretches of the methyl ligands in **1-h<sub>3</sub>** and **1-d<sub>3</sub>** were resolved using ATR-IR (see Figure 18 and 19 in Experimental section), corroborating the presence of the isotopically labelled ligand.<sup>7</sup>

**Selection of Pulse EPR Spectroscopic Techniques for the Detection of Cr(III) S = 3/2 Complexes.** Since deuterium nuclei have spin  $I = 1$ , they can induce deep modulation of the spin echo decay in pulse EPR, termed electron spin echo envelope modulation (ESEEM). ESEEM has been used to a significant extent in the characterization of biological and bioinorganic samples containing deuterated moieties (typically D<sub>2</sub>O ligands on metallocofactors).<sup>8</sup> ESEEM and its related two dimensional variant hyperfine sublevel correlation (HYSCORE) spectroscopy are advantageous for the detection of proximal nuclei to spin centers that exhibit relatively short-lived excited spin-state lifetimes. HYSCORE provides additional utility in comparison to the 1D ESEEM technique in that features arising from hyperfine couplings to different nuclei which are coupled to the same electron spin can be differentiated by the magnitude of their coupling relative to their characteristic nuclear Larmour frequency (see Experimental section for more details). For this reason, HYSCORE spectroscopy was utilized in the characterization of the series of complexes within the current study. The Cr(III) compounds studied herein exhibit spin lattice relaxation times that

are quite short ( $T_1 < 2 \mu\text{s}$ ), generally attributable to their high spin state ( $S=3/2$ ), making detection of nuclear hyperfine couplings by pulse electron nuclear double resonance (ENDOR) challenging. Despite this, in some cases, detection of  $^{31}\text{P}$  hyperfine couplings from the PNP ligand which are too large to be detected by HYSCORE was achieved via X-band Davies ENDOR (see Experimental section). This was only possible at the lowest temperatures we could obtain using a helium flow cryostat. We note that pulse ENDOR has rarely been used to study high spin ( $S > 1/2$ ) organometallic species.

**EPR Analysis of 1 and its Protonation Product.** With **1-h**<sub>3</sub> and **1-d**<sub>3</sub> in hand, a comparison of the spectral features of these complexes with their protonation products was possible. The preparation of activated precatalysts was performed as described in Chapter 2, using  $\text{HBAr}'_4$  in chlorobenzene solvent. We discovered that the addition of methylcyclohexane (MeCy) gave a higher-quality glass upon freezing the solutions. However, for solubility reasons, pure chlorobenzene was used if necessary. Good solubility and high quality glasses could also be obtained using toluene:Et<sub>2</sub>O or toluene:CH<sub>2</sub>Cl<sub>2</sub>, although such solvents were not appropriate for the spectroscopy under catalytic conditions.

The X-band CW spectrum of complex **1** can be simulated as an  $S = 3/2$  species exhibiting a relatively small axial zero-field splitting (ZFS)  $D = 0.64 \text{ cm}^{-1}$  and a Gaussian distribution of rhombic terms ( $E$ ) centered at  $E/D = 0.06$  with a full width at half-maximum (FWHM) of 0.08 (see Figure 2).

The small degree of rhombicity in this complex ( $E/D$  can vary between 0 and 0.33, i.e. a ZFS which is fully axial to rhombic, respectively) is consistent with this Cr(III) center possessing a ligand field symmetry of approximate octahedral symmetry in solution. The degree of rhombicity in the ZFS interaction can be quite sensitive to small changes in molecular geometry, thus the broad distribution of  $E/D$  values necessary to simulate the

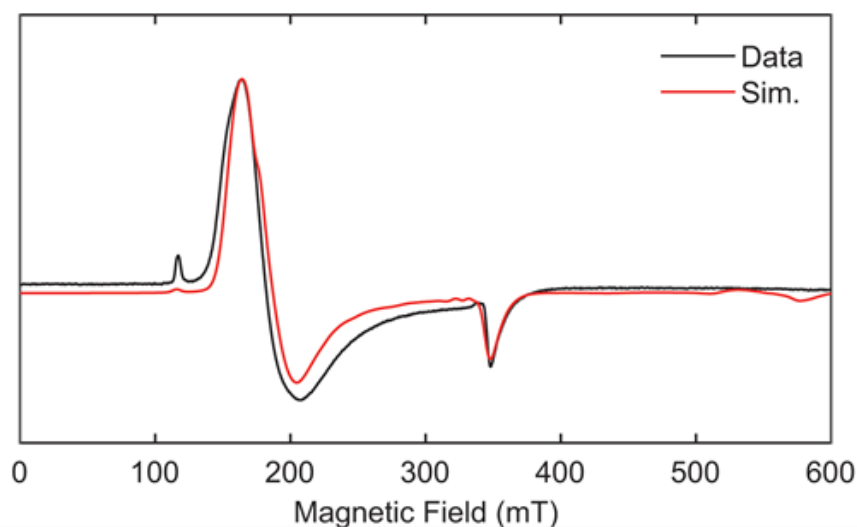


**Figure 2.** X-band CW-EPR spectrum of **1-h<sub>3</sub>**. Acquisition parameters: temperature = 5 K; MW frequency = 9.637 GHz; MW power = 2 mW; modulation amplitude = 0.4 mT; conversion time = 41 ms. Simulation parameters:  $S = 3/2$ ;  $g = 1.997$ ;  $D = 0.64$  cm<sup>-1</sup>;  $E/D = 0.06$ , FWHM of Gaussian distribution of  $E/D = 0.084$ .

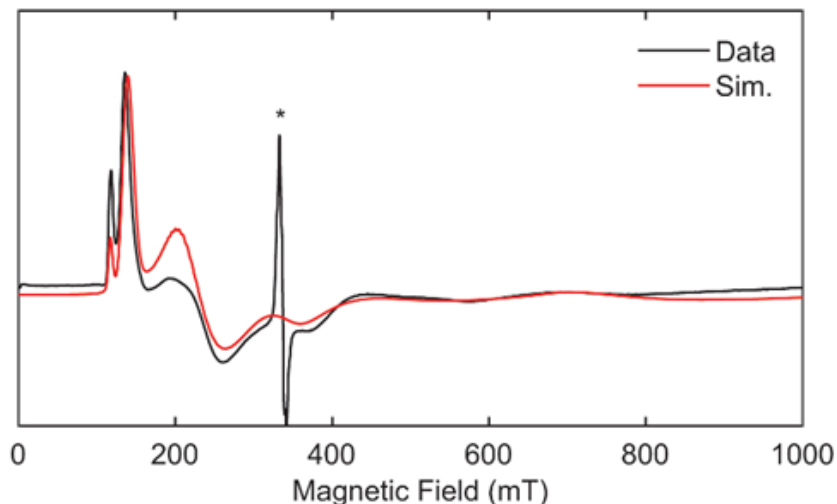


**Figure 3.** X-band CW-EPR spectrum of **2-h<sub>3</sub>**. Asterisk near 360 mT indicates a feature arising from a small amount of  $S = 1/2$  contaminant signal, likely a Cr(I) decomposition product formed upon protonation of **1-h<sub>3</sub>**. Acquisition parameters: temperature = 5 K; MW frequency = 9.371 GHz; MW power = 2 mW; modulation amplitude = 0.4 mT; conversion time = 41 ms. Simulation parameters:  $S = 3/2$ ;  $g = 1.970$ ;  $D = 0.50$  cm<sup>-1</sup>;  $E/D = 0.18$ , FWHM  $E/D$  distribution = 0.09.

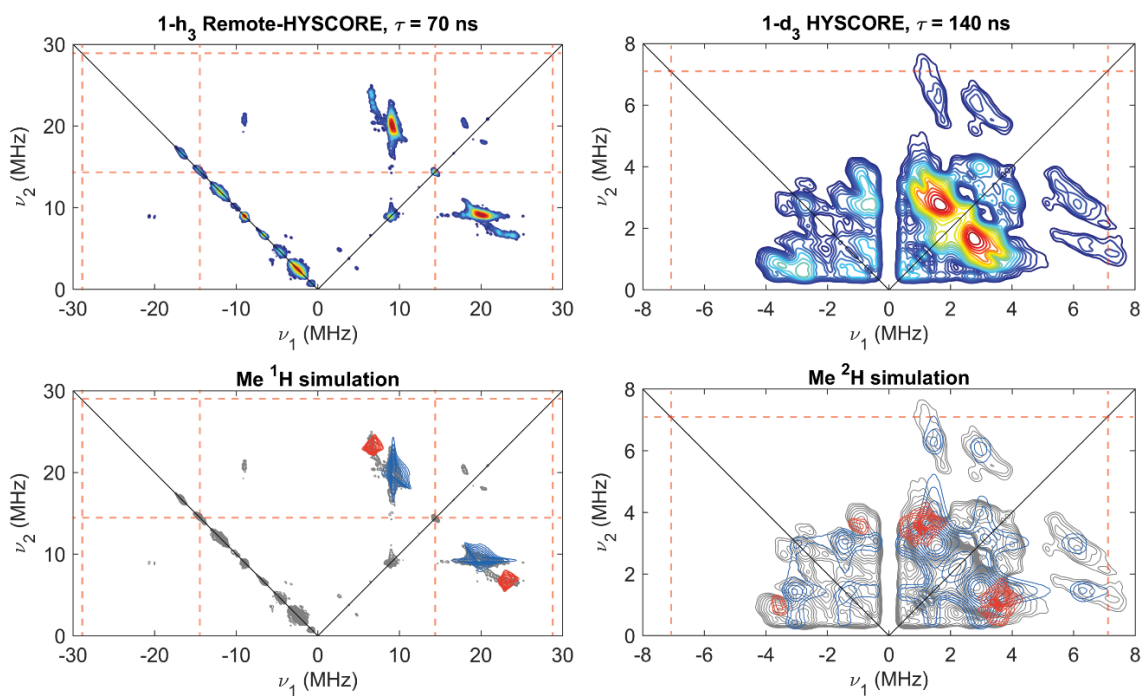


**Figure 4.** X-band HYSOCORE of natural abundance **1-h<sub>3</sub>** and **1-d<sub>3</sub>** acquired at 336.8 mT ( $g = 2.001$ ). Top panels show the experimental data, bottom panels show experimental data plotted as grey contours, with simulations of methyl <sup>1</sup>H or <sup>2</sup>H hyperfine coupling classes H<sub>a</sub> and H<sub>b</sub> are simulated in red and blue, respectively. Light red dotted lines represent HYSOCORE blind spots as a result of the tau value used. Acquisition parameters: temperature = 6.8 K; microwave frequency = 9.433 GHz; MW pulse length ( $\pi/2$ ,  $\pi$ ) = 8 ns, 16 ns;  $\tau = 70$  ns (**1-h<sub>3</sub>**), 140 ns (**1-d<sub>3</sub>**);  $t_1 = t_2 = 100$  ns;  $\Delta t_1 = \Delta t_2 = 16$  ns; shot repetition time (srt) = 1 ms).

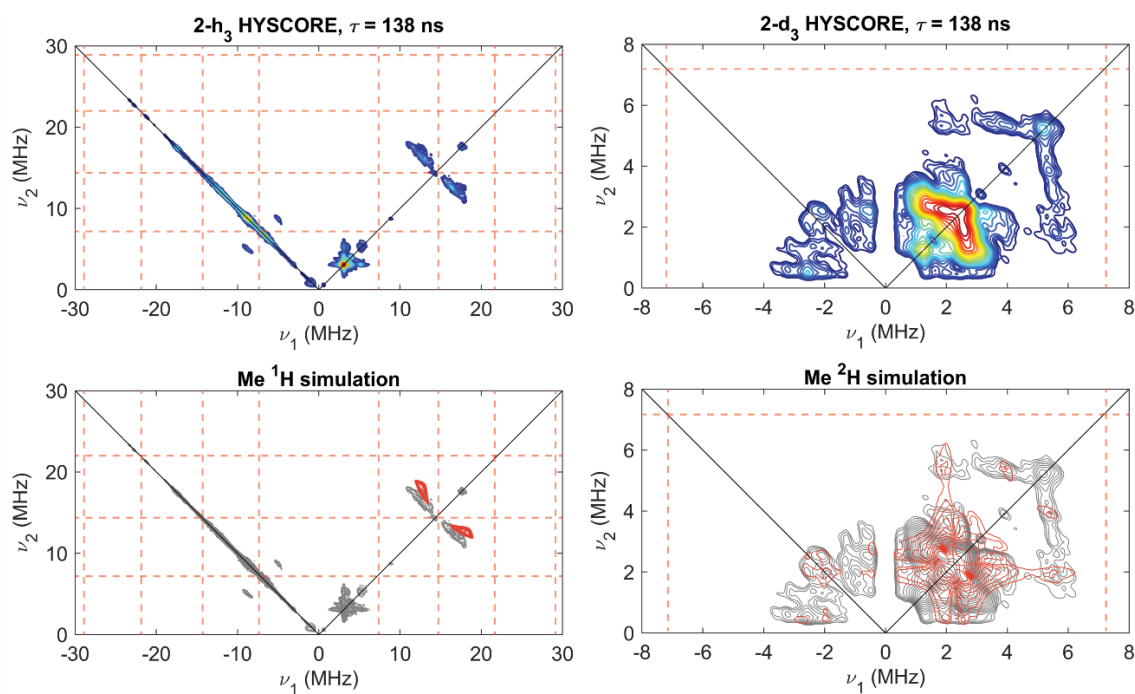


**Figure 5.** X-band HYSCORE of **2-h<sub>3</sub>** and **2-d<sub>3</sub>** acquired at 338.0 mT ( $g = 1.991$ ). Top panels show the experimental data, bottom panels show experimental data plotted as grey contours, with simulation of methyl <sup>1</sup>H and <sup>2</sup>H hyperfine couplings simulated in red. Light red dotted lines represent HYSCORE blind spots as a result of the tau value used. Acquisition parameters: temperature = 6.8 K; microwave frequency = 9.433 GHz; MW pulse length ( $\pi/2, \pi$ ) = 8 ns, 16 ns;  $\tau = 138$  ns,  $t_1 = t_2 = 100$  ns;  $\Delta t_1 = \Delta t_2 = 16$  ns; shot repetition time (srt) = 1 ms).

spectrum likely indicates some degree of variability of the ligand geometry in solution.

Following protonation of **1-h<sub>3</sub>**, a new  $S = 3/2$  CW EPR spectrum (see Figure 3) is observed which is distinct from that of the starting material (see Figure 2) which can be simulated with an axial zero field splitting term  $D = 0.50 \text{ cm}^{-1}$ , but a much higher degree of rhombicity, with the center of a Gaussian distribution of  $E/D$  at 0.18 with a (FWHM) of 0.09.

The higher degree of rhombicity in the zero field splitting interaction for this Cr(III) center is consistent with a lowering of the ligand symmetry from octahedral, as would be expected upon the loss of one of the aryl ligands upon protonation.

To substantiate the assignment of structure **2** as a product of stoichiometric activation of **1-h<sub>3</sub>**, HYSCORE spectroscopy was performed on **1-h<sub>3</sub>** and **1-d<sub>3</sub>**, as well as the products of protonation of these two isotopologues. Comparison of the HYSCORE spectra of **1-h<sub>3</sub>** and **1-d<sub>3</sub>** (see Figure 4) reveals correlation ridges arising from hyperfine coupling to two distinct classes of  $^1\text{H}$  nuclei simulated with two equivalent  $A(^1\text{H}_a) = [1, 7, 11]$  MHz, and a single larger coupling with  $A(^1\text{H}_b) = [8, 9, 17]$  MHz. These couplings correspond to the  $^2\text{H}$  correlation ridges evident in the HYSCORE spectrum of **1-d<sub>3</sub>** that are well simulated by scaling the  $^1\text{H}$  hyperfine tensor by the proportion of the  $^1\text{H}/^2\text{H}$  gyromagnetic ratios ( $\gamma^1\text{H}/\gamma^2\text{H} = 6.514$ ).

Notably,  $^2\text{H}$  features are also observed in HYSCORE spectra of the products of protonation of **1-d<sub>3</sub>** (Figure 5) substantiating the structural assignments of these products as **2-h<sub>3</sub>** and **2-d<sub>3</sub>**. Comparison of the HYSCORE spectra of **2-h<sub>3</sub>** and **2-d<sub>3</sub>** reveals correlation ridges arising from hyperfine coupling to a single class of  $^1\text{H}$  simulated with  $A(^1\text{H}) = [-2.5, -2.5, 10]$  MHz, which correspond to  $^2\text{H}$  correlation ridges evident in the HYSCORE spectrum of **2-d<sub>3</sub>** that, again, are well simulated by scaling the  $^1\text{H}$  hyperfine tensor by the

proportion of the  $^1\text{H}/^2\text{H}$  gyromagnetic ratios ( $\gamma^1\text{H}/\gamma^2\text{H} = 6.514$ ). Observation of deuterium HYSCORE features in the product of **1-d**<sub>3</sub> protonation confirms that **2-d**<sub>3</sub> is present in substantial concentrations (relative to **3**). It is reasonable that aryl protonolysis is kinetically favourable to methyl protonolysis. This cationic Cr(III) species likely undergoes further initiation steps to generate more reduced Cr capable of oxidative coupling of ethylene in a catalytic process. However, understanding the speciation of well-defined Cr precatalysts is a prerequisite to a more complete understanding of catalyst structure.

**EPR on Freeze-Quenched Chromium Catalytic Mixture Derived from 1-h<sub>3</sub>.** After successfully detecting  $^2\text{H}$  nuclei in organometallic Cr species by HYSCORE spectroscopy, we employed HYSCORE for the *in situ* characterization of Cr species following addition of ethylene gas.

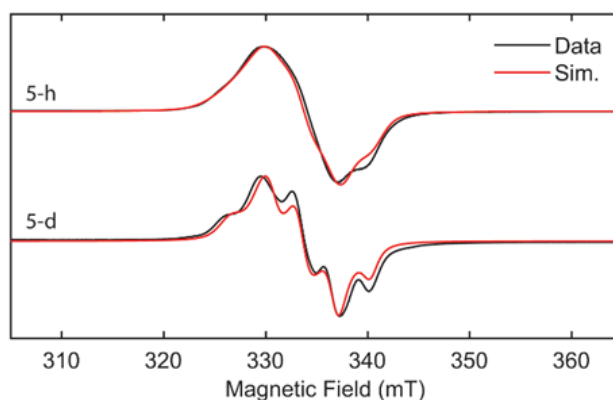


**Figure 6.** X-band CW-EPR spectra of **5-h** and **5-d**. Acquisition parameters: temperature = 77 K; MW frequency = 9.372 GHz; MW power = 6.4 mW; modulation amplitude = 0.4 mT; conversion time = 164 ms. Simulation parameters:  $S = 1/2$ ;  $g = [2.030, 2.006, 1.987]$ ;  $A(^{31}\text{P}_1) = [105, 86, 86]$  MHz;  $A(^{31}\text{P}_2) = [83, 84, 95]$  MHz;  $\text{HStrain}(\mathbf{5-h}) = [80, 60, 30]$  MHz;  $\text{HStrain}(\mathbf{5-d}) = [50, 30, 15]$  MHz.

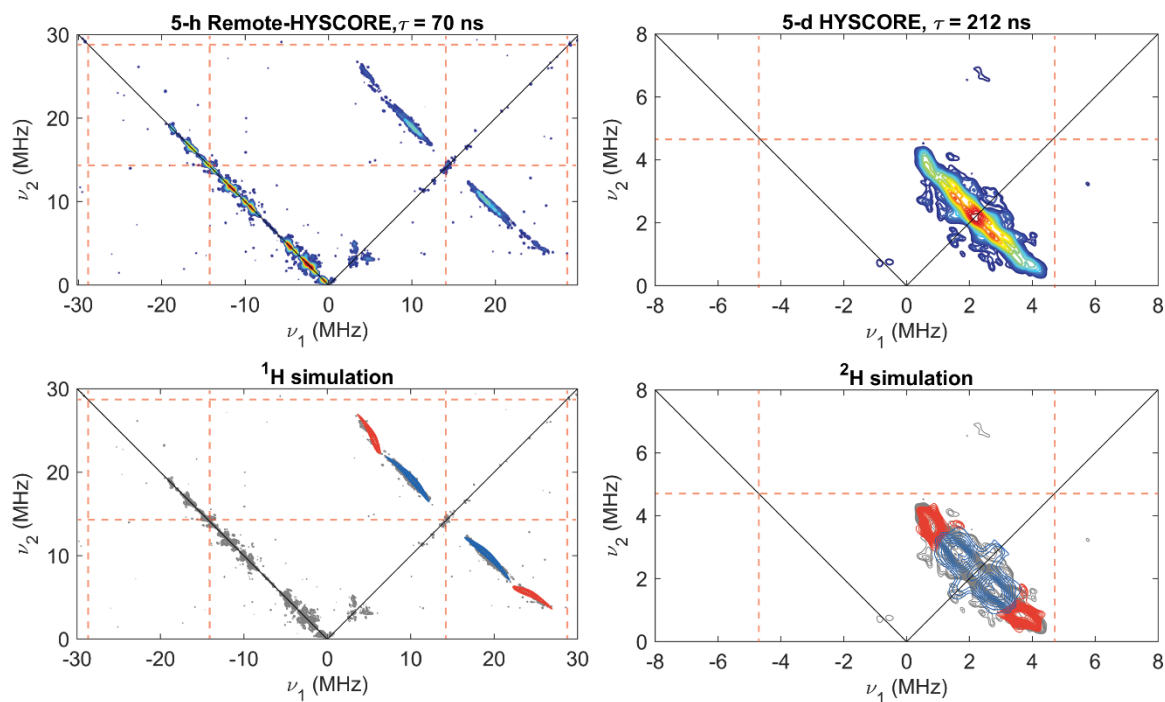


**Figure 7.** X-band HYSCORE of **5-h** and **5-d** acquired at 336.6 mT ( $g = 1.998$ ). Top panels show the experimental data, bottom panels show experimental data plotted as grey contours, with simulation of two distinct classes of  $^1\text{H}$  and  $^2\text{H}$  hyperfine coupling classes  $H_a$  and  $H_b$  simulated in red and blue, respectively. Acquisition parameters: temperature = 30 K; microwave frequency = 9.415 GHz; MW pulse length ( $\pi/2$ ,  $\pi$ ) = 8 ns, 16 ns;  $\tau = 212$  ns,  $t_1 = t_2 = 100$  ns;  $\Delta t_1 = \Delta t_2 = 16$  ns; shot repetition time (srt) = 1 ms).

Following the mixing of **2-h<sub>3</sub>** with ~100 equiv. C<sub>2</sub>H<sub>4</sub> in a flame-sealed quartz EPR tube, a color change in the solution from green-brown to orange was observed upon warming to RT. The poor solubility of the Cr complexes led to oily precipitation from the solution upon prolonged standing at -78 °C (using MeCy:PhCl). Therefore, pure PhCl was used, and the frozen samples were warmed directly to room temperature. Via CW EPR, a new, low-spin Cr species (**5**) was apparent (presumably Cr(I)). The remainder of the EPR-active material was unreacted **2-h<sub>3</sub>**.

In a separate experiment, this new species (**5**) was successfully formed in a Schlenk tube and the reaction mixture was analyzed by GC/MS to confirm the formation of 1-hexene (5 equiv.). An additional aliquot was analyzed by EPR to confirm the presence of **5**. The remaining mixture that included **5** was transferred to a high-pressure reactor for ethylene tetramerization catalysis at 100 psi.

Only 8 equiv. of 1-hexene was detected afterwards, which is very similar to the 5 equiv. detected beforehand. These experiments suggest that **5** is formed during, or as a result of, catalyst initiation and turnover. However, **5** itself is not an intermediate in the catalytic cycle, since it was not competent in the high-pressure ethylene oligomerization reaction. These experiments do not rule out an EPR-silent active species remaining in the mixture concomitant with formation of **5**, and then decomposing prior to high-pressure catalysis.

**EPR Analysis of 5-h and 5-d.** Utilizing natural abundance C<sub>2</sub>H<sub>4</sub> and isotopically enriched C<sub>2</sub>D<sub>4</sub>, **5** was formed in flame-sealed quartz EPR tubes by the same procedure. The X-band CW-EPR spectra of these reaction samples exhibit relatively narrow spectra centered at  $g = 2$ , consistent with  $S = 1/2$  paramagnetic species, likely representing Cr(I) species as opposed to Cr(III) (see Figure 6).

Via X-band HYSCORE (Figure 7), two distinct classes of C<sub>2</sub>H<sub>4</sub>-derived proton/deuterium hyperfine couplings were detected ( $A(^1\text{H}_1) = [29, 16, 16]$  MHz and  $A(^1\text{H}_2) = [16, 4, 4]$  MHz). This is consistent with the assignment of **5** as a Cr species with alkene or alkyl ligands derived from the ethylene gas (i.e. **5-d**). Despite this, the previously discussed experiment demonstrates that **5** is not an intermediate in the catalytic cycle.

Due to the significantly greater <sup>1</sup>H hyperfine couplings in **5** compared to the methyl species **1** and **2**, we assign **5** as the adduct of an alkene; either ethylene or 1-hexene would be reasonable. Notably, Theopold and coworkers observed a dinuclear Cr(I) species with a bridging ethylene as the product following ethylene trimerization catalysis.<sup>10</sup> Paramagnetic Cr(I) alkene species are rare, but we have evaluated one literature example (**6**, shown in the Experimental section) which has a conjugated diene bound to Cr(I).<sup>11</sup> HYSCORE spectroscopy of **6** reveals smaller <sup>1</sup>H hyperfine couplings than **5**, possibly due to delocalization of the spin density across the diene motif (see the Experimental section). We do not think this evidence rules out a Cr(I)/Cr(III) cycle, although therein a Cr(I) ethylene (or 1-hexene species) with PNP bound would be expected to be catalytically active. It is possible that endogenous or adventitious Lewis basic moieties have saturated the coordination sphere of Cr, rendering Cr(I) unreactive.

**EPR on Freeze-Quenched Chromium Catalytic Mixture Derived from MMAO-Activation of CrCl<sub>3</sub>(THF)<sub>3</sub>/PNP.** Although the stoichiometric activation mode provides potential practical advantages for catalysis, activation of Cr precatalysts with modified methylaluminoxane (MMAO) is still performed predominantly in both academic and industrial research. Therefore, a comparison was made between the spectral features observed for stoichiometrically-activated precatalyst **1-h<sub>3</sub>** and CrCl<sub>3</sub>-based precatalysts activated using MMAO.

The activation of  $\text{CrCl}_3(\text{THF})_3/\text{PNP}$  mixtures with an excess of MMAO is often used to generate a catalyst *in situ*. Despite our focus on a more well-defined activation method, we sought to compare the spectroscopic features of complexes derived from **1** with those of the MMAO-activated system. The MMAO-activated mixture was a green color that turned blue after 5 minutes at room temperature (as a result of degassing the EPR tube by freeze-pump-thaw cycles). Ethylene was condensed onto the frozen solution, and the mixture was warmed to room temperature, before freeze-quenching as in the other experiments. The resulting ESE EPR showed identical spectra between experiments using  $\text{C}_2\text{H}_4$  and  $\text{C}_2\text{D}_4$  gas. In the latter case, ESEEM analysis showed no effect of deuterium modulation. Therefore, the EPR-active material following ethylene addition to MMAO-activated precatalysts does not derive hydrocarbyl ligands from ethylene.

**Comments on EPR Investigation of Cr Catalysis.** In X-ray absorption studies, Cr(II) species have been observed,<sup>6d,12</sup> but Cr(II) would not be detected by the techniques employed here. Whereas **2** is a suitable precatalyst for reactions with ethylene under ambient conditions, its limited solubility in methylcyclohexane is problematic, as mentioned previously. We note that other EPR studies have leveraged specialized equipment to allow for studies at elevated ethylene pressures.<sup>6d</sup> Future *in situ* spectroscopic studies will have to balance the experimental constraints of the chosen spectroscopic technique with the known optimal reaction parameters of ethylene oligomerization catalysis (e.g. high ethylene pressures, high temperatures, and high dilution in methylcyclohexane).

## Conclusion.

We have established the presence of a methyl ligand on a reactive Cr(III) intermediate using isotopic labelling in combination with pulse EPR. This demonstrates the utility of pulse EPR in elucidating structural features of high-spin paramagnetic species of high relevance to organometallic catalysis. The methodology reported herein was applied to the *in situ* analysis of catalytic ethylene oligomerization.

We have derived structural information from pulse EPR on the freeze-quenched solutions of the catalytic mixture, following addition of ethylene. The observed Cr species was determined to be incompetent for catalysis. The conclusion is that catalytically active species in this system are either a) present in concentrations too low to detect, b) in oxidation states or spin states unsuitable for EPR detection or c) consumed on the timescale of the experiment (1 min).

This study highlights the applicability of well-defined Cr complexes in EPR spectroscopic investigations. More broadly, these methods may be applied to study transformations of paramagnetic metal-hydrocarbyl species in a variety of contexts.

## Experimental.

**Materials.** All synthetic procedures containing chromium were performed in a nitrogen-atmosphere glove box. All glassware was oven-dried and kept under active vacuum prior to use. Diethyl ether, tetrahydrofuran (THF), toluene, and pentane solvents were purified by sparging with nitrogen and then passing through a column of activated A2 alumina into sealed containers, degassed under active vacuum, and stored over activated molecular sieves prior to use. 1,4-Dioxane was dried over Na/benzophenone, vacuum distilled, and kept over

activated molecular sieves prior to use. Chlorobenzene was distilled from  $\text{CaH}_2$ , stored over activated molecular sieves for at least 24 hours, and filtered through activated alumina directly before use. Chlorobenzene- $\text{d}_5$  (from Acros Organics) was degassed using three freeze-pump-thaw cycles and stored over molecular sieves prior to use. M-MAO 3A was purchased from AkzoNobel as a 7% w/w Al solution in heptane. Ethylene gas (for high-pressure oligomerization trial) was purchased at polymer purity (99.9%) from Matheson, and was dried by passage through two 1L Swagelok steel columns packed with 3Å activated molecular sieves and Mn(II) oxide on vermiculite.<sup>13</sup> Ethylene- $\text{H}_4$  gas (for EPR sample preparation) was purchased from Sigma-Aldrich (99.99%) in a lecture bottle and immediately before use in catalysis was thawed under static vacuum from its condensed state in a cooled trap using high vacuum line techniques. Ethylene- $\text{D}_4$  gas was purchased from Cambridge Isotope Laboratories (98%-D) in a lecture bottle, and stored in a glass storage bulb under partial vacuum over dried, methylaluminoxane-treated silica (prepared using a similar procedure to that described by Bercaw and coworkers<sup>14</sup>) to remove traces of moisture. Immediately before use in catalysis, the ethylene- $\text{D}_4$  was thawed under static vacuum from its condensed state using high vacuum line techniques.  $\text{CrCl}_3(\text{THF})_3$  was synthesized according to the literature procedure, using  $\text{CrCl}_3$  (anhydrous) purchased from Strem.<sup>15</sup> The synthesis of  $^{\text{101}}\text{PNP}$ , and  $[\text{H}(\text{Et}_2\text{O})_2][\text{BAR}'_4]$  have been previously reported.<sup>16</sup>

**Instrumentation.** Gas chromatography (GC) was performed on an Agilent 6890A instrument using a DB-1 capillary column (10 m length, 0.10 mm diameter, 0.40  $\mu\text{m}$  film) and a flame ionization detector.

Continuous wave X-band EPR spectra were obtained on a Bruker EMX spectrometer using solutions prepared as frozen glasses in chlorobenzene or 1:1 chlorobenzene/methylcyclohexene. Pulse EPR spectroscopy: All pulse X-band (9.4-9.7) EPR,

electron nuclear double resonance (ENDOR), and hyperfine sublevel correlation spectroscopy (HYSCORE) experiments were acquired using a Bruker ELEXSYS E580 pulse EPR spectrometer. X-band ENDOR experiments were performed using a Bruker MD-4 X-band ENDOR resonator, and X-band HYSCORE experiments were performed using a Bruker MS-5 resonator. For experiments conducted at temperatures above 5 K, temperature control was achieved using an ER 4118HV-CF5-L Flexline Cryogen-Free VT cryostat manufactured by ColdEdge equipped with an Oxford Instruments Mercury ITC temperature controller. For experiments conducted below 5 K, an Oxford Cryogenic CF-935 helium flow cryostat and a Mercury ITC temperature controller was utilized with liquid helium.

**Pulse EPR Spectroscopy.** Pulse X-band ENDOR was acquired using the Davies pulse sequence ( $\pi - T_{RF} - \pi_{RF} - T_{RF} - \pi/2 - \tau - \pi - \text{echo}$ ), where  $T_{RF}$  is the delay between mw pulses and RF pulses,  $\pi_{RF}$  is the length of the RF pulse and the RF frequency is randomly sampled during each pulse sequence.

X-band HYSCORE spectra were acquired using the 4-pulse sequence ( $\pi/2 - \tau - \pi/2 - t_1 - \pi - t_2 - \pi/2 - \text{echo}$ ), where  $\tau$  is a fixed delay, while  $t_1$  and  $t_2$  are independently incremented by  $\Delta t_1$  and  $\Delta t_2$ , respectively. The time domain data was baseline-corrected (third-order polynomial) to eliminate the exponential decay in the echo intensity, apodized with a Hamming window function, zero-filled to eight-fold points, and fast Fourier-transformed to yield the 2-dimensional frequency domain. For  $^2\text{H}$ - $^1\text{H}$  difference spectra, the time domain of the HYSCORE spectrum of the  $^1\text{H}$  sample was subtracted from that of the  $^2\text{H}$  sample, and the same data processing procedure detailed above was used to generate the frequency spectrum.

In general, the ENDOR spectrum for a given nucleus with spin  $I = 1/2$  ( $^1\text{H}$ ,  $^{31}\text{P}$ ) coupled to the  $S = 1/2$  electron spin exhibits a doublet at frequencies

$$\nu_{\pm} = \left| \frac{A}{2} \pm \nu_N \right| \quad (1)$$

Where  $\nu_N$  is the nuclear Larmor frequency and  $A$  is the hyperfine coupling. For nuclei with  $I \geq 1$  ( $^2\text{H}$ ), an additional splitting of the  $\nu_{\pm}$  manifolds is produced by the nuclear quadrupole interaction (P)

$$\nu_{\pm, m_I} = \left| \nu_N \pm \frac{3P(2m_I - 1)}{2} \right| \quad (2)$$

In HYSCORE spectra, these signals manifest as cross-peaks or ridges in the 2-D frequency spectrum which are generally symmetric about the diagonal of a given quadrant. This technique allows hyperfine levels corresponding to the same electron-nuclear submanifold to be differentiated, as well as separating features from hyperfine couplings in the weak-coupling regime ( $|A| < 2|\nu_I|$ ) in the (+,+) quadrant from those in the strong coupling regime ( $|A| > 2|\nu_I|$ ) in the (-,+) quadrant. The (-,-) and (+,-) quadrants of these frequency spectra are symmetric to the (+,+) and (-,+) quadrants, thus typically only two of the quadrants are typically displayed in literature.

For systems with appreciable hyperfine anisotropy in frozen solutions or solids, HYSCORE spectra typically do not exhibit sharp cross peaks, but show ridges that represent the sum of cross peaks from selected orientations within the excitation bandwidth of the MW pulses at the magnetic field position at which the spectrum is collected. The length and curvature of these correlation ridges can allow for the separation and estimation of the magnitude of the isotropic and dipolar components of the hyperfine tensor, as shown in Fig. 8.

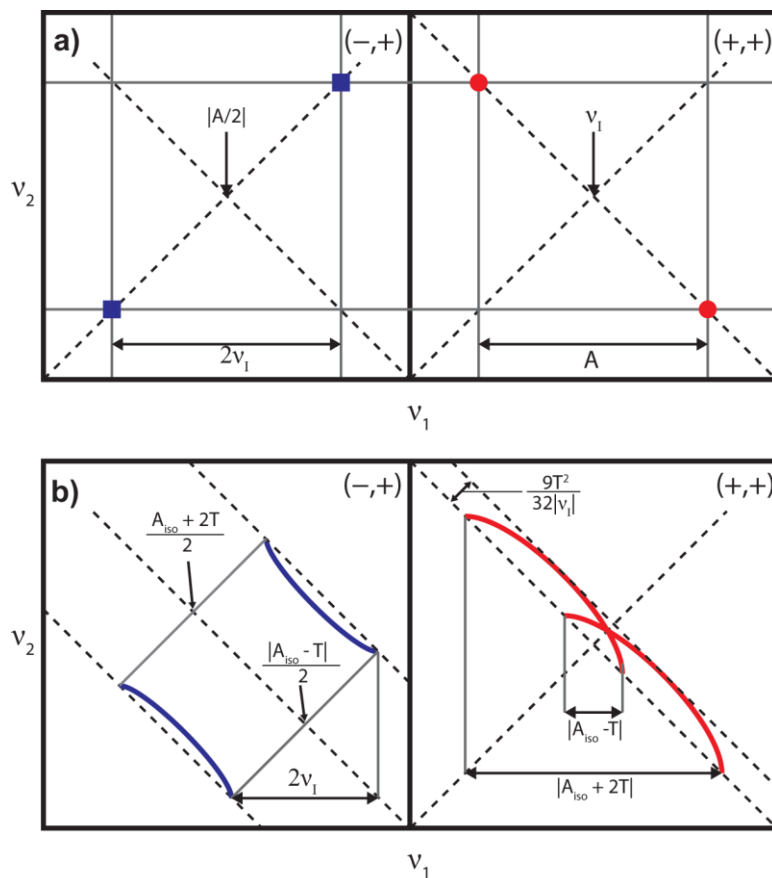


**Figure 8.** a) HYSCORE powder patterns for an  $S = 1/2$ ,  $I = 1/2$  spin system with an isotropic hyperfine tensor  $A$ . b) HYSCORE powder patterns for an  $S = 1/2$ ,  $I = 1/2$  spin system with an isotropic hyperfine tensor which contains isotropic ( $a_{\text{iso}}$ ) and dipolar ( $T$ ) contributions. Blue correlation ridges represent the strong coupling case; red correlation ridges represent the weak coupling case.

**EPR Simulations.** Simulations of all CW and pulse EPR data were achieved using the EasySpin simulation toolbox (release 5.2.25) with Matlab 2019a using the following Hamiltonian:

$$\hat{H} = \mu_B \vec{B}_0 g \hat{S} + \mu_N g_N \vec{B}_0 \hat{I} + h \hat{S} \cdot \mathbf{A} \cdot \hat{I} + h \hat{I} \cdot \mathbf{P} \cdot \hat{I} + h \hat{S} \cdot \mathbf{D} \cdot \hat{S} \quad (3)$$

In this expression, the first term corresponds to the electron Zeeman interaction term where  $\mu_B$  is the Bohr magneton,  $g$  is the electron spin  $g$ -value matrix with principle components  $g = [g_{xx}, g_{yy}, g_{zz}]$ , and  $\hat{S}$  is the electron spin operator; the second term corresponds to the nuclear

Zeeman interaction term where  $\mu_N$  is the nuclear magneton,  $g_N$  is the characteristic nuclear g-value for each nucleus (e.g.  $^1\text{H}$ ,  $^2\text{H}$ ,  $^{31}\text{P}$ ) and  $\hat{I}$  is the nuclear spin operator; the third term corresponds to the electron-nuclear hyperfine term, where  $\mathbf{A}$  is the hyperfine coupling tensor with principle components  $\mathbf{A} = [A_{xx}, A_{yy}, A_{zz}]$ ; and for nuclei with  $I \geq 1$ , the third term corresponds to the nuclear quadrupole (NQI) term which arises from the interaction of the nuclear quadrupole moment with the local electric field gradient (EFG) at the nucleus, where  $\mathbf{P}$  is the quadrupole coupling tensor. In the principle axis system (PAS),  $\mathbf{P}$  is traceless and parametrized by the quadrupole coupling constant  $e^2Qq/h$  and the asymmetry parameter  $\eta$  such that:

$$\mathbf{P} = \begin{pmatrix} P_{xx} & 0 & 0 \\ 0 & P_{yy} & 0 \\ 0 & 0 & P_{zz} \end{pmatrix} = \frac{e^2Qq/h}{4I(2I-1)} \begin{pmatrix} -(1-\eta) & 0 & 0 \\ 0 & -(1+\eta) & 0 \\ 0 & 0 & 2 \end{pmatrix} \quad (4)$$

where  $\frac{e^2Qq}{h} = 2I(2I-1)P_{zz}$  and  $\eta = \frac{P_{xx}-P_{yy}}{P_{zz}}$ . The asymmetry parameter may have values between 0 and 1, with 0 corresponding to an electric field gradient with axial symmetry and 1 corresponding to a fully rhombic EFG. For spin systems with more than one unpaired electron ( $S > 1/2$ ), the final term represents the zero-field splitting interaction (ZFS) between these electrons, where  $\mathbf{D}$  is the ZFS coupling tensor. In the principle axis system (PAS),  $\mathbf{D}$  is also diagonal and traceless, and is parametrized by the axial ( $D$ ) and rhombic ( $E$ ) terms such that:

$$\mathbf{D} = \begin{pmatrix} D_x & 0 & 0 \\ 0 & D_y & 0 \\ 0 & 0 & D_z \end{pmatrix} = \begin{pmatrix} -\frac{1}{3}D + E & 0 & 0 \\ 0 & -\frac{1}{3}D - E & 0 \\ 0 & 0 & \frac{2}{3}D \end{pmatrix} \quad (5)$$

Conventionally, the three principal axes are labelled such that  $|D_z| > |D_y| > |D_x|$ , and  $E/D$  is always positive and can vary between 0 and  $1/3$ , with  $E/D = 0$  corresponding to a zero-field splitting interaction of purely axial symmetry and  $E/D = 1/3$  corresponding to a fully rhombic ZFS.

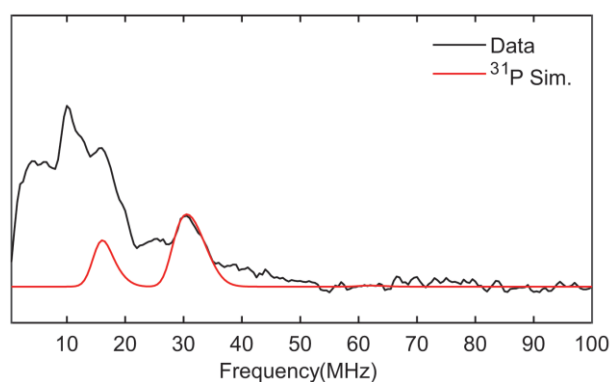


**Figure 9.** X-band Davies ENDOR of **1** acquired at 347 mT ( $g = 2.005$ ) with simulation of  $^{31}\text{P}$  hyperfine coupling overlaid in red. Acquisition parameters: temperature = 3.6 K; MW frequency = 9.737 GHz; MW pulse length ( $\pi/2$ ,  $\pi$ ) = 8 ns, 16 ns;  $\tau = 260$  ns; RF pulse length = 15  $\mu\text{s}$ ;  $T_{\text{RF}} = 2$   $\mu\text{s}$ ; shot repetition time = 1 ms. Simulation parameters:  $S = 3/2$ ;  $S = 3/2$ ;  $g = 1.997$ ;  $D = 0.64$  cm $^{-1}$ ;  $E/D = 0.06$ ;  $A(^{31}\text{P}_1) = A(^{31}\text{P}_2) = [44, 44, 44]$  MHz.

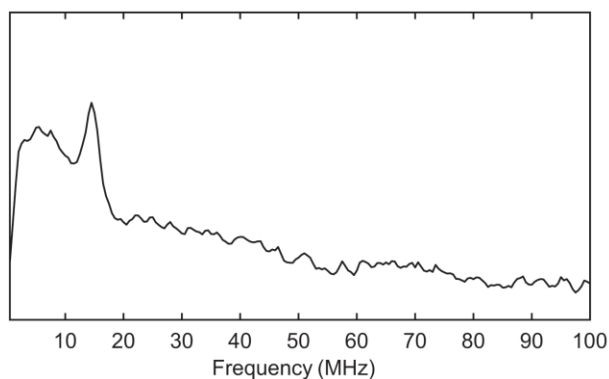


**Figure 10.** X-band Davies ENDOR of **2** acquired at 350 mT ( $g = 1.987$ ). Acquisition parameters: temperature = 3.6 K; MW frequency = 9.736 GHz; MW pulse length ( $\pi/2$ ,  $\pi$ ) = 8 ns, 16 ns;  $\tau = 260$  ns; RF pulse length = 15  $\mu\text{s}$ ;  $T_{\text{RF}} = 2$   $\mu\text{s}$ ; shot repetition time = 1 ms.

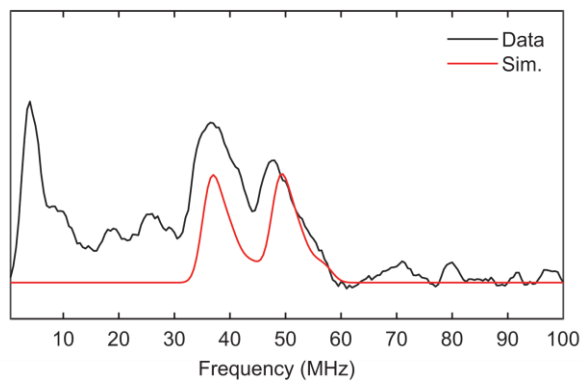


**Figure 11.** X-band Davies ENDOR of **5** acquired at 346 mT ( $g = 2.008$ ) with simulation of  $^{31}\text{P}$  hyperfine couplings overlaid in red. Acquisition parameters: temperature = 3.6 K; MW frequency = 9.737 GHz; MW pulse length ( $\pi/2$ ,  $\pi$ ) = 8 ns, 16 ns;  $\tau = 260$  ns; RF pulse length = 15  $\mu\text{s}$ ;  $T_{\text{RF}} = 2$   $\mu\text{s}$ ; shot repetition time = 5 ms. Simulation parameters:  $S = 1/2$ ;  $g = [2.030, 2.006, 1.987]$ ;  $A(^{31}\text{P}_1) = [105, 86, 86]$ ;  $A(^{31}\text{P}_2) = [83, 84, 95]$ .

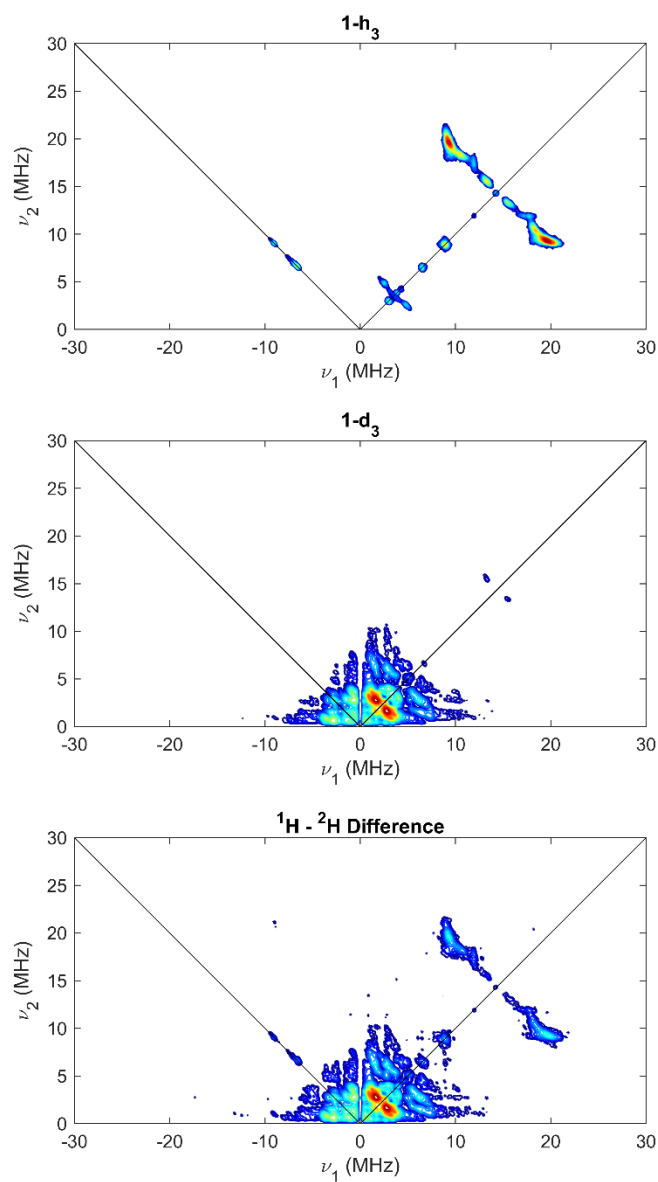


**Figure 12.** X-band HYSCORE of  $1\text{-h}_3$  (top panel),  $1\text{-d}_3$  (middle panel) acquired at 336.8 mT ( $g = 2.001$ ), and the  $1\text{H} - 2\text{H}$  difference spectrum (bottom panel). Acquisition parameters: temperature = 6.8 K; microwave frequency = 9.433 GHz; MW pulse length ( $\pi/2, \pi$ ) = 8 ns, 16 ns;  $\tau = 140$  ns,  $t_1 = t_2 = 100$  ns;  $\Delta t_1 = \Delta t_2 = 16$  ns; shot repetition time (srt) = 1 ms).

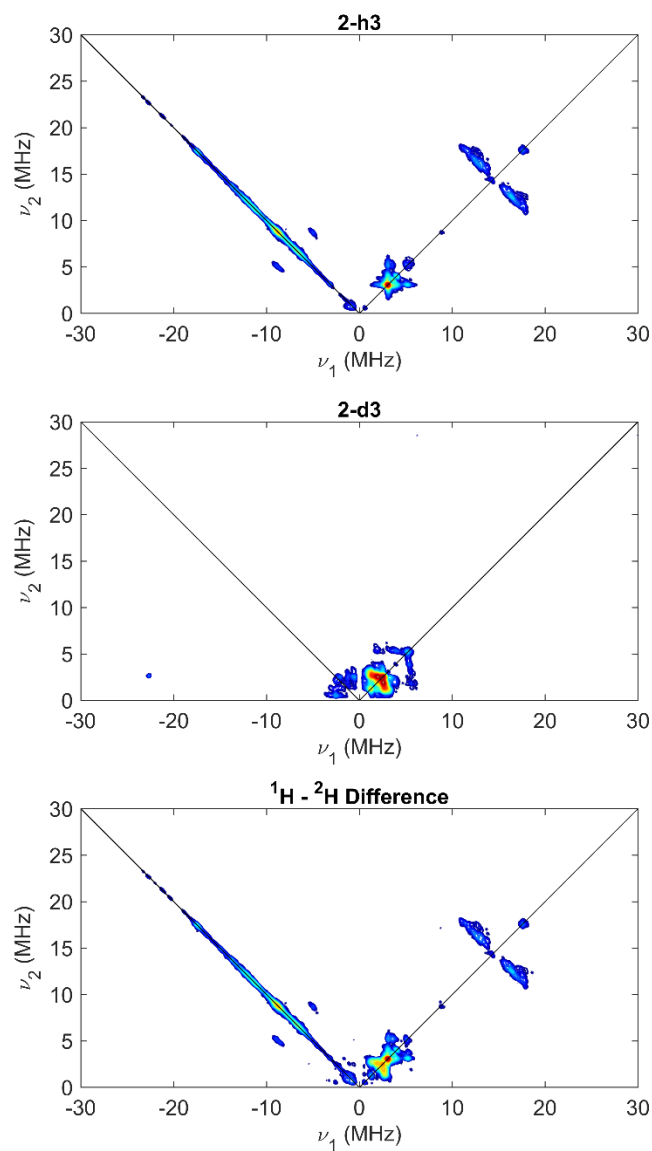


**Figure 13.** X-band HYSCORE of **2-h<sub>3</sub>** (top panel), **2-d<sub>3</sub>** (middle panel) acquired at 338.0 mT ( $g = 2.080$ ), and the  $^1\text{H} - ^2\text{H}$  difference spectrum (bottom panel). Acquisition parameters: temperature = 6.8 K; microwave frequency = 9.433 GHz; MW pulse length ( $\pi/2$ ,  $\pi$ ) = 8 ns, 16 ns;  $\tau = 140$  ns,  $t_1 = t_2 = 100$  ns;  $\Delta t_1 = \Delta t_2 = 16$  ns; shot repetition time (srt) = 1 ms).

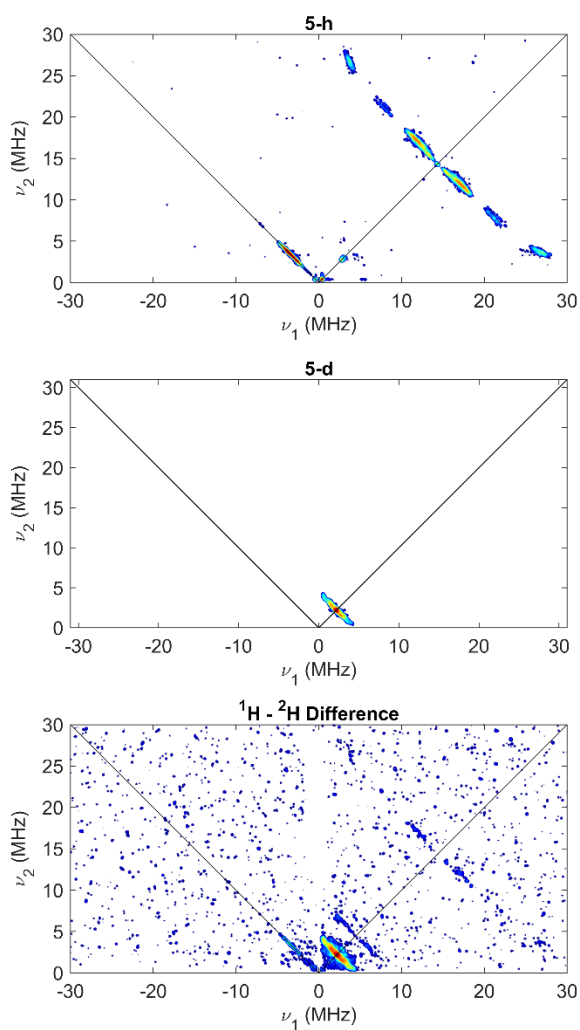


**Figure 14.** X-band HYSCORE of **5-h** (top panel), **5-d** (middle panel) acquired at 336.8 mT ( $g = 2.001$ ), and the  $^1\text{H} - ^2\text{H}$  difference spectrum (bottom panel). Acquisition parameters: temperature = 20 K; microwave frequency = 9.433 GHz; MW pulse length ( $\pi/2$ ,  $\pi$ ) = 8 ns, 16 ns;  $\tau = 140$  ns,  $t_1 = t_2 = 100$  ns;  $\Delta t_1 = \Delta t_2 = 16$  ns; shot repetition time (srt) = 1 ms).

### Synthetic Protocols.

**Cr(*o*-C<sub>6</sub>H<sub>4</sub>CH<sub>2</sub>)<sub>2</sub>O)(CD<sub>3</sub>)(THF)<sub>2</sub>. (A-d<sub>3</sub>)** We have previously reported the unlabeled version of this complex; the synthesis has been modified according to the following description. To a Schlenk tube containing Et<sub>2</sub>O (20 mL) and a slight excess of Mg turnings (60 mg, 2.5 mmol), CD<sub>3</sub>I (0.150 mL, 2.4 mmol) was added under N<sub>2</sub> counterflow via syringe. After several hours of stirring, most of the Mg was visibly consumed, and the solution was later filtered in a glovebox using glass wool, to obtain the CD<sub>3</sub>MgI solution. This solution was quickly added dropwise to a thawing suspension of CrCl<sub>3</sub>(THF)<sub>3</sub> (0.902 g, 2.4 mmol) in a mixture of 30 mL THF, 10 mL Et<sub>2</sub>O, and 1 mL 1,4-dioxane. As the suspension warmed over the course of 1 h, a bright green suspension was formed. The product, Cr(CD<sub>3</sub>)Cl<sub>2</sub>(THF)<sub>3</sub>, was not isolated since this often leads to reduced yields following recrystallization. Separately, the bis(aryl)ether magnesium reagent Mg(*o*-C<sub>6</sub>H<sub>4</sub>CH<sub>2</sub>)<sub>2</sub>O (2.4 mmol) was prepared in 80 mL 1:1 Et<sub>2</sub>O:THF, with 1 mL 1,4-dioxane, according to the previously reported procedure. The solution of Mg(*o*-C<sub>6</sub>H<sub>4</sub>CH<sub>2</sub>)<sub>2</sub>O was added dropwise over 10 min to the thawing suspension of Cr(CD<sub>3</sub>)Cl<sub>2</sub>(THF)<sub>3</sub>, which had been refrozen after stirring at RT for 4 h. An orange/brown solution with a pale precipitate formed after warming to room temperature. After 20 h, the solution was dark red, and was filtered from gray solids using Celite. The filtrate was reduced under vacuum to a red, dry solid. This solid was redissolved in THF (10 mL) and the solution was concentrated under vacuum to 5 mL. To this, pentane (5 mL) was added, causing some red precipitate to form. This precipitate was collected by filtration, and redissolved in THF (5 mL). From this solution, red crystals of Cr(*o*-C<sub>6</sub>H<sub>4</sub>CH<sub>2</sub>)<sub>2</sub>O)(CD<sub>3</sub>)(THF)<sub>2</sub> were grown at -35 °C over two weeks (0.33 g, 0.80 mmol, 33% yield). Anal. Calcd. for C<sub>23</sub>H<sub>28</sub>D<sub>3</sub>CrO<sub>3</sub>: C, 67.29; H, 7.61; N, 0.00. Found: C, 67.34; H, 7.56; N, 0.00.

**Synthesis of (<sup>tol</sup>PNP)Cr(*o*-C<sub>6</sub>H<sub>4</sub>CH<sub>2</sub>)<sub>2</sub>O)(CD<sub>3</sub>). (1-d<sub>3</sub>)** We have previously reported the unlabeled version of this complex. A solution of <sup>tol</sup>PNP (0.089 g, 0.19 mmol) in C<sub>6</sub>H<sub>6</sub> (2 mL) was used to dissolve Cr(*o*-C<sub>6</sub>H<sub>4</sub>CH<sub>2</sub>)<sub>2</sub>O)(CD<sub>3</sub>)(THF)<sub>2</sub> (0.077 g, 0.19 mmol). The resulting brown solution was stirred for five minutes, then lyophilized down to a dry brown powder. The solid was redissolved in C<sub>6</sub>H<sub>6</sub> (1 mL) and lyophilized again. The product (1-d<sub>3</sub>) was obtained in quantitative yield as a brown powder (0.139 g, 0.19 mmol). Anal. Calcd. for C<sub>46</sub>H<sub>39</sub>D<sub>3</sub>CrNOP<sub>2</sub>: C, 74.48; H, 5.71; N, 1.89. Found: C, 74.78; H, 5.85; N, 1.78.

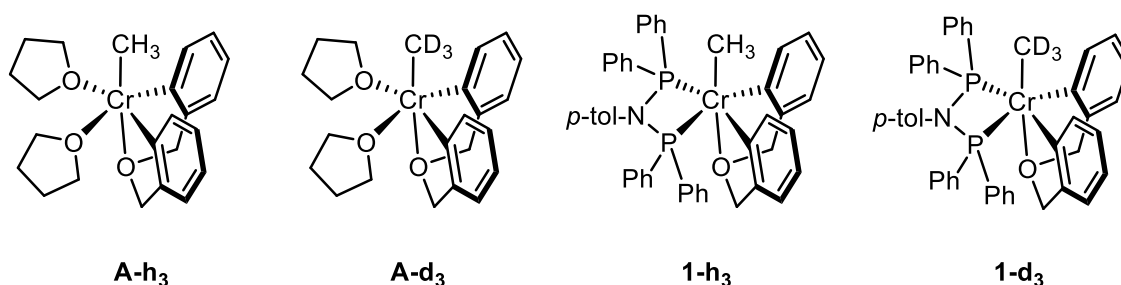


**Figure 15.** Molecular structures of **A-h<sub>3</sub>**, **A-d<sub>3</sub>**, **1-h<sub>3</sub>**, and **1-d<sub>3</sub>**.

### Preparation of EPR Samples

**Preparation of EPR Samples of 2-h<sub>3</sub> (or 2-d<sub>3</sub>).** In a 20 mL vial in the glovebox, equipped with a stirbar, compound **1** (7.0 mg) was dissolved in 0.25 mL PhCl. This solution was frozen in the glovebox cold well, then allowed to thaw while a solution of HBAR'<sub>4</sub> (9.6 mg) dissolved in 0.25 mL PhCl was added dropwise quickly (less than a minute). The resulting solution was then taken up in a syringe, and 0.1 mL transferred to a separate vial. This solution was diluted with 0.5 mL PhCl, to bring the volume to 0.6 mL, and [Cr] = 3 mM. Approximately 0.1 mL of this was transferred to an EPR tube (quartz glass, 4 mm o.d.), removed from the glovebox, and frozen in liquid nitrogen. To obtain a better-quality frozen

glass, dilution was performed with methylcyclohexene (rather than PhCl) so that the solvent composition was 4:1 methylcyclohexane:PhCl. However, this mixture was not ideal since solubility of the Cr complex(es) was poor. Ultimately, a high-quality frozen glass from a homogeneous solution was obtained by adding an Et<sub>2</sub>O solution of HBAR'<sub>4</sub> to a thawing toluene solution of the Cr compound. This resulted in a solvent composition of 1:1 toluene:Et<sub>2</sub>O; this mixture was ideal for characterization of the protonated Cr species (**2-h<sub>3</sub>** and **2-d<sub>3</sub>**), but was not used for reactions with ethylene.

**Preparation of EPR Samples in the Presence of Ethylene.** The sample of **2-h<sub>3</sub>** in PhCl described in the previous paragraph was transferred to an EPR tube (quartz glass, 4 mm o.d.) with a 14/20 ground glass joint affixed. This was connected to a 180° joint with a Teflon Kontes-pin using the 14/20 ground glass connection. This sealed apparatus was removed from the glovebox and attached to a high-vacuum line (< 1 mTorr) where the solution was degassed using 3 freeze-pump-thaw cycles. Into the degassed EPR tube, C<sub>2</sub>H<sub>4</sub> (or C<sub>2</sub>D<sub>4</sub>) was condensed from a calibrated gas bulb (17 mmHg, 36.7 mL). The tube was then sealed by closing the Kontes pin, and the sample kept in liquid nitrogen (the ethylene was frozen atop the PhCl solution at the bottom of the EPR tube). The apparatus was removed from the high vacuum line, then the EPR tube was flame-sealed to achieve a neat closure, in order to fit into the narrow spectrometer probe. The frozen sample was carefully warmed to the thawing point of the PhCl solution, then placed in a room-temperature water bath. It was quickly inverted several times to mix the solution. After a total of 1 minute at room temperature, the sample was frozen again in liquid nitrogen for the EPR measurements.



**Figure 16.** Photograph of the 180° joint with a Teflon Kontes-pin that connected the EPR tube (at the bottom) to the high-vacuum line (at the top).

## Infrared Spectra

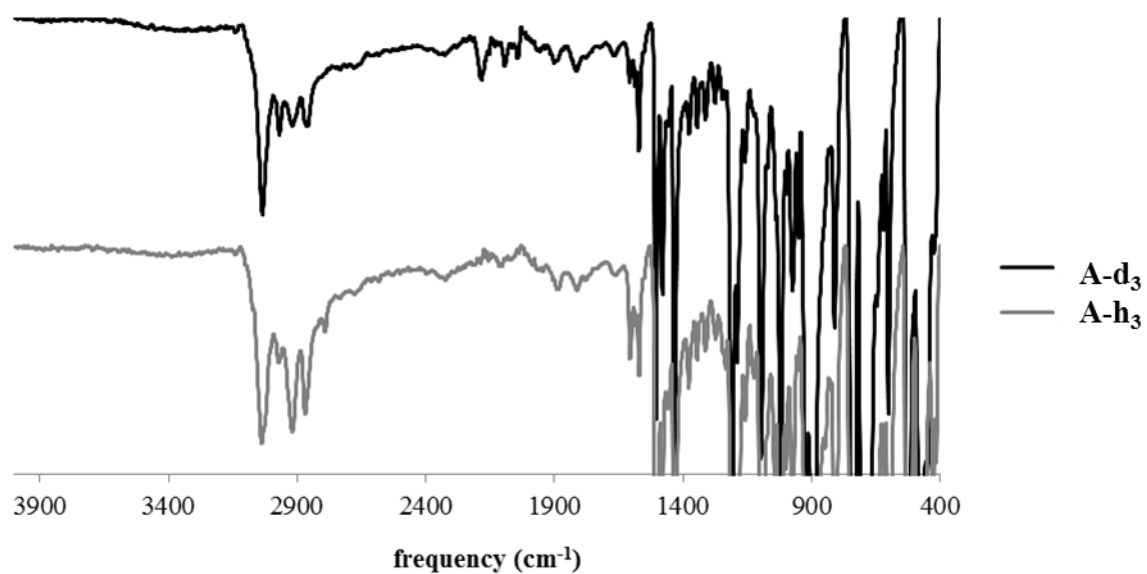


Figure 17. Infrared spectra for **A-d<sub>3</sub>** and **A-h<sub>3</sub>** (solid powders).

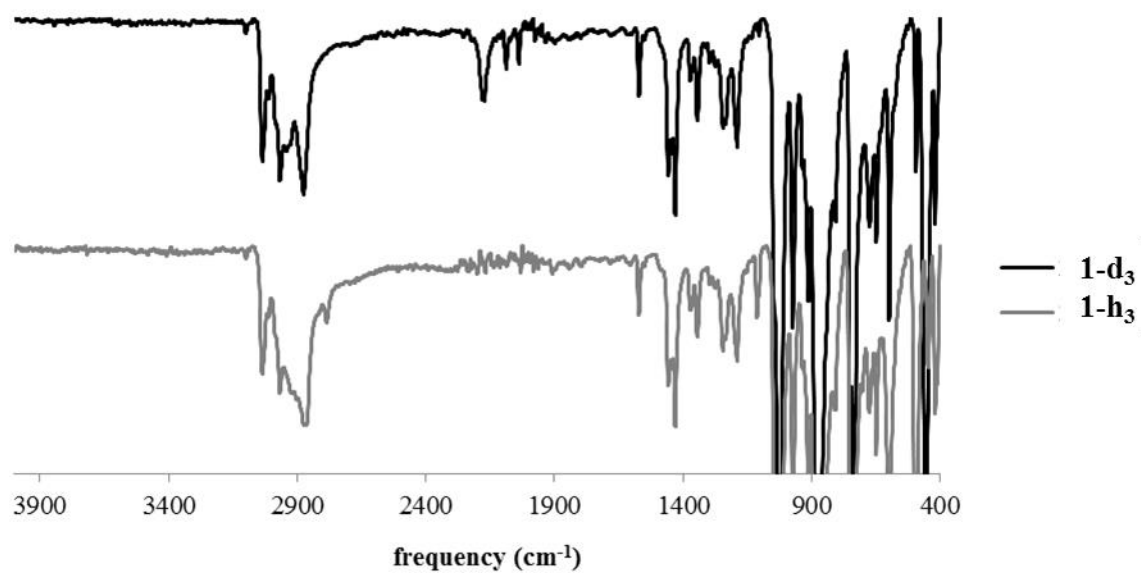
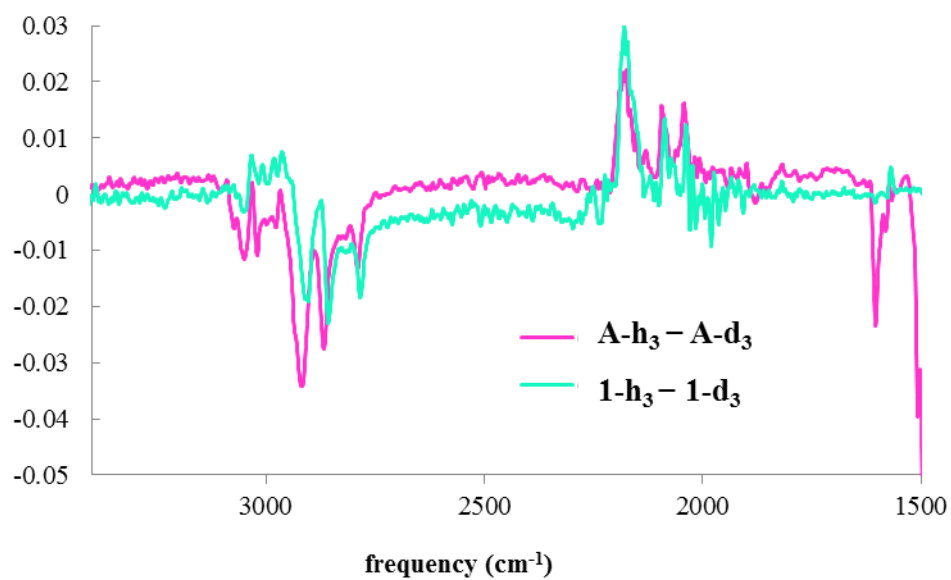


Figure 18. Infrared spectra for **1-d<sub>3</sub>** and **1-h<sub>3</sub>** (solid powders).



**Figure 19.** Difference infrared spectra ( $\mathbf{A-h_3}$  minus  $\mathbf{A-d_3}$  in pink *and*  $\mathbf{1-h_3}$  minus  $\mathbf{1-d_3}$  in green) highlighting the three C-H and/or C-D vibrations in each molecule.

Bond Vibrations for Methyl Ligands on Cr Complexes		
	C-H ( $\text{cm}^{-1}$ )	C-D ( $\text{cm}^{-1}$ )
$\mathbf{A-d_3}$	--	2180, 2087, 2039
$\mathbf{A-h_3}$	2904, 2857, 2785	--
$\mathbf{1-d_3}$	--	2175, 2094, 2043
$\mathbf{1-h_3}$	2918, 2869, 2791	--

**Table 1.** Bond vibrations (C-H or C-D) in  $\mathbf{A-h_3}$ ,  $\mathbf{A-d_3}$ ,  $\mathbf{1-h_3}$ , and  $\mathbf{1-d_3}$  determined from the IR spectroscopy.

## CW EPR Spectra.

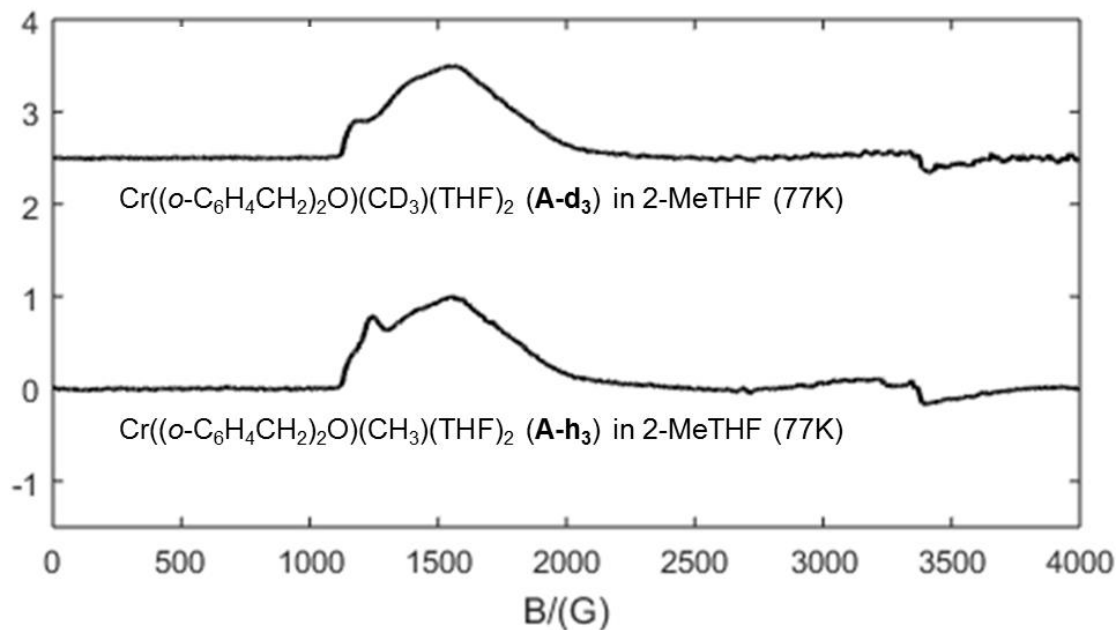


Figure 20. Comparison of CW EPR spectra of **A-d<sub>3</sub>** and **A-h<sub>3</sub>**.

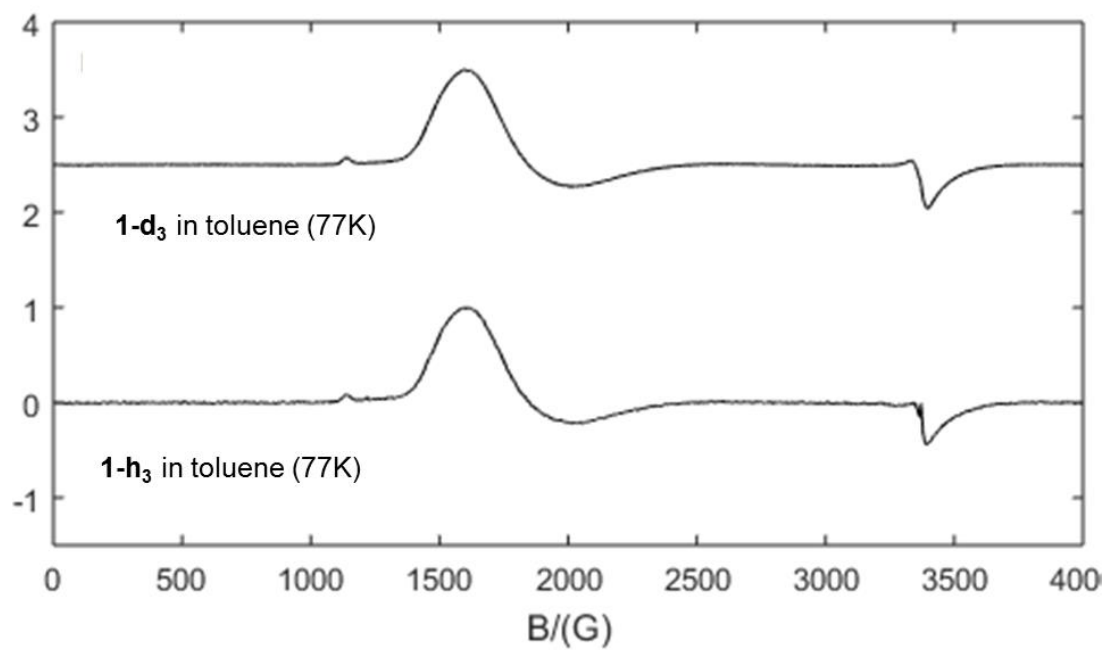
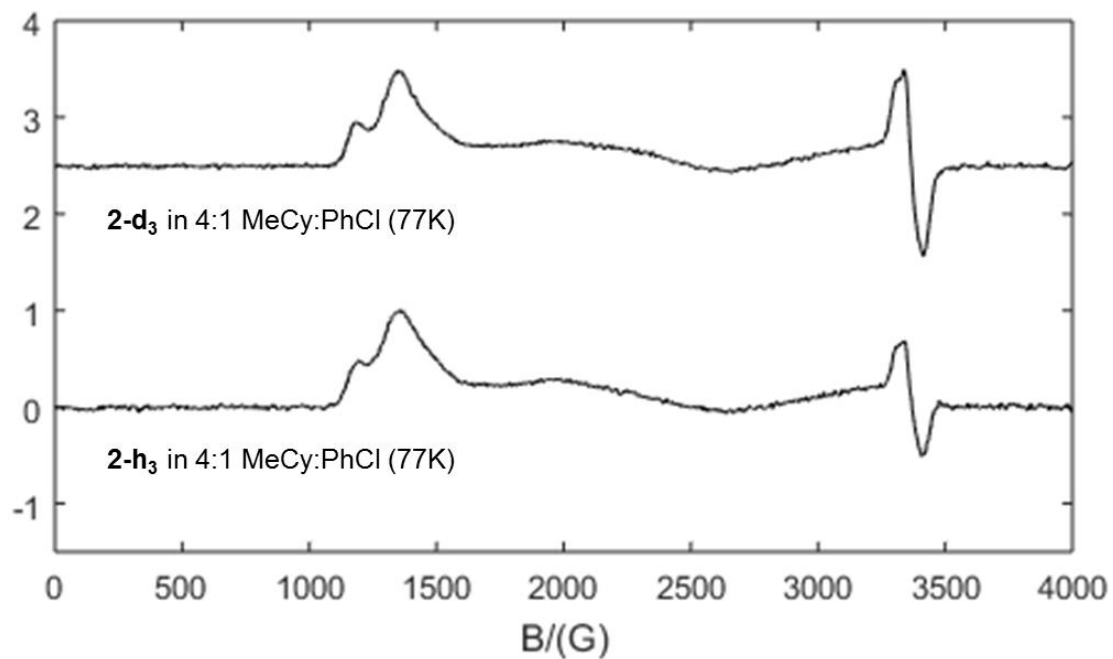
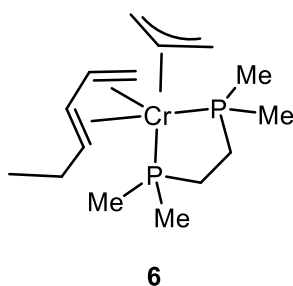


Figure 21. Comparison of CW EPR spectra of **1-d<sub>3</sub>** and **1-h<sub>3</sub>**.



**Figure 22.** Comparison of CW EPR spectra of **2-d<sub>3</sub>** and **2-h<sub>3</sub>**.



**Figure 23.** Complex **6** used as a reference compound.

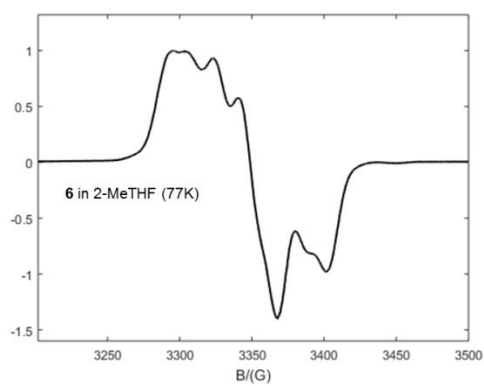


**Figure 24.** CW EPR spectrum of complex **6** in 2Me-THF.

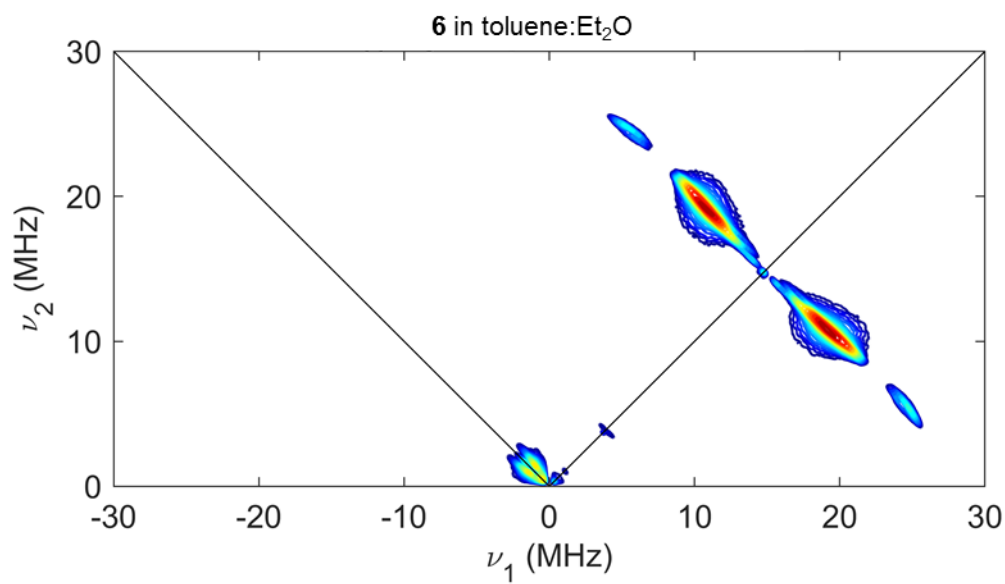


**Figure 25.** X-band HSCORE of **6**. Acquisition parameters: temperature = 40 K; microwave frequency = 9.723 GHz; MW pulse length ( $\pi/2$ ,  $\pi$ ) = 40 ns, 80 ns;  $\tau$  = 136 ns,  $t_1$  =  $t_2$  = 100 ns;  $\Delta t_1$  =  $\Delta t_2$  = 16 ns; shot repetition time (srt) = 2 ms.

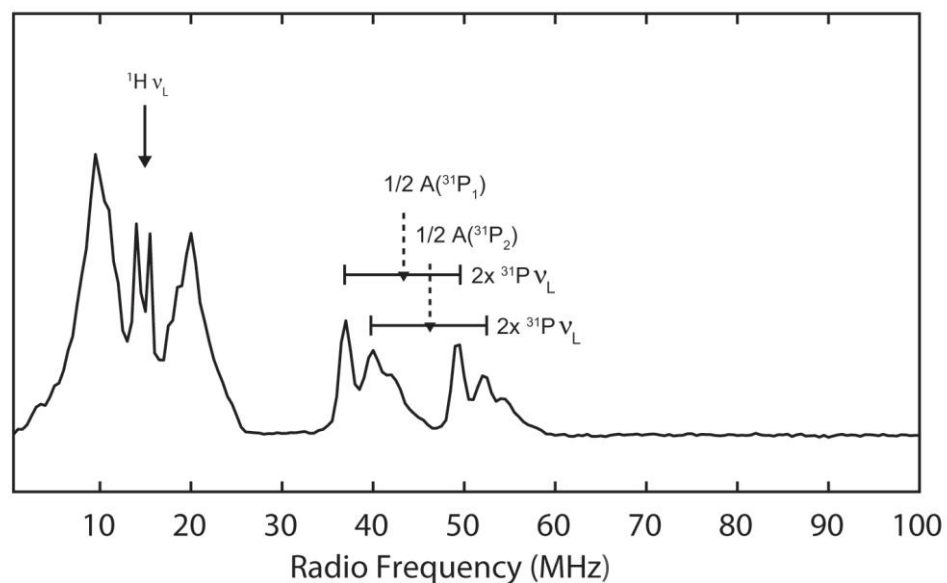


**Figure 26.** X-band Davies ENDOR of **6**. Acquisition parameters: temperature = 40 K; MW frequency = 9.723 GHz; MW pulse length ( $\pi/2$ ,  $\pi$ ) = 40 ns, 80 ns;  $\tau$  = 282 ns; RF pulse length = 15  $\mu$ s;  $T_{RF}$  = 2  $\mu$ s; shot repetition time = 5 ms.

**References.**

- (1) (a) Mohadjer Beromi, M.; Brudvig, G. W.; Hazari, N.; Lant, H. M. C.; Mercado, B. Q. *Angewandte Chemie International Edition* **2019**, *58*, 6094. (b) Neidig, M. L.; Carpenter, S. H.; Curran, D. J.; DeMuth, J. C.; Fleischauer, V. E.; Iannuzzi, T. E.; Neate, P. G. N.; Sears, J. D.; Wolford, N. J. *Accounts of Chemical Research* **2019**, *52*, 140. (c) Arevalo, R.; Chirik, P. J. *Journal of the American Chemical Society* **2019**, *141*, 9106.
- (2) Fernández, P.; Pritzkow, H.; Carbó, J. J.; Hofmann, P.; Enders, M. *Organometallics* **2007**, *26*, 4402.
- (3) (a) Bonomo, R. P.; Di Bilio, A. J.; Riggi, F. *Chemical Physics* **1991**, *151*, 323. (b) Pedersen, E.; Toftlund, H. *Inorganic Chemistry* **1974**, *13*, 1603.
- (4) (a) Deblon, S.; Liesum, L.; Harmer, J.; Schönberg, H.; Schweiger, A.; Grützmacher, H. *Chemistry – A European Journal* **2002**, *8*, 601. (b) Horitani, M.; Grubel, K.; McWilliams, S. F.; Stubbert, B. D.; Mercado, B. Q.; Yu, Y.; Gurubasavaraj, P. M.; Lees, N. S.; Holland, P. L.; Hoffman, B. M. *Chemical Science* **2017**, *8*, 5941. (c) Nesbit, M. A.; Oyala, P. H.; Peters, J. C. *Journal of the American Chemical Society* **2019**, *141*, 8116.
- (5) (a) Agapie, T. *Coordination Chemistry Reviews* **2011**, *255*, 861. (b) McGuinness, D. S. *Chemical Reviews* **2011**, *111*, 2321.
- (6) (a) Brückner, A.; Jabor, J. K.; McConnell, A. E. C.; Webb, P. B. *Organometallics* **2008**, *27*, 3849. (b) McDyre, L. E.; Hamilton, T.; Murphy, D. M.; Cavell, K. J.; Gabrielli, W. F.; Hanton, M. J.; Smith, D. M. *Dalton Transactions* **2010**, *39*, 7792. (c) Skobelev, I. Y.; Panchenko, V. N.; Lyakin, O. Y.; Bryliakov, K. P.; Zakharov, V. A.; Talsi, E. P. *Organometallics* **2010**, *29*, 2943. (d) Rabeah, J.; Bauer, M.; Baumann, W.; McConnell, A. E. C.; Gabrielli, W. F.; Webb, P. B.; Selent, D.; Brückner, A. *ACS Catalysis* **2012**, *3*, 95. (e) Do, L. H.; Labinger, J. A.; Bercaw, J. E. *ACS Catalysis* **2013**, *3*, 2582. (f) Venderbosch, B.; Oudsen,

J.-P. H.; Wolzak, L. A.; Martin, D. J.; Korstanje, T. J.; Tromp, M. *ACS Catalysis* **2019**, *9*, 1197.

(7) (a) McKean, D. C.; McQuillan, G. P.; Morrisson, A. R.; Torto, I. *Journal of the Chemical Society, Dalton Transactions* **1985**, 1207. (b) Robertson, A. H. J.; McQuillan, G. P.; McKean, D. C. *Journal of the Chemical Society, Dalton Transactions* **1995**, 3955. (c) McQuillan, G. P.; McKean, D. C.; Torto, I. *Journal of Organometallic Chemistry* **1986**, *312*, 183.

(8) (a) Hoogstraten, C. G.; Britt, R. D. *RNA* **2002**, *8*, 252. (b) Marchiori, D. A.; Oyala, P. H.; Debus, R. J.; Stich, T. A.; Britt, R. D. *The Journal of Physical Chemistry B* **2018**, *122*, 1588.

(9) Hirscher, N. A.; Agapie, T. *Organometallics* **2017**, *36*, 4107.

(10) (a) Monillas, W. H.; Yap, G. P. A.; MacAdams, L. A.; Theopold, K. H. *Journal of the American Chemical Society* **2007**, *129*, 8090. (b) Monillas, W. H.; Young, J. F.; Yap, G. P. A.; Theopold, K. H. *Dalton Transactions* **2013**, *42*, 9198.

(11) Iczek, F.; Jolly, P. W.; Krüger, C. *Journal of Organometallic Chemistry* **1990**, *382*, C11.

(12) Bartlett, S. A.; Moulin, J.; Tromp, M.; Reid, G.; Dent, A. J.; Cibir, G.; McGuinness, D. S.; Evans, J. *Catalysis Science & Technology* **2016**, *6*, 6237.

(13) Brown, T. L.; Dickerhoof, D. W.; Bafus, D. A.; Morgan, G. L. *Review of Scientific Instruments* **1962**, *33*, 491.

(14) Sattler, A.; Aluthge, D. C.; Winkler, J. R.; Labinger, J. A.; Bercaw, J. E. *ACS Catalysis* **2016**, *6*, 19.

(15) Herwig, W.; Zeiss, H. *The Journal of Organic Chemistry* **1958**, *23*, 1404.

(16) (a) Jiang, T.; Zhang, S.; Jiang, X.; Yang, C.; Niu, B.; Ning, Y. *Journal of Molecular Catalysis A: Chemical* **2008**, *279*, 90. (b) Brookhart, M.; Grant, B.; Volpe, A. F. *Organometallics* **1992**, *11*, 3920.

## Appendix 1

Chromium Complexes of Bidentate Aryl Amines and Tridentate Aryl Diamines

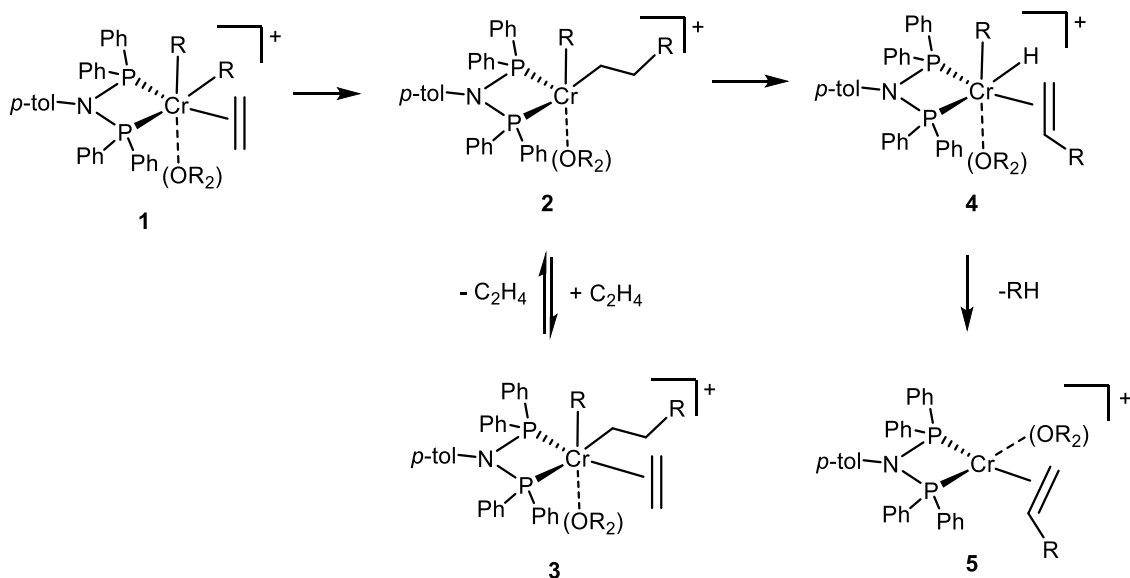
**Abstract.**

A monoanionic NCN (amine-aryl-amine) pincer ligand supported Cr(III) and Cr(II) complexes. Reduction to Cr(I) complexes was attempted but successful isolation of the product(s) was not achieved. A bidentate (aryl-amine) version was also used, but was likely too sterically open to prevent dimerization of Cr intermediates. The NCN Cr(III) complex was derivatized with pendant allyl groups to evaluate the potential for Cr-alkene interactions in a well-defined system. Alkene insertion into the Cr-aryl bond was determined to occur.

## Introduction.

Given the evidence surrounding a catalyst initiation pathway leading to a Cr(I) species, a strategy was devised to generate a well-defined Cr model complex. In particular, a isolable Cr(I) complex was targeted for spectroscopic benchmarking purposes, and in order to test for reactivity with ethylene. Further, it was theorized that catalyst initiation (from Cr(III) to Cr(I)) could have an inverse dependence on ethylene concentration leading to low concentrations of the Cr active species under typical tetramerization conditions (i.e. high ethylene pressures). More specifically, as shown in Scheme 1, the intermediate (2) that undergoes  $\beta$ -H elimination may be in equilibrium with a coordinatively-saturated Cr species (3). If [2] is low due to high  $[C_2H_4]$ , then the rate of  $\beta$ -H elimination is diminished. The implication of this hypothesis is that an appropriate Cr(I) precatalyst (if isolable) would not

**Scheme 1.** Proposed initiation mechanism from a Cr(III) precatalyst bound to ethylene (1), followed by subsequent insertion, then  $\beta$ -H elimination, and finally reductive elimination, to give Cr(I) species (5) which is suspected to lead to the active species following substitution for ethylenes in a Cr(I)/Cr(III) cycle.



have an initiation rate inversely dependent on ethylene concentration, and overall catalytic productivity could be increased as a result.

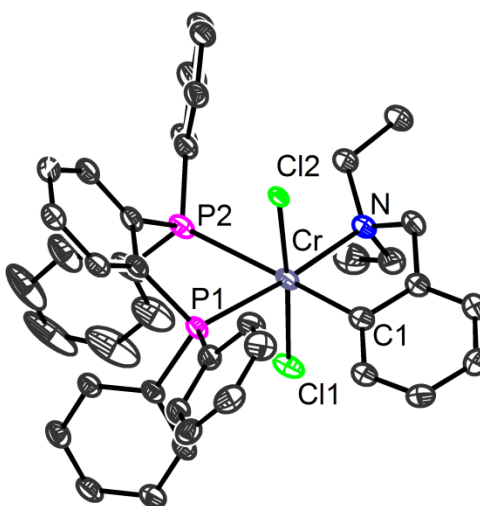
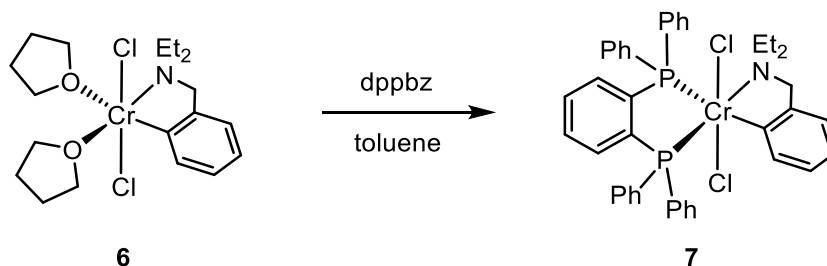
In several studies, Cr(I) precatalysts have been used for ethylene tetramerization, but they were saturated with carbonyl ligands and require alkyl-aluminum activators, so are not suitable for this direction.<sup>1</sup> There are relatively few examples of Cr(I) complexes that are not stabilized by strong donors like CO or Cp ligands.<sup>2</sup> Most relevant to the targeted structures are the Cr(I) monoaryl complexes from the Power lab, which are notable for their tendency to dimerize (and form Cr-Cr quintuple bonds).<sup>3</sup> In fact, only when the bulk of the aryl ligand is further increased can monomeric Cr(I) complexes be isolated.<sup>4</sup> The Cr(I) precatalysts needed to test the initiation hypothesis would be at least three-coordinate. Additional coordinating donors could be employed, if necessary, to achieve stable structures. To this end, several mono-, bi-, and tridentate aryl ligands were used towards reduced Cr(I) species. Ligation of the various Cr intermediates with a diphosphine (in this case, bis(diphenylphosphino)benzene (dppbz)) was attempted. Although not as optimal as the aminodiphosphines (PNP), dppbz has been reported to support ethylene tetramerization catalysis.<sup>5</sup> Importantly, it was expected to be more robust than PNP for these synthetic studies.

Some Cr(II) and Cr(III) complexes were isolated using the parent NCN pincer, but reductions to Cr(I) were not successful. The initiation hypothesis was not testable due to lack of suitable Cr(I) precatalysts. An interesting alkene insertion was observed from the allyl-derivatized NCN pincer complex.

## Results and Discussion.

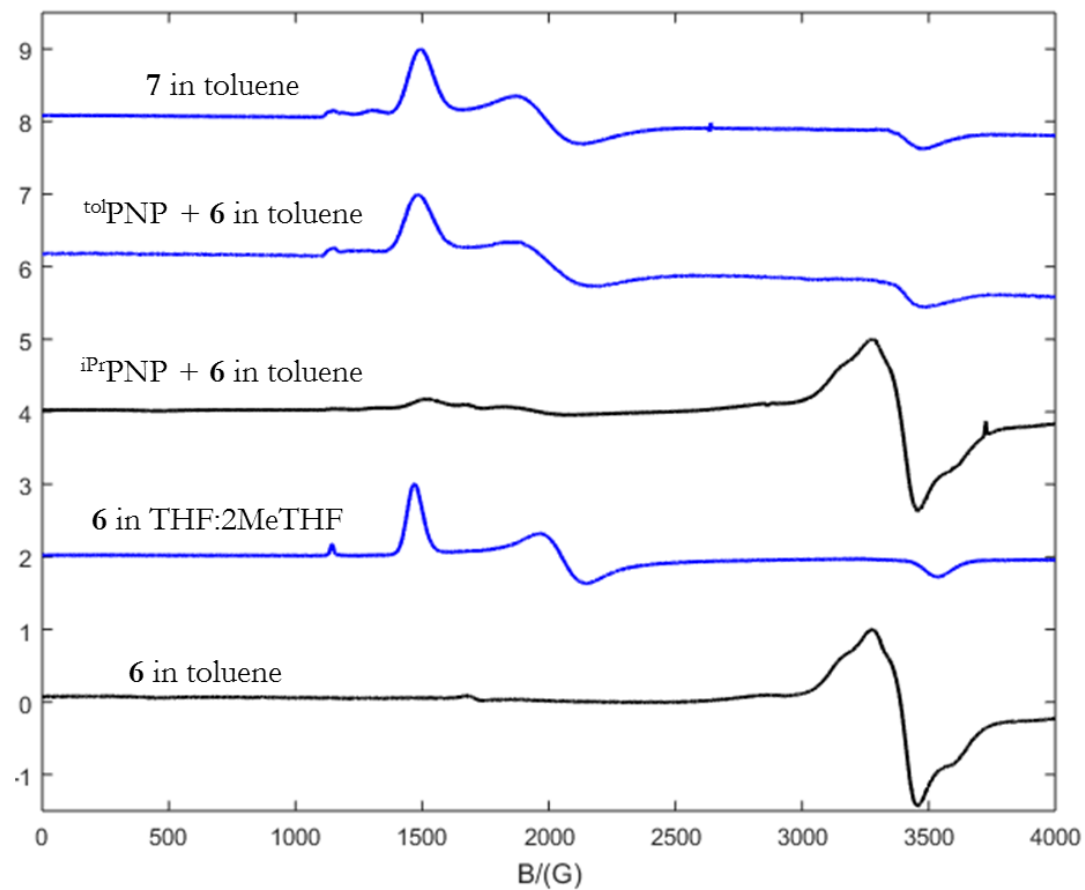
**Attempted Reductions of Monoaryl Cr Species.** Initial attempts to use bulky monoaryl Grignards without chelating groups (2,6-diisopropylphenyl, mesityl, or 2-biphenyl) to isolate Cr(III) precursors were not promising. Although  $\text{Cr}(\text{mesityl})\text{Cl}_2(\text{THF})_3$  was synthesized (structure shown in Appendix 4, Figure 11), reactions with dppbz and/or further reduction led only to the isolation of Cr(II) species (see Appendix 4, Figure 13). A chelating aryl Grignard could be used to isolate a monoaryl, Cr(III) bis-THF precursor (**6**). Subsequent metalation with dppbz was also successful, yielding **7**. Reductions of complex **7** were not tractable, however.

**Scheme 2.** Synthetic procedure allowing for structural characterization of compound **7**.

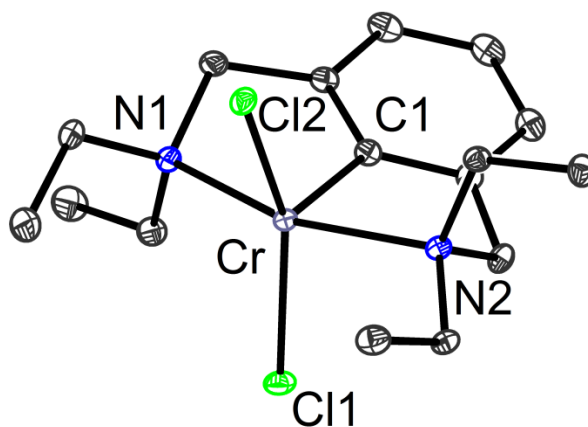
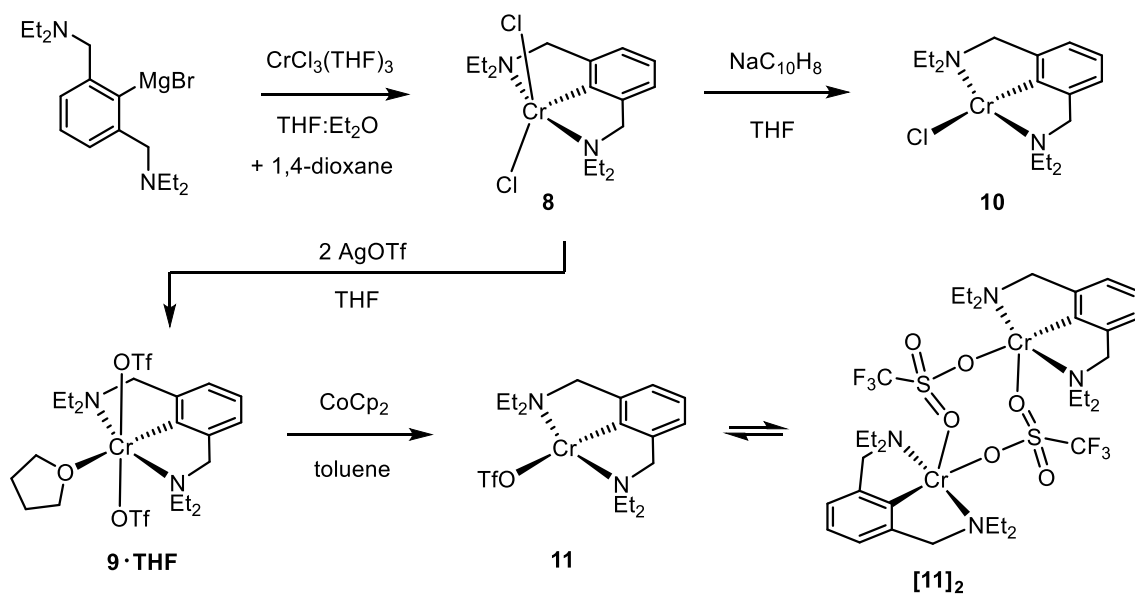


**Figure 1.** Molecular structure of  $(\text{dppbz})\text{CrCl}_2((\text{Et}_2\text{NCH}_2)\text{C}_6\text{H}_4)$  (**7**)

**Synthesis of Cr(III) and Cr(II) Complexes of an NCN Pincer Ligand.** Expecting that greater support of the Cr-aryl motif was necessary to stabilize the +1 oxidation state, an NCN pincer motif was used. Successful isolation of Cr(III) dichloride (**8**) and bis(triflate) (**9·THF**) complexes was achieved. These could be reduced to the Cr(II) analogs (**10** and **11**) using sodium naphthalenide or cobaltocene, respectively. Substitution for dppbz was targeted; it was hypothesized that an amine pincer arm might dissociate (or triflates, in the case of **9** and **11**). Since a monomer-dimer equilibrium was noticeable for **11** (dimeric blue crystals dissolve to give pink solution), it seemed likely that a six coordinate Cr(II) diphosphine complex would be formed. However, for neither of **8-11** was there an observable reaction with dppbz. The Cr(II) examples were tracked by  $^{31}\text{P}$  NMR, and  $^1\text{H}$  NMR; the Cr(III) examples were tracked by  $^{31}\text{P}$  NMR and cw EPR.



**Figure 2.** Stacked cw EPR spectra from top to bottom: **7** in toluene,  $^{\text{tol}}\text{PNP} + \mathbf{6}$  in toluene,  $^{\text{iPr}}\text{PNP} + \mathbf{6}$  in toluene, **6** in THF:2MeTHF, and **6** in toluene.

**Scheme 3.** Synthetic route to NCN pincer complexes of Cr.**Figure 3.** Molecular structure of  $\text{CrCl}_2((\text{Et}_2\text{NCH}_2)_2\text{C}_6\text{H}_3)$  (**8**) with thermal ellipsoids at the 50% probability level. H-atoms are omitted for clarity.

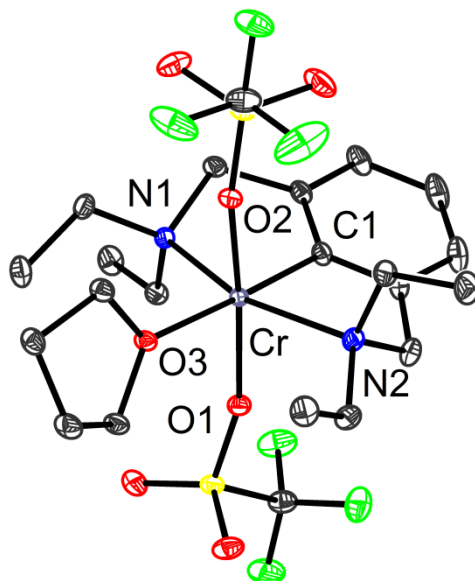


**Figure 4.** Molecular structure of  $\text{Cr}(\text{OTf})_2((\text{Et}_2\text{NCH}_2)_2\text{C}_6\text{H}_3)(\text{THF})$  (**9·THF**) with thermal ellipsoids at the 50% probability level. H-atoms are omitted for clarity.

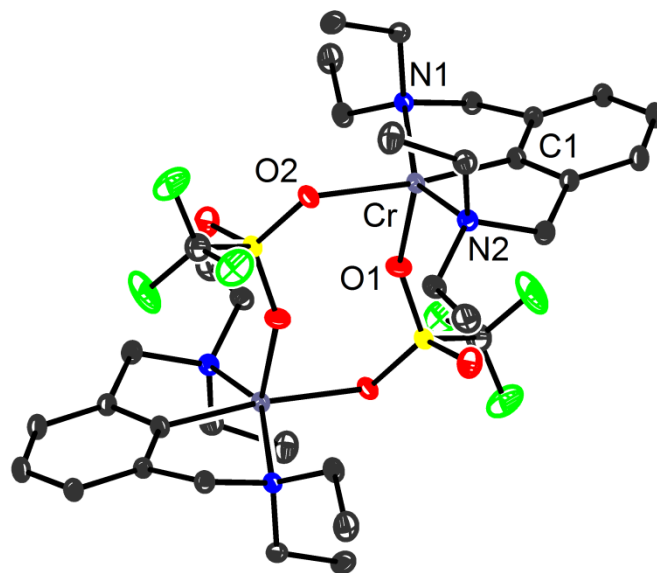


**Figure 5.** Molecular structure of  $[\text{Cr}(\text{OTf})((\text{Et}_2\text{NCH}_2)_2\text{C}_6\text{H}_3)]_2$  (**[11]<sub>2</sub>**) with thermal ellipsoids at the 50% probability level. H-atoms are omitted for clarity.

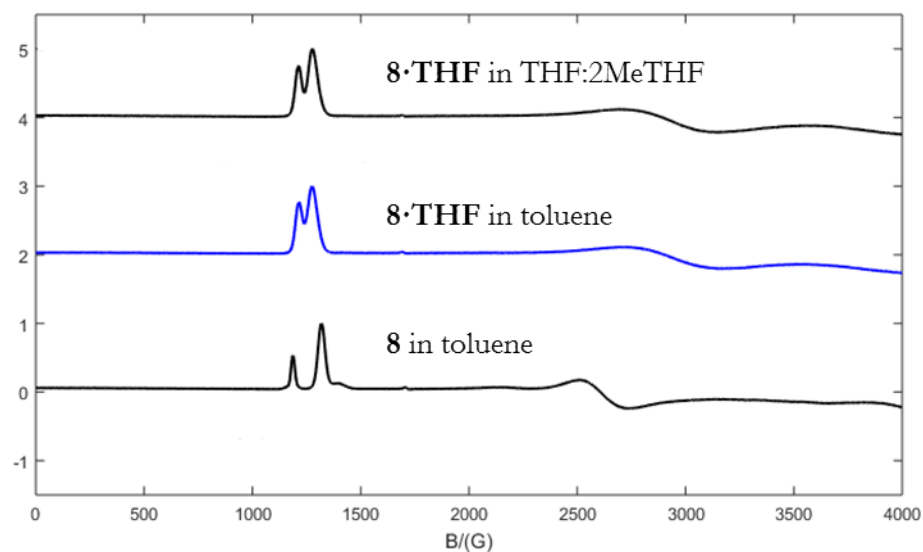


**Figure 6.** Stacked cw EPR spectra from top to bottom: **8•THF** in THF:2MeTHF, **8•THF** in toluene, and **8** in toluene.

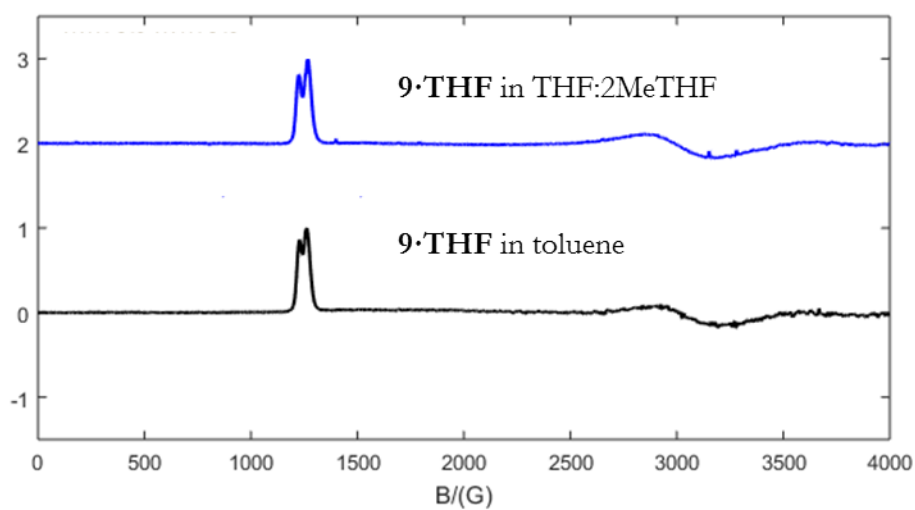


**Figure 7.** Stacked cw EPR spectra from top to bottom: **9•THF** in THF:2MeTHF, and **9•THF** in toluene.

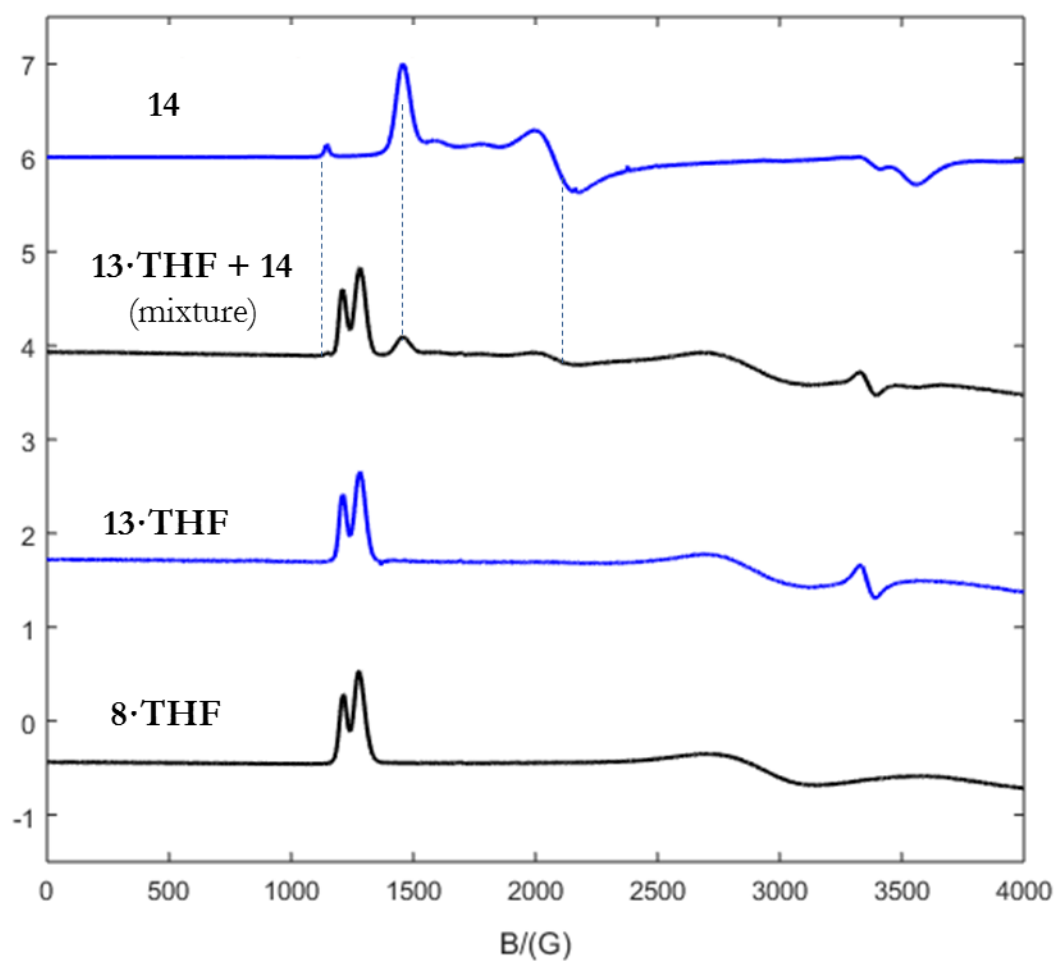


**Figure 8.** Stacked cw EPR spectra from top to bottom: **14** (proposed alkene insertion species), **13·THF + 14** mixture, **13·THF**, and **8·THF**.

**Reactions of an Allyl-Substituted NCN Cr Pincer Complex.** Noting the isomerization between five- and six-coordinate Cr(III) species (**8** and **8·THF** in Figure 6), a Cr-alkene intermediate was targeted by modifying the NCN pincer with pendant alkenes, designed to bind to the open coordination site. Using an NCN pincer with allyl substituents on the amine arms, rather than ethyl substituents, the analog of **8** was generated by the same synthetic route. In THF solution, the EPR spectrum was nearly identical to **8·THF**, substantiating the structural assignment as a six-coordinate species (Figure 8). Similarly to the conversion **8·THF** to **8**, **13·THF** converts to a new species (**14**). However, this conversion occurs in THF, rather than as a result of removing the solvent. Therefore, **14** has possibly undergone alkene insertion into the Cr-aryl bond. Quenched aliquots of **14** reveal an organic residue by GC/MS with a different retention time than the aryl residue from quenched aliquots of the corresponding Grignard formed from **12**. This is indirect evidence for **14** being an inserted species. However, single-crystals of **14** were not grown, only microcrystals were obtained.

Reductions of **13·THF** were attempted using  $KC_8$  and Na(Hg) but no crystals were isolated from the reaction mixture. Single crystals were obtained following the reaction of **14** with Na(Hg) (2 equiv. of sodium); the XRD structure showed a Cr(II) species bound to *two* NCN ligands, each exhibiting an alkene inserted into the Cr-aryl bond (see Figure 16 in Appendix 4). Such a product obviously was derived by ligand scrambling. Solely from this result, it is not clear at what stage the alkene insertion occurred, but clearly this side reactivity is problematic under reductive conditions (or even at the Cr(III) oxidation state, as discussed).

It was apparent that **14** already exhibited alkene insertion from the  $^1H$  NMR of the quenched aryl residue. It reveals a highly asymmetric structure, with seven distinct non-

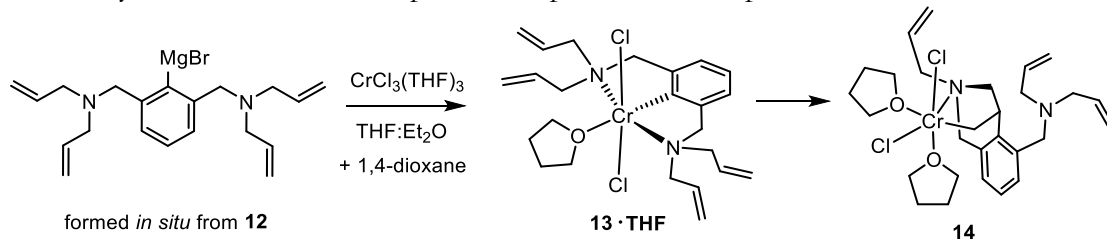
allylic, non-methyl aliphatic  $^1\text{H}$  resonances between 2.4 and 4.0 ppm, which is expected from the structure shown in Figure 9. The doublet at 1.3 ppm corresponds to the methyl group on the ring. The allylic protons resonate at 3.1 ppm, where the signals integrate to a total of six. The alkene proton resonances are also present (5.1 to 6.0 ppm) integrating to nine.

Additional evidence corroborating the structural assignment of **14** is the similarity between its cw EPR spectrum (in THF:2MeTHF) and the spectrum for **6** (in THF:2MeTHF), which are shown in Figure 8 and Figure 2, respectively. Thus, both are expected to exhibit a six-coordinate geometry about Cr(III), with two THF ligands, two chlorides, and a bidentate arylamine (in **6**) or bidentate alkylamine (in **14**).

The final evidence for the structure of **14** was the structure determination via XRD of crystals grown from dimethoxyethane (dme). The structure of **15** was identical to that assigned to **14**, except dme replaced the two THF ligands (Figure 10).

Noting that **14** does not have the second pincer “arm” bound, the analogous complex was sought from precursors without this extra functionality. Notably, the EPR spectrum of **16** was similar to **14** and **6**. However, GC/MS analysis of quenched aryl residues from **16** indicated a mixture of arylamine species, likely due to regioselectivity issues in the insertion (or degradation of **16**). Therefore, the preformation of the tridentate “pincer” motif **13** likely leads to cleaner conversion to **14**.

**Scheme 4.** Synthetic route to NCN pincer complex of Cr with pendant alkenes.



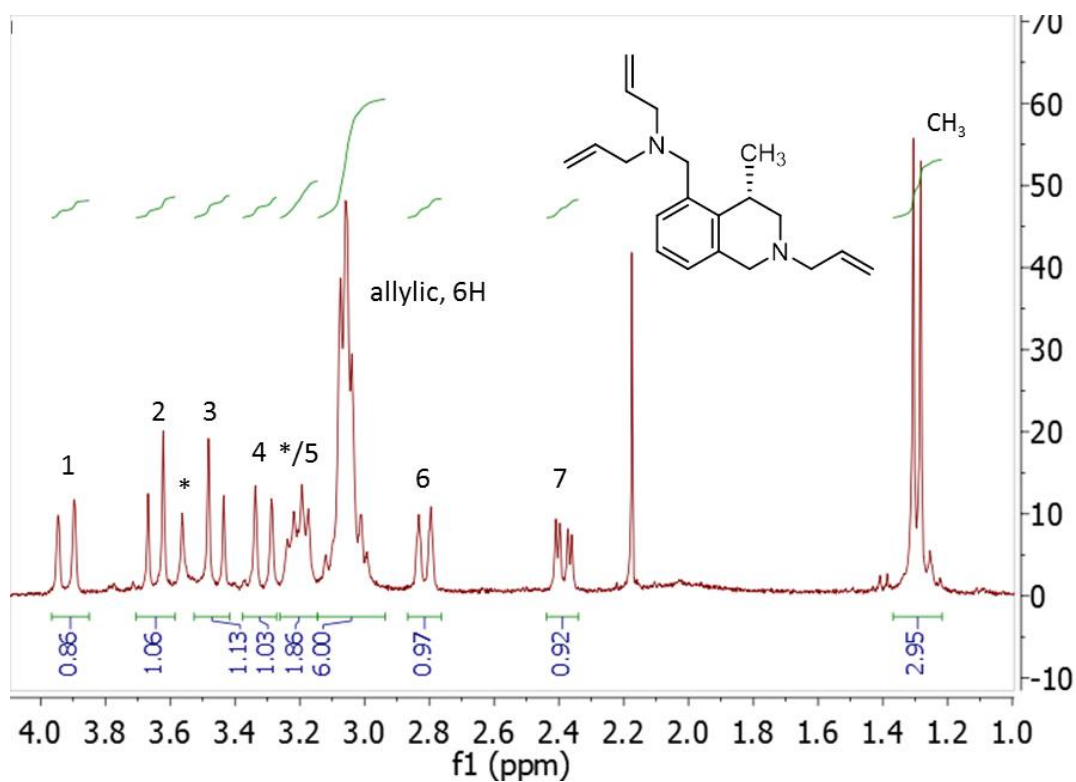


**Figure 9.**  $^1\text{H}$  NMR (CDCl<sub>3</sub>) of the organic residue derived from quenching **14** with methanol.

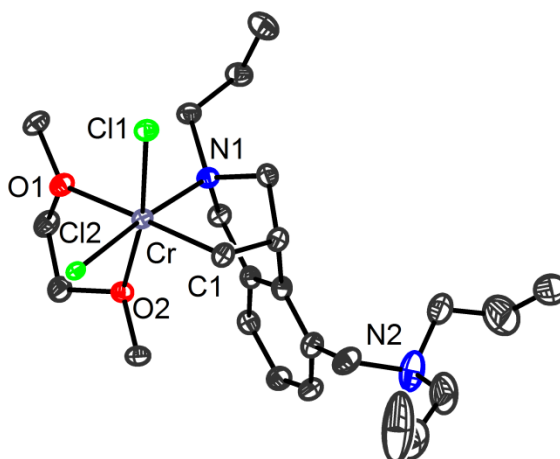
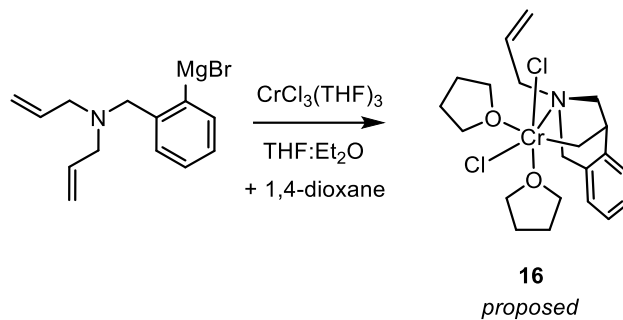


**Figure 10.** Molecular structure of dme adduct **15** (derived from **14**) with thermal ellipsoids at the 50% probability level. H-atoms are omitted for clarity.

**Scheme 5.** Synthetic route to alkene-inserted species from a bidentate aryl-amine proligand.



### Conclusion.

Building on the early examples of stabilized Cr-aryl complexes using chelating donors (primarily ethers) shown in Chapters 1-5, bidentate and tridentate aryl ligands with chelating amines were investigated. Although no Cr(I) complexes were isolated from these precursors, an interesting alkene insertion product was synthesized.

## Experimental.

General methods are identical to those described in the chapters of this thesis. 2-bromo-1,3-bis(bromomethyl)benzene and 1-bromo-2,6-bis((diethylamino)methyl)benzene were synthesized according to the published procedures.<sup>6</sup>

**Synthesis of  $\text{CrCl}_2((\text{Et}_2\text{NCH}_2)_2\text{C}_6\text{H}_3)(\text{THF})$  (**8**·THF).** A 4 mL THF solution of 1-bromo-2,6-bis((diethylamino)methyl)benzene (0.263 g, 0.804 mmol) was stirred over excess Mg turnings until Grignard formation was complete (as determined by GC/MS). This was filtered from the Mg, then added dropwise over two minutes to a thawing suspension of  $\text{CrCl}_3(\text{THF})_3$  in 8 mL THF. The reaction mixture was diluted to 16 mL using THF, then stirred at RT for 16 hours. The green solution was reduced *in vacuo* to approximately 6 mL, then 6 mL  $\text{Et}_2\text{O}$  and 0.25 mL 1,4-dioxane were added. This was stirred at RT for 20 hours, then a dark green solution was filtered from white solids using Celite. The filtrate was reduced to dryness, then redissolved in 2 mL THF. After storing at  $-35^\circ\text{C}$  for 2 days, some green powder was visible. The supernatant was decanted into a clean vial, and stored further at  $-35^\circ\text{C}$  for 3 days, yielding green crystalline blocks. Solid **8**·THF was isolated by decanting the supernatant and drying the crystals *in vacuo* briefly (0.229 g, 0.684 mmol, 85% yield). Yellow/red dichroic crystals of **8** suitable for XRD could be grown by vapor diffusion of hexanes into an  $\text{Et}_2\text{O}$  solution of **8** (which forms by pumping the THF off of **8**·THF).

**Synthesis of  $\text{Cr}(\text{OTf})_2((\text{Et}_2\text{NCH}_2)_2\text{C}_6\text{H}_3)(\text{THF})$  (**9**·THF).** A 6 mL toluene solution of **8**·THF (0.068 g, 0.15 mmol) was pumped to dryness *in vacuo*, and triturated with pentane to obtain 0.059 g of a red-violet residue (**8**). This was redissolved in THF (1 mL) then  $\text{AgOTf}$  (0.083 g, 0.032 mmol) was added in 2 mL THF. The green solution was stirred at RT, and after 10 min, filtered from pale solids (mostly  $\text{AgCl}$ ). The filtrate was reduced *in vacuo* to approximately 2 mL. This solution was stored at  $-35^\circ\text{C}$  for 3 days, during which time

blue-green blocks had crystallized. These were isolated by decanting the supernatant, and dried under vacuum (0.057 g, 0.085 mmol, 55% yield). The molecular structure was determined by XRD of a suitable crystal grown by this procedure.

**In Situ Formation of  $\text{CrCl}(\text{Et}_2\text{NCH}_2)_2\text{C}_6\text{H}_3$  (10).** To a 1 mL THF solution of **8·THF** (0.020 g, 0.045 mmol) stirring at RT, a 4 mL THF solution of sodium naphthalenide (1 equiv.) was added. This caused a color change in solution from green to blue, then finally purple.

**Synthesis of  $[\text{Cr}(\text{OTf})(\text{Et}_2\text{NCH}_2)_2\text{C}_6\text{H}_3]_2$  ([11]<sub>2</sub>).** To a stirring 3 mL toluene solution of **9·THF** (0.014 g, 0.021 mmol), a 1 mL toluene solution of cobaltocene (0.004 g, 0.02 mmol) was added dropwise. The blue-green solution changed color to red-orange. After five minutes, a pink solution was filtered from yellow-green solids. The pink solution was reduced *in vacuo* to dryness, causing a color change to violet-blue, corresponding to the dimer, **[11]<sub>2</sub>** (0.005 g, 0.006 mmol, 30% yield). Single crystals of **[11]<sub>2</sub>** suitable for XRD were grown by vapor diffusion of pentane into a toluene solution.

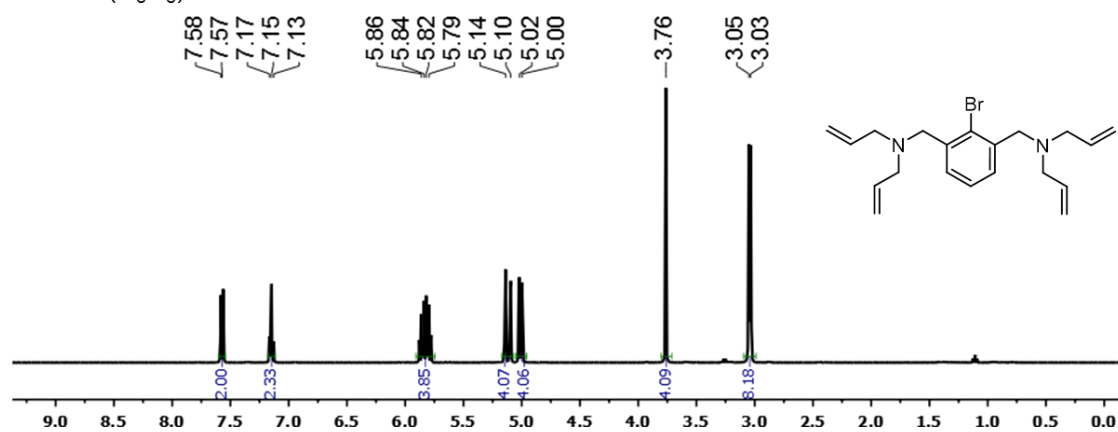
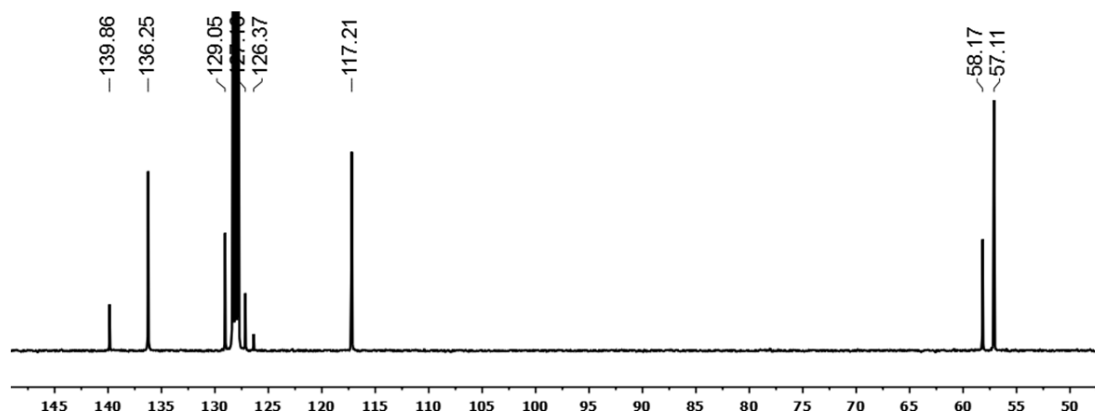
**Synthesis of 1-bromo-2,6-bis((diallylamino)methyl)benzene (12).** Freshly distilled diallylamine (4.3 g, 44 mmol) was added to a Schlenk flask under N<sub>2</sub> flow. A solution of 2-bromo-1,3-bis(bromomethyl)benzene (1.80 g, 5.25 mmol) in dry C<sub>6</sub>H<sub>6</sub> (20 mL) was added to the flask. The colorless solution was stirred vigorously at RT. After 1 hr, colorless precipitate was observed. After 44 hr, 1.8 g NaOH dissolved in H<sub>2</sub>O (50 mL) was added. The organic layer was collected, and the aqueous layer was extracted with 3 x 50 mL Et<sub>2</sub>O. The combined organics were rinsed with 50 mL H<sub>2</sub>O, and then dried over MgSO<sub>4</sub>, filtered, and reduced under vacuum to 1.8 g of pale yellow oil. This was distilled using a Kugelrohr apparatus (110-115°C, 50-100 mTorr) to collect the product as a colorless oil (1.76 g, 4.69 mmol, 89% yield). <sup>1</sup>H NMR (399.8 MHz, 23°C, C<sub>6</sub>D<sub>6</sub>): δ 7.58 (d, J<sub>H-H</sub> = 7.5 Hz, 2H, aryl-H), 7.16 (t, J<sub>H-H</sub>

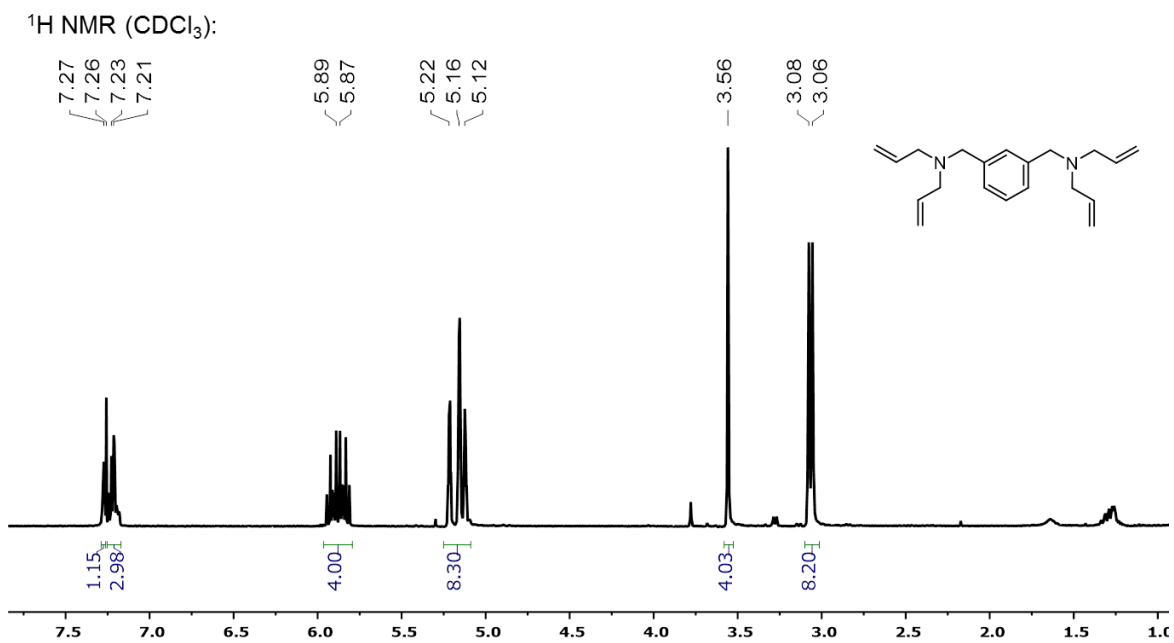
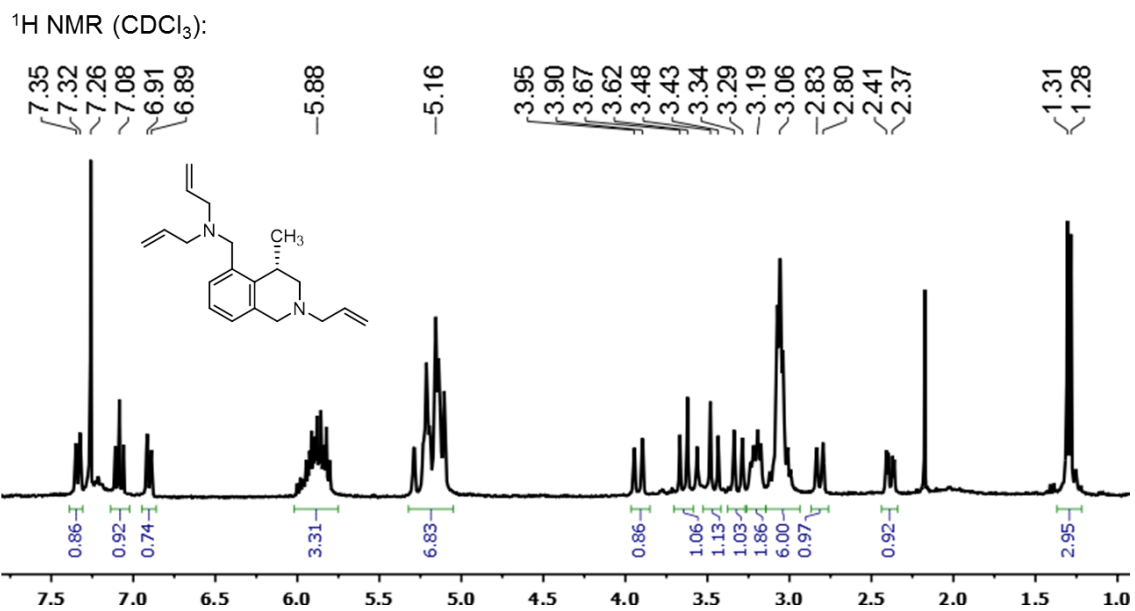
= 7.5 Hz, 1H, aryl-*H*), 5.83 (ddt,  $J_{\text{H-H}} = 17.1, 10.2, 6.2$  Hz, 4H,  $\text{CH}_2\text{CHCH}_2$ ), 5.12 (dd,  $J_{\text{H-H}} = 17.1, 1.9$  Hz, 4H,  $\text{CH}_2\text{CH-C(H)H}$ ), 5.01 (dd,  $J_{\text{H-H}} = 10.2, 1.9$  Hz, 4H,  $\text{CH}_2\text{CH-CH(H)}$ ), 3.76 (s, 4H, aryl- $\text{CH}_2\text{-N(allyl)}$ ), 3.04 (d,  $J_{\text{H-H}} = 6.2$  Hz, 8H,  $\text{NCH}_2\text{CHCH}_2$ ).  $^{13}\text{C}$  NMR (100.5 MHz, 23°C,  $\text{C}_6\text{D}_6$ ):  $\delta$  139.9, 136.3, 129.1, 127.2, 126.4, 117.2, 58.2, 57.1. EI/MS ( $m/z$ ): 376.

**Synthesis of  $\text{CrCl}_2((\text{allyl})_2\text{NCH}_2)_2\text{C}_6\text{H}_3$  (14).** In 3 mL THF, X (0.254 g, 0.677 mmol) was stirred over excess Mg turnings for several hours. Once Grignard formation was complete, as determined by as GC/MS of a quenched aliquot, the solution was filtered through glass wool, away from leftover Mg. To a thawing suspension of  $\text{CrCl}_3(\text{THF})_3$  (0.257 g, 0.686 mmol) in 3 mL THF, the Grignard solution was added over two minutes. The resulting green solution was diluted to 10 mL using THF. After 1 h at RT, the solution was reduced *in vacuo* to 3 mL, then 3 mL  $\text{Et}_2\text{O}$  and 0.25 mL 1,4-dioxane was added. This caused rapid precipitation of white solids. After 2 h, the green solution was filtered from the white solids. The filtrate was reduced *in vacuo* to yield a yellow-brown solid (0.255 g, 0.589 mmol, 87% yield).

**Synthesis of  $\text{CrCl}_2((\text{allyl})_2\text{NCH}_2)_2\text{C}_6\text{H}_4$  (16).** In 2 mL THF, 1-bromo-2-((diallylamino)methyl)benzene (0.148 g, 0.556 mmol) was stirred over excess Mg turnings for several hours. Once Grignard formation was complete, as determined by as GC/MS of a quenched aliquot, the solution was filtered through glass wool, away from leftover Mg. To a thawing suspension of  $\text{CrCl}_3(\text{THF})_3$  (0.210 g, 0.560 mmol) in 3 mL THF, the Grignard solution was added over two minutes, and the resulting solution warmed to RT, after adding 5 mL  $\text{Et}_2\text{O}$  and 0.1 mL 1,4-dioxane. After 90 minutes, a brown solution was filtered away from Mg salts. The filtrate was reduced *in vacuo* to 2 mL, then filtered away from more salts. The filtrate was reduced to dryness, and 2 mL toluene was used to rinse the yellow product, which was dried under vacuum (0.036 g).

## NMR Spectra.

 $^1\text{H}$  NMR ( $\text{C}_6\text{D}_6$ ): $^{13}\text{C}$  NMR ( $\text{C}_6\text{D}_6$ ):



Compound	7	8
Empirical formula	$C_{41}H_{40}Cl_2CrNP_2 \cdot 1.06(C_7H_8) \cdot 0.43(C_6H_6)$	$C_{16}H_{27}Cl_2CrN_2$
Formula weight	865.76	370.29
Temperature/K	100.0	100.0
Crystal system	monoclinic	orthorhombic
Space group	$P2_1/c$	$Pbca$
a/Å	13.1536(4)	16.7878(8)
b/Å	25.8833(7)	10.3585(5)
c/Å	13.1325(4)	20.2071(10)
$\alpha/^\circ$	90	90
$\beta/^\circ$	90.2970(10)	90
$\gamma/^\circ$	90	90
Volume/Å <sup>3</sup>	4471.0(2)	3513.9(3)
Z	4	8
$\rho_{calc}/cm^3$	1.286	1.400
$\mu/mm^{-1}$	4.147	0.951
F(000)	1815	1560
Crystal size/mm <sup>3</sup>	$0.13 \times 0.08 \times 0.07$	$0.217 \times 0.123 \times 0.103$
Radiation	CuK $\alpha$ ( $\lambda = 1.54178$ )	MoK $\alpha$ ( $\lambda = 0.71073$ )
2 $\Theta$ range for data collection/ $^\circ$	6.720 to 158.578	4.706 to 72.714
Index ranges	$-16 \leq h \leq 16, -32 \leq k \leq 32, -16 \leq l \leq 16$	$-27 \leq h \leq 27, -17 \leq k \leq 17, -33 \leq l \leq 33$
Reflections collected	84808	107601
Independent reflections	9445 [ $R_{int} = 0.0372,$ $R_{sigma} = 0.0205$ ]	8507 [ $R_{int} = 0.0512,$ $R_{sigma} = 0.0302$ ]
Data/restraints/parameters	9445/3/581	8507/0/194
Goodness-of-fit on F <sup>2</sup>	1.055	1.078
Final R indexes [ $I > 2\sigma(I)$ ]	$R_1 = 0.0536,$ $wR_2 = 0.0552$	$R_1 = 0.0381,$ $wR_2 = 0.0562$
Final R indexes [all data]	$R_1 = 0.1331,$ $wR_2 = 0.1341$	$R_1 = 0.0760,$ $wR_2 = 0.0814$
Largest diff. peak /hole / e Å <sup>-3</sup>	0.882/-0.629	0.611/-0.674

Compound	<b>9·THF</b>	<b>[11]<sub>2</sub></b>
Empirical formula	C <sub>22</sub> H <sub>35</sub> CrF <sub>6</sub> N <sub>2</sub> O <sub>7</sub> S <sub>2</sub>	C <sub>34</sub> H <sub>54</sub> Cr <sub>2</sub> F <sub>6</sub> N <sub>4</sub> O <sub>6</sub> S <sub>2</sub>
Formula weight	669.64	896.93
Temperature/K	100.01	99.97
Crystal system	monoclinic	monoclinic
Space group	<i>P</i> 2 <sub>1</sub> / <i>n</i>	<i>P</i> 2 <sub>1</sub> / <i>c</i>
a/Å	9.9599(5)	12.2477(6)
b/Å	22.4453(10)	17.3621(8)
c/Å	13.0487(6)	9.6451(4)
α/°	90	90
β/°	104.183(2)	98.743(2)
γ/°	90	90
Volume/Å <sup>3</sup>	2828.2(2)	2027.16(16)
Z	4	2
ρ <sub>calc</sub> /cm <sup>3</sup>	1.573	1.469
μ/mm <sup>-1</sup>	0.636	0.713
F(000)	1388	936
Crystal size/mm <sup>3</sup>	0.27 × 0.21 × 0.21	0.489 × 0.229 × 0.194
Radiation	MoKα (λ = 0.71073)	MoKα (λ = 0.71073)
2θ range for data collection/°	4.980 to 94.286	5.774 to 91.432
Index ranges	-20 ≤ h ≤ 20, -45 ≤ k ≤ 46, -26 ≤ l ≤ 26	-24 ≤ h ≤ 24, -34 ≤ k ≤ 34, -19 ≤ l ≤ 19
Reflections collected	224606	197527
Independent reflections	25792 [R <sub>int</sub> = 0.0444, R <sub>sigma</sub> = 0.0251]	17296 [R <sub>int</sub> = 0.0440, R <sub>sigma</sub> = 0.0194]
Data/restraints/parameters	25792/0/365	17296/0/248
Goodness-of-fit on F <sup>2</sup>	1.058	1.038
Final R indexes [I ≥ 2σ (I)]	R <sub>1</sub> = 0.0364, wR <sub>2</sub> = 0.0517	R <sub>1</sub> = 0.0291, wR <sub>2</sub> = 0.0375
Final R indexes [all data]	R <sub>1</sub> = 0.0837, wR <sub>2</sub> = 0.0895	R <sub>1</sub> = 0.0727, wR <sub>2</sub> = 0.0765
Largest diff. peak /hole / e Å <sup>-3</sup>	0.796/-0.790	1.099/-0.822

**References.**

(1) (a) Rucklidge, A. J.; McGuinness, D. S.; Tooze, R. P.; Slawin, A. M. Z.; Pelletier, J. D. A.; Hanton, M. J.; Webb, P. B. *Organometallics* **2007**, *26*, 2782. (b) Bowen, L. E.; Haddow, M. F.; Orpen, A. G.; Wass, D. F. *Dalton Transactions* **2007**, 1160. (c) McDyre, L. E.; Hamilton, T.; Murphy, D. M.; Cavell, K. J.; Gabrielli, W. F.; Hanton, M. J.; Smith, D. M. *Dalton Transactions* **2010**, *39*, 7792.

(2) (a) Cai, I. C.; Lipschutz, M. I.; Tilley, T. D. *Chemical Communications* **2014**, *50*, 13062. (b) Monillas, W. H.; Young, J. F.; Yap, G. P. A.; Theopold, K. H. *Dalton Transactions* **2013**, *42*, 9198. (c) Akturk, E. S.; Yap, G. P. A.; Theopold, K. H. *Chemical Communications* **2015**, *51*, 15402.

(3) (a) Wolf, R.; Ni, C.; Nguyen, T.; Brynda, M.; Long, G. J.; Sutton, A. D.; Fischer, R. C.; Fettinger, J. C.; Hellman, M.; Pu, L.; Power, P. P. *Inorganic Chemistry* **2007**, *46*, 11277. (b) Nguyen, T.; Sutton, A. D.; Brynda, M.; Fettinger, J. C.; Long, G. J.; Power, P. P. *Science* **2005**, *310*, 844.

(4) Wolf, R.; Brynda, M.; Ni, C.; Long, G. J.; Power, P. P. *Journal of the American Chemical Society* **2007**, *129*, 6076.

(5) Overett, M. J.; Blann, K.; Bollmann, A.; de Villiers, R.; Dixon, J. T.; Killian, E.; Maumela, M. C.; Maumela, H.; McGuinness, D. S.; Morgan, D. H.; Rucklidge, A.; Slawin, A. M. Z. *Journal of Molecular Catalysis A: Chemical* **2008**, *283*, 114.

(6) (a) Casitas, A.; Canta, M.; Solà, M.; Costas, M.; Ribas, X. *Journal of the American Chemical Society* **2011**, *133*, 19386. (b) van Beek, J. A. M.; van Koten, G.; Dekker, G. P. C. M.; Wissing, E.; Zoutberg, M. C.; Stam, C. H. *Journal of Organometallic Chemistry* **1990**, *394*, 659.

## Appendix 2

Soluble Cr Species for Ethylene Tetramerization in Methylcyclohexane, and  
High-Pressure Catalytic Trials of a Single-Component Precatalyst

**Abstract.**

A study of the effect of solvent on catalytic ethylene tetramerization was performed using two approaches. Firstly, a methylcyclohexane-soluble precatalyst and proton sources were used to generate a cationic activated species soluble in methylcyclohexane. However, it was determined that chlorobenzene was necessary for catalytic activity. Secondly, a variety of conditions were tested using the single-component precatalyst from Chapter 4. This showed that high 1-octene selectivity could be achieved at high ethylene pressures. However, the role of solvent was not fully deduced.

## Introduction.

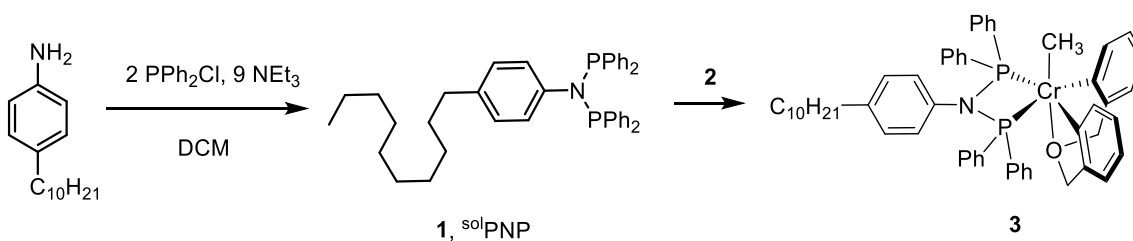
Since the well-defined chromium complexes reported in this thesis proved useful for the fundamental studies highlighted therein, they were evaluated under industrially-relevant catalytic conditions (solvent and pressure). Non-coordinating solvents must be used due to the electrophilicity of the Cr active species, as well as the likelihood of PNP displacement (e.g. by THF). Common solvents like toluene have been implicated in decomposition pathways *via* formation of Cr(I)-arene complexes.<sup>1</sup> One useful alkane solvent is methylcyclohexane (MeCy).<sup>2</sup> For our studies, methylcyclohexane was too nonpolar to dissolve the cationic Cr complexes (and some of the neutral ones). Therefore, chlorobenzene (PhCl) was used, which is reportedly less likely to facilitate decomposition to Cr(I)-arene species compared to toluene.<sup>1b</sup> Because of the preference by industrial researchers for MeCy, generating aliphatic-soluble versions of the Cr precatalysts was a goal of this work. Furthermore, MeCy coincidentally provides a very high-quality frozen glass, which is ideal for characterization of EPR solutions. This meant that spectroscopic and catalytic properties of a MeCy-soluble catalyst could be easily correlated, and compared to those in PhCl (see Chapter 5). To this end, a PNP ligand and a proton source each with long alkyl chains were synthesized in order to make a protonated species that could be dissolved in pure MeCy. Reactions showed that a soluble species was formed in MeCy, but catalytic activity was not achieved unless PhCl or toluene were used.

## Results and Discussion.

The commercially-available 4-(*n*-decyl)-aniline was successfully used to make the analog to <sup>101</sup>PNP. Now there is a long alkyl chain on the back of the ligand, instead of just a tolyl group. This approach was seen as complementary to other solubilizing PNP ligands, which

usually have substituents on the phosphine-aryl groups. The soluble PNP **1** (or <sup>sol</sup>PNP) was reacted with  $\text{Cr}((o\text{-C}_6\text{H}_4\text{CH}_2)_2\text{O})(\text{Me})(\text{THF})_2$  (**2**) to produce the analogous solubilizing PNP-ligated Cr precursor (<sup>sol</sup>PNP)Cr((*o*-C<sub>6</sub>H<sub>4</sub>CH<sub>2</sub>)<sub>2</sub>O)(Me) (**3**). In contrast to the original, <sup>tol</sup>PNP-ligated species (**4**) which was discussed in Chapter 2, **3** was found to be soluble in methylcyclohexane (MeCy). However, protonations with HBAR'<sub>4</sub> could not be performed directly in pure MeCy, since HBAR'<sub>4</sub> is not soluble. What is remarkable about industrial activation processes in MeCy is that very insoluble Cr precursors are used (e.g. CrCl<sub>3</sub>(THF)<sub>3</sub> or Cr(acac)<sub>3</sub>), but methylaluminoxane activation leads to a soluble species. So, activation and subsequent catalytic trials were performed with **3** using a variety of alkyl aluminum reagents (300 equiv.). All four examples (MMAO-3A, AlMe<sub>3</sub>, Al<sup>i</sup>Bu<sub>3</sub>, and AlMe<sub>2</sub>Cl) gave a homogeneous solution when mixed with **3** in pure MeCy, but only MMAO-3A gave catalytic activity (see Table 1).

**Scheme 1.** Synthesis of soluble PNP ligand **1** (<sup>sol</sup>PNP) and the corresponding Cr tris(hydrocarbyl) precatalyst **3**.



To achieve stoichiometric activation leading to catalysis in pure MeCy, suitable proton sources were sought. Two of these were utilized, one having a long alkyl chain on the proton source (**5**), the other having a long alkyl chain on both the proton source and the counteranion (**6**). A MeCy solution of **5** was added to a MeCy solution of **3**. Unfortunately, the resulting Cr product was insoluble and oiled out of solution. This highlighted the

necessity of using a soluble counteranion, which was achieved by making a perfluorinated borate monoanion derived from undecylimidazolate. A highly aliphatic amine was used as the proton source in conjunction with this anion (**6**). Therefore, all components of the targeted catalyst activation were equipped with long alkyl chains (# of carbons  $\geq 10$ ): the precatalyst, the proton source, and the counteranion. Indeed, protonation of **3** with **6** in pure MeCy gave a soluble species. However, pressurization with ethylene did not lead to catalytic production of oligomers, and precipitation was eventually observed from the solution. Tests of the **3/6** combination in other solvents showed that catalysis could be achieved in PhCl, although with very low productivity (see Table 2). In PhCl, **3** was successfully combined with HBAR'<sub>4</sub>. In PhCl and toluene, **4** was successfully combined with **6** in separate experiments. The conclusion is that the particular combination of the soluble precatalyst (**3**) and acid (**6**) was undesirable, even in PhCl. It could be that pure MeCy does not support efficient charge separation (but could only be tested for the **3/6** combination) and detrimental hydrophobic interactions occur (within the components of the Cr activated species) when PhCl is used for **3/6**. These reactions were performed in sealed tubes, leading to lower 1-octene selectivities

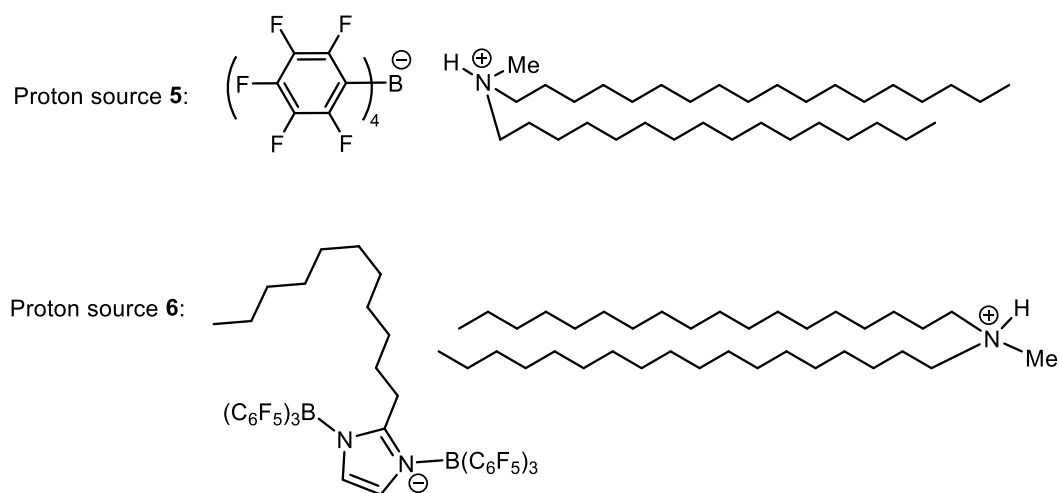


**Figure 1.** Soluble proton sources used in this study.

**Table 1.** Catalytic trials for ethylene oligomerization using **3** and alkyl aluminum-based activators.

Entry	Activator	Productivity (g/g Cr)	1-hexene (wt %)	1-octene (wt %)
1	300 MMAO-3A	720	21	76
2	300 AlMe <sub>3</sub>	< 3	--	--
3	300 Al( <sup>i</sup> Bu) <sub>3</sub>	7	--	--
4	300 AlMe <sub>2</sub> Cl	8	--	--
5	1 equiv. of <b>5</b>	--	--	--

Reaction vessel: glass Fisher-Porter bottle. [Cr] = 1 mM, Solvent: 7.5 mL PhCl. Pressure: 100 psig C<sub>2</sub>H<sub>4</sub>. Temperature: 25°C. Reaction time: 45 min.

**Table 2.** Catalytic trials for ethylene oligomerization using **3** or less-soluble **4**. Catalyst activation was performed by protonation using HBAR'<sub>4</sub> or **6**.

Entry	Cr/ H <sup>+</sup> source	Solvent	Productivity (g/g Cr)	Productivity (equiv. C <sub>2</sub> H <sub>4</sub> )	1-hexene (wt %)	1-octene (wt %)
1	<b>3/6</b>	PhCl	11	20	45	47
2	<b>3/6</b>	MeCy	--	--	--	--
3	<b>3/HBAR'</b> <sub>4</sub>	PhCl	370	690	46	40
4	<b>4/HBAR'</b> <sub>4</sub>	PhCl	553	1025	51	28
5	<b>4/6</b>	PhCl	180	330	41	49
6	<b>4/6</b>	toluene	22	40	78	22
7	<b>4/6</b>	benzene	--	--	--	--
8	<b>4/6</b>	Et <sub>2</sub> O	--	--	--	--

Reaction vessel: thick-walled, narrow glass Schlenk tube. [Cr] = 1 mM, Solvent: 7.5 mL PhCl. Initial pressure: ≈100 psig C<sub>2</sub>H<sub>4</sub>. Temperature: 25°C. Reaction time: 45 min.

than other trials reported in this thesis, especially when gas consumption was high (esp. Table 2, entry 4).

Attention was turned to evaluation of the effect of higher pressure, with the goal of achieving higher 1-octene selectivity and overall productivity. For this part of the study, the single-component catalyst highlighted in Chapter 4 was used (compound **7** in this appendix). Most catalytic trials (including in other chapters of this thesis) were run in glass reactors with a pressure rating of approximately 200 psig. To allow for even higher pressures, a steel reactor was used, lined with a glass insert, and equipped with a stirbar. Results of these catalytic trials are given in Table 3. Entries 1-3 indicate the effect of pressure increase from 100 to 600 psi. Notably, 1-octene selectivity increased (from 30% to 49%), but overall productivity did not change significantly. Although the results at 300 psi and 600 psi were similar, the remaining trials were conducted at the higher pressure. The effect of solvent was studied across a variety of the trials: fluorobenzene, and 4:1 mixtures of methylcyclohexane with various halogenated solvents were compared to chlorobenzene. There were no obvious trends, the likely combined effect of ethylene solubility and catalyst solubility differences make the analysis difficult.<sup>3</sup> In fluorobenzene, the catalyst concentration was varied (by changing the solvent volume). As shown in entries 4-6, higher concentration led to higher productivity, but lower 1-octene selectivity. The presence of trace solvent impurities could explain this result; entry 7 indicates no productivity at lower concentration in PhCl:MeCy solvent. The effect of temperature (0°C to 60°C) is shown in entries 8-10. It was found that 1-octene selectivity is higher at 25°C than 60°, attributable to the greater solubility of ethylene.<sup>3</sup> No productivity was seen at 0°C. The addition of alkyl aluminum reagents ( $\text{Al}^i\text{Bu}_3$  or MMAO) led to increased polymer production (entries 11-12).

Very high 1-octene selectivity was achieved by selecting the right solvent composition at 600 psi and 25°C. Fluorobenzene (entries 4 and 5), 4:1 MeCy:PhCl (entry 9), and 4:1 MeCy:difluorobenzene (entry 14) all gave  $\geq 79\%$  1-octene selectivity. Interestingly, 4:1 MeCy:fluorobenzene (entry 13) gave a low 1-octene selectivity (25%) despite the good selectivity in pure fluorobenzene. Again, this highlights the difficulty of disentangling the effects of gas/catalyst solubility and solvent impurity, not to mention the effects of solvent on catalyst initiation, propagation, or decomposition. Ultimately, most of the catalytic trials led to relatively low productivities ( $< 2000$  g/g Cr). It was suspected that lower chromium concentrations are important to avoid bimolecular decomposition pathways, but adventitious impurities (either in the solvent or the ethylene gas) shut down catalysis at those low concentrations (entry 4 and 7).

Because of the hypothesized competing effects of catalyst concentration (system impurities vs. bimolecular decomposition pathway), a scrubbing agent designed to scavenge system impurities was used. Although alkyl aluminum reagents are clearly not required to generate active ethylene tetramerization catalysts, they were targeted purely for their role as scavengers. Certain alkyl aluminums ( $\text{Al}^i\text{Bu}_3$  or MMAO) were already shown to be deleterious (Table 3, entries 11-12). Other studies successfully employed bulky ethyl aluminum bis(aryloxy) **8** for scavenging purposes.<sup>4</sup> The results of catalytic trials using **8** are given in Table 4. Higher productivities are obtained, suggestive of a benefit of using a scavenger. Notably, the Cr concentrations were lower even than those used in the previous trial. Despite this promise, the relatively high polyethylene production dissuaded further investigation.

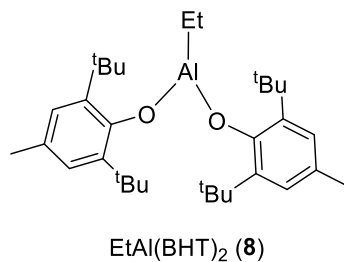


**Figure 2.** Bulky aluminum aryloxy compound, used as a scavenger.

**Table 3.** Catalytic trials for ethylene oligomerization using **7**.

Entry	Pressure (psi)	Solvent	[7] (mM)	Additive	Productivity (g/g Cr)	PE (wt %)	1-hexene (wt %)	1-octene (wt %)
1	100	PhCl	1.2	–	1000	0	58	30
2	300	PhCl	1.2	–	1400	2.4	45	45
3	600	PhCl	1.2	–	1300	4.2	42	49
4	600	PhF	0.4	–	250	n.d.	≈13	≈84
5	600	PhF	1.2	–	560	3.0	9	82
6	600	PhF	3.6	–	1300	n.d.	≈27	≈65
7	600	PhCl:MeCy <sup>c</sup>	0.4	–	–	–	–	–
8 <sup>a</sup>	600	PhCl:MeCy <sup>c</sup>	1.2	–	–	–	–	–
9	600	PhCl:MeCy <sup>c</sup>	1.2	–	700	6.3	8	79
10 <sup>b</sup>	600	PhCl:MeCy <sup>c</sup>	1.2	–	1600	n.d.	≈24	≈69
11	600	PhCl:MeCy <sup>c</sup>	1.2	50 Al <sup>i</sup> Bu <sub>3</sub>	1200	73	8	15
12	600	PhCl:MeCy <sup>c</sup>	1.2	50 MMAO	2500	14	12	65
13	600	PhF:MeCy <sup>d</sup>	1.2	–	1700	n.d.	≈70	≈25
14	600	o-F <sub>2</sub> C <sub>6</sub> H <sub>4</sub> :MeCy <sup>e</sup>	1.2	–	1600	0.8	9	83

Reaction vessel: Steel reactor. Reaction temperature: 25°C, except where noted otherwise. Reaction time: 45 min. <sup>a</sup>Reaction temperature: 0°C. <sup>b</sup>Reaction temperature: 60°C. <sup>c</sup>1:4 v/v PhCl:MeCy ratio. <sup>d</sup>1:4 v/v PhF:MeCy ratio. <sup>e</sup>1:4 v/v o-F<sub>2</sub>C<sub>6</sub>H<sub>4</sub>:MeCy ratio.

**Table 4.** Catalytic trials for ethylene oligomerization using **7** and **8** as a scavenger.

Entry	[ <b>7</b> ] (mM)	Equiv. <b>8</b>	Productivity (g/g Cr)	PE (wt %)	1-hexene (wt %)	1-octene (wt %)
1	0.12	100	6800	11	8	76
2	0.12	300	3800	44	7	47
3	0.05	300	7900	23	11	64

Reaction vessel: Steel reactor. Reaction temperature: 25°C, except where noted otherwise. Reaction time: 45 min. Solvent: 1:4 v/v PhCl:MeCy ratio. Pressure: 600 psig C<sub>2</sub>H<sub>4</sub>.

### Conclusion.

A fully methylcyclohexane-soluble activated Cr species was developed by incorporation of a long alkyl chain into the PNP ligand, ammonium acid, and non-coordinating anion. However, despite the successful catalysis for ethylene tetramerization observed using this combination in chlorobenzene, there was no activity in methylcyclohexane. This indicates the important role of solvent beyond simply that of solubility. Notably, MMAO activation of the same Cr precatalyst gave good catalytic productivity.

High pressure ethylene tetramerization trials using a single-component catalyst species showed that 1-octene selectivity (up to 83 wt%) could be achieved at 600 psi of ethylene, and by using solvents other than chlorobenzene. The role of solvent in this study was not fully rationalized, but the existence of trace system impurities was suggested due to the successful use of a bulky alkyl aluminum scavenging reagent.

## Experimental.

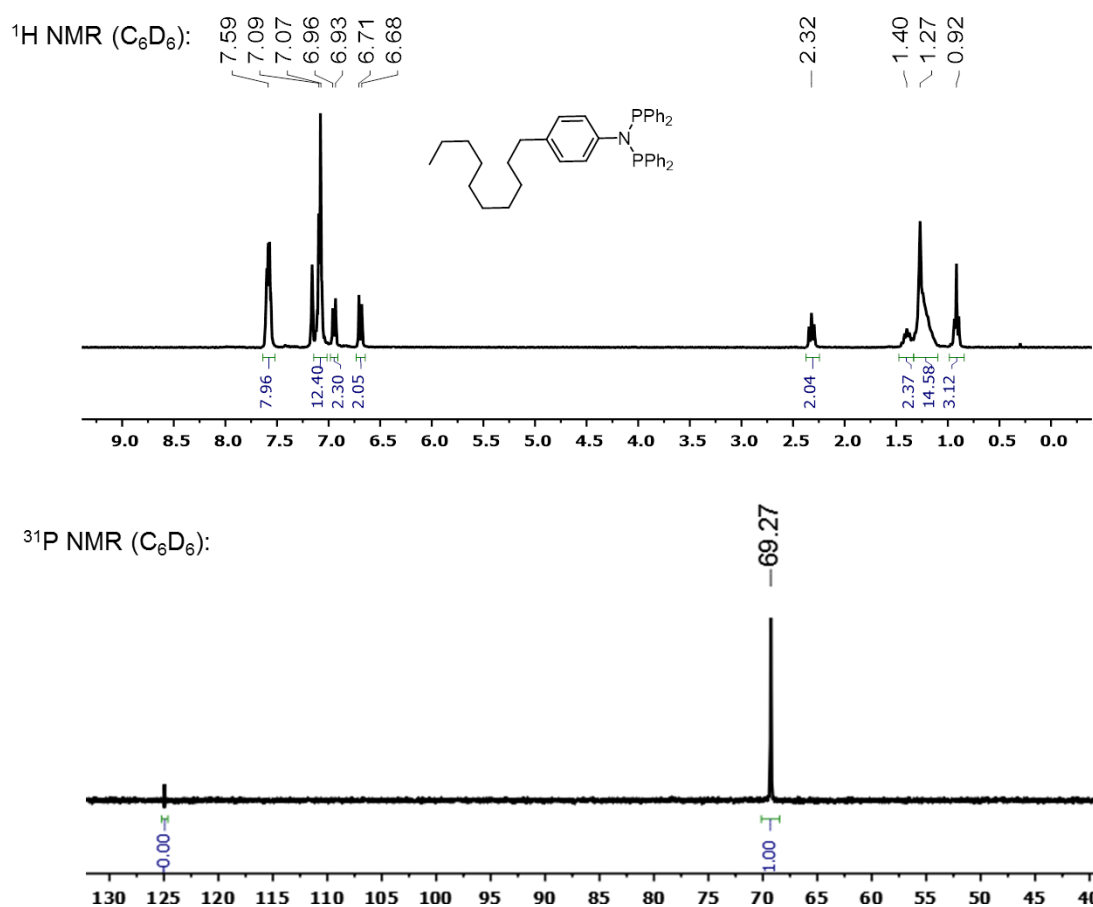
**Synthesis of 4-(n-decyl)(C<sub>6</sub>H<sub>4</sub>)N(PPh<sub>2</sub>)<sub>2</sub>. (1)** To a flask under N<sub>2</sub>, NEt<sub>3</sub> (8.5 mL) and DCM (10 mL) were added. This was cooled to 0°C, then Ph<sub>2</sub>PCL (3.0 mL) was added via syringe to the stirring solution. After the solution was stirred for 30 min, 4-(n-decyl)-aniline (1.94 g) was added via syringe (it was gently warmed to melt). After 30 minutes at 0°C, the suspension was warmed to RT, then stirred for 16 hr more. It was then reduced to dryness *in vacuo*, and 40 mL C<sub>6</sub>H<sub>6</sub> was used to rinse an orange solution from white ammonium salts. The filtrate was reduced *in vacuo* to 4.5 g amber-colored oil. To obtain pure product, 0.670 mg of the oil was dissolved in 5 mL hexanes, and run through an alumina plug, rinsing with 15 mL hexanes. This was reduced *in vacuo* to 0.483 g of a golden oil (9.6% overall yield). <sup>1</sup>H NMR (300.8 MHz, 27°C, C<sub>6</sub>D<sub>6</sub>): δ 7.59 (m, 8H), 7.08 (m, 12H), 6.95 (d, J<sub>HH</sub> = 8.3 Hz, 2H), 6.69 (d, J<sub>HH</sub> = 8.3 Hz, 2H), 2.32 (t, J<sub>HH</sub> = 7.7 Hz, 2H), 1.40 (m, 2H), 1.27 (m, 14H), 0.92 (t, J<sub>HH</sub> = 6.7 Hz, 3H). <sup>31</sup>P NMR (121.5 MHz, 27°C, C<sub>6</sub>D<sub>6</sub>): δ 69.27.

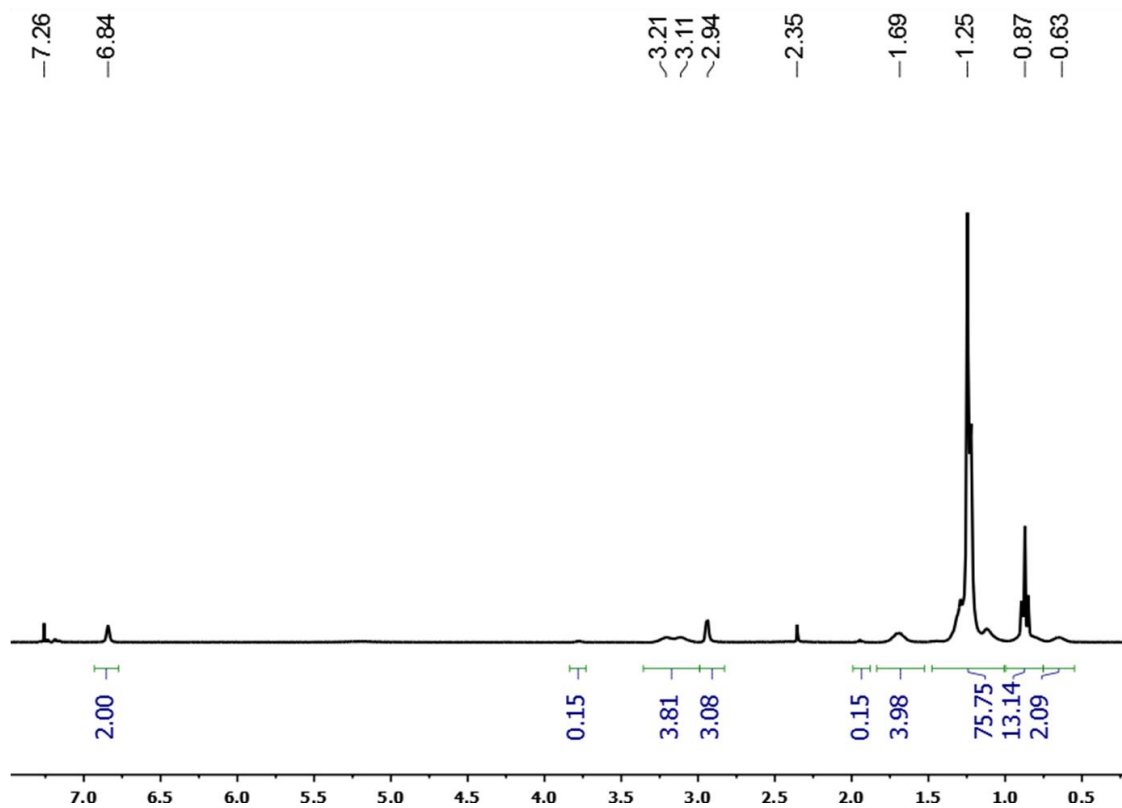
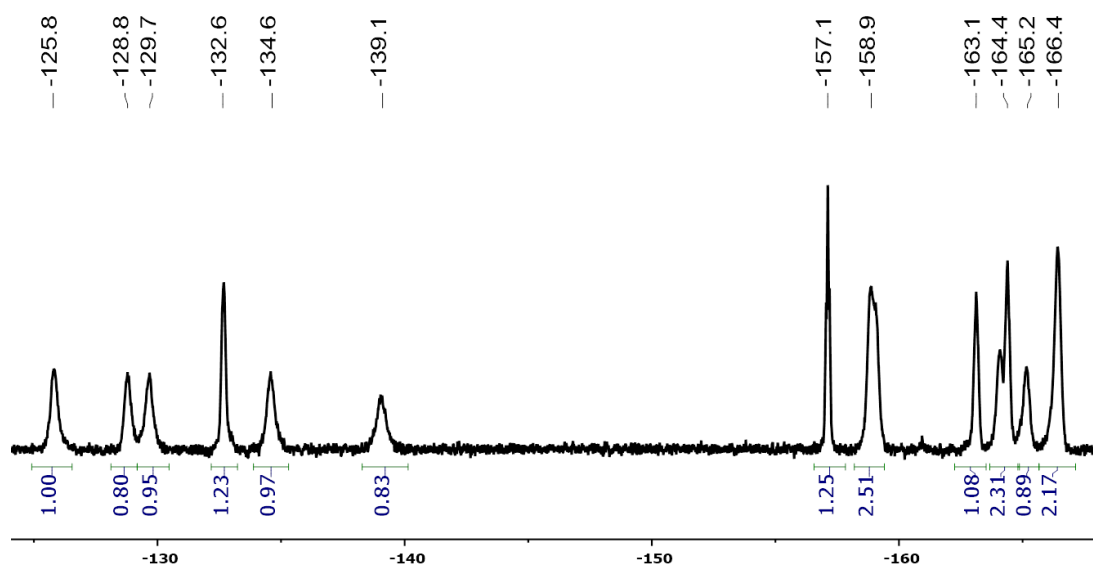
**Synthesis of (<sup>sol</sup>PNP)Cr((*o*-C<sub>6</sub>H<sub>4</sub>CH<sub>2</sub>)<sub>2</sub>O)(Me). (3)** A solution of 4-(n-decyl)(C<sub>6</sub>H<sub>4</sub>)N(PPh<sub>2</sub>)<sub>2</sub> (0.074 g, 0.12 mmol) in 10 mL hexanes was added to a vial containing solid **2** (0.050 g, 0.12 mmol). After 1 hr of stirring at RT, a brown solution containing brown solids was obtained. Then, 1 mL C<sub>6</sub>H<sub>6</sub> was added and the brown suspension was reduced to dryness *in vacuo*, yielding a brown solid (0.102 g, 95% yield).

**Synthesis of 6.** A modification of the procedure(s) reported for related compounds was used.<sup>5</sup> Asymmetry in the <sup>19</sup>F NMR spectrum is attributed to hindered rotation of the fluorinated aryls about the C-B bond. <sup>1</sup>H NMR (299.8 MHz, 25°C, CDCl<sub>3</sub>): δ 6.84 (s, 2H), 3.16 (m, 4H), 2.94 (s, 3H), 1.69, (m, 4H), 1.25 (m, 75H), 0.87 (m, 12H), 0.63 (m, 2H). <sup>19</sup>F NMR (282.3 MHz, 27°C, CDCl<sub>3</sub>): δ -125.8 (s, 1F), -128.8 (s, 1F), -129.7 (s, 1F), -132.6 (s, 1F),

-134.6 (s, 1F), -139.1 (s, 1F), -157.1 (s, 1F), -158.9 (2F), -163.1 (s, 1F), -164.4 (2F), -165.2 (s, 1F), -166.4 (2F).

### NMR Spectra.



$^1\text{H}$  NMR for **6** ( $\text{CDCl}_3$ ): $^{19}\text{F}$  NMR for **6** ( $\text{CDCl}_3$ ):

**References.**

- (1) (a) McDyre, L.; Carter, E.; Cavell, K. J.; Murphy, D. M.; Platts, J. A.; Sampford, K.; Ward, B. D.; Gabrielli, W. F.; Hanton, M. J.; Smith, D. M. *Organometallics* **2011**, *30*, 4505. (b) Rabeah, J.; Bauer, M.; Baumann, W.; McConnell, A. E. C.; Gabrielli, W. F.; Webb, P. B.; Selent, D.; Brückner, A. *ACS Catalysis* **2012**, *3*, 95.
- (2) Kim, E. H.; Lee, H. M.; Jeong, M. S.; Ryu, J. Y.; Lee, J.; Lee, B. Y. *ACS Omega* **2017**, *2*, 765.
- (3) Kuhlmann, S.; Dixon, J. T.; Haumann, M.; Morgan, D. H.; Ofili, J.; Spuhl, O.; Taccardi, N.; Wasserscheid, P. *Advanced Synthesis & Catalysis* **2006**, *348*, 1200.
- (4) (a) Stapleton, R. A.; Al-Humydi, A.; Chai, J.; Galan, B. R.; Collins, S. *Organometallics* **2006**, *25*, 5083. (b) Stapleton, R. A.; Galan, B. R.; Collins, S.; Simons, R. S.; Garrison, J. C.; Youngs, W. J. *Journal of the American Chemical Society* **2003**, *125*, 9246.
- (5) LaPointe, R. E.; Roof, G. R.; Abboud, K. A.; Klosin, J. *Journal of the American Chemical Society* **2000**, *122*, 9560.

## Appendix 3

Deposition of a Bipyridine Re Carbonyl Complex onto Electrodes for CO<sub>2</sub>

Reduction

**Abstract.**

A bipyridine Re carbonyl complex was synthesized, containing a cationic pyridinium group on the bipyridine ligand. This facilitated deposition of the Re coordination complex onto glassy carbon or copper electrodes following electroreduction and C-C coupling. This electrode functionalization method led to CO<sub>2</sub> electrocatalysis on glassy carbon from the deposited material. On copper, current diminishment suggested that the film inhibited the intrinsic catalytic activity of the electrode.

## Introduction.

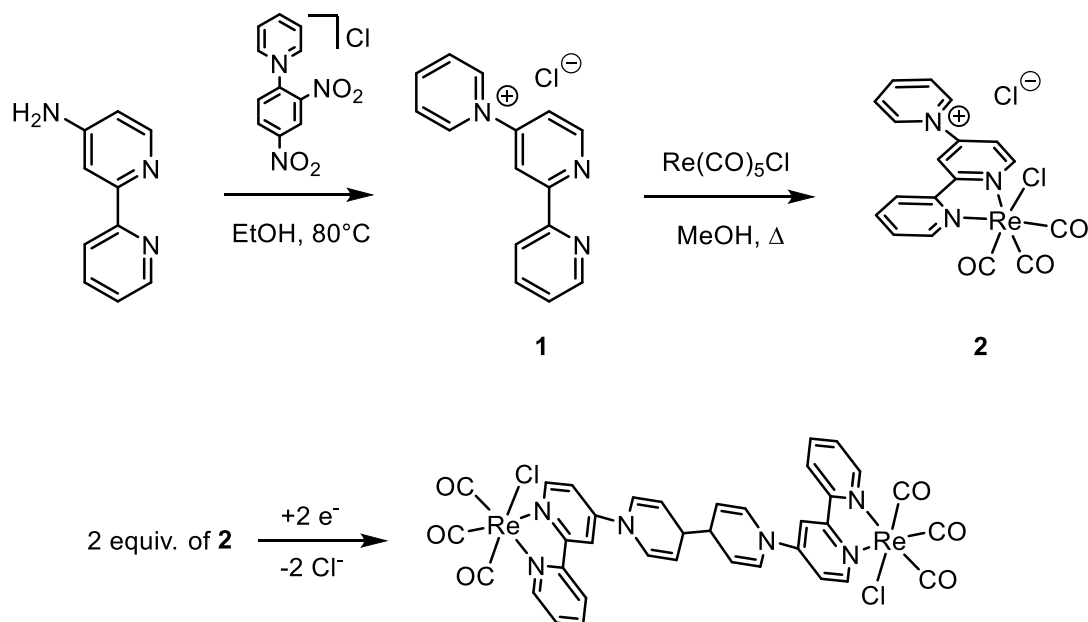
The conversion of CO<sub>2</sub> to reduced carbon products (e.g. alkanes, alkenes) is promising for the sustainable synthesis of higher-density fuels and chemicals. Especially when coupled to renewable energy sources, CO<sub>2</sub> electroreduction by copper is particularly attractive because of the high selectivity for two- and three-carbon products (esp. ethylene).<sup>1</sup> Many studies have targeted enhanced catalytic performance by modifying the copper electrode.<sup>2</sup> An important mechanistic detail of the copper electrocatalysts is that carbon monoxide is an intermediate to C-C coupled products.<sup>3</sup> One way to improve catalysis is to incorporate co-catalysts that can perform CO<sub>2</sub> to CO reduction at lower overpotentials than copper.<sup>4</sup>

Functionalization of inert electrodes with molecular CO<sub>2</sub> electroreduction catalysts is a highly explored field.<sup>5</sup> The functionalization of catalytically-active electrodes with molecular catalysts (e.g. making a tandem catalytic system) is much less common. Recently, it was shown that functionalization of copper electrodes with simple organics could dramatically affect product selectivity.<sup>6</sup> This project targeted the functionalization of copper with known molecular catalysts for the conversion of CO<sub>2</sub> to CO (bipyridine rhenium carbonyls). This strategy is attractive because electrodeposition could occur under the same conditions as catalysis, removing the need for pre-functionalization or other fabrication steps.

## Results and Discussion.

The Zincke salt reaction<sup>7</sup> of 4-aminobipyridine proved useful for the synthesis of **1**, which was then metallated with Re(CO)<sub>5</sub>Cl to generate the Re bipyridine complex **2**. This was soluble in water and CO<sub>2</sub>-saturated bicarbonate buffer, making it directly useful for the catalytic trials.

**Scheme 1.** Top: synthesis of **1**, and subsequent metalation to form **2**. Bottom: proposed electroreduction, followed by dimerization of **2** to give a neutral dimer that deposits on the electrode as a film.



Electrochemical analysis of **2** was performed by cyclic voltammetry (CV) using a glassy carbon disc electrode. Upon scanning reductively, a feature at  $-0.77$  V attributable to pyridinium reduction was observed. Dimerization by C-C coupling of the organic radical is expected to occur at this point. In  $\text{Na}_2\text{SO}_4$  electrolyte (no  $\text{CO}_2$ ), Re complex reduction occurs with several features observable between  $-1.1$  and  $-1.5$  V. The same is true for  $\text{CO}_2$ -saturated bicarbonate electrolyte (see Figure 1). Onset of electrocatalysis occurs at approximately  $-1.6$  V (vs. Ag/AgCl) in both cases. However, the current is significantly higher in the presence of  $\text{CO}_2$ , confirming that  $\text{CO}_2$  electrocatalysis occurs.

Repeated CV cycles lead to eventual diminishment of the catalytic current (see Figure 2). This is attributable to passivation of the glassy carbon electrode by additional layers of deposited material. Attempted bulk electrolysis at  $-1.7$  V vs. Ag/AgCl using **2** in  $\text{CO}_2$ -

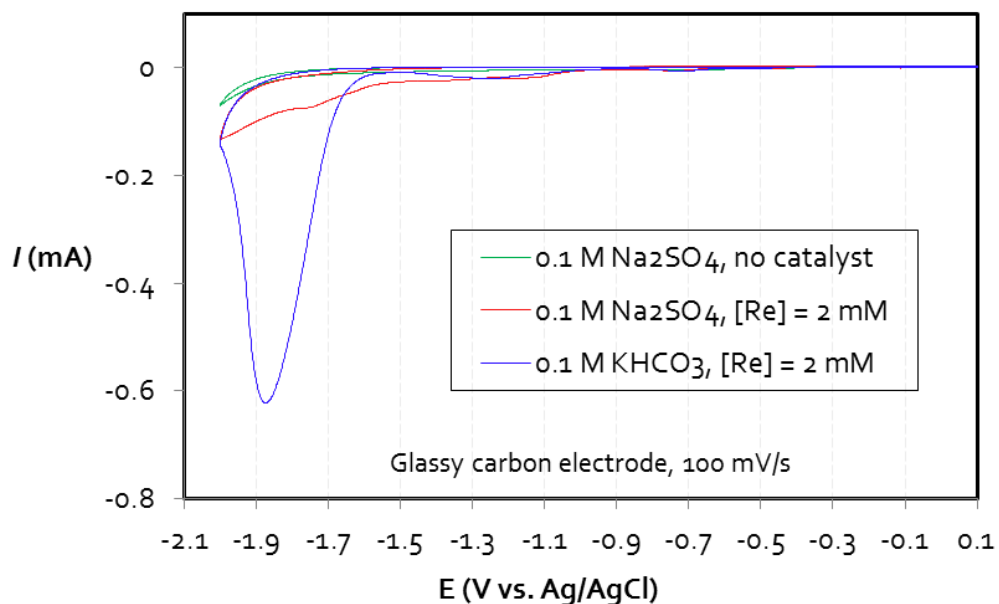


**Figure 1.** Cyclic voltammetry of blank aqueous  $\text{Na}_2\text{SO}_4$  under  $\text{N}_2$  (green trace), compound **2** in aqueous  $\text{Na}_2\text{SO}_4$  under  $\text{N}_2$  (red trace), and compound **2** in  $\text{CO}_2$ -saturated  $\text{KHCO}_3$  (blue trace).

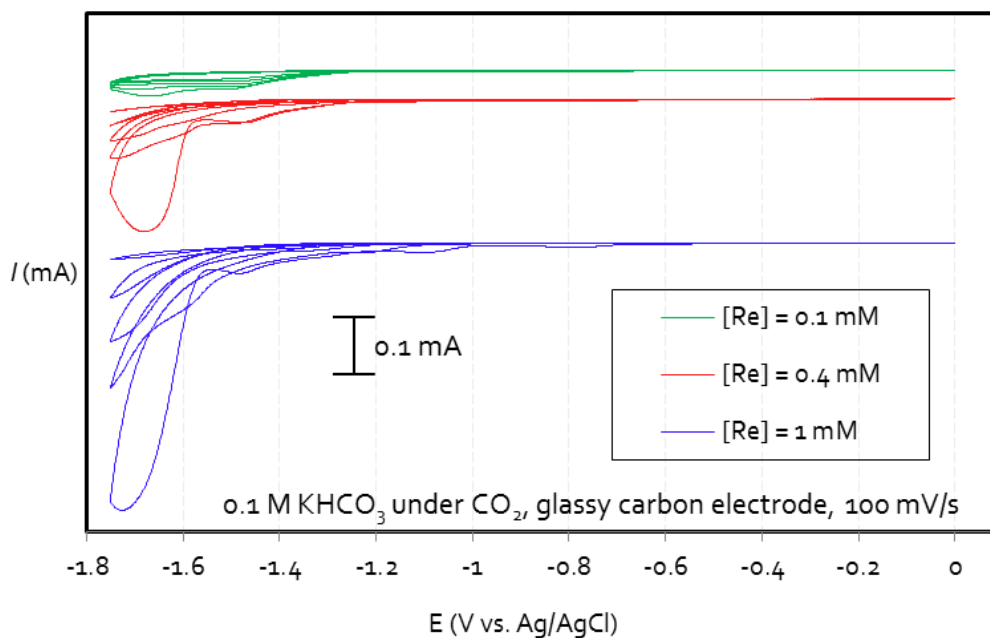


**Figure 2.** Cyclic voltammetry of compound **2** in  $\text{CO}_2$ -saturated  $\text{KHCO}_3$  at three different concentrations using a glassy carbon electrode. Over five consecutive scans, current diminished in each experiment.

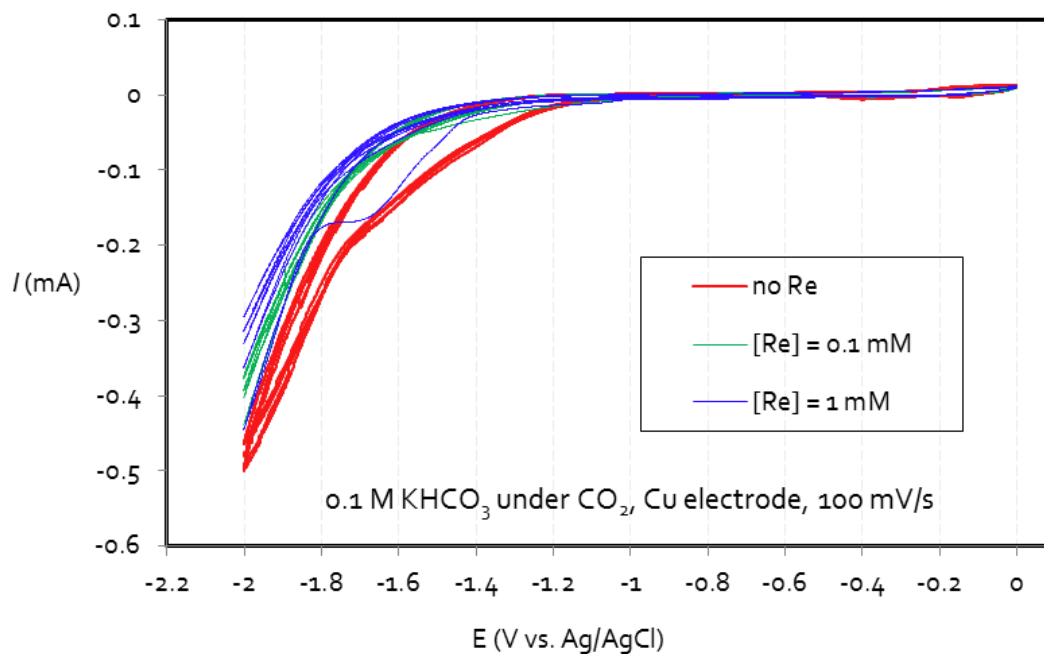


**Figure 3.** Cyclic voltammetry of compound **2** (blue and green traces) in  $\text{CO}_2$ -saturated  $\text{KHCO}_3$  at two different concentrations using a copper electrode. Catalytic onset potential (attributable to the copper electrode) shifted positive in the absence of **2** (red trace).

saturated  $\text{KHCO}_3$  electrolyte led to rapid diminishment of current, attributable to this passivation effect. By GC,  $\text{H}_2$  and traces of CO were observed.

Cyclic voltammetry of solutions of **2** using a copper electrode led to the shift of the onset potential of catalysis (intrinsic to the copper itself) by about 300 mV more negative. This is a deleterious effect, the reason for which is not certain. Bulk electrolysis at -1.7 V vs. Ag/AgCl using **2** in  $\text{CO}_2$ -saturated  $\text{KHCO}_3$  electrolyte led to primarily  $\text{H}_2$  formation (80% Faradaic efficiency) and low ethylene production (3% Faradaic efficiency). This is in comparison to a blank trial (no **2** in solution) where  $\text{H}_2$  Faradaic efficiency was 56%, and ethylene Faradaic efficiency was 12%. Furthermore, total current density (over 1 hr) dropped from  $5.3 \text{ mA/cm}^2$  to  $2.3 \text{ mA/cm}^2$ . After bulk electrolysis, there was a visible yellow film on

the copper electrode, which was not soluble in water. Together, this was consistent with deposition of a film derived from **2**, but which poisoned copper catalytic sites selective for ethylene, relative to those that generate H<sub>2</sub>.

### **Conclusion.**

A molecular CO<sub>2</sub> electroreduction catalyst based on Re was appended to a pyridinium group. This was designed to deposit as a neutral film following reduction and dimerization via C-C coupling. This complex was used for CO<sub>2</sub> reduction, assessed by cyclic voltammetry, but the resulting film was either not stable or passivated the electrode, making bulk electrolysis ineffective.

## Experimental.

**Materials.** Copper foil (99.999% Cu, 25 mm × 50 mm × 1 mm) and potassium carbonate (99.995%), were purchased from Sigma-Aldrich. Carbon rods (99.999% C) were purchased from Strem Chemicals. Water was purified by a Nanopure Analytical Ultrapure Water System (Thermo Scientific) or a Milli-Q Advantage A10 Water Purification System (Millipore) with specific resistance of 18.2 MΩ·cm at 25 °C. Natural abundance carbon dioxide (Research grade) was purchased from Airgas. Upon receiving, copper foil was polished to a mirror-like finish using alumina pastes (0.05 μm, Buehler) followed by rinsing and sonicating in water to remove residual alumina. Before each experiment, the copper foil was electropolished in a 85% phosphoric acid bath, +2.1 V versus a carbon rod counter electrode was applied to the Cu foil for 5 minutes and the foil was subsequently washed with ultra-pure water and dried under a stream of nitrogen gas. Potassium bicarbonate electrolytes (KHCO<sub>3</sub>(aq), 0.1 M) were prepared by sparging an aqueous solution of potassium carbonate (K<sub>2</sub>CO<sub>3</sub>(aq), 0.05 M) with CO<sub>2</sub> for at least 1 hour prior to electrolysis. Such process converts K<sub>2</sub>CO<sub>3</sub> into KHCO<sub>3</sub> and saturates the electrolyte solution with CO<sub>2</sub>.

**Synthesis of Compound 1.** To a 20 mL EtOH solution of 4-aminobipyridine (0.760 g, 4.44 mmol), Zincke salt was added (1.19 g, 4.74 mmol) The dark red suspension was heated to 80°C for 84 hours, then cooled to RT. The solution was filtered through a frit, using 10 mL EtOH to rinse. The filtrate was reduced *in vacuo* to dryness. It was rinsed into a separatory funnel using 40 mL H<sub>2</sub>O and 20 mL CHCl<sub>3</sub>. The aqueous layer was rinsed with 2 x 20 ml CHCl<sub>3</sub>, then reduced *in vacuo* to 1.2 g amber oil and brown solid. This was dissolved in 6 mL of warm EtOH, and 50 mL CHCl<sub>3</sub> was added, causing colorless crystals to form after several minutes. The supernatant was filtered, then reduced to dryness *in vacuo*. The orange tacky solid was dissolved in 5 mL warm EtOH, and 140 mL CHCl<sub>3</sub> was added; again,

crystals formed and the supernatant was collected and dried. This was dissolved in 6 mL warm EtOH and 30 mL Et<sub>2</sub>O was added (to remove a different impurity). Orange solids precipitated from the yellow solution, which was collected by filtration and dried to obtain 380 mg. The Et<sub>2</sub>O precipitation process was repeated, and the solution reduced to dryness to obtain pure **1** as a pale powder (0.334 g, 1.18 mmol, 25% yield). <sup>1</sup>H NMR (399.8 MHz, 25°C, CD<sub>3</sub>OD): δ 9.44 (d, J<sub>HH</sub> = 5.8 Hz, 2H), 9.06 (d, J<sub>HH</sub> = 5.5 Hz, 1H), 8.90 (t, J<sub>HH</sub> = 7.8 Hz, 1H), 8.86 (d, J<sub>HH</sub> = 1.7 Hz, 1H), 8.74 (d, J<sub>HH</sub> = 4.3 Hz, 1H), 8.56 (d, J<sub>HH</sub> = 7.8 Hz, 1H), 8.38 (t, J<sub>HH</sub> = 7.8 Hz, 2H), 8.02 (dt, J<sub>HH</sub> = 7.8, 1.4 Hz, 1H), 7.92 (dd, J<sub>HH</sub> = 5.5, 2.1 Hz, 1H), 7.53 (dd, J<sub>HH</sub> = 7.8, 5.5 Hz, 1H). <sup>13</sup>C NMR (100.6 MHz, 25°C, CD<sub>3</sub>OD): δ 160.3, 155.3, 153.0, 152.0, 150.7, 149.3, 145.9, 138.9, 129.8, 126.4, 122.9, 119.9, 117.2.

**Synthesis of Compound 2.** An 8 mL MeOH solution of **1** (0.066 g, 0.24 mmol) was added to dry Re(CO)<sub>5</sub>Cl (0.082 g, 0.23 mmol). The pale suspension of white solids was heated to 60°C for 5 hours, then the resulting orange solution was cooled to RT, and reduced to dryness *in vacuo*. The residue was mostly dissolved in 4 mL warm EtOH, which was decanted from insoluble solids. Small portions of Et<sub>2</sub>O were added (4 mL total) to gradually precipitate pale yellow crystals of **2**. To the mixture, 2 mL Et<sub>2</sub>O was further added, causing more crystallization. The supernatant was decanted, and the crystals washed with 3 x 1 mL of 1:1 EtOH:Et<sub>2</sub>O. The yellow crystals were dried *in vacuo* (0.089 g, 0.15 mmol, 65% yield). <sup>1</sup>H NMR (399.8 MHz, 25°C, CD<sub>3</sub>OD): δ 9.55 (d, J<sub>HH</sub> = 6.0 Hz, 2H), 9.40 (d, J<sub>HH</sub> = 6.0 Hz, 1H), 9.26 (d, J<sub>HH</sub> = 1.7 Hz, 1H), 9.13 (d, J<sub>HH</sub> = 5.4 Hz, 1H), 8.98 (t, J<sub>HH</sub> = 7.9 Hz, 1H), 8.80 (d, J<sub>HH</sub> = 7.9 Hz, 1H), 8.46 (t, J<sub>HH</sub> = 7.0 Hz, 2H), 8.35 (t, J<sub>HH</sub> = 7.9, 1H), 8.23 (dd, J<sub>HH</sub> = 6.4, 1.7 Hz, 1H), 7.81 (t, J<sub>HH</sub> = 6.4 Hz, 1H). <sup>13</sup>C NMR (100.6 MHz, 25°C, CD<sub>3</sub>OD): δ 198.1, 197.9, 189.8, 160.3, 156.6, 155.9, 154.6, 152.6, 150.3, 146.1, 141.5, 129.9, 129.8, 126.4, 123.7, 121.3.





**References.**

- (1) (a) Gattrell, M.; Gupta, N.; Co, A. *Journal of Electroanalytical Chemistry* **2006**, *594*, 1. (b) Yoshio, H.; Katsuhei, K.; Akira, M.; Shin, S. *Chemistry Letters* **1986**, *15*, 897. (c) Nitopi, S.; Bertheussen, E.; Scott, S. B.; Liu, X.; Engstfeld, A. K.; Horch, S.; Seger, B.; Stephens, I. E. L.; Chan, K.; Hahn, C.; Nørskov, J. K.; Jaramillo, T. F.; Chorkendorff, I. *Chemical Reviews* **2019**, *119*, 7610.
- (2) (a) Higgins, D.; Hahn, C.; Xiang, C.; Jaramillo, T. F.; Weber, A. Z. *ACS Energy Letters* **2019**, *4*, 317. (b) Mistry, H.; Varela, A. S.; Kühn, S.; Strasser, P.; Cuenya, B. R. *Nature Reviews Materials* **2016**, *1*, 16009.
- (3) (a) Kortlever, R.; Shen, J.; Schouten, K. J. P.; Calle-Vallejo, F.; Koper, M. T. M. *The Journal of Physical Chemistry Letters* **2015**, *6*, 4073. (b) Wang, L.; Nitopi, S. A.; Bertheussen, E.; Orazov, M.; Morales-Guio, C. G.; Liu, X.; Higgins, D. C.; Chan, K.; Nørskov, J. K.; Hahn, C.; Jaramillo, T. F. *ACS Catalysis* **2018**, *8*, 7445.
- (4) (a) Lum, Y.; Ager, J. W. *Energy & Environmental Science* **2018**, *11*, 2935. (b) Morales-Guio, C. G.; Cave, E. R.; Nitopi, S. A.; Feaster, J. T.; Wang, L.; Kuhl, K. P.; Jackson, A.; Johnson, N. C.; Abram, D. N.; Hatsukade, T.; Hahn, C.; Jaramillo, T. F. *Nature Catalysis* **2018**, *1*, 764.
- (5) (a) Orchanian, N. M.; Hong, L. E.; Skrainka, J. A.; Esterhuizen, J. A.; Popov, D. A.; Marinescu, S. C. *ACS Applied Energy Materials* **2018**. (b) Rotundo, L.; Filippi, J.; Gobetto, R.; Miller, H. A.; Rocca, R.; Nervi, C.; Vizza, F. *Chemical Communications* **2019**, *55*, 775. (c) Sun, C.; Gobetto, R.; Nervi, C. *New Journal of Chemistry* **2016**, *40*, 5656. (d) Willkomm, J.; Bertin, E.; Atwa, M.; Lin, J.-B.; Birss, V.; Piers, W. E. *ACS Applied Energy Materials* **2019**, *2*, 2414.
- (6) Han, Z.; Kortlever, R.; Chen, H.-Y.; Peters, J. C.; Agapie, T. *ACS Central Science* **2017**, *3*, 853.

(7) Zeghib, N.; Thelliere, P.; Rivard, M.; Martens, T. *The Journal of Organic Chemistry* **2016**, *81*, 3256.

## Appendix 4

Miscellaneous X-Ray Crystal Structures

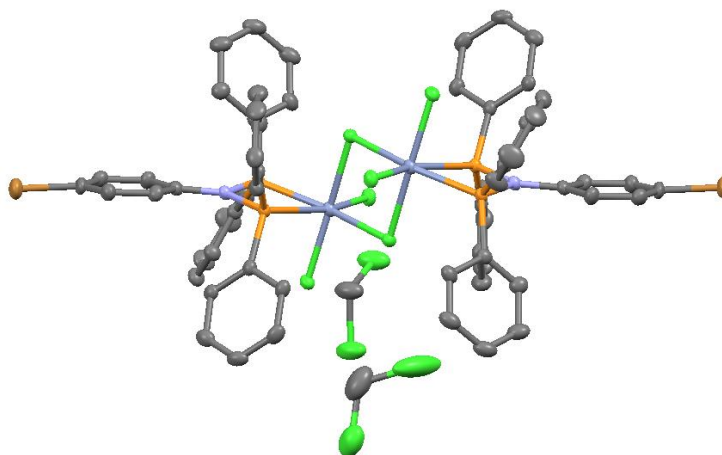


**Figure 1.** Dimeric Cr(III) structure  $[(\text{BrC}_6\text{H}_4\text{N}(\text{PPh}_2)_2\text{CrCl}_3)_2]$  with DCM solvent molecules shown.

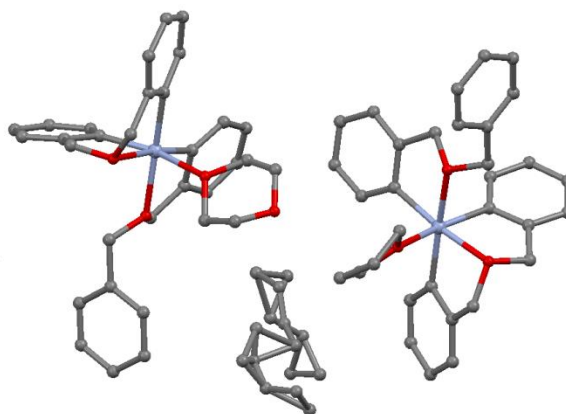


**Figure 2.** Cr(III) structures derived from protonolysis of bis(aryl)ether ligand arm (probably due to traces of water) and ligand scrambling, with dioxane or THF bound. Disordered solvent shown.

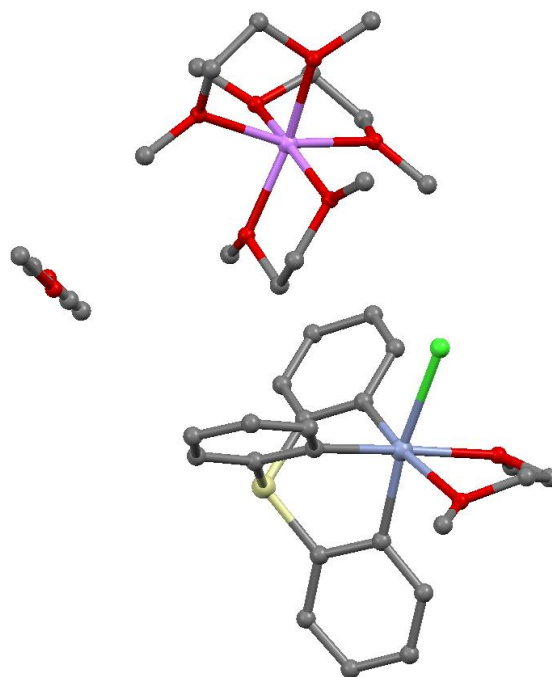


**Figure 3.** Cr(III) triarylsilane (based on the Si-H version) with dimethoxyethane (dme) bound, and outer-sphere lithium cation, coordinated to dme.

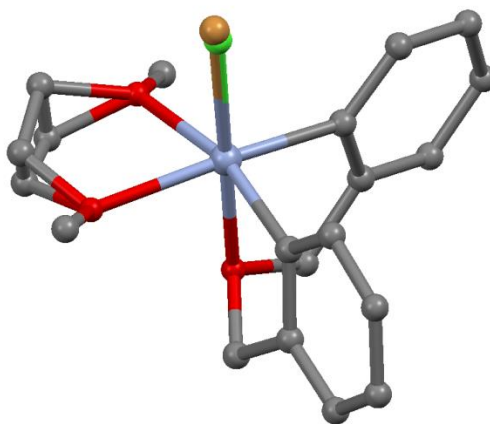


**Figure 4.** Cr(III) halide (Cl/Br) bis(aryl)ether, with dme bound (disorder shown).

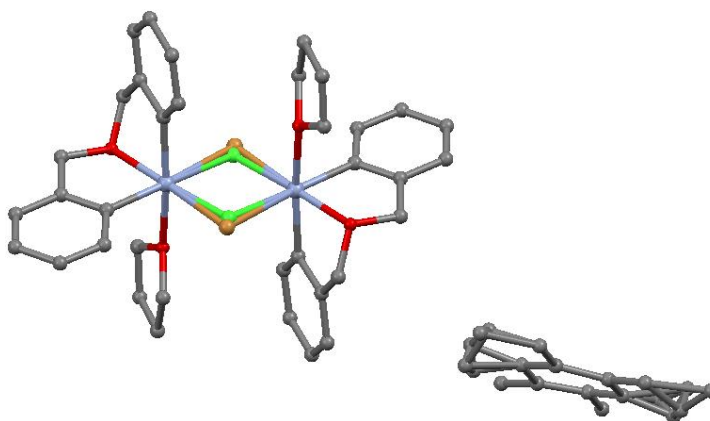


**Figure 5.** Dimeric, halide bridged (Cl/Br) Cr(III) bis(aryl)ether structure. Disordered toluene solvent channel shown.

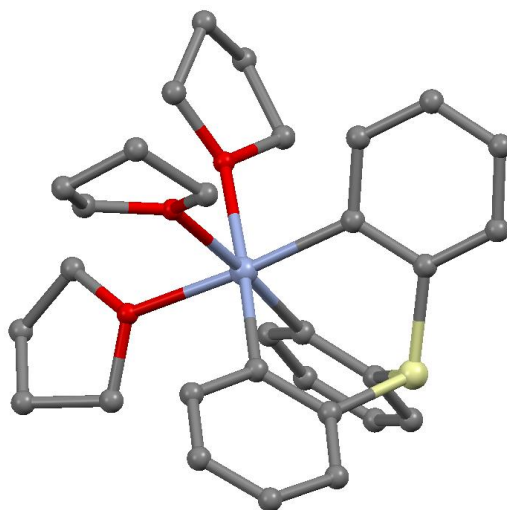


**Figure 6.** Triarylsilane Cr(III) tris-THF structure, with the Si-H linker, rather than Si-Me.

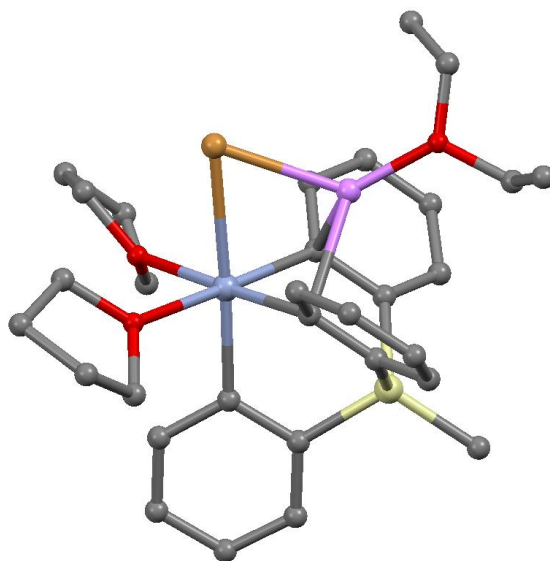


**Figure 7.** Triarylsilane Cr(III) complex, with lithium halide (Cl/Br) coordinated.

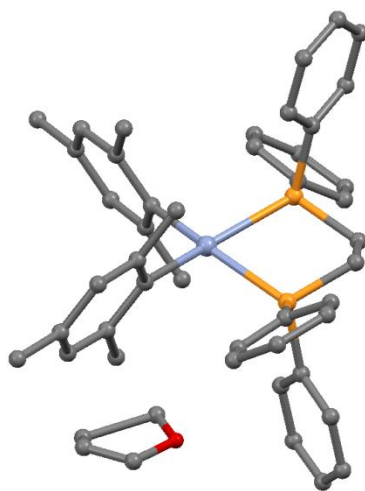


**Figure 8.** Bis(dimethylphosphino)ethane Cr(II) dimesityl. THF solvent molecule shown.

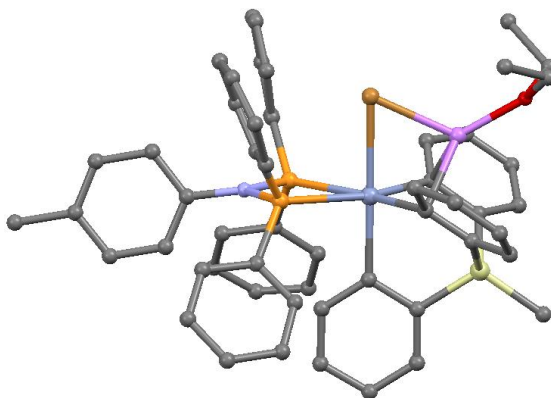


**Figure 9.** Triarylsilane Cr(III) bound to <sup>tol</sup>PNP and a lithium halide (Cl/Br) equivalent.

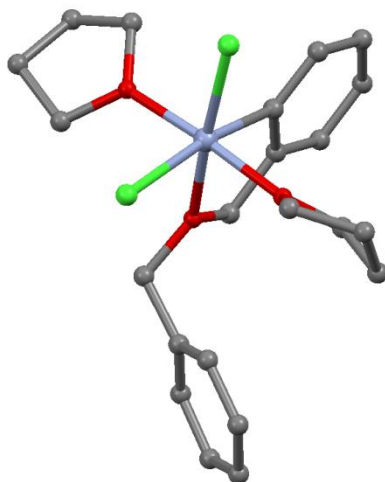


**Figure 10.**  $\text{CrCl}_2(o\text{-(C}_6\text{H}_5\text{CH}_2\text{OCH}_2\text{)-C}_6\text{H}_4)_3(\text{THF})_2$ .

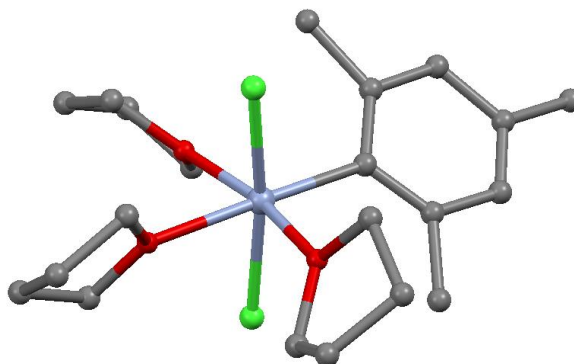


**Figure 11.**  $\text{CrCl}_2(\text{mesityl})(\text{THF})_3$ .

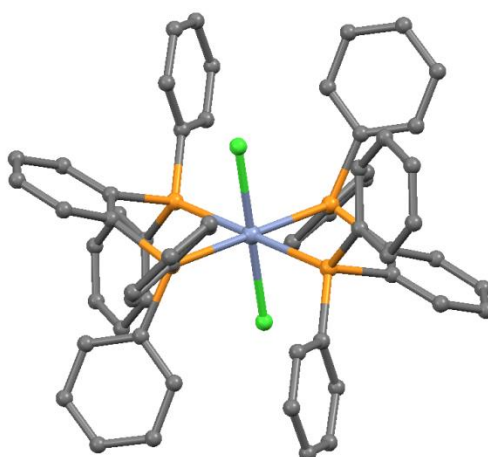


**Figure 12.**  $\text{CrCl}_2(\text{dppbz})_2$ .

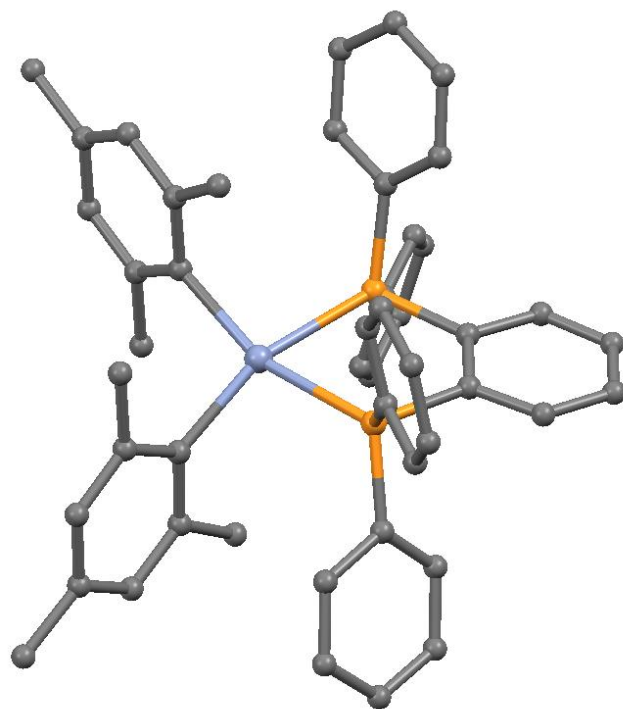


**Figure 13.**  $\text{Cr}(\text{mesityl})_2(\text{dppbz})$

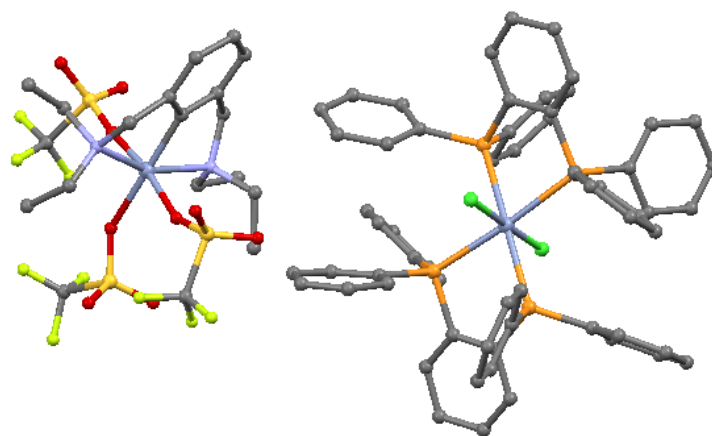


**Figure 14.**  $(\text{NCN})\text{Cr}$  tris(triflate) and  $\text{CrCl}_2(\text{dppbz})_2$  in the same crystal lattice.

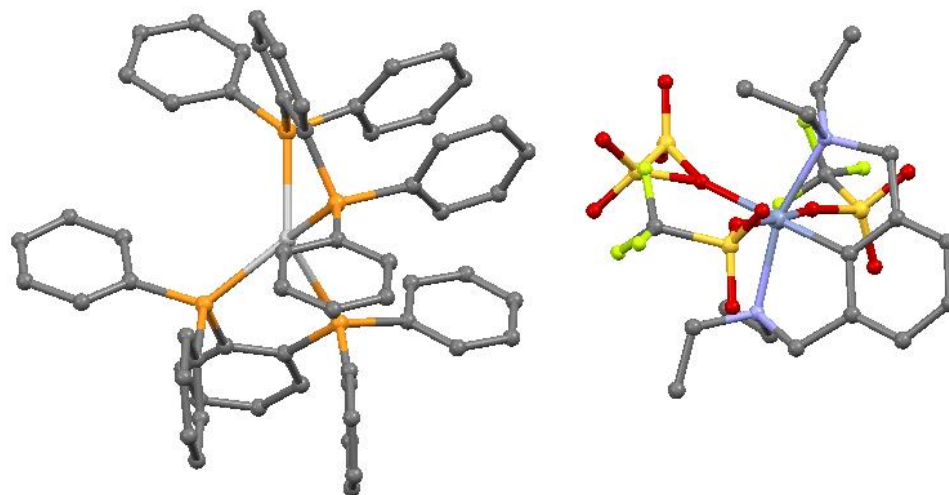


**Figure 15.** (NCN)Cr tris(triflate) (partially modelled triflate trans to the aryl donor) and Ag(dppbz)<sub>2</sub> in the same crystal lattice.

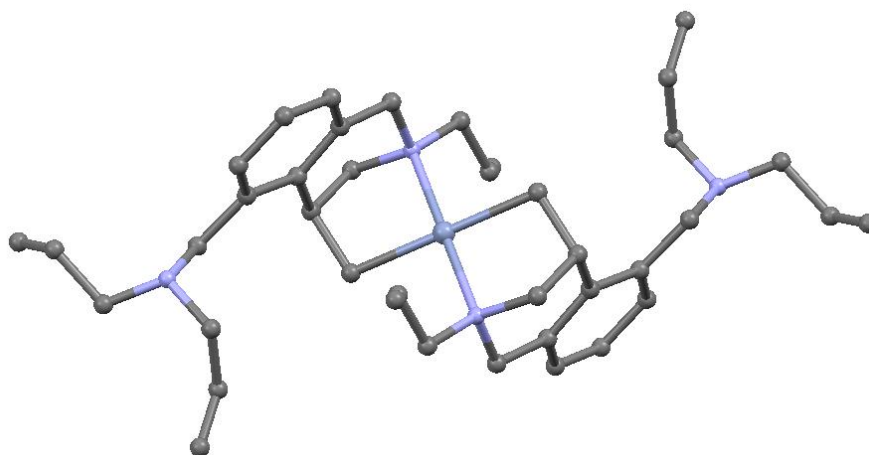


**Figure 16.** Two amine-alkyl ligands (derived from alkene-derivatized NCN-pincer complex) on Cr(II).

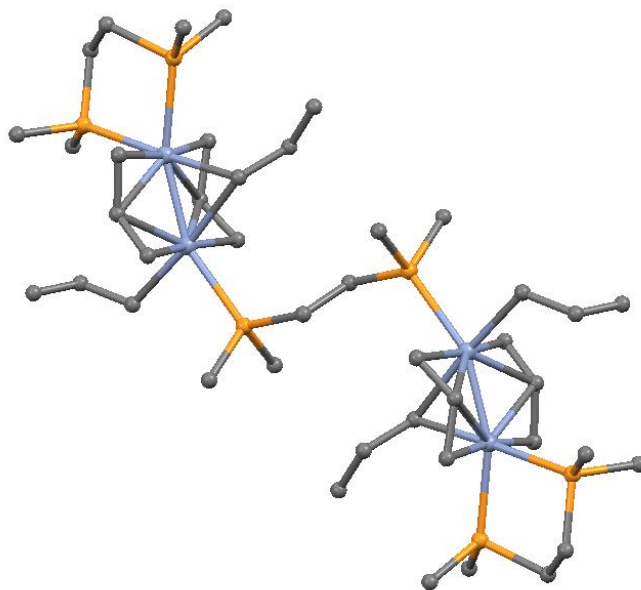


**Figure 17.** Bis(dimethylphosphino)ethane (dmpe) bridges two dichromium units with the following formula:  $(\text{dmpe})\text{Cr}_2(\text{allyl})_4$ .

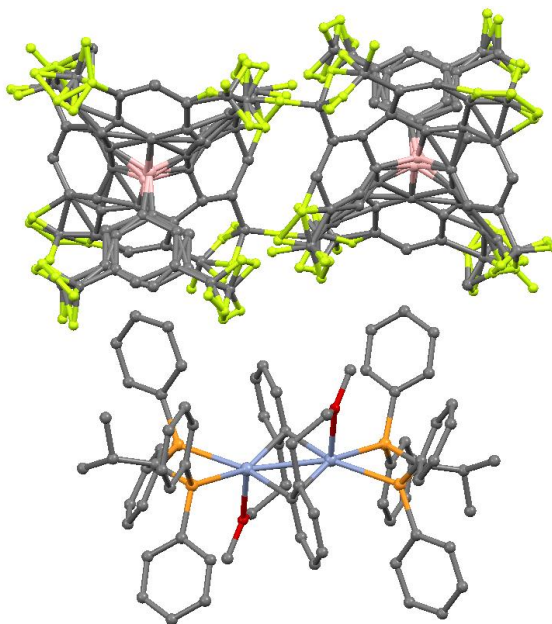


**Figure 18.**  $[(^i\text{Pr})\text{PNP}]\text{Cr}(\text{MeO}(\text{CH}_2)_2\text{C}_6\text{H}_4)_2$  with two outer sphere  $\text{BAR}_4^-$  anions (disorder shown).

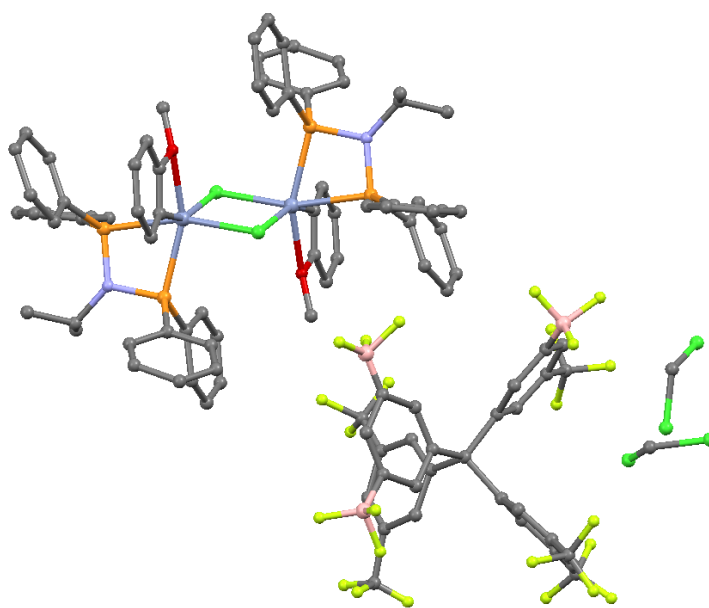


**Figure 19.** Dimeric,  $[(^i\text{PrPNP})\text{Cr}(\text{MeOC}_6\text{H}_4)\text{Cl}]_2$  with two outer sphere  $\text{BAr}'_4$  anions (only one shown). DCM solvent molecules shown.

### About the Author



Nate Hirscher was born in Manassas, Virginia. His parents raised him there, along with four siblings. After graduating with a Virginia home-school high-school diploma in 2010, he attended the University of Virginia in Charlottesville, VA. He obtained his B.Sc. in Chemistry, graduating in 2014. It was there that he found two loves: chemistry (now his career) and Emily (now his wife). Nate's passion for transition metal reaction chemistry took him through College Station, TX for a summer research appointment with Prof. Oleg Ozerov at Texas A&M University, then finally to Pasadena, CA for his Ph.D. studies with Prof. Theodor Agapie at Caltech. Following graduation in 2019, Nate is heading to the University of Pennsylvania in Philadelphia, PA to postdoc in the labs of Profs. Karen Goldberg and Eric Schelter.